

# **Mechanistic insight into virus disinfection: Influence of virus characteristics, solution composition and surface interactions**

THÈSE N° 6166 (2014)

PRÉSENTÉE LE 23 MAI 2014

À LA FACULTÉ DE L'ENVIRONNEMENT NATUREL, ARCHITECTURAL ET CONSTRUIT  
LABORATOIRE DE CHIMIE ENVIRONNEMENTALE  
PROGRAMME DOCTORAL EN GÉNIE CIVIL ET ENVIRONNEMENT

ÉCOLE POLYTECHNIQUE FÉDÉRALE DE LAUSANNE

POUR L'OBTENTION DU GRADE DE DOCTEUR ÈS SCIENCES

PAR

**Anne Thérèse SIGSTAM**

acceptée sur proposition du jury:

Prof. K. Schirmer, présidente du jury  
Prof. T. Kohn, directrice de thèse  
Prof. A. M. de Roda Husman, rapporteuse  
Dr M. Sander, rapporteur  
Prof. U. von Gunten, rapporteur



ÉCOLE POLYTECHNIQUE  
FÉDÉRALE DE LAUSANNE

Suisse  
2014



**“When you drink the water, remember the spring”**

Chinese proverb





# Acknowledgements

First and foremost I'd like to thank my thesis supervisor **Tamar** who guided me through these four years of PhD. Thanks to her, I've discovered the interesting domain of water disinfection and in particular the amazing world of viruses. I'd also like to thank her for her support to drive this project forward, her critical and constructive reviews, the interesting conferences abroad as well as her outstanding availability to answer questions at all times. For all these reasons, it has been a pleasure working at LCE and I wish her all the best for the continuation of her career.

I also kindly thank the president of the jury, Prof. **Kristin Schirmer**, and all the members of the jury: Prof. **Urs von Gunten**, Prof. **Ana Maria de Roda Husman** and Dr. **Michael Sander** for accepting this task.

Special thanks go to **Andreas**, who spent 6 months in the lab working on disinfection by chlorine dioxide, hence greatly contributing to the second chapter of this thesis. Thanks also to **Moritz** for having shared with me his master thesis results which also contributed to the second chapter of this work. Another special acknowledgement goes to Prof. **Satoshi Takahama**, without whom I would probably still be stuck on the statistical significance of the Hom model.

This PhD thesis was part of the SINERGIA project which involved other research groups that I also would like to acknowledge. In particular, I'd like to thank **Tony**, who has always answered all my stupid questions about adsorption and SAMs with tremendous patience and **Michael Sander** for welcoming me in his lab for a week and for his valuable and creative reviews to my work. I am also very grateful for the nice collaboration with Prof. **Michele Cascella's** group: **Greg** (who does magic to explain virus behaviors towards disinfectants) and **Kristos**. In this collaborative project I also would like to thank Prof. **Kris McNeill** and **Elena** for valuable inputs to my work.

Merci également à **Sylvain** et **Dominique** pour leur aide et leur efficacité dans les analyses chimiques.

Mes quatre ans au sein du LCE n'auraient pas été les mêmes sans la présence du **König der Party** (**Michael**) et **Lucky Loïc** avec qui j'ai partagé le bureau le plus proche de Sat. Merci à eux pour les débats scientifiques mais également pour les moments de détente, de bricolage et de rigolade entre deux

## Acknowledgements

expériences. Un grand merci à **Karine** qui a résolu pour moi tous les problèmes administratifs. Un grand merci à **Flo** pour les évasions gustatives plus succulentes les unes que les autres. All my gratitude also goes to a former member of LCE **Krista Wigginton** who taught me everything there was to know about virus manipulations and transmitted me her interest in viral proteomics. Thanks also to **Brian Pecson**, our father of PCR for his unconditional good humor and all the fun wine tastings. Thanks also to all the present and former group members of LCE: **Heather, Anna, Qingxia, Julien, Franziska, Shinobu, Rebecca, Corinne, Jessi, Ariane, Alex, Vincent** and **Manfred**, without whom, these four years wouldn't have been as exciting.

Ich möchte auch oftmals **Michèle** danken für alle Stunden, dass sie mit viel Geduld mit mir Deutsch gesprochen hat. Merci également à **Kathi** pour avoir toujours été motivée pour jouer aux cartes et pour avoir rendu plus agréables mes trajets entre Lausanne et Fribourg.

Mon temps à l'EPFL n'aurait pas eu la même saveur sans la présence de **Valérie** qui m'a permis de m'échapper de mes virus le temps d'un match de badminton. Merci également à son cher et tendre **Franzi** pour tous les taboulés et autre soupes Dong.

Ces quatre années ne se seraient jamais aussi bien passé sans la présence de mes amis qui ont toujours été là pour me soutenir, mais surtout pour tous les moments de plaisir lors de soirées, jeux de cartes, sorties à ski et autres moments. Et pour cela je remercie mille fois **Sof, Flo, Nat, Cyril** ainsi que toute Steak'Hip d'allumés de Nyon: **Séb, Alex, Lolo, Quanou, Pascal** et **Florent**. J'aimerais également remercier **Mestre Paulão** et tout le groupe **ACL** sans qui je n'aurais pas découvert la capoeira ainsi que la magnifique culture brésilienne. Merci également à **Sévrine** avec qui je partage une grande amitié depuis plus de 25 ans maintenant, qui malgré l'éloignement est toujours là pour la petite pensée qui fait chaud au cœur. Un merci tout particulier à **Mél** pour les nombreuses années d'amitié et pour m'avoir donné l'immense bonheur d'être la marraine de la magnifique petite **Léa**. Dans ce sens, j'aimerais aussi remercier **Nadia** et **Julien** qui m'ont accordé la confiance d'être la marraine du plus beau des petit **Romeo**.

Enfin, le plus grand remerciement va à toute ma famille. Och framför allt, vill jag tacka min mamma **Susann** och min pappa **Kaj**. Ni har givit mig en väldigt glad barndom, gjort så att jag lärt mig stå på ett par skidor och givit mig en utmärkt utbildning som har tagit mig ända hit idag. Ni har alltid stått

bakom mig och trott på vad jag gör och för allt det vill jag nu ta tillfället att tacka Er. Jag vill också tacka alla mina syskon i Sverige: **Anna-Lena**, **Karin**, **Ia** och **Pelle** för trevliga tider på Långhäll, eller på andra roliga ställen i världen och en väldigt rolig båtresa föra året. Puis finalement, un grand merci pour son soutien et sa présence à mon cher petit frangin **Arvid**, à mes côtés depuis 30 ans maintenant avec qui j'ai toujours autant de plaisir à partager une journée à ski ou un bon souper.



# Abstract

Waterborne viruses are responsible for major outbreaks of diarrhea and other diseases throughout the world. Efficient virus inactivation during water and wastewater treatment is therefore important to prevent the contamination of water resources by inadequately treated wastewater, and to ensure the microbial safety of drinking and recreational water. This thesis discusses the kinetics and mechanisms of virus inactivation in commonly used homogeneous (chlorine dioxide, chlorine, UV and singlet oxygen) and heterogeneous (copper surfaces) disinfection systems, in order to obtain a better understanding of these processes.

In order to compare the efficiency of different disinfection treatments within a wide variety of viruses or among different disinfectants, the Chick-Watson first-order model is frequently used. It allows determination of virus inactivation rate constants as a function of disinfectant dose. However, virus inactivation by chlorine dioxide shows a deviation from this first-order model, namely a tailing curve. The mechanisms underlying this deviation are currently not understood. Tailing has been previously reported, but is typically attributed to the decay in disinfectant concentration. However, present results showed that tailing occurs even at constant  $\text{ClO}_2$  concentrations. Four working hypothesis to explain the cause of tailing were tested, specifically changes in the solution's disinfecting capacity, aggregation of viruses, resistant virus subpopulations, and changes in the virus properties during disinfection. In experiments using MS2 as a model virus, it was possible to rule out the solution's disinfecting capacity, virus aggregation and the resistant subpopulation as reasons for tailing. Instead, the cause for tailing is the deposition of an adduct onto the virus capsid over the course of the experiment, which protects the viruses. This adduct could easily be removed by washing, which restored the susceptibility of the viruses to  $\text{ClO}_2$ . This finding highlights an important shortcoming of  $\text{ClO}_2$ , namely its self-limiting effect on virus disinfection. It is important to take this effect into account in treatment applications to ensure that the water is sufficiently disinfected before human consumption.

Besides its deviation from first-order kinetics,  $\text{ClO}_2$  also exhibits drastically different inactivation kinetics for different viruses, even if viruses are closely related. These differences can only be rationalized if the underlying disinfection mechanisms are understood. Herein, we therefore determined how small

## Abstract

differences in the composition of the viral genome and proteins impact the disinfection kinetics and mechanisms of  $\text{ClO}_2$  and other disinfectants. To this end, we investigated the inactivation of three related bacteriophages (MS2, fr, and GA) by  $\text{UV}_{254}$ , singlet oxygen ( $^1\text{O}_2$ ), free chlorine (FC), and  $\text{ClO}_2$ . Genome damage was quantified by q-PCR, and protein damage was assessed by quantitative matrix-assisted laser desorption ionization (MALDI) mass spectrometry.  $\text{ClO}_2$  caused great variability in the inactivation kinetics between viruses and was the only treatment that did not induce genome damage. In contrast, the inactivation kinetics were similar for all viruses when treated with disinfectants possessing a genome-damaging component (FC,  $^1\text{O}_2$ , and  $\text{UV}_{254}$ ). On the protein level,  $\text{UV}_{254}$  subtly damaged MS2 and fr capsid proteins, whereas GA's capsid remained intact. Singlet oxygen oxidized a methionine residue in MS2 but did not affect the other two viruses. In contrast, FC and  $\text{ClO}_2$  rapidly degraded the capsid proteins of all three viruses. Protein composition alone could not explain the observed degradation trends; instead, molecular dynamics simulations indicated that degradation is dictated by the solvent-accessible surface area of individual amino acids. Finally, despite the similarities of the three viruses investigated, their mode of inactivation by a single disinfectant varied. This explains why closely related viruses can exhibit drastically different inactivation kinetics.

Compared to the homogeneous disinfection methods mentioned above, even less is known regarding the mode of action of heterogeneous disinfectants. In heterogeneous systems, disinfection is mediated by virus-surface interactions. A prominent example of a heterogeneous disinfection system is the copper jar, which is widely used in Indian homes to store water, and which has been shown to possess antiviral activity. However, it is not understood which virus-copper interactions lead to disinfection, or how the viruses are affected by these interactions. To better understand this system, adsorption-inactivation experiments were performed with two bacteriophages, MS2 and Qbeta, on metallic copper. Hereby, the contributions of both the metallic copper and the dissolved copper leached from the solid surface were investigated. MS2 was found to be inactivated by dissolved copper only, whereas the metallic copper had an important role in the inactivation of Qbeta. To shed light on which virus-surface interactions cause inactivation, adsorption-inactivation processes were studied on self-assembled monolayers (SAMs) which allow studying the effect of a single type of interaction at a time. The two viruses were found to differ in their adsorption behavior, but not their inactivation trends: hydrophobic and hydrogen-bonding surfaces led to efficient adsorption and inactivation of both viruses; positively charged surfaces led to adsorption via electrostatic attraction, but not to inactivation; and finally, pure gold surfaces (exhibiting van der Waals interactions) adsorbed Qbeta more efficiently than MS2, but did not inactivate either

virus. Based on these results, it was suggested that the different inactivation behavior of the two viruses observed in presence of metallic copper was a result of their differing adsorption, rather than inactivation tendencies. The stronger surface interactions of Qbeta may furthermore be rationalized by the presence of disulfide bridges in its capsid protein, which can form thiolate bonds with the copper surface. Then concurrent reduction of the disulfide bridges may cause important distortions of Qbeta's capsid's conformation, or may result in its disintegration.

Overall this thesis has shed new light on the mechanisms involved in virus inactivation and on how to relate them to inactivation predictions of nonculturable viruses. The use of surrogates to this purpose showed to be reliable for genome-active disinfection treatments but care should be taken when predicting inactivation by protein-active treatments. This mechanistic insight into viral inactivation also allowed understanding the mechanisms causing tailing by protein-active disinfectants.

**Keywords:** Virus inactivation, chlorine dioxide, tailing effect, inactivation mechanisms by oxidants, genome degradation, protein degradation, virus-surface interaction, copper, self-assembled monolayers (SAMs)





# Résumé

Les virus transmis par l'eau sont responsables de grandes épidémies de diarrhée et d'autres maladies dans le monde entier. Il est donc d'importance capitale que lors du traitement de l'eau et des eaux usées, l'inactivation virale soit efficace afin de prévenir la contamination des ressources en eau par les eaux usées insuffisamment traitées, et pour assurer la sécurité microbienne de l'eau potable et des zones de baignade. Cette thèse traite de la cinétique et des mécanismes d'inactivation de virus dans des systèmes de désinfections homogènes (dioxyde de chlore, chlore, oxygène singulet et UV) et hétérogènes (surfaces de cuivre) couramment utilisés, pour obtenir une meilleure compréhension de ces processus.

Afin de comparer l'efficacité de différents traitements de désinfection entre eux et/ou pour différents virus, le modèle cinétique de premier ordre de Chick-Watson est fréquemment utilisé. Il permet la détermination de constantes de vitesse d'inactivation de virus en fonction de la dose de désinfectant. Cependant, l'inactivation de virus par le dioxyde de chlore présente une importante déviation de ce modèle de premier ordre, plus précisément, par la formation d'un plateau. La formation de plateau a été détectée à plusieurs reprises, mais les mécanismes sous-jacents à ce type de déviation ne sont actuellement pas connus. La formation de plateau est en général simplement attribuée à la diminution de la concentration de désinfectant. Cependant les résultats obtenus dans cette thèse ont montré que ce phénomène se produit même à des concentrations de dioxyde de chlore constantes. Quatre hypothèses de travail ont été émises et testées pour expliquer la cause de ce plateau; *i)* l'altération de la capacité de désinfection de la solution au cours du traitement; *ii)* l'agrégation des virus; *iii)* la présence de sous-populations de virus résistants; *iv)* les changements de propriété virale au cours de la désinfection. Les résultats des expériences utilisant MS2 comme modèle de virus, ont montré qu'il était possible d'exclure la diminution de la capacité de désinfection de la solution, l'agrégation des virus et la présence de sous-populations résistantes comme cause du phénomène de plateau. Au lieu de cela, nous avons pu démontrer que la cause de la formation du plateau est le dépôt d'un produit sur la capsid du virus au cours de la désinfection, lui conférant ainsi une protection. Ce produit déposé peut facilement être éliminé par rinçage, ce qui rétablit la sensibilité des virus au dioxyde de chlore. Ce constat a mis en évidence un important défaut du traitement par le dioxyde de chlore, c'est-à-dire son effet d'auto-

limitation de la désinfection des virus. Il est donc important de prendre en compte cet effet lors du dimensionnement des systèmes de traitement de l'eau.

Outre la déviation de la cinétique de premier ordre, la désinfection par le dioxyde de chlore a également présenté des cinétiques d'inactivation radicalement différentes pour des virus distincts bien qu'étroitement apparentés. Ces différences ne peuvent être rationalisées que si les mécanismes moléculaires induisant l'inactivation sont compris. Nous avons par conséquent déterminé comment de subtiles différences dans la composition du génome et des protéines virales peuvent avoir un impact sur la cinétique de désinfection ainsi que sur les mécanismes d'inactivation par le dioxyde de chlore et d'autres désinfectants communément utilisés. Dans ce but, nous avons étudié l'inactivation par l'UV<sub>254</sub>, l'oxygène singulet (<sup>1</sup>O<sub>2</sub>), le chlore, et le dioxyde de chlore (ClO<sub>2</sub>) de trois bactériophages, MS2, fr et GA, similaires par leur forme et leur structure. Les lésions au niveau du génome ont été quantifiées par la méthode de réaction en chaîne par polymérase quantitative (q-PCR) et les lésions au niveau de la capside protéique ont été évaluées par spectrométrie de masse quantitative (MALDI). La désinfection par le dioxyde de chlore a causé une grande variabilité dans la cinétique d'inactivation des virus et a été le seul traitement ne provoquant aucune lésion du génome. En revanche, les cinétiques d'inactivation se sont montrées similaires pour tous les virus étudiés lorsqu'ils étaient traités avec un désinfectant possédant la capacité d'endommager le génome (chlore, <sup>1</sup>O<sub>2</sub> et UV<sub>254</sub>). Concernant la capside protéique, l'UV<sub>254</sub> l'a sensiblement endommagée dans le cas de MS2 et fr, mais elle est restée intacte pour GA. L'oxygène singulet a oxydé un résidu méthionine dans MS2 mais n'a pas eu d'incidence sur les deux autres virus. En revanche, le chlore et le dioxyde de chlore ont rapidement dégradé les protéines de la capside de l'ensemble des trois phages. En tenant compte uniquement de la composition (séquence d'acides aminés) de la protéine, les tendances de dégradation observées ici ne pouvaient être expliquées. Cependant, grâce à des simulations de dynamique moléculaire, il a été possible de déterminer que la dégradation était dictée par la capacité des solvants à accéder à la surface des acides aminés individuels. Ainsi, malgré les similitudes entre les trois virus étudiés, leur mécanisme d'inactivation par un même désinfectant peut varier, engendrant des cinétiques d'inactivation radicalement différentes.

Par rapport aux méthodes de désinfection homogènes mentionnées ci-dessus, nous disposons d'encore moins de connaissance sur le mode d'action des désinfectants hétérogènes. Dans les systèmes hétérogènes, la désinfection des virus se fait par l'intermédiaire des interactions virus-surface. Un exemple bien connu d'un système de désinfection hétérogène est la jarre de cuivre, qui est

fréquemment utilisée dans les maisons indiennes pour stocker l'eau, et qui a démontré une activité antivirale. Toutefois, la manière dont ces interactions virus-cuivre conduisent à la désinfection, ou le procédé par lequel les virus sont affectés, ne sont pas encore connus. Afin de mieux comprendre ce système, des expériences d'adsorption-inactivation ont été réalisées avec deux bactériophages, MS2 et Qbeta, dans une solution contenant une feuille de cuivre. De cette manière, les contributions du cuivre métallique et du cuivre dissout ont pu être étudiées. L'inactivation de MS2 a été provoquée par le cuivre dissout uniquement, alors que la feuille de cuivre a joué un rôle important dans l'inactivation de Qbeta. Afin de mettre en lumière les interactions virus-surface susceptibles de provoquer l'inactivation, les processus d'adsorption-inactivation ont été examinés sur des monocouches auto-assemblées permettant d'étudier l'effet d'un seul type d'interaction à la fois. Le comportement d'adsorption des deux virus se sont révélés différents, cependant leurs tendances d'inactivation étaient similaires: les surfaces hydrophobes ainsi que celles induisant des ponts hydrogène ont conduit à une adsorption efficace et à l'inactivation des deux virus; les surfaces chargées positivement ont conduit à une adsorption efficace par l'attraction électrostatique, mais aucune inactivation n'a été observée; les surfaces d'or pur (présentant des interactions de type van der Waals) ont adsorbés Qbeta plus efficacement que MS2, mais n'ont pas engendré d'inactivation. Sur la base de ces résultats, il a été suggéré que la différence d'inactivation observée entre les deux virus en présence d'une feuille de cuivre est la conséquence de leur différente capacité d'adsorption, plutôt que de la possibilité d'inactivation une fois adsorbés. Les interactions exacerbées avec la surface de cuivre ou d'or de Qbeta peuvent être expliquées par la présence de ponts disulfure dans sa capsidie protéique, qui peuvent former des liaisons thiolate avec ces surfaces. De plus, la réduction chimique des ponts disulfure peut provoquer des déformations importantes de la conformation de la capsidie, ou même aboutir à sa désintégration.

Globalement, cette thèse a mis en lumière les mécanismes impliqués lors de l'inactivation de virus et sur la manière de relier ces résultats afin de permettre des prédictions d'inactivation de virus non cultivables. Cette approche mécanistique de l'inactivation virale a également permis de comprendre les mécanismes à l'origine du phénomène de plateau observé lors de traitement visant principalement l'intégrité des protéines.

**Mots-clés:** Inactivation de virus, dioxyde de chlore, formation de plateau, mécanismes d'inactivation par des oxydants, dégradation de génome, dégradation de protéines, interaction virus-surface, cuivre, monocouche auto-assemblées



# Contents

Acknowledgements .....	V
Abstract.....	IX
Résumé.....	XIII
Contents.....	XVII
List of figures .....	XXI
List of tables .....	XXV
Introduction.....	1
1.1    From microorganisms to pathogens .....	1
1.2    Viruses .....	2
1.2.1    Origin and occurrence of viruses.....	2
1.2.2    Virus characteristics.....	4
1.2.3    Transmission of viruses.....	5
1.2.4    Detection and composition of viruses .....	7
1.3    Virus inactivation by homogeneous disinfectants .....	11
1.3.1    Disinfection kinetics.....	13
1.3.2    Disinfection mechanisms .....	15
1.4    Virus inactivation by heterogeneous disinfectants .....	17
1.4.1    Importance of viral adsorption .....	17
1.4.2    Mechanisms of viral adsorption .....	18
1.5    Research objectives of this thesis .....	20
On the cause of the tailing phenomenon during virus disinfection by chlorine dioxide.....	23
2.1    Introduction .....	23
2.2    Materials and methods.....	25
2.2.1    Chemicals .....	25
2.2.2    Microorganisms.....	25
2.2.3    Chlorine dioxide production and experimental setup.....	25
2.2.4    Re-growth of MS2 after inactivation .....	26

## Contents

2.2.5	Particle size measurement by Dynamic Light Scattering (DLS) .....	26
2.2.6	Analysis of the capsid protein by Matrix Assisted Laser Desorption Ionization (MALDI) ....	26
2.2.7	Analysis of disinfection kinetics.....	27
2.3	Results and discussion .....	27
2.3.1	Changes in solution properties.....	29
2.3.2	Aggregation .....	31
2.3.3	Resistant subpopulation .....	35
2.3.4	Changes in virus properties.....	36
2.4	Conclusions .....	39
Subtle differences in virus composition affect disinfection kinetics and mechanisms: effect of genome composition.....		41
3.1	Introduction .....	41
3.2	Materials and Methods .....	43
3.2.1	Chemicals .....	43
3.2.2	Microorganisms.....	43
3.2.3	Disinfection experiments .....	43
3.2.4	Analysis of disinfection kinetics.....	45
3.2.5	Quantitative Polymerase Chain Reaction (q-PCR).....	45
3.2.6	Quantification of damage to entire genome .....	46
3.2.7	Experimental and predicted degradation rate constants of amplicons .....	47
3.3	Results.....	48
3.3.1	Comparison of inactivation kinetics .....	48
3.3.2	Comparison of levels of genome degradation .....	51
3.3.3	Distribution of genome damage.....	54
3.4	Discussion .....	56
3.4.1	Influence of genome composition on degradation and inactivation .....	56
3.4.2	UV <sub>254</sub> .....	57
3.4.3	Singlet oxygen .....	58
3.4.4	Free chlorine .....	58
3.4.5	Chlorine dioxide.....	59
3.4.6	Location in genome damage influences degradation .....	60
3.5	Conclusion.....	61

Subtle differences in virus composition affect disinfection kinetics and mechanisms: effect of protein composition.....	63
4.1    Introduction .....	63
4.2    Materials and methods.....	65
4.2.1    Chemicals .....	65
4.2.2    Microorganisms.....	65
4.2.3    Propagation of <sup>15</sup> N-labeled bacteriophages.....	65
4.2.4    Disinfection assays for protein damage assessment.....	66
4.2.5    Analysis of peptide damage by Matrix Assisted Laser Desorption Ionization (MALDI) .....	66
4.2.6    Quantification of capsid protein degradation.....	71
4.2.7    Prediction of capsid protein degradation rate constants .....	72
4.2.8    Computational modeling of methionine oxidation in fr and MS2 .....	73
4.3    Results.....	74
4.3.1    Comparison of capsid protein degradation .....	74
4.3.2    Identification of susceptible capsid protein domains.....	78
4.3.3    Identification of susceptible A protein domains .....	82
4.3.4    MS/MS identification of amino acids modified by singlet oxygen .....	82
4.3.5    Computational rationalization of singlet oxygen findings .....	83
4.4    Discussion .....	85
4.4.1    Influence of protein composition on degradation and inactivation .....	85
4.4.2    UV <sub>254</sub> .....	86
4.4.3    Singlet oxygen .....	86
4.4.4    Free chlorine .....	87
4.4.5    Chlorine dioxide.....	88
4.5    Conclusion.....	90
MS2 and Qbeta inactivation at the copper-water interface .....	91
5.1    Introduction .....	91
5.2    Materials and Methods .....	94
5.2.1    Chemicals .....	94
5.2.2    Microorganisms.....	95
5.2.3    Batch experiments with copper .....	95
5.2.4    RNA extraction and quantitative Polymerase Chain Reaction (q-PCR) .....	96

## Contents

5.2.5	Analysis of copper disinfection kinetics .....	96
5.2.6	Self-assembled monolayers (SAMs): description and preparation .....	97
5.2.7	Adsorption and inactivation experiments in a teflon QCM-D flow-through cell .....	99
5.2.8	Analysis of Qbeta genome damage by q-PCR .....	101
5.2.9	Analysis of Qbeta capsid protein damage by Matrix Assisted Laser Desorption Ionization (MALDI) .....	101
5.3	Results and discussion .....	103
5.3.1	Inactivation kinetics by copper .....	103
5.3.2	Surface interactions of MS2 and Qbeta .....	106
5.3.3	Probing the effect of different interactions on virus infectivity .....	108
5.3.4	Assessment of the mechanism of inactivation by copper .....	112
5.3.5	Limitations of the current study .....	114
5.4	Conclusion .....	115
Conclusions and perspectives .....		117
6.1	Inactivation mechanism determines disinfection model .....	119
6.2	Mechanistic information explains differences in viruses' susceptibility to disinfection .....	120
6.3	Interactions leading to heterogeneous inactivation .....	121
6.4	Future work .....	122
Appendix A – Chapter 1 .....		125
Appendix B – Chapter 2 .....		127
Appendix C – Chapter 3 .....		131
Appendix D – Chapter 4 .....		133
References .....		141



# List of figures

Figure 1.1: Effect of TBV on tulips .....	3
Figure 1.2: Variety of shapes in the virus family .....	4
Figure 1.3: Schematic representation of a virus.....	4
Figure 1.4: Fecal-oral transmission route .....	6
Figure 1.5: Agar plate with plaques .....	8
Figure 1.6: Cross-section and outside view of MS2 and Picornavirus .....	9
Figure 1.7: Amino acid sequence of MS2, fr, GA and Qbeta .....	10
Figure 1.8: Possible shapes of inactivation curves of microorganisms.....	14
Figure 1.9: Disinfection mechanisms of MS2 .....	16
Figure 1.10: DLVO theory representation .....	18
Figure 1.11: Mechanism of inactivation at virus-surface interface .....	19
Figure 2.1: Inactivation of MS2 by chlorine dioxide .....	28
Figure 2.2: Impact on $k_H$ due to changes in solution properties .....	30
Figure 2.3: Size distribution of MS2 at different ionic strengths.....	32
Figure 2.4: Impact of aggregate dispersion on $k_H$ .....	34
Figure 2.5: Effect of washing on the inactivation of MS2 by chlorine dioxide.....	36
Figure 2.6: MALDI spectra of washed and unwashed MS2 samples before and after $\text{ClO}_2$ treatment.....	38
Figure 3.1: Location and distribution of analyzed genome regions. ....	46
Figure 3.2: Comparison of disinfection kinetics .....	49
Figure 3.3: Overview of the inactivation rate constants (hexagons) and genome degradation rate constants (spirals) for all four disinfecting treatments .....	50
Figure 3.4: Comparison of genome damage of the three phages upon inactivation by the four disinfectants investigated .....	51
Figure 3.5: Comparison of genome damage and virus inactivation of the three bacteriophages upon inactivation by the four disinfectants.....	53
Figure 3.6: Comparison of predicted and experimental amplicon degradation rate constants for MS2 upon $\text{UV}_{254}$ , $^1\text{O}_2$ , FC and $\text{ClO}_2$ .....	54
Figure 4.1: Example calibration curves for the quantification of peptides.....	69

## List of figures

Figure 4.2: Comparison of capsid protein damage versus disinfectant dose between the three viruses upon inactivation by the four disinfectants .....	75
Figure 4.3: Overview of inactivation, genome degradation and protein degradation rate constants .....	76
Figure 4.4: Protein degradation per log inactivation between the three viruses upon inactivation by the four disinfectants.....	77
Figure 4.5: Degradation rate constants $k_{\text{peptide}}$ for the individual peptides within the capsid proteins of the three viruses.....	79
Figure 4.6: Linear mode MALDI spectra after disinfection by UV <sub>254</sub> and free chlorine .....	81
Figure 4.7: GA A protein peptide degradation after UV <sub>254</sub> and <sup>1</sup> O <sub>2</sub> .....	82
Figure 4.8: MALDI-TOF-TOF fragmentation spectra of oxidation product m/z 2687.89 .....	83
Figure 4.9: Capsid protein views of MS2 and fr.....	84
Figure 4.10: Location of degraded peptides after ClO <sub>2</sub> treatment on the outside (A) and inside (B) of the MS2 capsid .....	89
Figure 5.1: MS2 and Qbeta bacteriophage, surface characteristics.....	93
Figure 5.2: Representation of the self-assembled monolayers on gold sensors used in this study.....	97
Figure 5.3: QCM-D output for adsorption monitoring.....	100
Figure 5.4: Schematic representation of inactivation experiments on SAMs.....	101
Figure 5.5: Inactivation kinetics of MS2 and Qbeta with copper .....	104
Figure 5.6: Kinetics of copper dissolution .....	105
Figure 5.7: Adsorption efficiency onto SAMs .....	107
Figure 5.8: Infectivity and genome concentration after adsorption-desorption to a surface .....	109
Figure 5.9: Inactivation after adsorption-desorption on SAMs.....	110
Figure 5.10: Qbeta genome damage after exposure to copper .....	112
Figure 5.11: Qbeta peptide damage after treatment with copper .....	113
Figure A.1: Table of amino acids.....	125
Figure B.1: Inactivation curve with fit to the Hom model for a control and for the experiment with added carbonate buffer instead of DB.....	127
Figure B.2: Inactivation curve with fit to the Hom model for a control and for the experiment with added chlorite in the beginning.....	127
Figure B.3: Inactivation curve with fit to the Hom model for a control and for the second spike of MS2 in the spent solution.....	128

Figure B.4: Inactivation curve with fit to the Hom model for a control and for the experiment with sonication pre-treated virus stock.....	128
Figure B.5: Inactivation curve with fit to the Hom model for a control and for the experiment with chloroform pre-treated virus stock .....	129
Figure B.6: Inactivation curve with fit to the Hom model for a control and for the experiment with 0.1 $\mu\text{m}$ filtered virus stock. ....	129
Figure B.7: Inactivation curve with fit to the Hom model for a control and for the experiment in high ionic strength (500 mM NaCl). ....	130
Figure B.8: Inactivation curve of a control experiment and a sample with increased $\text{ClO}_2$ concentration after 120 seconds .....	130
Figure D.1: Schematic representation of the thermodynamic cycle used for the calculation of energy difference in the oxidation of methionine in an aqueous environment relative to a protein environment.....	135
Figure D.2: Schematic representation of the thermodynamics cycle used for the calculation of the electrostatic component of the inter-triplet capsid binding energy .....	136
Figure D.3: Distance to the sulfur atom of Met88 for a single atom in the surrounding residues .....	137
Figure D.4: Radial distribution function of the Met 88 sulfur atom in chain A and the oxygen atoms of water for the MS2 and fr virus capsid .....	138



# List of tables

Table 1.1: Common waterborne viruses and MS2 bacteriophage, and their associated diseases. ....	7
Table 1.2: Coagulation, sedimentation, filtration.....	12
Table 1.3: IEP and PZC examples. ....	19
Table 3.1: Reported nucleotide degradation rate constants, molar absorptivities ( $\epsilon_{254}$ ) and quantum yields ( $\phi$ ).....	47
Table 3.2: Number of copies and percentage of each nucleotide in the genome of each bacteriophage. ....	48
Table 3.3: Inactivation rate constants for each virus and each disinfectant .....	50
Table 3.4: Predicted and experimental genome degradation rate constants for each virus and each disinfectant .....	52
Table 3.5: Experimental and predicted degradation rate constants ( $k_{amp}$ ) for each amplicon.....	55
Table 4.1: Peptide sequences for each virus and each protease .....	68
Table 4.2: A protein peptide sequence for GA digested by trypsin.....	70
Table 4.3: Summary of reaction rate constants, molar absorptivities ( $\epsilon$ ) and quantum yields ( $\phi$ ) for the reactions of free amino acids with the disinfectants considered herein .....	73
Table 4.4: Experimental and predicted single protein degradation rate constants.....	78
Table 5.1: Description of SAMs.....	98
Table 5.2: Peptide sequences for Qbeta after trypsin digestion .....	102
Table C.1: Description of primers for PCR.....	131
Table C.2: q-PCR thermocycling conditions.....	132
Table D.1: Location and mass of each peptide with its corresponding [ $^{14}\text{N}$ ] and [ $^{15}\text{N}$ ] peak mass .....	133
Table D.2: The change in Gibbs energy for the oxidation of methionine in a capsid protein environment relative to an aqueous environment .....	138
Table D.3: The APBS calculated electrostatic component of the MS2 and fr intra-capsid binding energies and its ionic strength dependency. ....	139



## Chapter 1

# Introduction

### 1.1 From microorganisms to pathogens

Microorganisms are the family of all living organisms invisible to the human eye. They can range from simple unicellulars as bacteria and archaea to more complex organisms such as protozoa, fungi or algae. The term microorganisms may furthermore encompass viruses, though they are not technically a living organism, as they lack the ability to replicate independently.

The mentioning of microorganisms often invokes the idea of disease. However, microorganisms play beneficial roles in many fields as:

- *Food production:* fermentation is a process that involves yeast or bacteria and that is responsible for the production of bread, yoghurt or cheese and are also present in winemaking and beer brewing
- *Digestion:* more than 500 species of bacteria are present in the digestive system of humans and they contribute, for example, to gut immunity and synthesis of some vitamins
- *Water treatment:* Different microorganisms are responsible of recovering nutrients as nitrogen or phosphorous from waste water
- *Ecology:* microorganisms are responsible for the decomposition process of dead plants or animals
- *Energy:* various researchers are now studying the possibility to use microorganisms to convert agricultural or urban waste into reusable energy

A variety of microorganisms have also developed methods to adjust to extreme conditions (temperature, pH, pressure, etc...),<sup>1-3</sup> which allow them to survive in environments such as geysers, deserts or the poles.

Some microorganisms, known as pathogens, cause diseases when invading humans, animals or plants. These microorganisms infect and replicate in higher organisms, and thereby induce an immune response. Prominent examples of diseases caused by pathogenic bacteria in humans include cholera, typhoid fever, diphtheria, tetanus or tuberculosis, while protozoa can cause malaria, toxoplasmosis and dysentery. Finally, pathogenic viruses are responsible for a wide range of diseases including influenza, hepatitis, measles, poliomyelitis, AIDS and herpes, to cite just a few.

Some of these infectious diseases can be treated with antibiotics or antivirals. For others, though, no such cure exists, or it is not accessible to those who need it. A more effective way to deal with infectious diseases is therefore to implement strategies to control their transmission, and thereby reduce or prevent their occurrence. The control of virus transmission is the framework for this work. Specifically, this thesis deals with the disinfection of viruses that can be transmitted by water, also known as waterborne viruses.

This introduction will give an overview over the discovery of viruses and their transmission routes, with an emphasis on the field of environmental virology. Then different homogeneous disinfection methods will be discussed, including introduction to disinfection kinetics and mechanisms of inactivation. Finally, heterogeneous disinfection processes are introduced, along with the physico-chemical characteristics of viruses that influence them.

## 1.2 Viruses

### 1.2.1 Origin and occurrence of viruses

Viruses were first discovered at the end of the 19<sup>th</sup> century by Dmitry Iwanovsky, who discovered that a non-self-replicating pathogenic agent passed through filters small enough to retain bacteria.<sup>4</sup> Since then, three hypotheses have been suggested concerning the origin of viruses:<sup>5</sup>

- *Virus-first hypothesis*: viruses are relics of pre-cellular life-forms and they have co-evolved at the same time as the appearance of the first cells on earth
- *Reduction hypothesis*: viruses may have derived from unicellular organisms, losing the genes allowing them to replicate on their own



- *Escape theory*: they evolved from genetic material (RNA or DNA) that may have escaped from larger organisms

These hypotheses are still actively debated, and there is no unified explanation yet regarding the origin of viruses.

Viruses can infect all living organisms, both prokaryotic and eukaryotic. Furthermore, they are the most abundant entity on earth with about  $10^{31}$  particles,<sup>6</sup> making them  $10^{21}$  times more abundant than humans. The great majority of viruses resides in the seas, where about  $10^8$  viruses are found per milliliter of seawater.<sup>7</sup> Marine viruses have been found to kill about 20% of the ocean's living biomass every day.<sup>8</sup> As such, viruses play a major role in the regulation of this ecosystem. Viruses also affect growth, fitness and appearance of terrestrial organisms. For example, infection by the Tulip Breaking virus (TBV) causes the color-breaking of tulip flowers (Fig. 1.1).



**Figure 1.1: Effect of TBV on tulips.** Left: Healthy tulips; Right: TBV infected tulips.

For mankind, viruses are estimated to be the source of about 60% of all illnesses<sup>9</sup> ranging from a simple cough to serious diseases such as AIDS or Ebola. They have also been responsible for enormous human disasters such as the smallpox pandemic, which killed 300-500 million people during the 20<sup>th</sup> century,<sup>10</sup> or the influenza pandemic at the beginning of the 20<sup>th</sup> century responsible for more than 50 million deaths.<sup>11</sup>

### 1.2.2 Virus characteristics

Viruses are the smallest microorganisms known, ranging in size between 20 and 300 nm. Even though they are very small, they can still exhibit a great variety of shapes as shown in Fig. 1.2. For example, Tobacco Mosaic virus has a rod-like appearance, whereas Influenza virus is spherical with spikes and Rabies virus looks like a bullet with spikes. The appearance of bacteriophage T4 is often likened to a spaceship.

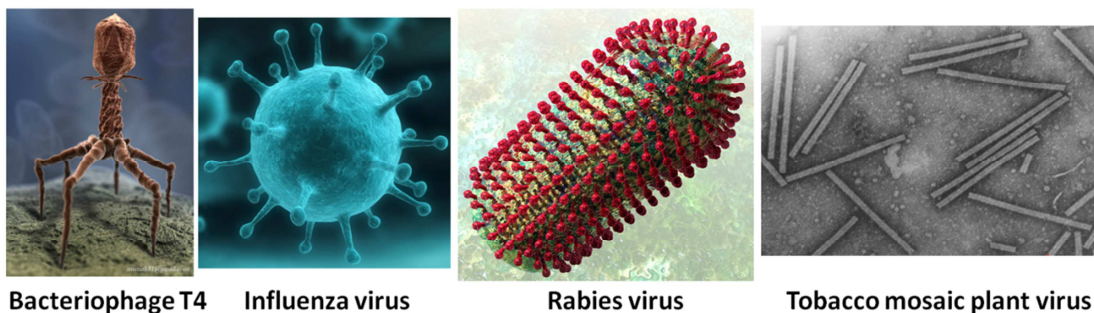


Figure 1.2: Variety of shapes in the virus family.

Despite of this variety in shapes, all viruses can simply be represented by a genome consisting of either RNA or DNA, surrounded by a protein capsid and sometimes enveloped by a lipidic membrane (e.g. Influenza or Rabies virus) as shown in Fig. 1.3.

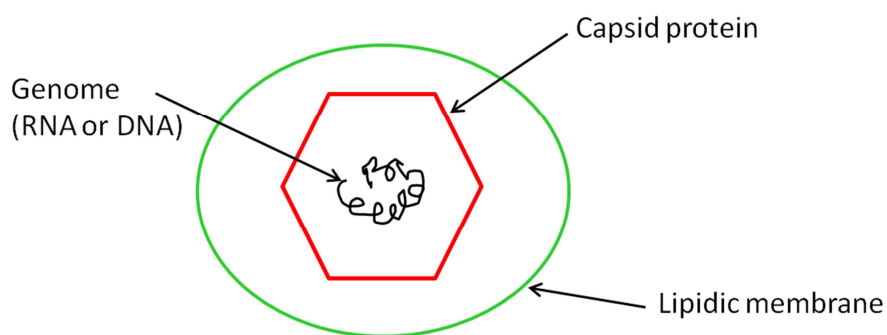


Figure 1.3: Schematic representation of a virus. The lipidic membrane is not present in all viruses.

Viruses are different from any other organism because they are obligate parasites: they are not capable of replicating independently, but depend on specific hosts for reproduction. To replicate, they first need to transfer their genomic material into the host cell, where they use the cellular machinery to replicate their genome and produce proteins. Finally, they emerge from the host cell in their final configuration by

lysis or budding out, in some cases taking a part of the cellular membrane with them. Then they are transported in the organism or in the environment until they encounter a new host and can start a new infection cycle.<sup>12</sup> Outside of their host, viruses do not require any sustenance (e.g. air or food), making them very persistent and capable of surviving for long periods of time before infecting a new host. The replication of viruses is very effective; one human virus can produce up to 1'000 progeny in a single infection.<sup>4</sup> This leads to large viral loads in infected individuals. For example, in the case of Norwalk viruses more than  $10^9$  viruses per gram feces can be shed during about 28 days after infection.<sup>13</sup> To allow viruses to replicate, specific conditions are required. In addition to be in contact with its specific host cell, they also need to be at an optimal temperature, which for most human pathogenic viruses is 37°C. However some viruses have adapted and are most infectious at 33°C as some Rhinoviruses infecting cells in the nose where the temperature is lower than in the rest of the body.<sup>14</sup> If the temperature is too low, the viruses may still bind to their host cell but won't be able to inject their genome into the cell.<sup>15</sup> On the other hand if the temperature increases the proteins may start to denature, which will inactivate the viruses.

### 1.2.3 Transmission of viruses

Human viruses are often spread between individuals, either by vertical transmission (from mother to child), via horizontal transmission (from person to person) by exchange of body fluids (e.g. HIV, Hepatitis C), or via inhalation of contaminated aerosols or droplets excreted from an infected individual (e.g. Influenza virus, Rhinovirus). Furthermore, some viruses are transmitted by a vector (often insects, e.g. Dengue virus, Yellow Fever). To avoid these types of transmission, the strategy is to build up barriers that the viruses are not able to penetrate (membranes, masks, repellants, etc). Finally, viruses can be transmitted by the so-called fecal-oral route, i.e., the consumption of food or water contaminated by excreta from infected individuals (e.g., Norovirus, Hepatitis A virus; see Fig. 1.4).

The fecal-oral transmission route gained prominence in late 1955, when a large hepatitis outbreak in India led scientists to a new discipline: water virology, also called environmental virology.<sup>16</sup> The origin of the epidemic was the contamination by sewage of the Jumna River, the source of water for the drinking water plant. Since then many viruses have been recognized as waterborne, indicating that they can remain infective during transport in the water to a new host. Waterborne viruses give rise to worldwide illnesses such as poliomyelitis. In 2004, it was estimated that 1.8 million people die of diarrheal diseases

## Introduction

arising from waterborne illnesses often caused by viruses, and that 90% of those deaths affect children under 5 years old.<sup>17</sup>

Fig. 1.4 shows the transmission of waterborne viruses via the fecal-oral route. The figure indicates where it is possible to introduce barriers to impede the progression of the viruses. The efforts that need to be achieved to render water consumption safer are: improved sanitation (installation of toilets and behavioral changes with respect to sanitation), improved hygiene (hands washing), and water treatment (disinfection processes). Improved sanitation could reduce diarrhea morbidity by 32%, hygiene interventions (such as hygiene education and promotion of hand washing) could lead to a reduction of diarrheal cases by up to 45%, and finally improvement in drinking water quality through household water treatment (such as chlorination) could reduce it by 35%.<sup>17</sup>

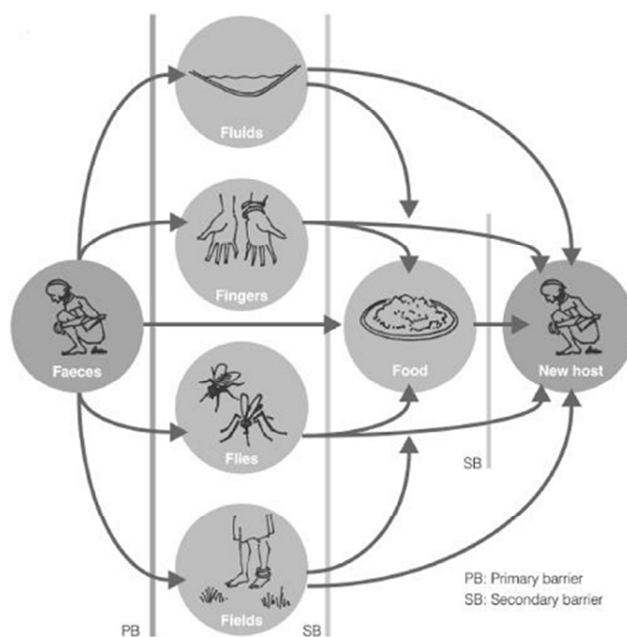


**Figure 1.4: Fecal-oral transmission route.** Increased sanitation is mainly responsible for the primary barrier whereas increased hygiene and water treatment represent the secondary barrier. Figure reproduced from WHO report (Domestic water quantity, service level and health, by Howard and Bartram, 2003).<sup>18</sup>

In Table 1.1, several waterborne viruses are described along with the diseases they cause. It also shows the great genetic variety that is present among viruses.

**Table 1.1: Common waterborne viruses and MS2 bacteriophage, and their associated diseases.**<sup>19</sup> kbp = kilo base pairs; kb = kilo bases.

<b>Virus</b>	<b>Size</b>	<b>Genome size</b>	<b>Human disease</b>
Adenovirus	95 nm	dsDNA, 26-45 kbp	Respiratory infection, conjunctivitis, gastroenteritis
Poliovirus	30 nm	ssRNA, 6.8-8.5 kb	Poliomyelitis
Rotavirus	70 nm	dsRNA, 18.5 kbp	Gastroenteritis
Norwalk virus	32 nm	ssRNA, 6.8-8.5 kb	Gastroenteritis
Echovirus	28 nm	ssRNA, 6.8-8.5 kb	Fever, rash, aseptic meningitis
Coxsackievirus	28 nm	ssRNA, 6.8-8.5 kb	Aseptic meningitis
Hepatitis A virus	28 nm	ssRNA, 6.8-8.5 kb	Hepatitis
MS2 bacteriophage	25 nm	ssRNA, 3.5 kb	None, surrogate for human viruses

#### 1.2.4 Detection and composition of viruses

For water treatment, it is of great interest to know if viruses are effectively inactivated during different disinfection treatments. For this purpose, it is crucial to distinguish between infective and non-infective viruses. This can, for the moment, only be achieved by culturing. However, many of the hundreds of viruses transported by sewage are not detectable by a cell culture protocol, or the protocols are tedious and time-consuming. This is in particular the case of many of the human pathogenic viruses, which may have long incubation periods before obtaining any results concerning their infectivity or which do not replicate in vitro (nonculturable viruses). Therefore, Polymerase Chain Reaction (PCR) is often used for viral diagnosis,<sup>20</sup> though this method cannot distinguish between infective and inactivated viruses. To nevertheless obtain an indication of viral infectivity, indicator organisms are frequently used. A good indicator organism should fulfill the following criteria:<sup>21,22</sup>

- It should be consistently and exclusively associated with the source of the pathogens

## Introduction

- It should be present in sufficient numbers to assure an accurate estimation of the contamination
- It should be similarly susceptible to disinfection as the pathogens of interest
- It should be easy and cheap to quantify them precisely from any water of interest
- It should behave in the environment in the same manner as pathogens with respect to:  
Transport, inactivation, interaction with solids and plants, etc...

The most commonly used indicators are bacterial indicators, namely *Escherichia coli* and *Enterococci*. However it has been shown that viruses such as Hepatitis A or Rotavirus are more resistant to disinfection than these bacterial indicator organisms, making the water unsafe for consumption even though it may comply with water quality standards.<sup>23</sup> It is therefore of interest to find more closely related, viral indicator organisms that have a similar susceptibility to disinfectants as waterborne viruses. A good viral indicator should have the same type of genome (RNA or DNA, single or double-stranded), a similar size and a similar shape as the virus of interest. For this purpose the use of bacteriophages is increasingly common, as they have been shown to better correlate with the presence and inactivation of enteric viruses.<sup>24</sup>

Bacteriophages are viruses that infect bacteria. They offer the great advantage that simple and rapid culturing assays exist. The virus is mixed with its host bacteria, spread on a petri dish containing growth media, and incubated. Within some hours, the bacteria overgrow the petri dish. The less mobile viruses infected and replicated at specific spots on the bacterial lawn, forming plaques as is shown in Fig. 1.5. It is assumed that each plaque originates from one virus, making it possible to determine the titer of the starting solution.



**Figure 1.5: Agar plate with plaques.** Each plaque represents one virus.

In Fig. 1.6, two representations of bacteriophage MS2 and Picornavirus (a member of the Enterovirus genus) are depicted, showing the simplicity of their composition and the high level of similarity between them. They are both icosahedral viruses of 26-30 nm in diameter, and contain a positive sense single-stranded RNA. Their capsids differ by the fact that MS2's capsid is composed of multiple copies of one single protein, whereas Picornavirus consists of multiple copies of four different proteins. Their conformational and structural similarities with many enteric viruses (Fig. 1.6 and Table 1.1) as well as the easier working methods, make bacteriophages good models to understand processes occurring during disinfection. Furthermore, they are not threatening to human health, making them safer to work with.<sup>25,26</sup>

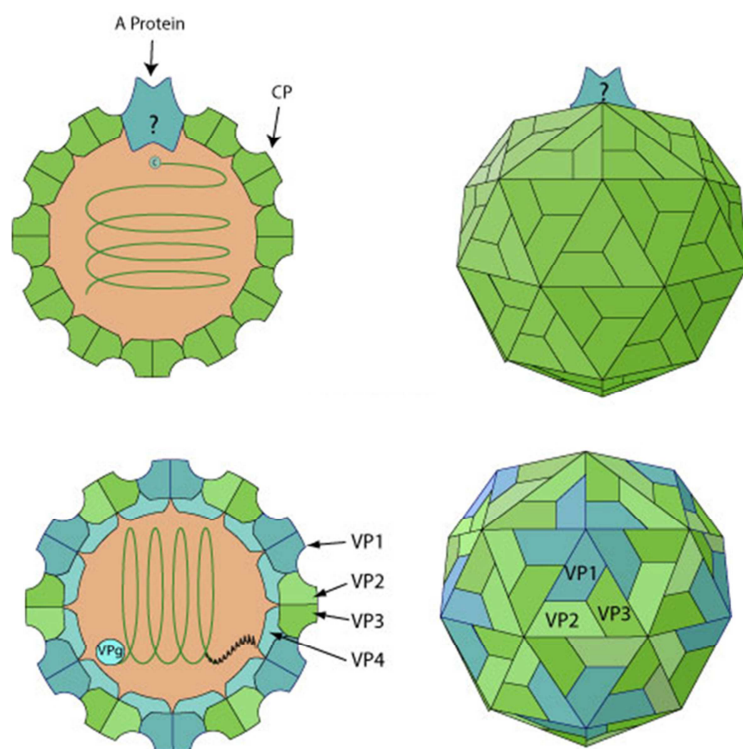


**Figure 1.6: Cross-section and outside view of MS2 and Picornavirus.** Up: Bacteriophage MS2, 26 nm, genome: positive sense single-stranded RNA of 3.5 kb, capsid protein: 180 copies of one protein. Down: Picornavirus, 30 nm, genome: positive sense single-stranded RNA of 7.2-8.5 kb, capsid protein: 60 protomers consisting of four polypeptides.<sup>27</sup>

The main bacteriophage used in this thesis is MS2 coliphage. It is an icosahedral virus with a linear single stranded RNA genome containing 3569 nucleotides, surrounded by a capsid composed of 180 copies of a protein containing 129 amino acids. The capsid protein is involved in the binding of the virus to the bacteria and in the injection of the genome into the host, but it also plays the important role of barrier

## Introduction

protecting the genome from oxidizing agents or nucleases permanently present in the environment. In the core of the virus, there is a single copy of a second protein, called A protein or maturation protein, which contains 393 amino acids. This protein is assumed to be involved in the attachment of the virus to the bacteria, in the injection process of the genome inside the cell as well as in the assembly process of the virus after replication.<sup>28</sup> Additional bacteriophages investigated in the framework of this thesis are fr, GA and Qbeta. Like MS2, they all belong to the *Leviviridae* family and infect male *Escherichia coli*. Fig. 1.7 shows the composition of the capsid proteins of each one of these bacteriophages and a table of all amino acids as well as their structure and physical properties can be found in appendix (Fig. A.1). These four bacteriophages are all very similar. The homology of the capsid protein of MS2 with the other phages is 87% for fr, 61% for GA, and 22% for Qbeta.<sup>29</sup>

MS2	A	S	N	F	T	Q	F	V	L	V	D	N	G	G	T	G	D	V	T	V	A	.	.	.	.	P	S	N	F	A <sup>26</sup>	
fr	A	S	N	F	E	E	F	V	L	V	D	N	G	G	T	G	D	V	K	V	A	.	.	.	.	P	S	N	F	A <sup>26</sup>	
GA	.	A	T	L	R	S	F	V	L	V	D	N	G	G	T	G	N	V	T	V	V	.	.	.	.	P	V	S	N	A <sup>25</sup>	
Qbeta	.	A	K	L	E	T	V	T	L	G	N	I	G	K	D	G	K	Q	T	L	V	L	N	P	R	G	V	N	P	T <sup>29</sup>	
MS2	N	G	V	A	E	W	I	S	S	N	S	R	S	Q	A	Y	.	.	K	V	T	C	S	V	R	Q	S	S	A	Q <sup>54</sup>	
fr	N	G	V	A	E	W	I	S	S	N	S	R	S	Q	A	Y	.	.	K	V	T	C	S	V	R	Q	S	S	A	N <sup>54</sup>	
GA	N	G	V	A	E	W	L	S	N	N	S	R	S	Q	A	Y	.	.	R	V	T	A	S	Y	R	A	S	G	A	D <sup>53</sup>	
Qbeta	N	G	V	A	.	S	L	S	Q	A	G	A	V	P	A	L	E	K	R	V	T	V	S	V	S	Q	P	S	R	N <sup>50</sup>	
MS2	N	R	K	Y	T	I	K	V	E	V	P	K	V	A	T	Q	T	V	G	G	V	E	L	P	V	A	A	W	R	S <sup>34</sup>	
fr	N	R	K	Y	T	V	K	V	E	V	P	K	V	A	T	Q	V	Q	G	G	V	E	L	P	V	A	A	W	R	S <sup>34</sup>	
GA	K	R	K	Y	T	I	K	L	E	V	P	K	I	V	T	Q	V	V	N	G	V	E	L	P	V	S	A	W	K	A <sup>33</sup>	
Qbeta	R	K	N	Y	K	V	Q	V	K	I	Q	N	P	T	A	C	T	A	N	G	S	C	D	P	S	V	T	R	Q	A <sup>38</sup>	
MS2	Y	L	N	M	E	L	T	I	P	I	F	A	T	N	S	D	C	E	L	I	V	K	A	M	Q	G	L	L <sup>112</sup>			
fr	Y	M	N	M	E	L	T	I	P	V	F	A	T	N	D	D	C	A	L	I	V	K	A	L	Q	G	T	F <sup>112</sup>			
GA	Y	A	S	I	D	L	T	I	P	I	F	A	A	T	D	D	V	T	V	I	S	K	S	L	A	G	L	F <sup>111</sup>			
Qbeta	Y	A	D	V	T	F	S	F	T	Q	Y	S	T	D	E	E	R	A	F	V	R	T	E	L	A	A	L	L <sup>116</sup>			
MS2	K	D	G	.	N	P	I	P	S	A	I	A	A	N	S	G	I	Y <sup>129</sup>													
fr	K	T	G	.	N	P	I	A	T	A	I	A	A	N	S	G	I	Y <sup>129</sup>													
GA	K	V	G	.	N	P	I	A	E	A	I	S	S	Q	S	G	F	Y	A <sup>129</sup>												
Qbeta	.	.	A	S	P	L	L	I	D	A	I	D	Q	L	N	P	A	Y <sup>132</sup>													

**Figure 1.7: Amino acid sequence of MS2, fr, GA and Qbeta.** The colors represent the amino acid similarity of fr, GA and Qbeta to MS2: blue indicates a common amino acid of one virus with MS2; yellow is for two viruses and MS2, and green is for all four viruses having the same amino acid at one site.

Some notable facts regarding the composition of these phages are firstly that GA does not contain any methionine or cysteine. This is important because these amino acids are the only ones containing sulfur,



which renders them sensitive towards oxidation.<sup>30</sup> Secondly, the capsid of Qbeta contains disulfide bonds bridging the individual capsid proteins.<sup>31</sup> These were observed to hold together the capsid protein and stabilize its conformation. These structural details are of importance when studying the mechanisms of inactivation.

### **1.3 Virus inactivation by homogeneous disinfectants**

An important part of viruses can be transmitted through the fecal-oral route. It is therefore important to stop the progression of the viruses at an early stage, by good sanitary utilities and proper hygiene habits. Infection can nevertheless occur through exposure to, or consumption of, water contaminated by wastewater-derived viruses. Therefore, raw or insufficiently treated wastewater is often the source of virus contamination in water sources used for drinking water production or for recreational purposes.

Because viruses are often present in raw drinking water<sup>32</sup> many utilities apply a disinfection step before distributing the water to households. Increasingly, wastewater disinfection is also practiced. The easiest method to reduce the load of pathogenic organisms in water is to set up a physical barrier, which can be achieved in the form of filters or membranes. Successful reduction of bacteria has been observed with these methods, but viruses are often too small to be retained. Although membrane filters do exist that have small enough pores to retain viruses, their implementation is technologically challenging and generates very high costs and energy demands. In Table 1.2 the removal efficiency by sedimentation and filtration methods is shown. It can be seen that rapid filtration can reduce the enteric virus population by 99% (2 log<sub>10</sub>). However the minimum treatment objective for drinking water is a 99.99% (or 4 log<sub>10</sub>) reduction or inactivation (according to US EPA surface water treatment rule), indicating that supplementary treatment is needed. Slow sand filtration could potentially be used for this purpose but this treatment requires extensive land areas and long treatment periods. For these reasons, it is of interest to apply other methods of pathogen control, in particular disinfection.

**Table 1.2: Coagulation, sedimentation, filtration.** Typical removal efficiencies and effluent quality.

Organisms	Coagulation and sedimentation (% removal)	Rapid filtration (% removal)	Slow sand filtration (% removal)
Total coliforms	74-97	50-98	>99.999
Fecal coliforms	76-83	50-98	>99.999
Enteric viruses	88-95	10-99	>99.999
<i>Giardia</i>	58-99	97-99.9	>99
<i>Cryptosporidium</i>	90	98-99	99

From US EPA (1988)

Homogeneous chemical disinfection (e.g chlorine, chlorine dioxide, ozone), UV irradiation and reactive oxygen species (ROS) created by advanced oxidation processes are common disinfection methods used in domestic water treatment. A good disinfectant should be highly toxic to a wide range of microorganisms at low (but detectable) concentrations, and safe to handle and apply.

The first major step toward water disinfection was the introduction of chlorination. It started to be applied routinely in treatment plants at the beginning of the 20<sup>th</sup> century in the United States, and along with filtration it has contributed to an increased life expectancy by 50% over the century.<sup>33</sup> Ever since, chlorine has been extensively used, and is still one of the most efficient disinfectants available. An advantage of chlorine over many other disinfectants is that a low concentration can be added to the treated water before discharge into the distribution system, such that a chlorine residual is left in the water pipes to ensure its safety up to the consumer's tap. However, chlorine is not always easy to handle. Its reactivity is greatly dependant on pH and on the chlorine demand of the water. It also has a very pronounced, unpleasant taste, and an infamously low efficiency in inactivating *Cryptosporidium* oocysts. Finally, since the 1970's it has been increasingly shown that chlorine also reacts with organic and inorganic matter in the water to form toxic byproducts.<sup>34</sup> Some of the major disinfection byproducts (DBPs) formed are trihalomethanes or haloacetic acids, which have been recognized to have potential carcinogenic effects.<sup>35,36</sup> To date, more than 600 DBPs have been identified worldwide,<sup>37</sup> of which less than 20 are regulated in the USA.<sup>38</sup> A recent study showed that more than 90 DBPs can be detected in drinking water in Europe and that their presence was significantly correlated with chronic mammalian cell cytotoxicity.<sup>39</sup> For these reasons, it has been of great interest to study alternatives to chlorine in

order to disinfect water. Important replacements for chlorine that are already used in many treatment plants are UV and ozone.<sup>40</sup> Recent studies have also focused on the possibility of using chlorine dioxide or ferrate.<sup>41,42</sup>

In natural waters, the impact of sunlight on microorganisms is also an important feature to take into account. Solar treatment of water is a naturally occurring process, and has been engineered for use in wastewater treatment, for example in waste stabilization ponds. Three distinct mechanisms can lead to photoinactivation of pathogens; direct, indirect endogenous and indirect exogenous inactivation.<sup>43</sup> In the first case, irradiation (mainly by sunlight in the UVB range) directly causes damage to the components that are able to absorb light, such as nucleotides and aromatic amino acids. In indirect inactivation, light absorbing components or sensitizers transfer energy or an electron to dissolved oxygen, thereby forming reactive oxygen species (ROS). In endogenous indirect inactivation the sensitizer is part of the organism that gets oxidized by the ROS. For exogenous indirect inactivation, the sensitizer producing ROS is located outside the organism. This is often important in waters where natural organic matter (NOM) is present, which can act as a sensitizer for ROS production. ROS include singlet oxygen ( $^1\text{O}_2$ ), superoxide ( $\text{O}_2^-$ ), hydroxyl radical ( $\text{OH}\cdot$ ), peroxy radical ( $\text{RO}_2\cdot$ ) and hydrogen peroxide ( $\text{H}_2\text{O}_2$ ). ROS are very short-lived species as they are very reactive, but if in their lifespan they encounter a virus, they will react with it, causing oxidation of its components.<sup>44</sup>

### 1.3.1 Disinfection kinetics

In order to compare the inactivation efficiency of a disinfectant on various microorganisms, or the efficiency of different disinfectants on a single organism, models have been developed that describe the inactivation as a function of exposure time and concentration of disinfectant. The best-known disinfection model is the Chick-Watson model (Eq. 1.1):<sup>45,46</sup>

$$\ln(C_v/C_{v,0}) = -k_{\text{CW}} C^n t \quad \text{Eq. 1.1}$$

where  $t$  is the time of exposure,  $C_v$  is the infective virus concentration at time  $t$ ,  $k_{\text{CW}}$  is the Chick-Watson inactivation rate constant,  $C$  is the disinfectant concentration (or irradiance for UV treatments) and  $n$  is an empirical constant, also called dilution factor. Frequently  $n$  is equal to 1, in which case the Chick-Watson model becomes first-order with respect to disinfectant dose (expressed as  $Ct$ ). With this model, it is possible to describe the inactivation of many microorganisms with a wide variety of disinfectants,

and to determine the required dose of disinfectant to obtain a given level of inactivation. Even though this model is the reference when kinetics of inactivation are studied, it has been shown that deviations from this ideal model frequently occur.<sup>47</sup> Fig. 1.8 shows the different inactivation behaviors that can be encountered:

- **Linear:** Inactivation of the microorganism is first-order with respect to the disinfectant dose applied and follows the ideal model described by Chick-Watson (Eq. 1.1). The slope of the line represents the inactivation rate constant  $k_{CW}$ .
- **Tailing:** The first part of the inactivation curve follows the Chick-Watson model, but inactivation eventually slows down. Many factors have been suggested to explain this behavior, such as heterogeneity in the virus population, consumption of the disinfectant, or changes in the solution over time of reaction.
- **Shoulder:** Contrary to the tailing scenario, this case shows a slow inactivation in the beginning of the disinfection process, followed by faster inactivation after some time or disinfectant dose. This behavior can be explained by the fact that the microorganisms require multiple hits before starting to inactivate. It can be compared to the activation energy necessary for a chemical reaction to start.

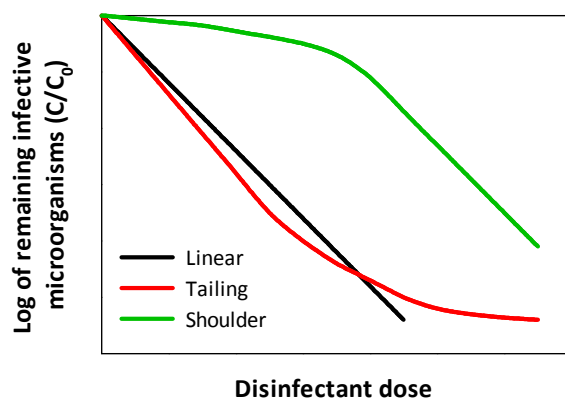


Figure 1.8: Possible shapes of inactivation curves of microorganisms. C is the concentration of infective microorganisms.

It is important to know which kinetic scheme a combination of microorganism and disinfectant follows, in order to properly decide on a disinfection treatment to adopt. In the last decades many studies have focused on determining the rates of inactivation of various microorganisms with different types of disinfectants. Great differences were found between the disinfection efficiency of bacteria and viruses, and between the efficiencies of different disinfectants. For example, it was shown that the inactivation of *Bacillus subtilis* by chlorine was far slower than that of MS2.<sup>48</sup> In contrast, a study by Koivunen et al.

showed that inactivation of *Enterococcus faecalis* by hypochlorite was more efficient than the inactivation of MS2 under the same conditions.<sup>49</sup> They also found that a more efficient disinfection of these organisms could be achieved when using PAA coupled with UV, compared to disinfection by HOCl. Furthermore, it has been observed that even among viruses, major differences in disinfection efficiency can occur for a specific treatment. For example, Adenovirus 2 was more resistant to UV irradiation than Echovirus 1 and 11, Coxsackievirus B5 and Poliovirus 1.<sup>50</sup> Shin et al. observed that for the same UV dose, enteric RNA viruses such as Poliovirus or Coxsackievirus were more readily inactivated than RNA bacteriophages.<sup>51</sup> This indicated that inactivation by UV irradiation was not simply predictable by the type and size of the virus or by its genome's characteristics. Finally, differences in inactivation rate constants have been observed within viruses of the same family. For example Coxsackievirus A9 was inactivated faster by chlorine than Coxsackievirus B5.<sup>52</sup> Similar behavior was also observed for different species of Echovirus as well as Poliovirus.<sup>52</sup>

All these studies show that there is not a single rule to describe the inactivation of a microorganism by a specific treatment. The specifics of any combination of disinfection treatment and microorganisms are important to take into account when dimensioning a treatment process.

### 1.3.2 Disinfection mechanisms

To obtain a better understanding of the differences in disinfection kinetics discussed above, it is essential to consider the mechanisms of inactivation. The majority of studies on virus inactivation have focused on inactivation rates differences of bacteriophages and human viruses, but only few report the mechanisms involved.<sup>48,50,52-54</sup> Most mechanistic work to date has focused on damage to the genome,<sup>55</sup> but protein damage may also contribute to inactivation.<sup>56,57</sup> Chlorine is known to cause multiple alterations to proteins, such as oxidation, chlorination, carbonylation and backbone cleavage.<sup>58,59</sup> UV treatment is well-known for its genome-damaging properties, but proteins also contain light absorbing amino acids and can therefore also be affected.<sup>60-62</sup> Specifically, three aromatic amino acids (tyrosine, tryptophan and phenylalanine) are susceptible to damage by UV light.<sup>63</sup> Finally, a recent study in our laboratory investigated the disinfection of MS2 by several disinfectants and demonstrated that each disinfectant acted by a distinctly different pattern, ranging from damaging only the viral proteins (ClO<sub>2</sub>, pasteurization) to predominantly the viral genome (UV), to a combination of both (singlet oxygen, chlorine) as is shown in Fig. 1.9.<sup>56</sup> This illustrates that a wide variety of inactivation mechanisms exist, and that generalizations across disinfectants are not possible.

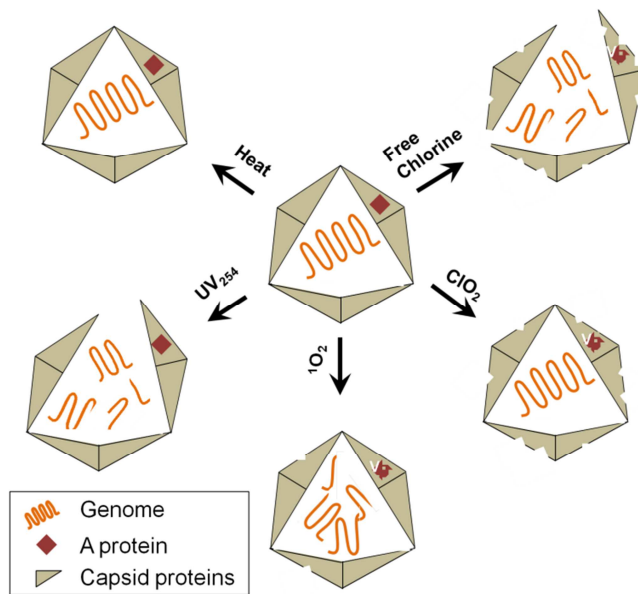


**Figure 1.9: Disinfection mechanisms of MS2.** Effect on genome, A protein and capsid protein by heat, free chlorine,  $\text{ClO}_2$ ,  $^1\text{O}_2$  and  $\text{UV}_{254}$ . Figure reproduced from Wigginton et al. 2012.<sup>56</sup>

In order to cause inactivation, the damage to genomes and proteins must lead to a loss in the essential virus functions. Hereby, several functions involved in virus replication can be disrupted. Firstly the virus could be prevented from binding to its host cell, which would result in the incapacity of transferring its genome into the host. Secondly, viruses could maintain their ability to bind to the host cell, but not to transfer their genome into the host. This, too, may be a result of damage to the viral proteins. Finally, the viruses may be able to bind and transfer their genome, but the genome may fail to replicate. This can be caused by extensive, irreparable damage to the genome, which renders it impossible to be transcribed by the viral polymerase. These processes have been studied by Page et al. for the case of Adenovirus treated by chlorine.<sup>64</sup> They observed that after inactivation, the virus was still able to bind to its host cell, and that its genome could be amplified by PCR, suggesting that genome damage could not account for inactivation. By immunoblotting, they found that Adenovirus was unable to express the viral proteins necessary for endocytosis, endosomal lysis or nuclear delivery during infection. This study thus showed that free chlorine inactivated Adenovirus by affecting the post-host attachment processes associated with transferring the genome to the host cell.

An additional interest in understanding virus inactivation mechanisms is that it may ultimately allow us to develop an alternative to culturing to investigate virus disinfection. As mentioned above (see 1.2), many human enteric viruses do not have an *in vitro* culturing assay. This renders it impossible to study their disinfection kinetics. If the mechanisms of inactivation are well understood, however, we may

ultimately be able to extrapolate this knowledge to non-culturable viruses, by quantifying the damage to their genomes and proteins, and hence determining their state of infectivity.

## **1.4 Virus inactivation by heterogeneous disinfectants**

### **1.4.1 Importance of viral adsorption**

A problem with many water disinfection studies is that they do not take into account the portion of viruses that are sorbed onto solids. It has been shown that association of viruses with solids can protect them from inactivation by chlorine and natural inactivating factors.<sup>65-67</sup> In water and wastewater, viruses are likely encountered in a sorbed state. For example, Gerba et al.<sup>68</sup> showed that in secondarily treated sewage discharges, the proportion of solid-adsorbed viruses can be up to 100%. In a laboratory setup, bacteriophages have been shown to adsorb efficiently to clay minerals.<sup>69,70</sup> Generally it can be stated that viruses easily adsorb to surfaces such as soil and sediment particles, but also to air and water filters, walls and door handles in hospitals, schools and other public spaces. Upon changes in solution conditions, viruses can then be eluted from solids and surfaces and re-enter the solution in an infectious state. Adhesion should thus be taken into account at all time, as it is a reversible process<sup>71</sup> that may lead to underestimation of viral loads.<sup>72</sup>

Besides serving as a protective substrate, some surfaces and particles may also have antiviral potentials. For example, metallic copper has been used for decades to store water, as it has been shown to inactivate pathogens.<sup>73</sup> Furthermore copper is starting to be introduced in many different materials that would benefit of disinfecting properties, such as latex gloves or socks.<sup>74,75</sup> Finally, it was shown that the presence of copper in pipes instead of only polyethylene, considerably reduced the growth of biomass during 200 days.<sup>76</sup>

### 1.4.2 Mechanisms of viral adsorption

Viral particles are bio-colloids, therefore their adsorption behavior is frequently described by theories applied to inorganic colloids. Interactions between colloids have been best described by the Derjaguin-Landau-Verwey-Overbeek theory (DLVO theory), which is represented in Fig. 1.10.

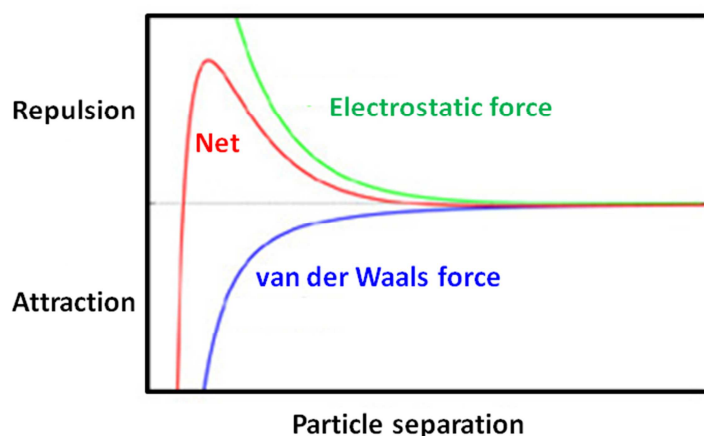


**Figure 1.10: DLVO theory representation.** The interplay of attractive van der Waals forces and repulsive electrostatic forces is shown as a function of the separation distance of two like-charged particles.

It takes into account the electrostatic interactions as well as the positive van der Waals interaction as a function of distance between particles. Van der Waals interactions are relatively weak and arise from the instantaneous dipole moments within the particles.<sup>77</sup> At small virus-surface distances, short-range forces become increasingly important. Experimental data has shown that DLVO theory alone cannot appropriately describe virus – particle interactions. Therefore so-called extended-DLVO (XDLVO) models were constructed, which involve steric interactions,<sup>78</sup> ionic strength<sup>79</sup> as well as hydrophobic interactions.<sup>80</sup> Even though this representation is a better approximation, recent studies have shown that in fact viruses may not be treated as hard colloidal spheres but rather as permeable soft particles composed of concentric soft layers,<sup>81</sup> and that it is important to take into account the roughness of the surface.<sup>82</sup>

The electrostatic interactions between viruses and surfaces may either be repulsive or attractive. Depending on the solution pH, the point of zero charge (PZC, pH at which the net charge on the surface is neutral) of a surface and the isoelectric point (IEP, pH at which the net charge on the surface of a protein is neutral) of a virus may exhibit opposite charges, which will lead to attraction. High ionic strength can help shield charges, and multivalent cations may act as a salt bridge to bring two particles



into contact.<sup>83</sup> It has also been shown that small ions can promote hydrophobic interactions by increasing the structure of water, rendering it less able to accommodate hydrophobic groups.<sup>84</sup> In Table 1.2 the IEP or PZC of different viruses and surfaces of interest are described.

**Table 1.3: IEP and PZC examples.** IEP of MS2 and some enteric viruses as well as PZC of solids of interest.

Microorganism	IEP	Solid	PZC
MS2	3.9 <sup>85</sup>	CuO	9.5 <sup>86</sup>
Qbeta	5.3 <sup>85</sup>	Al <sub>2</sub> O <sub>3</sub>	8-9 <sup>87</sup>
Hepatitis A	2.8 <sup>85</sup>	Magnetite (Fe <sub>3</sub> O <sub>4</sub> )	6-6.8 <sup>88</sup>
Echovirus 1	5-6 <sup>85</sup>	TiO <sub>2</sub>	6.1 <sup>89</sup>
Norwalk virus	5.5 <sup>85</sup>	NOM	< 4 <sup>90</sup>

Several particles and surfaces have been found to have virucidal effects. For example, CuO and metallic aluminum provoke extensive virus inactivation, whereas glass, Al<sub>2</sub>O<sub>3</sub> and hematite (Fe<sub>2</sub>O<sub>3</sub>) do not. Strong interactions between a virus and a mineral surface have been suggested to denature proteins by dehydration and disruption of interactions between peptide chains.<sup>91</sup>

Several mechanisms may lead to surface-mediated inactivation, as is depicted in Fig. 1.11. The interaction with the surface may create a distortion of the capsid, which prevents the virus from binding to its host cell (left panel in Fig 1.11). This distortion may be sufficiently important to cause denaturation and disruption of the capsid, which could allow the genome to escape (middle panel in Fig 1.11).<sup>92,93</sup>

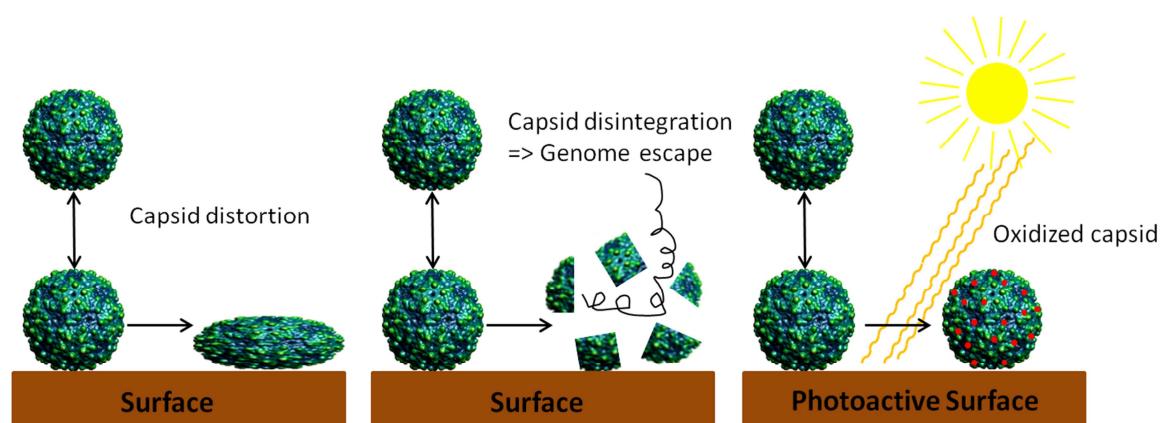


**Figure 1.11: Mechanism of inactivation at virus-surface interface.** Left: Inactivation by capsid distortion; Middle: Inactivation by capsid denaturation and disintegration; Right: Inactivation by oxidation of the capsid by surface-produced ROS.

The last mechanism described in Fig. 1.11 is inactivation promoted by the production of ROS by photoactive surfaces. For example, solutions containing  $\text{TiO}_2$  particles exposed to light were more effective in inactivating viruses than solutions without the  $\text{TiO}_2$  particles.<sup>94,95</sup> Furthermore, viruses adsorbed onto  $\text{TiO}_2$  were found to be inactivated more readily than free viruses. This may be due to the close proximity of the viruses to the ROS source, i.e., the particle surface. This proximity allows the ROS to immediately react with the virus components, before being quenched by any other solution constituents. The production of ROS from surfaces could arise in three ways:

- *Semiconductors*: When irradiated by light of higher energy than the band gap, it causes the separation of electrons ( $e^-$ ) and positive holes ( $h^+$ ). The electrons can further react with oxygen to form superoxide ( $\cdot\text{O}_2^-$ ), which can get further reduced to peroxides ( $\text{H}_2\text{O}_2$ ) and hydroxyl radicals ( $\cdot\text{OH}$ ). The most studied semiconductor to date is  $\text{TiO}_2$ . Inactivating UV doses could drastically be reduced when coupled with  $\text{TiO}_2$  adsorption.<sup>95</sup> Other oxides that have been shown to react comparably to  $\text{TiO}_2$  are  $\text{ZnO}$  and hematite ( $\text{Fe}_2\text{O}_3$ ).
- *Fenton-active surfaces*: Electron transfer from a reduced transition metal (usually iron or copper) to hydrogen peroxide causes formation of ROS. This reaction creates hydroxyl radicals ( $\text{OH}\cdot$ ) and hydroperoxyl radicals ( $\text{OOH}\cdot$ ).
- *Sensitizing surfaces (containing a light absorbing component)*: Excited sensitizers on a surface can interact via electron or energy transfer with dissolved  $\text{O}_2$  to form  $^1\text{O}_2$  under sunlight.

Even though heterogeneous disinfectants have been studied for some decades, there are still many mechanisms that are unknown and need further investigation. For water treatment it would be of great interest to develop pipes or containers that could reduce the microbial load without adding any chemical disinfectant. In public places (companies, schools, hospitals, etc...), it would decrease many contamination opportunities if doorknobs or the buttons on the coffee machine could self-disinfect. In medical centers, where high hygiene levels are mandatory, gloves or masks containing inactivating surfaces could potentially greatly reduce contamination risks.

### 1.5 Research objectives of this thesis

The current lack of understanding of the fundamental mechanisms of virus disinfection is a major limitation that prevents us from executing optimal virus control. This thesis contributes to a deeper mechanistic understanding of virus disinfection processes. In particular, this work aims at identifying the molecular-level processes that influence the kinetics and efficiency of virus inactivation by homogeneous

and heterogeneous disinfectants, linking it to the damage incurred by viral components during disinfection, and assessing how damage and inactivation are affected by the composition of viruses.

This PhD research project is part of a larger Sinergia project, which involves several institutions in Switzerland (Swiss Federal Institute of Technology (Lausanne and Zurich) and Bern University). This project is a combined computational and experimental approach of physical and chemical processes that lead to virus inactivation at solid-water interfaces. Each group is responsible for one aspect of the project in order to give a complete understanding on the behavior of viruses on solid surfaces.

In the following paragraphs, a short overview over the research chapters of this thesis is given.

## **Chapter 2**

Inactivation of viruses by chlorine dioxide exhibits significant deviation from Chick-Watson kinetics, in the form of a tailing curve. Tailing has been previously reported, but is typically attributed to the decay in disinfectant concentration. This chapter shows that tailing occurs even at constant  $\text{ClO}_2$  concentrations. Four working hypothesis to explain the cause of tailing were tested, namely changes in the solution's disinfecting capacity, aggregation of viruses, resistant virus subpopulations, and changes in the virus properties over the course of reaction. Bacteriophage MS2 was used as a model and was subjected to inactivation by chlorine dioxide in various conditions, allowing to selectively test the different hypothesis for tailing. Its capsid protein was also assessed by mass spectrometry to determine if protein damage was responsible for the change in susceptibility towards chlorine dioxide disinfection over time.

## **Chapter 3**

Kinetics of inactivation have been studied in depth, but the molecular level inactivation mechanisms are not fully understood. It is known that even viruses that are similar in shape, size and composition may differ greatly in their inactivation behavior. This chapter, along with chapter 4, aims at identifying how subtle differences in virus composition affect inactivation. To do so, inactivation of three closely related bacteriophages (MS2, fr and GA) by free chlorine,  $\text{UV}_{254}$ , chlorine dioxide and singlet oxygen was studied. The inactivation kinetics were assessed and the impact of each treatment on the genome was measured by the means of q-PCR. In order to assess the distribution of the damage inflicted on the genome, about half of the entire RNA chain was analyzed. The experimental measurements of genome damage were compared to the estimated extent of damage based on the genome composition, to assess if the composition of the genome is sufficient to predict its damage during inactivation.

## **Chapter 4**

Chapter 3 treated the damage inflicted to the genome during disinfection by four disinfectants; in this chapter the corresponding damage to the capsid protein was assessed. By the development of a quantitative mass spectrometry method it was possible to identify susceptible regions of the capsids and compare capsid degradation patterns among the three viruses. One important goal was to determine if the absence of cysteine in the capsid protein of GA had any impact on its inactivation. Predictions of capsid protein damage were made based on the susceptibility of the amino acids composing the capsids of MS2, fr and GA, and were compared to the experimentally determined damage.

## **Chapter 5**

After discussing kinetics and mechanisms of inactivation in homogeneous solutions in the previous chapters, chapter 5 focuses on the interaction between viruses and surfaces, and in particular, the inactivation potential of metallic copper. This effect was studied for bacteriophage MS2 and Qbeta in batch experiments containing either metallic copper or dissolved copper. To understand which interactions contribute to adsorption and furthermore cause inactivation, specific virus interactions were probed using self-assembled monolayers exposing different chemical functionalities. This approach allowed us to study the effect of individual interactions in a very controlled manner. Finally, the effect of surface inactivation on the different virus components was assessed.

# On the cause of the tailing phenomenon during virus disinfection by chlorine dioxide

## 2.1 Introduction

Chlorination is among the oldest and most commonly used disinfection process worldwide. However, over the years it has been shown that chlorine produces harmful by-products such as trihalomethanes and other halogenated compounds with potential carcinogenic effects.<sup>34</sup> It is therefore of interest to investigate other disinfectants that have a similar disinfection potential but generate fewer problematic by-products. As a good alternative, chlorine dioxide (ClO<sub>2</sub>) has shown to efficiently disinfect water for human consumption.<sup>96,97</sup> Importantly, it is effective at inactivating *Cryptosporidium*, whereas free chlorine is not.<sup>98</sup> Except from exhibiting a good disinfection capacity, ClO<sub>2</sub> can also oxidize iron and manganese, as well as help controlling taste and odor compounds.<sup>99,100</sup> The disadvantage of using chlorine dioxide is that it reacts to chlorite, which may be neurotoxic at high doses.<sup>34,42</sup>

In 1908, Chick published the first model for describing bacteria inactivation by disinfecting agents.<sup>45</sup> The model suggests that the fraction of surviving organisms ( $C_v/C_{v,0}$ ) exponentially decreases with time, which then leads to a linear decrease of  $\ln(C_v/C_{v,0})$  with time (Eq. 2.1):

$$\ln(C_v/C_{v,0}) = -kt \quad \text{Eq. 2.1}$$

Here,  $k$  represents the inactivation rate constant,  $C_v$  is the concentration of infective virus and  $t$  the time of disinfection.

In order to be able to compare different disinfectant concentration, this model was expanded by Watson<sup>46</sup> to yield the well-known Chick-Watson model (Eq. 2.2):

$$\ln(C_v/C_{v,0}) = -k_{cw}C^n t \quad \text{Eq. 2.2}$$

where  $k_{cw}$  is the Chick-Watson inactivation rate constant,  $C$  is the disinfectant concentration, and  $n$  is an empirical constant also called the dilution coefficient. Frequently it is found that  $n = 1$ , in which case the Chick-Watson model is first order with respect to the disinfectant dose (expressed as  $Ct$ ). This model thus allows calculating the disinfectant dose necessary to obtain a certain amount of inactivation. It was quickly discovered, however, that inactivation kinetics occasionally deviate from this simple model. In particular, inactivation curves frequently exhibit tailing after an initial exponential decay. The reason for this observed deviation divided the researchers into two main groups: the *vitalistics*, who argued that this deviation originated from heterogeneity in the population of microorganisms, and the *mechanistics*, who attributed these deviations to factors occurring during the disinfection process.<sup>47</sup> To date, the mechanism underlying this deviation from Chick-Watson's first-order model still hasn't been fully assessed and understood.<sup>101</sup> Cerf stated in his review on tailing of survival curves that: "People who have observed tails or who have considered the question, either accept tails as facts or reject them as artefacts".<sup>102</sup> In other words, even though tailing is frequently observed, little attention has been given to its underlying cause. The occurrence of tailing, however, may lead to incomplete inactivation and ultimately may cause the disinfection process to fall short of the treatment goal. It is thus important to account for tailing, in order to ensure that water or food is sufficiently disinfected prior to human consumption.

Tailing appears to be particularly common in the case of virus disinfection by  $\text{ClO}_2$ . Examples include the inactivation of Adenovirus, feline Calicivirus, Enterovirus 71, murine Norovirus and human and simian Rotavirus.<sup>96,103–106</sup> Yet its occurrence was either not mentioned or simply attributed to the decay in chlorine dioxide concentration over time of reaction. In a recent study, Hornstra et al.<sup>107</sup> performed an in-depth investigation on the disinfection of bacteriophage MS2 at low  $\text{ClO}_2$  concentrations, and suggested that heterogeneity of the virus population (either in the original virus stock or acquired during disinfection) could be the reason for the tailing behavior. This hypothesis, however, was not proven, nor were other possible causes for the tailing behavior investigated in depth.

In the present work, we test the resistant subpopulation hypothesis, along with three other possible mechanisms that can lead to tailing: the presence of viral aggregates; changes in the solution properties during disinfection that diminish the efficiency of  $\text{ClO}_2$ ; and changes in the virus properties during disinfection that protect them from  $\text{ClO}_2$ .

## 2.2 Materials and methods

Virus disinfection experiments were conducted in stirred dilution buffer (DB: 5 mM  $\text{PO}_4^{2-}$ , 10 mM NaCl, pH 7.4) at room temperature. MS2 was used as the test organism, because it is a commonly used surrogate for human viruses<sup>25</sup> and to facilitate the comparison of our results with the study by Hornstra et al.<sup>107</sup> At several time points during the inactivating treatment, samples were analyzed for the remaining virus infectivity. Experiments were typically conducted in two or more replicates with good reproducibility. Exceptions are the tests involving pretreatments with sonication, chloroform and filtration (see section 2.3.2), which were conducted only once.

### 2.2.1 Chemicals

NaCl (99.5%), NaOH (extrapure),  $\text{NaH}_2\text{PO}_4 \cdot \text{H}_2\text{O}$  (99%),  $\text{K}_2\text{S}_2\text{O}_8$  (99%),  $\text{NaHCO}_3$  (99.7%) and  $\text{CHCl}_3$  (99.8%) were purchased from Acros Organics (Geel, Belgium).  $\text{Na}_2\text{S}_2\text{O}_3$  (98%), sinapinic acid (98%) and  $\text{NaClO}_2$  (puriss.) was obtained from Sigma-Aldrich (Germany). HCl (25%) was obtained from Merck (Darmstadt, Germany). Ultrapure water ( $>18 \text{ M}\Omega\text{cm}^{-1}$ ) was used for all aqueous solutions.

### 2.2.2 Microorganisms

Bacteriophage MS2 (DSMZ 13767) and its *Escherichia coli* host (DSMZ 5695) were purchased from the German Collection of Microorganisms and Cell Cultures (Braunschweig, Germany). It was propagated as described previously<sup>108</sup> and infectivity was assessed by enumeration of plaque forming units (pfu) using the double agar layer method.<sup>109</sup>

### 2.2.3 Chlorine dioxide production and experimental setup

Chlorine dioxide was produced by mixing 100 mL 4%  $\text{K}_2\text{S}_2\text{O}_8$  with 100 mL 2%  $\text{NaClO}_2$ <sup>110</sup> and was stored at 4°C. The resulting  $\text{ClO}_2$  stock concentration (250 to 1000 mg/L) was determined by spectrophotometry ( $\epsilon_{358\text{nm}} = 1200 \text{ M}^{-1}\text{cm}^{-1}$ ).<sup>111</sup> Prior to experiments, the stock solution was diluted to a working solution of 0.4-0.7 mg/L  $\text{ClO}_2$ , and was spiked with virus stock solution to a concentration of  $0.5 \cdot 10^{12}$  pfu/mL. To

compensate for ClO<sub>2</sub> evaporation and consumption throughout the experiment, concentrated ClO<sub>2</sub> (16 mg/L) was added at a rate of 8-20 µl/min by means of a peristaltic pump (KdScientific, Holliston, MA). Prior to the start of each experiment it was ensured that this setup maintained a constant ClO<sub>2</sub> concentration under the given solution conditions. To halt the disinfection, ClO<sub>2</sub> was quenched by addition of sodium thiosulfate (0.63 M) at a 20:1 sample:quenching agent ratio. Control samples confirmed that the addition of sodium thiosulfate did not result in inactivation.

#### **2.2.4 Re-growth of MS2 after inactivation**

After disinfection, the solution was centrifuged using a 100 kDa Microcon centrifugal filter (Millipore, Billerica, MA) and concentrated to 20 µL. The centrifuged sample was washed 5 times with DB, and 50 µL of DB was added. Of this solution, 50 µL were spiked into a 12 mL *E. coli* culture in exponential growth phase at an optical density of 0.04. After 5 hours of incubation at 37 °C, 1 mL of CHCl<sub>3</sub> was added to lyse the bacteria. The solution was then centrifuged at 3000 g for 5 minutes to pellet the bacteria. The supernatant was concentrated to 1 mL in a 100 kDa Microcon centrifugal filter and was washed 4 times with DB. Finally the virus solution was passed through a 0.1 µm filter and was used for the next inactivation-growth cycle. This procedure was repeated after each disinfection experiment for 5 cycles.

#### **2.2.5 Particle size measurement by Dynamic Light Scattering (DLS)**

Hydrodynamic size measurements were performed by Zetasizer (Malvern Instruments, Nano ZS) in disposable 120 µl cuvettes. The cuvettes were always placed in the instrument with the same orientation and care was taken to avoid air bubbles. The data acquisition software (Dispersion Technology Software 5.10, Malvern Instruments Ltd.) was set to 13 runs of 10 seconds in each measurement. Each measurement was repeated at least three times.

#### **2.2.6 Analysis of the capsid protein by Matrix Assisted Laser Desorption Ionization (MALDI)**

To assess the effect of ClO<sub>2</sub> on the capsid proteins, 10 mL of 1.5 mg/L chlorine dioxide were spiked to a final MS2 concentration of 1×10<sup>12</sup> pfu/mL. Because thiosulfate can back-reduce oxidized protein residues, disinfection experiments in which protein integrity was assessed were conducted by the one-time addition of ClO<sub>2</sub>, which was then left to evaporate as was described before.<sup>112</sup> All MALDI measurements were performed with an ABI 4800 MALDI-TOF-TOF (Applied Biosystems, Rotkreuz, Switzerland), using the instrument settings and sample deposition methods described previously.<sup>61</sup>



### 2.2.7 Analysis of disinfection kinetics

As described in previous work,<sup>112</sup> chlorine dioxide inactivation kinetics of MS2 deviate from the first-order Chick-Watson model and can be described by the Hom model according to the following equation(Eq. 2.3):<sup>113</sup>

$$\ln(C_v/C_{v,0}) = -k_H C^n t^{m-1} \quad \text{Eq. 2.3}$$

where C is the disinfectant concentration (constant over the time of reaction),  $k_H$  is the Hom rate constant  $[(\text{mgL}^{-1}\text{sec}^{m-1})^{-1}]$ , n is the dilution coefficient (set to 1 as only a single  $\text{ClO}_2$  concentration was used), and m is an empirical constant that describes the deviation from the ideal Chick-Watson model. The parameters for the Hom model were fitted in Sigmaplot (version: 12.0, 2011). Model fits were compared by ANCOVA analysis as described previously.<sup>112</sup> The correlation coefficient (R) for all fits varied between 0.97 and 0.99.

## 2.3 Results and discussion

Fig. 2.1 shows an example inactivation curve obtained for MS2 after exposure to a constant concentration of 0.5 mg/L chlorine dioxide. It is readily seen that after 4 logs inactivation a tail starts to form. The most obvious reason for a tailing disinfection curve is the consumption of the disinfectant over time, as has been suggested in other studies.<sup>106,114</sup> As can be seen in Fig. 2.1, however, we demonstrate that  $\text{ClO}_2$  consumption is not the sole reason for tailing, as this feature is evident even though the chlorine dioxide concentration in our experiments was maintained constant.

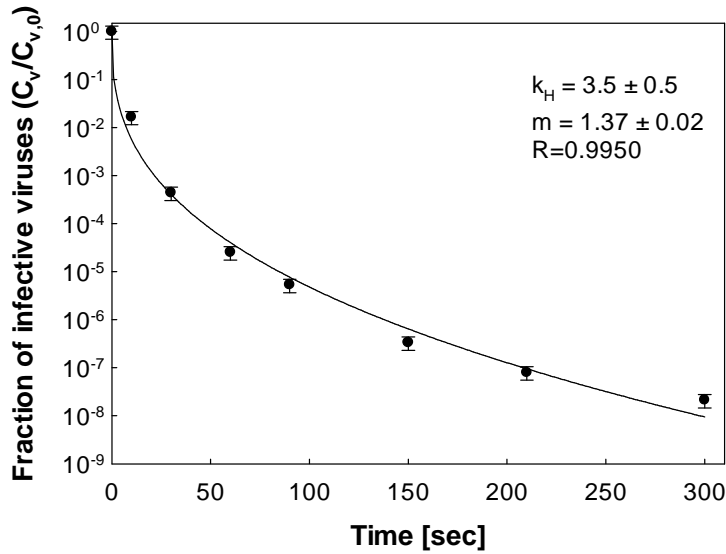


**Figure 2.1: Inactivation of MS2 by chlorine dioxide.**  $\text{ClO}_2$  concentration was 0.6 mg/L. Measured data are present as data points. The line represents the fit to the Hom model (Eq. 2.3). The error bars represent the standard deviation associated with virus enumeration.

Interestingly, no tailing effect was observed for the inactivation of MS2 by other oxidants, such as free chlorine, peracetic acid or singlet oxygen.<sup>56,112,115</sup> The tailing feature must therefore be related to the specific mode of action of  $\text{ClO}_2$ . An important feature in  $\text{ClO}_2$ 's mode of action is that, unlike other oxidants studied, it does not act on the MS2 genome, but solely on its proteins.<sup>56,112</sup> Recombination of damaged genomes, which has been suggested as the cause for tailing during  $\text{UV}_{254}$  disinfection,<sup>116</sup> can therefore be ruled out for  $\text{ClO}_2$ . The tailing observed in  $\text{ClO}_2$  disinfection must instead stem from an increasingly inhibited reactivity or accessibility of  $\text{ClO}_2$  toward MS2 proteins.

Starting from this insight, the present study intended to determine the feature specific to  $\text{ClO}_2$  disinfection that results in tailing. To do so, four main factors can be hypothesized as the underlying cause:

1. *Changes in solution properties:* The disinfecting capacity of the chlorine dioxide solution changes over time of reaction.
2. *Aggregation:* In the virus stock, a fraction of viruses are in an aggregated state which may protect them from inactivation. Aggregation could also occur over time of reaction.
3. *Resistant subpopulation:* The initial virus stock contains different subpopulations with variable resistance to chlorine dioxide.

4. *Changes in virus properties*: The disinfection process changes virus properties such that they are increasingly protected against the disinfectant.

Of these four causes, the first three were suggested by Hornstra et al.<sup>107</sup> and are investigated in detail here. The fourth cause, however, has not previously been considered. In the following, we discuss our experimental results leading to the inclusion or rejection of each of these four hypotheses.

### **2.3.1 Changes in solution properties**

To assess if changes in solution properties over the course of a disinfection experiment are the cause of tailing, three factors were examined: the influence of the buffer, the role of the accumulating disinfection by-product chlorite, and the disinfection efficiency of spent solution.

The influence of the buffer was tested to ensure that the observed disinfection behavior was not an artifact arising from interactions of  $\text{ClO}_2$  with the matrix. Specifically, we exchanged DB for carbonate buffer (5 mM). In Fig. 2.2, a comparison of the inactivation rate constants determined for an experiment in carbonate buffer and in DB is shown. The corresponding inactivation curves and Hom model fits are shown in the appendix (Fig. B1). It can be seen that this buffer exchange didn't affect the observed inactivation kinetics, indicating that the phosphate is not essential to the tailing process.

On the cause of the tailing phenomenon during virus disinfection by chlorine dioxide

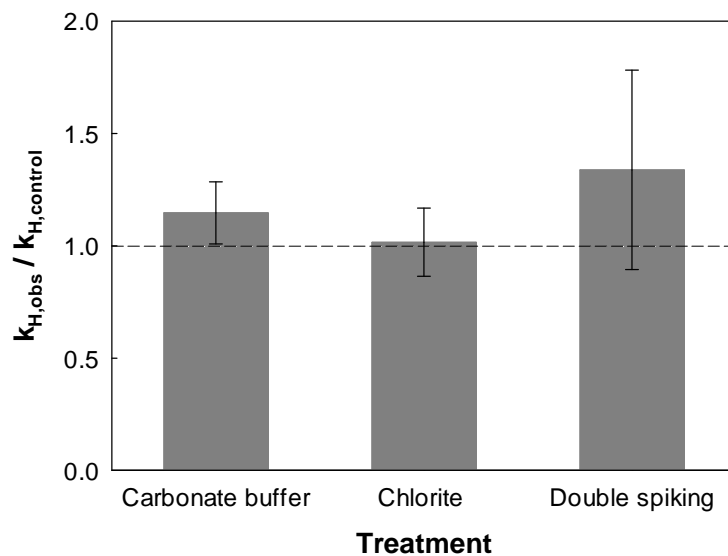


**Figure 2.2: Impact on  $k_H$  due to changes in solution properties.** Ratio of  $k_H$  obtained in a control experiment (0.5 mg/L  $\text{ClO}_2$ ) and in experiments with changed solution conditions: left: experiment conducted in carbonate buffer instead of DB; middle: experimental solution contained chlorite (6.0 mg/L); right: solution was re-spiked with fresh MS2 after 120 seconds of reaction. The dashed line represents equal  $k_H$  in the sample and the control. The error bars represent the propagated standard error associated with the model fits of  $k_H$ .

The disinfection by-product chlorite is formed during the reaction between chlorine dioxide and amino acids,<sup>117</sup> thereby changing the composition of the matrix during the experiment. If chlorite interfered with the disinfection efficiency of  $\text{ClO}_2$ , its accumulation in solution over time may explain the tailing effect. Figs. 2.2 and B2 show a comparison of the inactivation rate constants and curves determined from an experiment with chlorite added to the solution at the beginning of the disinfection process and the control experiment (without added chlorite). The amount of chlorite added corresponded to the amount chlorite produced over the time of a control experiment (3-6 mg/L). As can be seen in Fig. 2.2, addition of chlorite did not cause a significant change in  $k_H$  ( $p = 0.98$ ). Similarly,  $m$  did not change significantly ( $p = 0.42$ ). The lack of change in  $k_H$  and  $m$  values in the presence of chlorite implies that the tailing effect was present, and that its onset occurred at the same extent of inactivation as in the control experiment. The gradual accumulation of chlorite during disinfection can therefore not explain tailing.

The most conclusive experiment in this series consisted of spiking fresh virus into a spent solution. This experiment was performed to confirm the findings by Hornstra et al.<sup>107</sup> Specifically, MS2 disinfection was monitored for 120 seconds, well into the tailing zone (Fig. 2.1). Then the solution was re-spiked with fresh viruses, and disinfection was monitored for an additional 120 seconds. The second virus spike

showed the same kinetic parameters as the first spike (Figs. 2.2 and B3), indicating that exposing fresh viruses to a spent solution didn't change the disinfection kinetics. This is in agreement with the result of a similar experiment obtained by Hornstra et al.<sup>107</sup> Combined, the results from these experiments conclusively confirm that changes in solution properties are not responsible for the observed tailing effect.

### 2.3.2 Aggregation

A previous study has shown that strong disinfectants are readily consumed at the outermost layer of virus aggregates, and therefore only a reduced disinfectant concentration reaches the aggregate core.<sup>115</sup> The innermost viruses thus become inactivated at a slower rate. Furthermore, if viruses are enumerated in an aggregated state, it is not possible to distinguish if only one or several viruses in the aggregate remain infective. The number of surviving viruses therefore appears constant, even if disinfection within the aggregate continues. Both these factors lead to a tailing feature in the disinfection curve of partially or fully aggregated samples, as has been reported in various studies.<sup>118,119</sup>

MS2 has an isoelectric point of 3.9, which means that at the working pH of this study (7.5), most viruses should be dispersed. However, it is possible that the solution contains aggregates that were formed in the host cell during the virus propagation process. In Fig. 2.3, the size measurement of the viruses in solution is shown; the first peak at about 30 nm represents single MS2 particles, (MS2 diameter = 26 nm). In addition, a larger particle population can be seen, which could be virus aggregates or impurities arising from the virus propagation or sample handling. Note that Fig. 2.3 shows the signal intensity, which is proportional to  $r^6$ , where  $r$  is the particle radius. Even though the intensity peaks in Fig. 2.3 for the small and large particles have similar areas, the number of larger particles is thus very small compared to the single viruses.

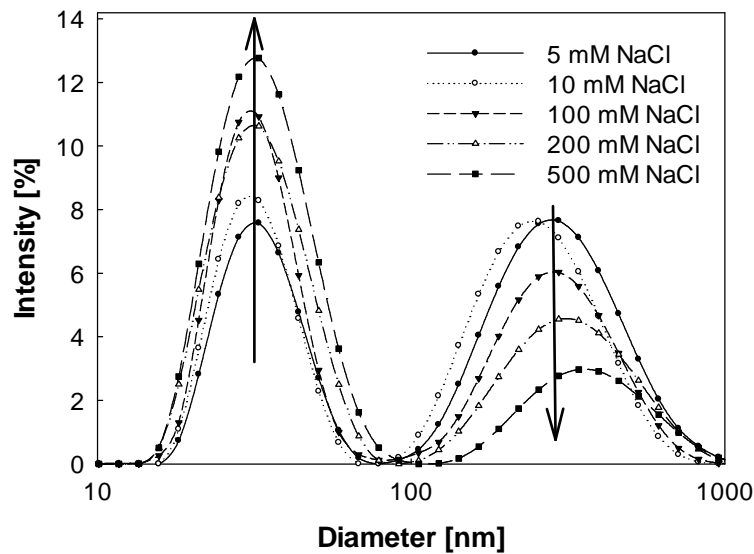


**Figure 2.3: Size distribution of MS2 at different ionic strengths.** The MS2 concentration was  $5 \times 10^{11}$  pfu/mL. Each data point represents the average of three DLS measurements.

To determine if the tailing phenomenon arises from the presence of few small aggregates seen in Fig. 2.3, it was attempted to break up any aggregates in solution. To do so, the virus solution was subjected to different treatments prior to disinfection. Firstly, the sample was sonicated during 30 minutes. This treatment has previously been shown to be efficient in dispersing aggregated viruses.<sup>120</sup> Secondly, the virus stock was subjected to chloroform extraction. Chloroform extraction is used during virus production to purify and disperse viruses after propagation.<sup>119</sup> Therefore it was assumed that treating the stock solution with chloroform before the disinfection treatment may break up residual aggregates. Thirdly, the virus stock was filtered through a 0.1  $\mu\text{m}$  pore size filter. This ensured that no particles larger than 0.1  $\mu\text{m}$  in diameter stayed in solution. But given that the diameter of one virus is 26 nm, an aggregate of 100 nm in diameter could still be composed of 10-20 viruses, which may have a protective effect on the viruses located in the core of the aggregate. Finally, the ionic strength of the buffer solution was increased, as previous studies have suggested that high ionic strength disperses viral aggregates.<sup>121</sup> As shown in Fig. 2.3, this effect was also evident in our experimental system. The intensity of the single virus peak increased slightly and the intensity of larger particles decreased with higher salt concentrations. This indicates a shift from aggregates to single particles. This finding may be surprising, as it is contrary to the double layer theory, which suggests that the interaction between equally charged particles should increase with increasing NaCl concentration, due to increasing charge shielding.<sup>122</sup> However, a similar finding was reported previously for polio and Reovirus by Floyd et al.,<sup>123</sup> who

suggested that dispersion could be due to cations binding to the virus, which results in positively charged particles with repulsive forces.

Fig. 2.4 shows a comparison of the inactivation rate constants determined from experiments with broken up aggregates compared to a control experiment (without any pre-treatment on the virus or the solution). The corresponding inactivation curves and model fits are shown in the appendix (Figs. B4-B7). While none of the treatments described above eliminated tailing, filtration and increasing ionic strength slightly increased the inactivation rate constant ( $p = 0.05$  for filtration and  $p < 0.01$  for the high ionic strength solution). An increase in  $k_H$  represents more rapid inactivation before as well as after the onset of tailing. This behavior can be interpreted as the removal or break up of some, but not all aggregates. The biggest increase in  $k_H$  was found for the solution with high ionic strength (Fig. B7). However, even in this solution a tailing still appeared. In fact, no significant differences were found among these experiments and the control for the second model parameter,  $m$  (data not shown). This indicates that all experiments deviated similarly from first-order Chick-Watson kinetics, and that the dispersal or removal of aggregates in the virus stock solution could not explain the tailing effect. In addition, aggregation would also affect the inactivation curves of other disinfectants. However, as mentioned above, no tailing effect was observed for free chlorine or singlet oxygen.<sup>112</sup> This further indicates that aggregates in the viral stocks do not contribute to the tailing exhibited during chlorine dioxide disinfection.

On the cause of the tailing phenomenon during virus disinfection by chlorine dioxide

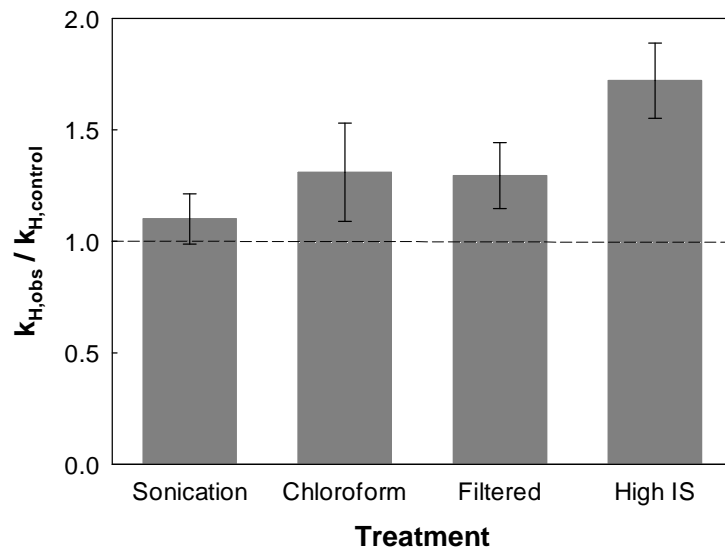


**Figure 2.4: Impact of aggregate dispersion on  $k_H$ .** Ratio of  $k_H$  obtained in pre-treated virus samples and control experiment at 25°C. Sonication = sample sonicated for 30 minutes; Chloroform = sample extracted using chloroform; Filtered = sample passed through a filter of 0.1  $\mu\text{m}$  pore size; High IS = sample exposed to a solution of high ionic strength containing 500 mM NaCl. The dashed line indicates equal  $k_H$  in the sample and the control. The error bars represent the propagated standard error associated with the model fits of  $k_H$ .

An aggregation effect on inactivation could also occur if aggregates form during, rather than prior to, the disinfection process. While the size measurements by DLS didn't indicate any change in the particle size during disinfection, small aggregates may have formed at concentrations below the detection limit of the DLS. To assess if any aggregation occurred during the experiment, the disinfection was stopped (by discontinuing the addition of  $\text{ClO}_2$ ) after 120 seconds, and the sample was subjected to 10 minutes of sonication to break any newly formed aggregates before re-starting the disinfection. The disinfection kinetics in this experiment showed no difference to the non-sonicated control experiment, neither in  $k_H$  ( $p = 0.09$ ) nor in  $m$  ( $p = 0.39$ ). This indicates either that no aggregates formed during the short time of reaction or that the aggregates formed are not dispersible.

For more conclusive evidence that aggregation during disinfection did not play a role, the MS2 starting concentration was lowered. Fewer viruses in solution lead to fewer chances of virus encounter, and hence to less aggregation. Experiments were therefore performed at starting concentrations of  $1 \times 10^7$  pfu/mL and  $5 \times 10^9$  pfu/mL. The inactivation behavior was not significantly different from that of the control experiments with  $5 \times 10^{11}$  pfu/mL as the starting MS2 concentration ( $p = 0.16$ ). Furthermore, the



onset of tailing occurred after the same extent of inactivation for all starting concentrations, confirming that aggregation during disinfection was not the cause for tailing.

### 2.3.3 Resistant subpopulation

So far we established that neither changes in solution properties, nor aggregation could explain the tailing feature. As proposed by Hornstra et al.,<sup>107</sup> tailing could arise from the presence of a resistant subpopulation in the starting virus stock. To support this theory they re-spiked the viruses from the tail directly in fresh chlorine dioxide solution and found that the inactivation continued in the slow, tailing phase. This finding is consistent with the presence of a resistant subpopulation, but doesn't exclude the possibility of a change in the virus properties. We therefore conducted two additional experiments to determine if a resistant sub-population was present in the virus stock.

First, the potentially resistant virus population, i.e., the virus population surviving throughout the tailing phase of the experiment, was isolated and re-grown, and the re-grown viruses were re-exposed to  $\text{ClO}_2$ . After five such disinfection and re-growth cycles, no change in virus disinfection kinetics was observed. In other words, repeated re-growth of the surviving population and re-exposure to  $\text{ClO}_2$  did not yield a more resistant MS2 population. This indicates that either no resistant sub-population was present, or that the remaining wild types dominated the re-growth phase.

Second, the chlorine dioxide concentration in solution was increased five-fold after 120 seconds to attempt to disinfect the potentially resistant subpopulation with a higher  $\text{ClO}_2$  dose (Fig. B8). This measure did not cause any change in the inactivation behavior of the virus. In other words, the tailing part of the curve exhibited the same slow inactivation as seen in Fig. 2.1 ( $p = 0.20$ ). This indicates that, if a resistant sub-population is present, it exhibits slow inactivation kinetics that are in conflict with Chick-Watson kinetics, as they are independent of the  $\text{ClO}_2$  concentration. While this finding does not conclusively rule out the hypothesis of a resistant subpopulation, it appears unlikely that a subpopulation exists that has  $\text{ClO}_2$ -independent disinfection kinetics. Instead, this result appears to be more consistent with our final hypothesis, namely a change in virus properties during disinfection.

### 2.3.4 Changes in virus properties

In order to evaluate if changes in the virus properties caused the virus to become more protected toward  $\text{ClO}_2$  over the course of the experiment, the virus solution was first subjected to inactivation into the tailing region. It was then washed in 100 kDa Microcon centrifugal filters (Millipore, Billerica, MA) with DB, and subsequently re-exposed to chlorine dioxide. The important difference in this experiment to that by Hornstra et al.<sup>107</sup> discussed above is the washing step prior to re-exposure to  $\text{ClO}_2$ . As shown in Fig. 2.5, the washed sample exhibited fully restored reactivity toward chlorine dioxide, manifested by an initial exponential decay, followed by tailing after 3-4 logs of inactivation. In contrast, as reported by Hornstra et al., unwashed samples from the tailing region remained protected toward  $\text{ClO}_2$ .<sup>107</sup> This observation indicates that the viruses acquire protection during the disinfection process, but that the protection is easily reversible by washing with DB. This recovery of biphasic disinfection kinetics weakens the argument of a resistant subpopulation.

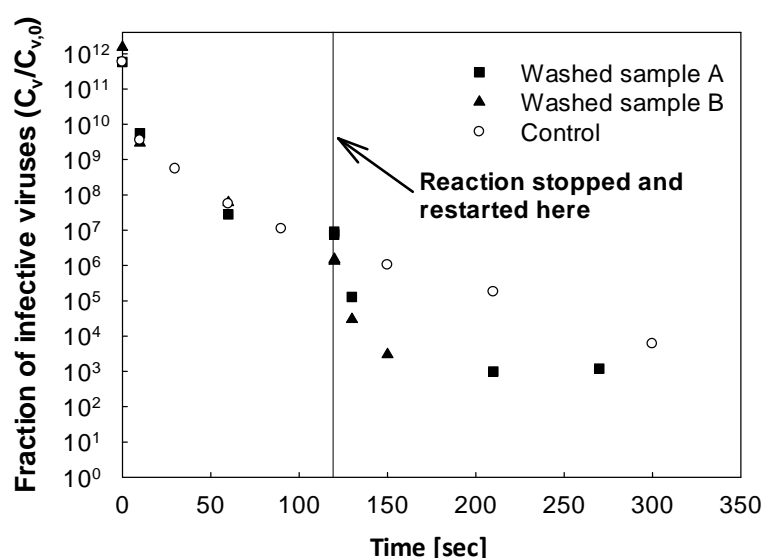


**Figure 2.5: Effect of washing on the inactivation of MS2 by chlorine dioxide.** At time = 0, the solution was spiked to a MS2 concentration of  $1 \times 10^{12}$  pfu/mL. The reaction was stopped after 120 seconds (solid line), and the viruses were washed with DB and re-exposed to chlorine dioxide. The starting concentration after washing was  $5 \times 10^6$  pfu/mL. Triangles and squares indicate duplicate experiments, and a control sample (not washed; empty circles) is shown for comparison.

To better understand the effect of the washing step, the samples were subjected to MALDI mass spectrometry before and after washing, to determine if there was any change in the mass of the viral capsid protein. MS2's capsid protein is composed of 180 copies of one single protein of 129 amino acids, which is readily detectable by protein mass spectrometry. Results from the MALDI analyses are

illustrated in Fig. 2.6. Untreated control samples show a strong peak at a mass over charge ratio ( $m/z$ ) of 13.7 kDa, consistent with the mass of the MS2 capsid protein. After treatment with  $\text{ClO}_2$ , the capsid protein peak shifted and appeared as a broad peak consisting of several masses. When the sample was washed after treatment, however, the intact capsid protein peak re-emerged. These mass spectrometry results showed that indeed a protected population of viruses is created during the disinfection process by deposition of disinfection products onto the viral capsid proteins. However, the viruses can shed their protective layer relatively easily by washing. The masses observed in the unwashed mass spectra (Fig. 2.6) cannot be readily assigned to a specific reaction product. The +67 peak may result from adsorbed chlorite formed from the reaction between chlorine dioxide and an amino acid, but more work is needed to conclusively assign the individual peaks to specific capsid protein adducts, and to determine their effect with respect to protection from  $\text{ClO}_2$ .

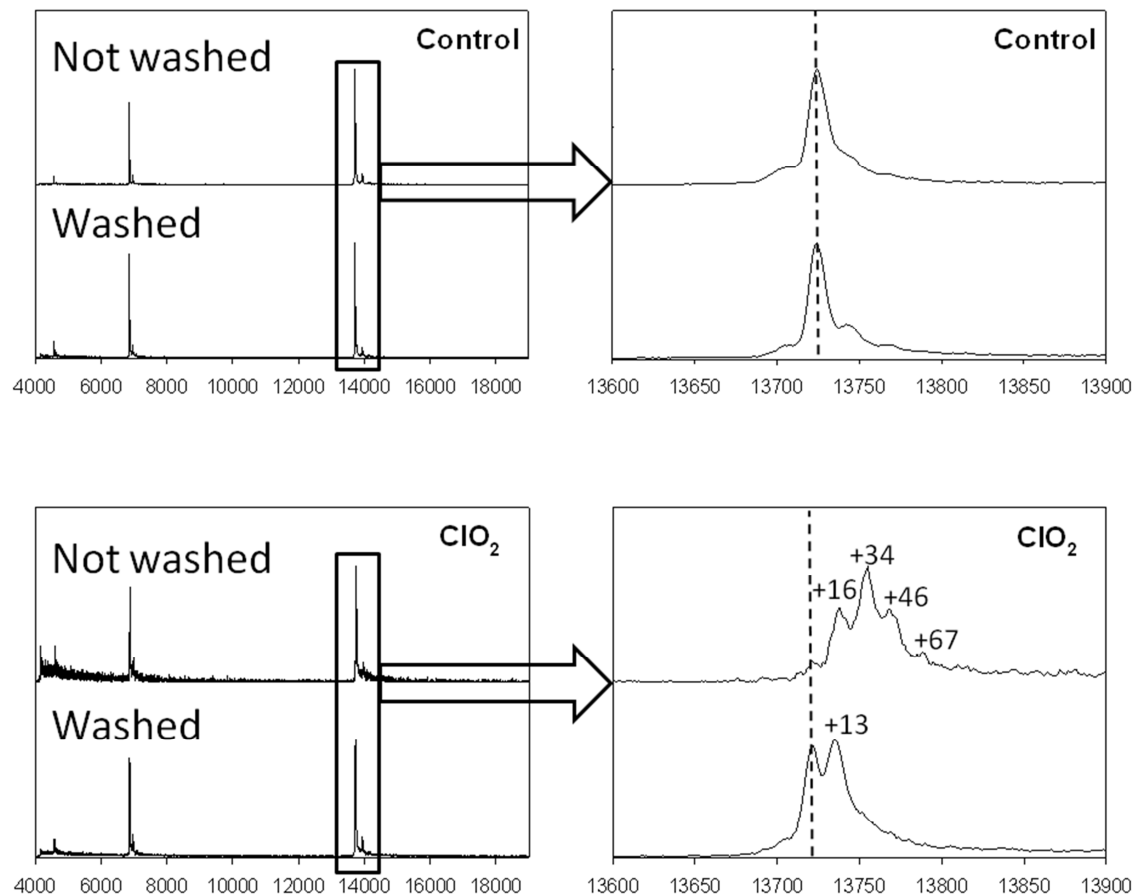


**Figure 2.6: MALDI spectra of washed and unwashed MS2 samples before and after  $\text{ClO}_2$  treatment.** Top panel: sample before  $\text{ClO}_2$  treatment (control); bottom panel: sample after inactivation ( $\text{ClO}_2$ ). Left: overview spectra over the whole measured mass to charge ( $m/z$ ) range. Right: Zoom on the  $M^{+1}$  capsid protein peak. The boxes and dashed lines indicate the  $m/z$  ratio of the intact capsid protein peak. Numbers in plot indicate the mass difference between the intact capsid protein and the products formed during inactivation.

Previous work in our group<sup>112</sup> showed that damage to the capsid protein incurred during chlorine dioxide exposure is directly proportional to inactivation, suggesting that capsid protein damage may be involved in the inactivation of the virus. In the present study it is shown that disinfection products bind to the protein and protect the virus from further inactivation. This corroborates that the capsid protein is an important feature controlling the inactivation of MS2 by chlorine dioxide.

## 2.4 Conclusions

This study shows that the main cause for tailing during the disinfection of MS2 by chlorine dioxide is a change in the virus properties during the course of the experiment. Specifically, the reaction of  $\text{ClO}_2$  with MS2 creates products that deposit onto the viruses and protect them from further disinfection. This protection takes place on the capsid protein, which gets extensively but reversibly modified during the disinfection process. Other proposed causes for tailing, namely changes to the reactivity of the disinfecting solution, virus aggregation, and the presence of resistant subpopulations, could be ruled out. Virus disinfection by  $\text{ClO}_2$  is thus a self-limiting process, in that it increasingly inhibits its own inactivation efficiency as the disinfection treatment proceeds. This is an important and potentially detrimental characteristic of this disinfectant, which should be recognized by water utilities working with  $\text{ClO}_2$ . Specifically, the self-limiting effect may cause the disinfection of viruses to fall short of the required treatment goal.

Further work is needed, however, to determine if the protective effect is observed to the same extent for other  $\text{ClO}_2$  doses. Similarly, in the application of  $\text{ClO}_2$  for virus disinfection in actual drinking water matrices should be tested to establish if protecting adducts preferably bind to organic matter rather than the virus, which may reduce the tailing effect. Finally, more work is required using a selection of different viruses, to establish if this effect is equally important across virus species and families.



# Subtle differences in virus composition affect disinfection kinetics and mechanisms: effect of genome composition

### 3.1 Introduction

Many important illnesses such as gastroenteritis, poliomyelitis, aseptic meningitis and some variants of hepatitis are transmitted by viruses via the fecal-oral route.<sup>124</sup> One main route of exposure occurs when populations are exposed to drinking or recreational water that has been impacted by wastewater. To prevent viral disease outbreaks, it is therefore important that water be appropriately treated before it is brought into contact with humans.

Inactivation kinetics of viruses upon treatment by various disinfectants including UV, singlet oxygen ( $^1\text{O}_2$ ), free chlorine (FC), chloramines and chlorine dioxide ( $\text{ClO}_2$ ) have been studied in depth.<sup>43,52,60,103,106,125,126</sup> Even though these disinfectants have been used for decades or even centuries, we still lack a fundamental understanding of their mode of action. Several studies have investigated the role of damage to either the viral genomes or proteins, but rarely were both considered simultaneously. Consequently, different studies reach different conclusions regarding the important disinfection targets. For example, it has been postulated<sup>55,127</sup> that chlorine dioxide and free chlorine inactivate Poliovirus and Hepatitis A virus, respectively, by damaging the viral genome. Contradictorily, Lim et al.<sup>106</sup> report that genome damage is not sufficient to explain inactivation by chlorine dioxide. This is supported by the work of Napolitano et al., who suggested that inactivation should be due to protein damage, as  $\text{ClO}_2$  reacts more readily with amino acids than with nucleotides.<sup>128</sup> UV is often reported to cause fatal genome damage by forming pyrimidine dimers,<sup>60,129,130</sup> yet protein damage has also been reported.<sup>61,62</sup>

Singlet oxygen has been found to cause protein cross linking<sup>131</sup> whereas other studies report genome damage as the main target for disinfection.<sup>108,132</sup>

Interestingly, different serotypes within a family of viruses can exhibit very different susceptibilities to disinfectants. For example, the inactivation of Coxsackievirus A9 by free chlorine was ten to 44-times more rapid than the inactivation of Coxsackievirus B5 depending on the pH.<sup>52</sup> Similarly, UV<sub>254</sub> inactivation of Adenovirus type 41 was significantly slower than for Adenovirus types 2 and 5.<sup>133</sup> These substantial differences in inactivation kinetics arise even though the serotypes exhibit only minor differences in composition. To rationalize this behavior, the molecular-level effects of the disinfectants on the different virus components must be understood.

In previous work, we investigated the main targets of disinfection of MS2 bacteriophage by UV<sub>254</sub>, <sup>1</sup>O<sub>2</sub>, FC and ClO<sub>2</sub>.<sup>56</sup> The present work's goal was to assess how subtle changes in the composition of three closely related viruses affect the kinetics of inactivation by these disinfectants, and to determine to what extent the observed differences can be rationalized by damage incurred by the viral genomes and capsid proteins. Specifically, we compared the inactivation of MS2 with that of two other phages of the *Leviviridae* family, fr and GA. These phages serve as ideal models for this work as they are among the most simply structured viruses: they consist of a positive sense, single-stranded RNA genome (approximately 3500 nucleotides), which is surrounded by an icosahedral capsid containing 180 copies of a capsid protein (composed of 129 amino acids), as well as one copy of an assembly protein (A protein; composed of 393 amino acids for MS2 and fr; 390 for GA). The genomes of fr and GA are 85 and 74% identical to that of MS2, respectively, while the capsid proteins are 87 and 61% homologous. The ultimate goal was to establish how these differences in capsid and genome content influence the kinetics and mechanisms of inactivation upon treatment by different disinfectants.

The results of this work are divided into two chapters; the present one discusses the effect of genome composition on inactivation kinetics and mechanisms; the next chapter (chapter 4) is dedicated to the contribution of the viral proteins.



### 3.2 Materials and methods

Virus inactivation experiments were conducted using three different phages (MS2, fr and GA) and four disinfectants (UV<sub>254</sub>, <sup>1</sup>O<sub>2</sub>, FC and ClO<sub>2</sub>). All experiments were conducted in stirred dilution buffer (DB: 5 mM PO<sub>4</sub><sup>2-</sup>, 10 mM NaCl, pH 7.4) at room temperature with a starting concentration of 1×10<sup>10</sup> pfu/mL. Throughout the disinfection experiments, sample aliquots of 10 to 100 µL were periodically removed and infective viruses were enumerated. A second set of aliquots (10 to 100 µL) was collected for genome extraction and analysis as described below. All experiments were conducted in duplicate (two separate experiments for each combination of virus and disinfectant).

#### 3.2.1 Chemicals

NaCl (99.5%), NaOH (extrapure), NaH<sub>2</sub>PO<sub>4</sub>·H<sub>2</sub>O (99%), EDTA-dihydrate (99%), CaCl<sub>2</sub>·2H<sub>2</sub>O (99%), HPLC grade acetonitrile, Rose Bengal (85%) were purchased from Acros Organics (Geel, Belgium). H<sub>3</sub>BO<sub>3</sub> (99%), KMnO<sub>4</sub> (99%), KI (99%) and Na<sub>2</sub>S<sub>2</sub>O<sub>3</sub> (98%), were obtained from Sigma-Aldrich (Germany). The following products were obtained from Merck (Darmstadt, Germany): HCl (25%) and H<sub>2</sub>SO<sub>4</sub> (95-97%). Tris (ultrapure) was purchased from AppliChem (Darmstadt, Germany). KIO<sub>3</sub> was purchased from Siegfried AG (Zofingen, Switzerland). N,N-Diethyl-p-phenylenediamine oxalate (DPD) (90%) and furfuryl alcohol (98%) were obtained from Fluka (Steinheim, Germany). Sodium hypochlorite (13-14%) was obtained from Reactolab SA (Servion, Switzerland). Ultrapure water (>18 MΩcm<sup>-1</sup>) was used for all aqueous solutions.

#### 3.2.2 Microorganisms

Bacteriophage MS2 (DSMZ 13767) and its *E. coli* host (DSMZ 5695) were purchased from the German Collection of Microorganisms and Cell Cultures (Braunschweig, Germany). Bacteriophage fr (ATCC-15767-B1) was purchased from LGC Standards (Molsheim, France). Bacteriophage GA was kindly provided by Dr. Joan Jofre (University of Barcelona). GA and fr were cultured in the same *E. coli* host as MS2. They were propagated as described previously<sup>108</sup> and infectivity was assessed by enumeration of plaque forming units (pfu) using the double agar layer method.<sup>109</sup>

#### 3.2.3 Disinfection experiments

UV<sub>254</sub>. Black reactors (5 ml) containing 2 mL virus samples were placed in black plastic tubes (3 cm in diameter and 17.5 cm in height) to optimize beam collimation, as described previously.<sup>116</sup> A low-pressure

18-W UV-C lamp (253.7 nm; model TUV T8; Philips) in a quasi-parallel beam setup was used to inactivate the phages. Samples were exposed to  $UV_{254}$  irradiance for periods between 0 and 10 min. The disinfection process was halted by removing the sample from the light source. The fluence entering the reactor was measured by actinometry<sup>134</sup> and corresponded to  $2.4 \text{ W/m}^2$ .

*Singlet oxygen.* 100  $\mu\text{L}$  of a 50 mg/L Rose Bengal (RB) solution was added to 2-ml virus samples, and reactors were exposed for periods between 0 and 45 min to light emitted from a Sun 2000 solar simulator (ABET Technologies, Milford, CT) equipped with a 1-kW Xe lamp and an AM1.5 and a UVB cutoff filter.<sup>108</sup> To compensate for RB photobleaching during the course of the experiments, 40  $\mu\text{L}$  and 27  $\mu\text{L}$  of the RB stock solution were added to the samples after 15 and 30 minutes, respectively. This enabled maintaining a stable singlet oxygen concentration of  $1.1 \cdot 10^{-11} \text{ M}$  ( $3.52 \cdot 10^{-7} \text{ mg/L}$ ) as determined by reaction with the probe compound furfuryl alcohol.<sup>43</sup> Disinfection was halted by removing the reactors from the light source. Control experiments conducted in the absence of light or RB did not show any inactivation.

*Free chlorine.* 10 mL virus samples containing FC (1.5 to 3 mg/liter FC) were stirred in chlorine-demand-free beakers (prepared by overnight soaking in concentrated FC solution). The FC concentration was monitored with the N,N-diethyl-p-phenylenediamine (DPD) colorimetric method<sup>109</sup> and FC loss throughout the kinetic experiments did not exceed 15%. To halt the disinfection process, samples were diluted into a 9-fold volume of Tris buffer (10 mM Tris, pH 7.4) to quench the FC.

*Chlorine dioxide.* Chlorine dioxide was produced by mixing 100 mL 4%  $\text{K}_2\text{S}_2\text{O}_8$  with 100 mL 2%  $\text{NaClO}_2$ <sup>110</sup> and was stored at 4°C. The resulting  $\text{ClO}_2$  stock concentration (250 to 1000 mg/L) was determined by spectrophotometry ( $\epsilon_{358\text{nm}} = 1200 \text{ M}^{-1}\text{s}^{-1}$ ).<sup>111</sup> Prior to experiments, the stock solution was diluted to a working solution of 0.5-2 mg/L  $\text{ClO}_2$  and was spiked with virus stock solution to the desired virus concentration. To compensate for  $\text{ClO}_2$  evaporation and consumption throughout the experiment, concentrated  $\text{ClO}_2$  (16 mg/L) was added at a rate of 20  $\mu\text{L/min}$  by means of a peristaltic pump (KdScientific, Holliston, MA). To halt the disinfection,  $\text{ClO}_2$  was quenched by addition of sodium thiosulfate (0.63 M) at a 20:1 sample/quenching agent ratio. Control samples confirmed that the addition of sodium thiosulfate did not result in inactivation.

### 3.2.4 Analysis of disinfection kinetics

For free chlorine, singlet oxygen and UV<sub>254</sub>, inactivation kinetics were fitted to a first-order Chick-Watson model (Eq.3.1):

$$\ln (C_v/C_{v,0}) = -k_{CW}C_d t \quad \text{Eq. 3.1}$$

where  $k_{CW}$  is the inactivation rate constant,  $C_d$  is the disinfectant concentration or UV<sub>254</sub> fluence (constant over the time of reaction), and  $C_v$  is the concentration of infective virus. For ClO<sub>2</sub>, virus inactivation was described by the Hom model according to the following equation (Eq. 3.2):

$$\ln (C_v/C_{v,0}) = -k_H C_d^n t^{m-1} \quad \text{Eq. 3.2}$$

where  $k_H$  is the Hom rate constant [(mgL<sup>-1</sup>sec<sup>m-1</sup>)<sup>-1</sup>],  $n$  is the dilution coefficient (set to 1 as only a single ClO<sub>2</sub> concentration was used), and  $m$  is the constant for the inactivation rate law that describes the deviation from the ideal Chick-Watson model (Eq. 3.1). The parameters for the Hom model were fitted in Sigmaplot (version: 12.0, 2011).

### 3.2.5 Quantitative Polymerase Chain Reaction (q-PCR)

200 µl RNA samples were extracted with a PureLink<sup>TM</sup> Viral RNA/DNA Kit (Invitrogen). Extracts were reverse transcribed and amplified with a Rotorgene 3000 quantitative PCR platform (Corbett Life Science, Sydney, Australia) as described previously.<sup>108</sup> For each virus, several genome segments (amplicons) were amplified, such that approximately 50% of the genome was covered. Fig. 3.1 shows the distribution and location of the analyzed amplicons. Additional details pertaining to the exact location and length of each amplicon analyzed, as well as the thermocycles used during the amplification, are given in the appendix in Tables C1 and C2. At the end of the 45<sup>th</sup> cycle a melting ramp from 72°C to 95°C with a 45 sec hold on the first step and a 5 sec hold on the following temperatures was performed. RNA standards were prepared for all viruses as described previously.<sup>108</sup>



Figure 3.1: Location and distribution of analyzed genome regions.

### 3.2.6 Quantification of damage to entire genome

The integrity of each amplicon was assessed, and the results were extrapolated as described by Pecson et al.<sup>135</sup> to quantify damage across the whole genome. Briefly, the probability of finding an intact amplicon  $i$  after a given level of inactivation corresponds to  $n_i/n_{i,0}$  for each amplicon, where  $n_{i,0}$  and  $n_i$  represent the number of intact genome copies detected before and after treatment, respectively. The probability of all tested amplicons being intact in one genome copy then corresponds to  $\prod n_i/n_{i,0}$ . The probability that an entire RNA strand is intact,  $N/N_0$ , can be extrapolated according to the following relationship (Eq. 3.3):

$$N/N_0 = (\prod n_i/n_{i,0})^{\left(\frac{\text{genome length}}{\text{total length of } i \text{ amplicons}}\right)} \quad \text{Eq. 3.3}$$

This extrapolation is valid only if the damage is evenly distributed across the entire genome, or if a large fraction of the entire genome is assayed. In this study, we measured approximately half of the entire genome, a strategy that we have previously shown to account for variability in the distribution of damage across the genome.<sup>135</sup>

Genome degradation rate constants ( $k_G$ ) were determined from first-order fits of genome degradation versus dose ( $C_d t$ ) (Eq. 3.4):<sup>136</sup>

$$\ln(N/N_0) = -k_G C_d t \quad \text{Eq. 3.4}$$

To determine if significant differences existed between genome degradation and inactivation of each phage, or if genome degradation or inactivation differed among the three phages, rate constants were compared by analysis of covariance (ANCOVA), whereby a  $p$  value of  $<0.05$  was deemed significant.

### 3.2.7 Experimental and predicted degradation rate constants of amplicons

Amplicon degradation rate constants ( $k_{\text{amp}}$ ) were determined from first-order fits of genome degradation versus dose ( $C_d t$ ) (Eq. 3.5):

$$\ln(n_i/n_{i,0}) = -k_{\text{amp}} C_d t \quad \text{Eq. 3.5}$$

where  $n_{i,0}$  and  $n_i$  represent the number of intact genome copies detected at time 0 and time  $t$ , respectively.

Degradation of free nucleotides by the disinfectants considered herein has been extensively studied, and the reported 2<sup>nd</sup> order rate constants for the reactions with  $^1\text{O}_2$ , FC and  $\text{ClO}_2$ ,<sup>137–140</sup> as well as the quantum yields and molar absorptivities for photolysis by  $\text{UV}_{254}$ <sup>136,141</sup> are summarized in Table 3.1.

**Table 3.1: Reported nucleotide degradation rate constants, molar absorptivities ( $\epsilon_{254}$ ) and quantum yields ( $\phi$ ).** FC measured at pH 7. \* Values for adenosine monophosphate (AMP), cytosine monophosphate (CMP), guanosine monophosphate (GMP) and uridine monophosphate (UMP). \*\* Value is for T-T dimer.

Nucleotide	$\text{UV}_{254}$		$^1\text{O}_2$	FC	$\text{ClO}_2$
	$\epsilon_{254\text{nm}} [\text{M}^{-1}\text{cm}^{-1}]^{136}$	$\Phi [\%]^{141}$	$k [\text{M}^{-1}\text{s}^{-1}]^{137}$	$k [\text{M}^{-1}\text{s}^{-1}]^{138,139}$	$k [\text{M}^{-1}\text{s}^{-1}]^{140}$
Adenine	$1.19 \cdot 10^4$	$4.4 \cdot 10^{-4}$	$3.85 \cdot 10^4$	$6.40^*$	
Cytosine	$3.50 \cdot 10^3$	$5.3 \cdot 10^{-4}$	$3.08 \cdot 10^5$	$6.60 \cdot 10^{1*}$	
Guanine	$1.02 \cdot 10^4$	$2.1 \cdot 10^{-4}$	$1.00 \cdot 10^6$	$2.10 \cdot 10^{4*}$	$1.50 \cdot 10^{3*}$
Uracil	$7.69 \cdot 10^3$	$1.4 \cdot 10^{-3}$	$5.00 \cdot 10^5$	$5.5 \cdot 10^{3*}$	
Uracil dimer	$1.54 \cdot 10^4$	$2.6 \cdot 10^{-3**}$			

Based on these values, in conjunction with the abundance of each nucleotide in the different viral genomes or amplicons depicted in Table 3.2, a predicted degradation rate constant for each genome or amplicon and disinfectant. For  $\text{UV}_{254}$ , the first order rate constant was calculated by multiplying the molar absorption by the quantum yield. Hereby not only the nucleotide content was taken into account but also the quantity of adjacent uracils, as uracil dimers are the most important genome photoproduct.<sup>142</sup>

**Table 3.2: Number of copies and percentage of each nucleotide in the genome of each bacteriophage.**

	Adenine		Cytosine		Guanine		Uracil		UU dimers
	number	%	number	%	number	%	number	%	
<b>MS2</b>	835	23.4	933	26.1	927	26.0	874	25.5	169
<b>fr</b>	875	24.5	887	24.8	950	26.6	863	24.1	172
<b>GA</b>	844	24.3	838	24.2	821	23.7	963	27.8	217

### 3.3 Results

#### 3.3.1 Comparison of inactivation kinetics

Inactivation kinetics for each virus upon treatment by the different disinfectants is shown in Fig. 3.2. Inactivation by  $UV_{254}$ ,  $^1O_2$  and FC was first-order with respect to dose (Eq. 3.1). For  $ClO_2$ , in contrast, inactivation deviated from first-order and exhibited significant tailing at higher doses. Consequently, inactivation rate constants for  $ClO_2$  were determined by a fit to the Hom model (Eq. 3.2).

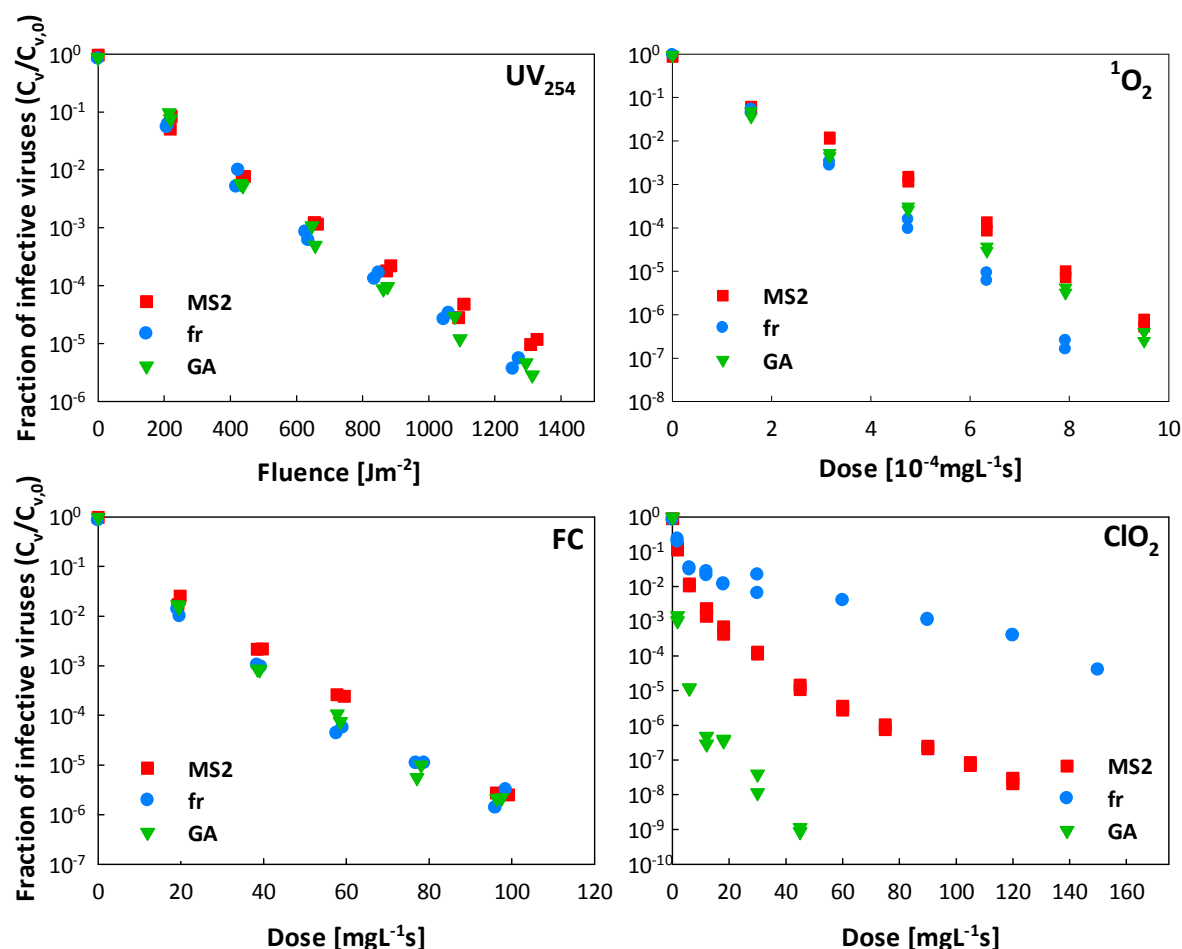


**Figure 3.2: Comparison of disinfection kinetics.** Representation of kinetics of the three phages upon treatment by the four disinfectants investigated. Statistically significant differences in inactivation were found for the following combinations: UV<sub>254</sub>: GA-MS2 ( $p = 0.027$ );  $^1\text{O}_2$ : MS2-fr ( $p < 0.001$ ), MS2-GA ( $p = 0.022$ ), fr-GA ( $p < 0.001$ );  $\text{ClO}_2$ : MS2-fr ( $p = 0.026$ ), MS2-GA ( $p = 0.007$ ), fr-GA ( $p = 0.001$ ).

The inactivation rate constants for all treatments are summarized in Fig. 3.3 and the exact values and associated uncertainties are listed in Table 3.3. For free chlorine, the inactivation rate constants did not significantly differ between the three viruses. In contrast, for UV<sub>254</sub> a significantly higher rate constant was found for GA compared to MS2 ( $p = 0.027$ ). For singlet oxygen and  $\text{ClO}_2$  all three viruses were inactivated at different rates: for  $\text{ClO}_2$  the sequence of inactivation in the initial, linear part of the inactivation curve followed the order  $\text{fr} < \text{MS2} < \text{GA}$  ( $p = 0.026$  for MS2 vs fr;  $p = 0.007$  for MS2 vs GA;  $p = 0.001$  for fr vs GA), whereas for singlet oxygen, the order was  $\text{MS2} < \text{GA} < \text{fr}$  ( $p < 0.001$  for MS2 vs fr;  $p = 0.022$  for MS2 vs GA;  $p < 0.001$  for fr vs GA).

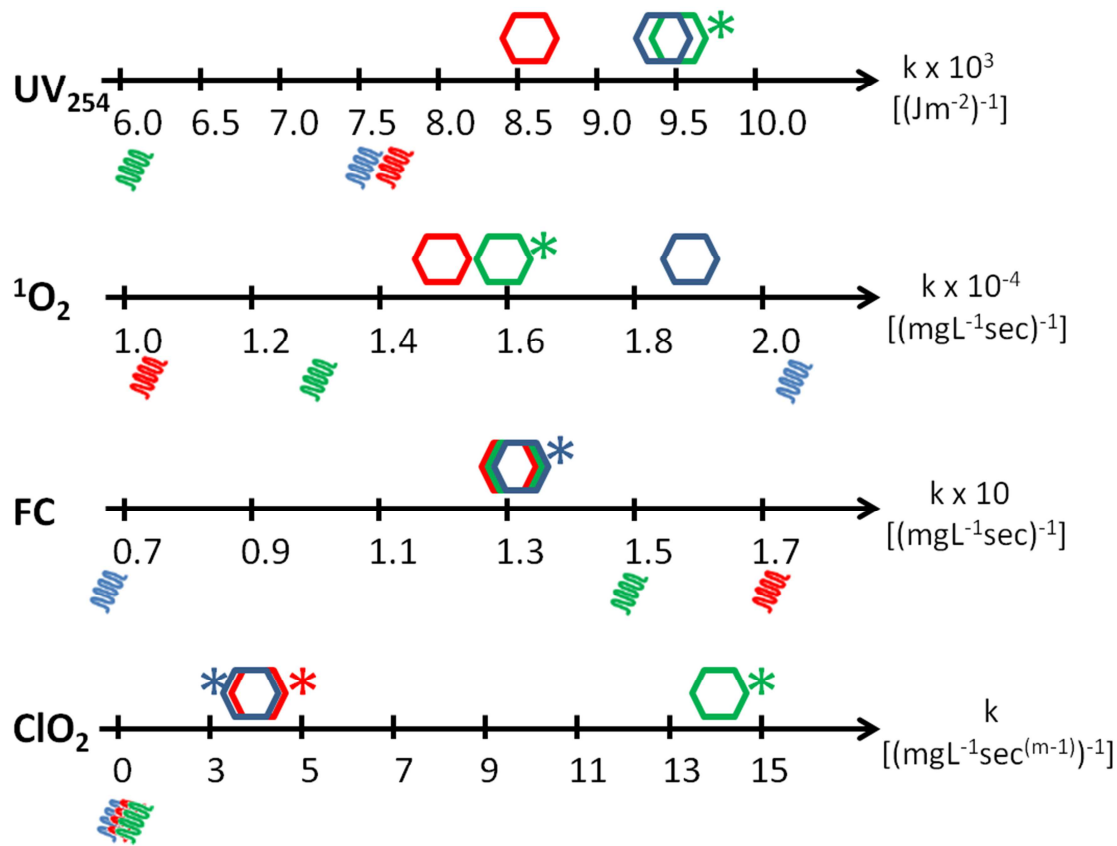


**Figure 3.3: Overview of the inactivation rate constants (hexagons) and genome degradation rate constants (spirals) for all four disinfecting treatments.** Values for MS2 are shown in red, those for fr are shown in blue and those for GA are shown in green. The asterisks indicate virus-treatment pairs where genome degradation could not account for inactivation. Exact values and associated errors are listed in Table 3.3 (inactivation) and Table 3.4 (genome damage).

**Table 3.3: Inactivation rate constants for each virus and each disinfectant.** The error represents the standard error.

Bacteriophage	UV <sub>254</sub> , $k_{CW}$ [[Jm <sup>-2</sup> ) <sup>-1</sup> ]	<sup>1</sup> O <sub>2</sub> , $k_{CW}$ [(mgL <sup>-1</sup> sec) <sup>-1</sup> ]	FC, $k_{CW}$ [(mgL <sup>-1</sup> sec) <sup>-1</sup> ]	ClO <sub>2</sub> , $k_H$ [(mgL <sup>-1</sup> sec <sup>m-1</sup> ) <sup>-1</sup> ]
MS2	$8.6 \cdot 10^{-3} \pm 1.1 \cdot 10^{-3}$	$1.5 \cdot 10^4 \pm 0.3 \cdot 10^3$	$1.3 \cdot 10^{-1} \pm 0.1 \cdot 10^{-1}$	$3.7 \pm 0.1$ $m = 1.46 \pm 0.01$
fr	$9.5 \cdot 10^{-3} \pm 1.1 \cdot 10^{-3}$	$2.0 \cdot 10^4 \pm 0.3 \cdot 10^3$	$1.3 \cdot 10^{-1} \pm 0.1 \cdot 10^{-1}$	$3.3 \pm 0.5$ $m = 1.35 \pm 0.03$
GA	$9.6 \cdot 10^{-3} \pm 1.0 \cdot 10^{-3}$	$1.6 \cdot 10^4 \pm 0.3 \cdot 10^3$	$1.3 \cdot 10^{-1} \pm 0.1 \cdot 10^{-1}$	$14.2 \pm 1.1$ $m = 1.31 \pm 0.02$



### 3.3.2 Comparison of levels of genome degradation

Genome degradation as a function of disinfectant dose is shown in Fig. 3.4. This representation illustrates the genome-damaging capacity of a specific treatment, as well as the differences between each virus. The corresponding experimental degradation rate constants as well as the predicted ones are summarized in Figure 3.3 and Table 3.4.  $UV_{254}$ , FC and  $^1O_2$  were all capable of degrading the genome in each virus. Only subtle differences were observed among the three viruses: for  $UV_{254}$ , genome degradation proceeded at the same rate for all viruses; upon treatment by  $^1O_2$ , the fr genome degraded slightly faster than the MS2 ( $p = 0.029$ ) and GA ( $p = 0.005$ ) genomes; the opposite was found for free chlorine, which degraded the fr genome more slowly than it did the MS2 ( $p = 0.006$ ) and GA ( $p = 0.011$ ) genomes. Notably,  $ClO_2$  did not induce genome damage in any of the viruses.

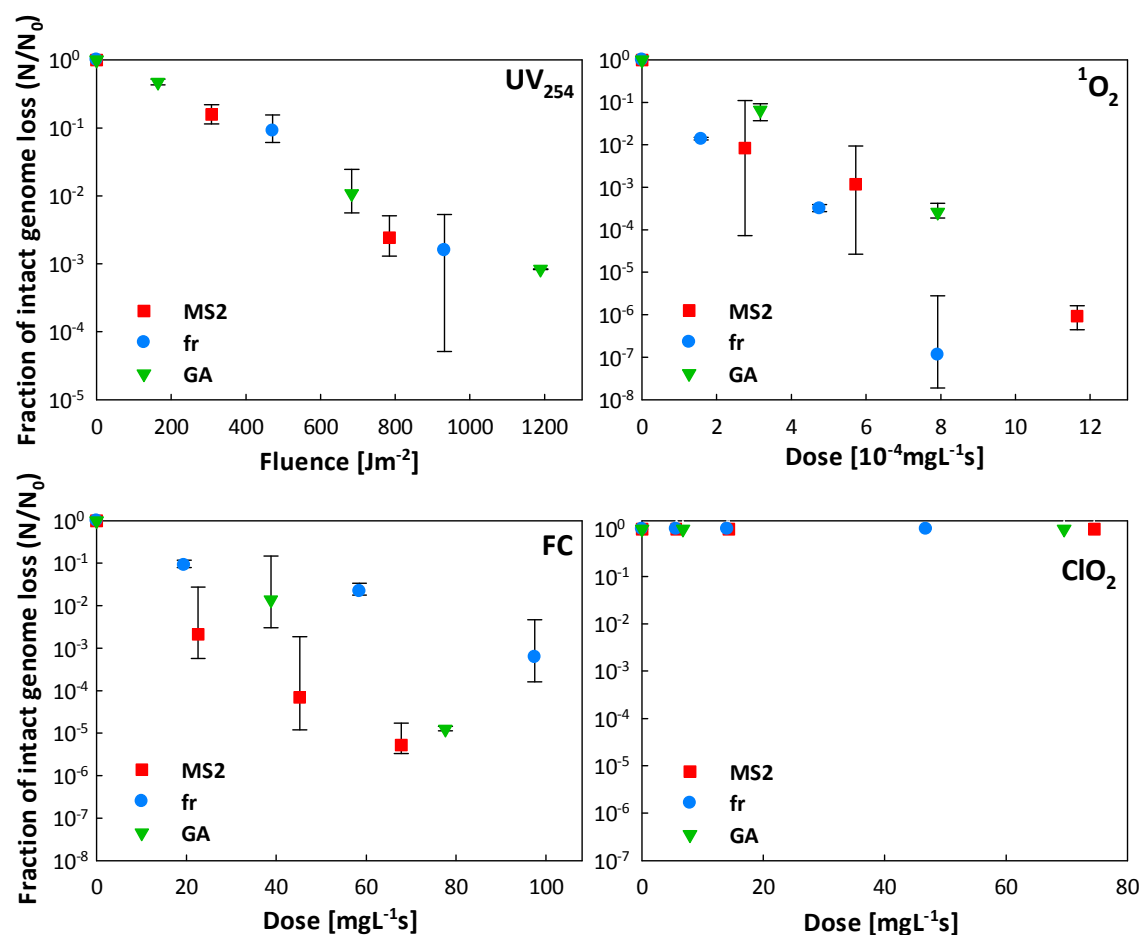


**Figure 3.4: Comparison of genome damage of the three phages upon inactivation by the four disinfectants investigated.** Statistically significant differences in genome degradation were found for the following combinations:  $^1O_2$ : fr-MS2 ( $p = 0.029$ ), fr-GA ( $p = 0.005$ ); FC: MS2-fr ( $p = 0.006$ ), fr-GA ( $p = 0.011$ ). Genome degradation upon exposure to  $ClO_2$  was not different from zero.

**Table 3.4: Predicted and experimental genome degradation rate constants for each virus and each disinfectant.** The uncertainties are given as standard error. The experimental rate constants for  $\text{ClO}_2$  were not significantly different from 0 (NS).

Bacteriophage	$\text{UV}_{254}, k_G [(\text{Jm}^{-2})^{-1}]$		$^1\text{O}_2, k_G [(\text{mgL}^{-1}\text{sec})^{-1}]$	
	Predicted	Experimental	Predicted	Experimental
<b>MS2</b>	$4.6 \cdot 10^{-3}$	$7.7 \cdot 10^{-3} \pm 1.4 \cdot 10^{-3}$	$5.2 \cdot 10^4$	$1.1 \cdot 10^4 \pm 0.2 \cdot 10^4$
<b>fr</b>	$4.6 \cdot 10^{-3}$	$7.5 \cdot 10^{-3} \pm 1.6 \cdot 10^{-3}$	$5.3 \cdot 10^4$	$2.0 \cdot 10^4 \pm 0.2 \cdot 10^4$
<b>GA</b>	$4.9 \cdot 10^{-3}$	$6.1 \cdot 10^{-3} \pm 0.7 \cdot 10^{-3}$	$5.0 \cdot 10^4$	$1.3 \cdot 10^4 \pm 0.2 \cdot 10^4$
Bacteriophage	$\text{FC}, k_G [(\text{mgL}^{-1}\text{sec})^{-1}]$		$\text{ClO}_2, k_G [(\text{mgL}^{-1}\text{sec})^{-1}]$	
	Predicted	Experimental	Predicted	Experimental
<b>MS2</b>	$4.6 \cdot 10^2$	$1.7 \cdot 10^{-1} \pm 0.3 \cdot 10^{-1}$	$2.1 \cdot 10^1$	NS
<b>fr</b>	$4.7 \cdot 10^2$	$6.9 \cdot 10^{-2} \pm 1.4 \cdot 10^{-2}$	$2.1 \cdot 10^1$	NS
<b>GA</b>	$4.3 \cdot 10^2$	$1.5 \cdot 10^{-1} \pm 0.2 \cdot 10^{-1}$	$1.8 \cdot 10^1$	NS

To measure the importance of genome damage as a mechanism of inactivation, the extent of genome damage was directly compared to inactivation (Fig. 3.5). Three possibilities exist: *i*) if  $N/N_0 < C_v/C_{v,0}$  (slope of genome degradation versus inactivation in Fig. 3.5  $< 1$ ), there is more virus inactivation than genome damage, and therefore, genome damage can only partially contribute to the overall inactivation. In this scenario, some population of inactivated viruses must contain intact genomes. *ii*) If  $N/N_0 = C_v/C_{v,0}$  (slope in Fig. 3.5  $= 1$ ), there is sufficient genome damage to fully account for the loss of infectivity, assuming that each genome lesion causes inactivation (single-hit model). And *iii*), if  $N/N_0 > C_v/C_{v,0}$  (slope in Fig. 3.5  $> 1$ ), then infective viruses with damaged genomes are present. This implies that the virus can sustain multiple genome lesions before becoming inactivated.

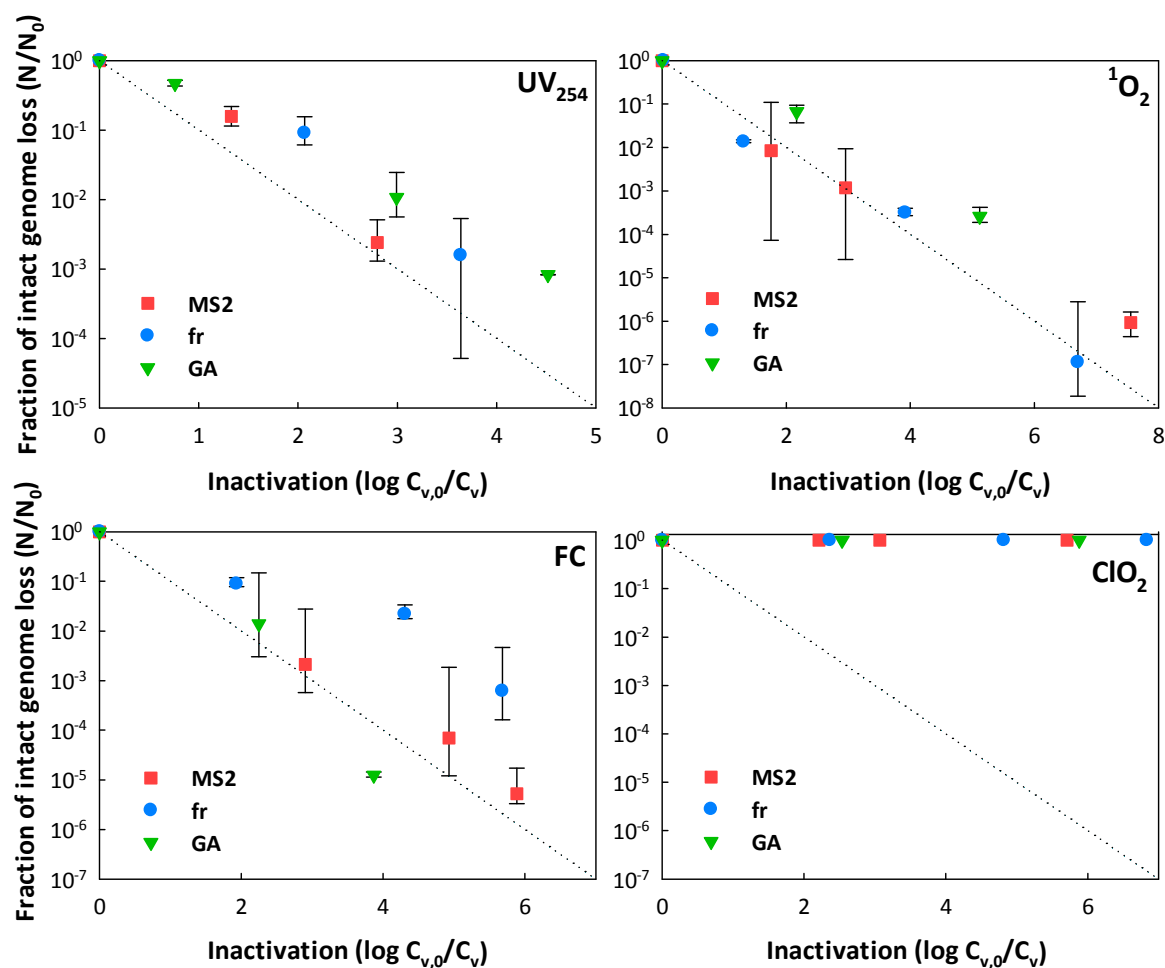


**Figure 3.5: Comparison of genome damage and virus inactivation of the three bacteriophages upon inactivation by the four disinfectants.** The dotted line represents a 1:1 relation between inactivation and genome degradation. Besides  $\text{ClO}_2$ , which did not induce genome damage, significantly slower genome degradation than inactivation was observed for the following combinations: fr-FC ( $p = 0.004$ ), GA- $\text{UV}_{254}$  ( $p = 0.003$ ) and GA- $^1\text{O}_2$  ( $p = 0.033$ ).

As can be seen from Figure 3.5, genome damage could not fully account for inactivation of any virus by  $\text{ClO}_2$  (slope < 1). In addition, three further virus-disinfectant combinations yielded less genome damage than inactivation: fr-FC ( $p = 0.004$ ), GA- $\text{UV}_{254}$  ( $p = 0.003$ ), and GA- $^1\text{O}_2$  ( $p = 0.033$ ). For these combinations of virus and disinfectant, protein degradation must therefore play a role in the inactivation process. For the remaining virus-disinfectant pairs, the extent of inactivation corresponded to that of genome degradation (slope = 1). No virus-disinfectant combination yielded an obvious multihit scenario (slope > 1).

### 3.3.3 Distribution of genome damage

To investigate the effect of genome structure on susceptibility to disinfectants, approximately half of the genomes were assayed for each of the viruses, and the degradation of small genome segments (amplicons of 300-700 nt lengths; Fig. 3.1 and Table C1) distributed across the genome were analyzed and compared. These measured degradation rate constants were also compared to the ones predicted based on both the amplicon composition and the reported reaction rates of free nucleotides with the given disinfectant (Table 3.5). The predicted and experimental amplicon degradation rate constants are shown in Figure 3.6. For the sake of clarity, only MS2 is represented in the figure; however, similar trends were observed for all three viruses, and the corresponding values are shown in Table 3.5.

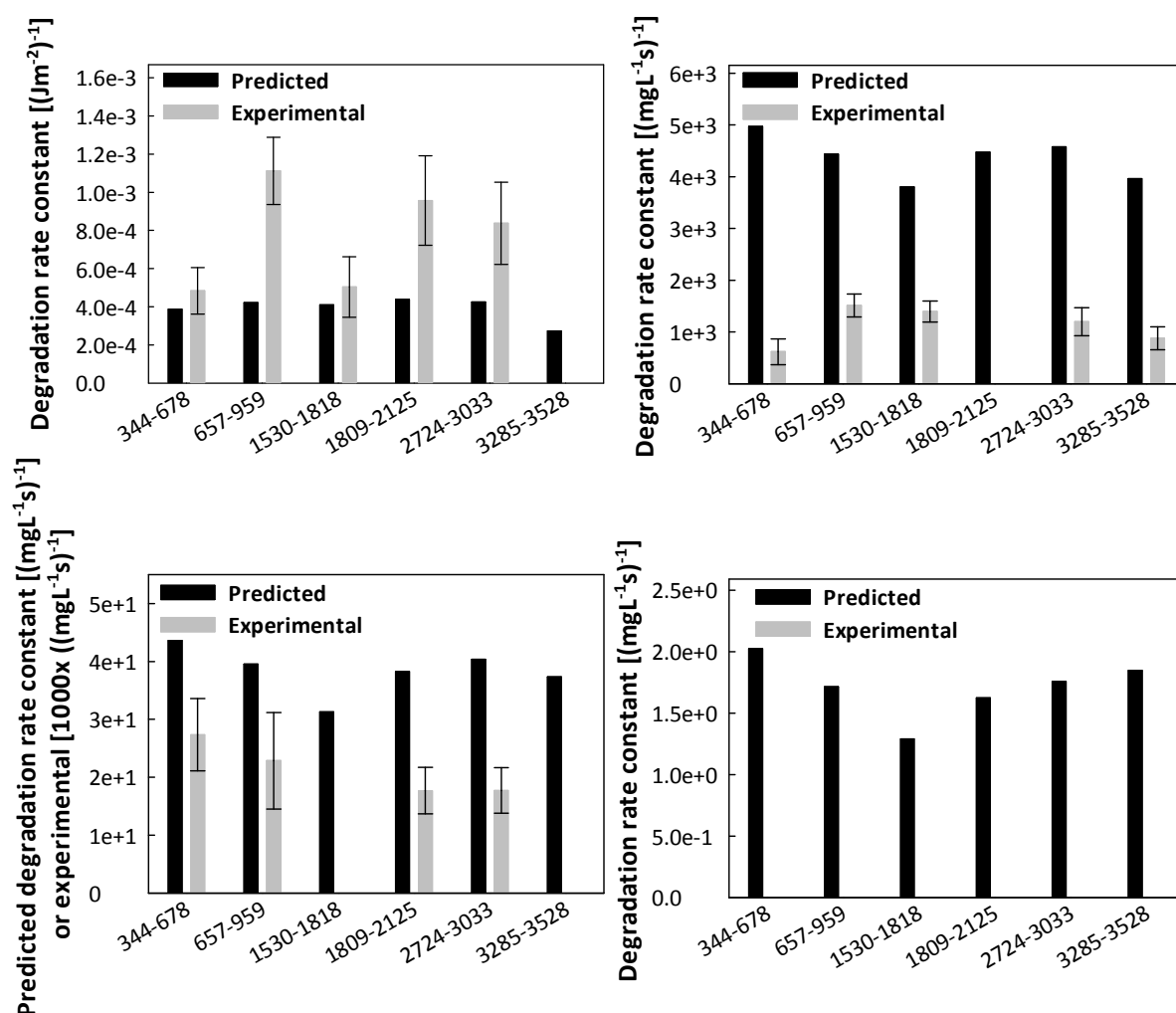


**Figure 3.6: Comparison of predicted and experimental amplicon degradation rate constants for MS2 upon UV<sub>254</sub>, <sup>1</sup>O<sub>2</sub>, FC and ClO<sub>2</sub>.** Experimental values for FC were multiplied by 1000 to allow comparison. Error bars indicate the standard error. For ClO<sub>2</sub>, only predicted values are shown, as no degradation was observed experimentally.

**Table 3.5: Experimental and predicted degradation rate constants ( $k_{\text{amp}}$ ) for each amplicon.** The uncertainties represent the standard error. NS indicates non-significant decay.

Bacteriophage	Amplicon	UV <sub>254</sub> , $k_{\text{amp}}$ [(Jm <sup>-2</sup> ) <sup>-1</sup> ]		<sup>1</sup> O <sub>2</sub> , $k_{\text{amp}}$ [(mgL <sup>-1</sup> sec) <sup>-1</sup> ]	
		Predicted	Experimental	Predicted	Experimental
MS2	344-678	$3.9 \cdot 10^{-4}$	$4.8 \cdot 10^{-4} \pm 1.2 \cdot 10^{-4}$	$5.0 \cdot 10^3$	$6.0 \cdot 10^2 \pm 3.0 \cdot 10^2$
	657-959	$4.2 \cdot 10^{-4}$	$1.1 \cdot 10^{-3} \pm 0.2 \cdot 10^{-3}$	$4.4 \cdot 10^3$	$1.5 \cdot 10^3 \pm 0.2 \cdot 10^3$
	1530-1818	$4.1 \cdot 10^{-4}$	$5.0 \cdot 10^{-4} \pm 1.6 \cdot 10^{-4}$	$3.8 \cdot 10^3$	$1.4 \cdot 10^3 \pm 0.2 \cdot 10^3$
	1809-2125	$4.4 \cdot 10^{-4}$	$9.6 \cdot 10^{-4} \pm 2.4 \cdot 10^{-4}$	$4.5 \cdot 10^3$	NS
	2724-3033	$4.3 \cdot 10^{-4}$	$8.4 \cdot 10^{-4} \pm 2.2 \cdot 10^{-4}$	$4.6 \cdot 10^3$	$1.2 \cdot 10^3 \pm 0.3 \cdot 10^3$
	3285-3528	$2.7 \cdot 10^{-4}$	NS	$4.0 \cdot 10^3$	$9.0 \cdot 10^2 \pm 2.0 \cdot 10^2$
fr	90-765	$8.2 \cdot 10^{-4}$	$1.8 \cdot 10^{-3} \pm 0.4 \cdot 10^{-3}$	$10.1 \cdot 10^3$	$3.8 \cdot 10^3 \pm 0.3 \cdot 10^3$
	1935-2566	$8.0 \cdot 10^{-4}$	$2.0 \cdot 10^{-3} \pm 0.5 \cdot 10^{-3}$	$9.3 \cdot 10^3$	$3.2 \cdot 10^3 \pm 0.3 \cdot 10^3$
	3018-3503	$5.7 \cdot 10^{-4}$	NS	$7.6 \cdot 10^3$	$2.8 \cdot 10^3 \pm 0.4 \cdot 10^3$
GA	967-1559	$5.9 \cdot 10^{-4}$	$1.1 \cdot 10^{-3} \pm 0.7 \cdot 10^{-4}$	$5.7 \cdot 10^3$	$3.0 \cdot 10^3 \pm 0.4 \cdot 10^3$
	1587-1945	$8.6 \cdot 10^{-4}$	$8.9 \cdot 10^{-4} \pm 1.1 \cdot 10^{-4}$	$8.5 \cdot 10^3$	$1.8 \cdot 10^3 \pm 0.4 \cdot 10^3$
	2143-2523	$5.1 \cdot 10^{-4}$	$5.1 \cdot 10^{-4} \pm 0.9 \cdot 10^{-4}$	$5.0 \cdot 10^3$	NS
	2533-2926	$5.1 \cdot 10^{-4}$	$7.0 \cdot 10^{-4} \pm 0.9 \cdot 10^{-4}$	$5.7 \cdot 10^3$	$2.0 \cdot 10^3 \pm 0.4 \cdot 10^3$
	2958-3343	$5.3 \cdot 10^{-4}$	$5.8 \cdot 10^{-4} \pm 1.1 \cdot 10^{-4}$	$5.8 \cdot 10^3$	$1.2 \cdot 10^3 \pm 0.3 \cdot 10^3$
Bacteriophage	Amplicon	FC, $k_{\text{amp}}$ [(mgL <sup>-1</sup> sec) <sup>-1</sup> ]		ClO <sub>2</sub> , $k_{\text{amp}}$ [(mgL <sup>-1</sup> sec) <sup>-1</sup> ]	
		Predicted	Experimental	Predicted	Experimental
MS2	344-678	$4.4 \cdot 10^1$	$2.7 \cdot 10^{-2} \pm 0.6 \cdot 10^{-2}$	2.0	NS
	657-959	$4.0 \cdot 10^1$	$2.3 \cdot 10^{-2} \pm 0.8 \cdot 10^{-2}$	1.7	NS
	1530-1818	$3.1 \cdot 10^1$	NS	1.3	NS
	1809-2125	$3.8 \cdot 10^1$	$1.8 \cdot 10^{-2} \pm 0.4 \cdot 10^{-2}$	1.6	NS
	2724-3033	$4.0 \cdot 10^1$	$1.8 \cdot 10^{-2} \pm 0.4 \cdot 10^{-2}$	1.8	NS
	3285-3528	$3.7 \cdot 10^1$	NS	1.9	NS
fr	90-765	$9.1 \cdot 10^1$	$1.0 \cdot 10^{-2} \pm 0.2 \cdot 10^{-2}$	4.2	NS
	1935-2566	$8.4 \cdot 10^1$	$0.9 \cdot 10^{-2} \pm 0.3 \cdot 10^{-2}$	3.8	NS
	3018-3503	$7.1 \cdot 10^1$	$1.4 \cdot 10^{-2} \pm 0.2 \cdot 10^{-2}$	3.3	NS
GA	967-1559	$4.8 \cdot 10^1$	$1.3 \cdot 10^{-2} \pm 0.2 \cdot 10^{-2}$	1.9	NS
	1587-1945	$7.4 \cdot 10^1$	$8.0 \cdot 10^{-3} \pm 1.0 \cdot 10^{-3}$	3.1	NS
	2143-2523	$4.2 \cdot 10^1$	$7.0 \cdot 10^{-3} \pm 1.0 \cdot 10^{-3}$	1.7	NS
	2533-2926	$5.2 \cdot 10^1$	$9.0 \cdot 10^{-3} \pm 1.0 \cdot 10^{-3}$	2.3	NS
	2958-3343	$5.1 \cdot 10^1$	$9.0 \cdot 10^{-3} \pm 1.0 \cdot 10^{-3}$	2.2	NS

Fig. 3.6 illustrates that the measured amplicon degradation was heterogeneously distributed across the genome, yet it never differed by more than a factor of 3 for any disinfectant. Furthermore, except for FC, the measured degradation did not follow the trend of the predicted, more homogeneously distributed one. Finally, the experimental and predicted values for FC differed by three orders of magnitude. For UV<sub>254</sub> and <sup>1</sup>O<sub>2</sub>, in contrast, the experimental values were close to the predicted ones. For ClO<sub>2</sub>, only the predicted values are plotted as the experimental ones are not significant.

### 3.4 Discussion

The inactivation kinetics results (Figs. 3.2-3.3 and Table 3.3) illustrate the complexity of predicting virus inactivation: depending on the disinfectant, the three viruses exhibited equal, similar, or greatly different inactivation rates; furthermore, their relative susceptibilities changed with disinfectant. However, our data indicate that, despite their (small) differences in composition, the genomes of all three viruses were affected by the disinfectants in roughly the same way: genome damage was strong for inactivation by UV<sub>254</sub>, free chlorine and singlet oxygen, and not measurable for chlorine dioxide (Figs. 3.4 and 3.5).

Our previous work on MS2 has shown that for UV<sub>254</sub> and <sup>1</sup>O<sub>2</sub>, the main disinfection target is the viral genome.<sup>56</sup> In contrast, ClO<sub>2</sub> leaves the genome intact and acts solely on the viral proteins. Inactivation by free chlorine, finally, is mediated by damage to both genome and proteins. If the inactivation mechanisms are the same for all three phages, then one would expect that differences in the genome composition can account for the observed differences in inactivation by UV<sub>254</sub> and <sup>1</sup>O<sub>2</sub>, to a lesser extent by FC, but not at all for ClO<sub>2</sub>. In other words, if the composition of the genomes directly influences genome degradation, then it should also govern the inactivation of the three phages by UV<sub>254</sub> and <sup>1</sup>O<sub>2</sub>. This effect is expected to be less apparent for FC, and absent for ClO<sub>2</sub>.

To test these assumptions, the observed genome degradation rate constants were compared with those predicted based on composition (Table 3.4), as well as with the concurrent inactivation rate constants (Table 3.3).

#### 3.4.1 Influence of genome composition on degradation and inactivation

Genome degradation may be related to genome length, nucleotide content, and genome structure. More specifically, longer genomes offer more targets for attack, higher contents of guanine (the most easily oxidizable nucleobase; Table 3.1) may increase the susceptibility to oxidants, and genome

structure may dictate the accessibility of oxidants to the reactive sites. *fr*, which contains 3575 nucleotides in its genome compared to MS2's 3569 and GA's 3466, should thus be slightly more susceptible to disinfection. In addition to having the longest genome, *fr* contains the highest proportion of guanine (G; 26.6%; Table 3.2), which is the most easily oxidizable nucleotide. Consequently, if the main inactivation mechanism is genome damage, *fr* is predicted to be the most readily inactivated by oxidants. In contrast, for UV<sub>254</sub>, adjacent uracils are the most important feature, of which GA contains the most (Table 3.2).

It should be noted at this point that the predicted genome degradation is based solely on the reported rate constants for free nucleotides. However, incorporation of nucleotides into viral RNA may alter their reactivity. In addition, the packing of the genome inside the virus as well as the binding sites between RNA and capsid protein have been investigated by electron microscopy<sup>143,144</sup> and have been shown to exhibit a partly specific secondary structure.<sup>145</sup> This secondary structure may create genome regions that are not solvent accessible, and hence not easily accessible to dissolved disinfectants, resulting in less degradation than expected based on the nucleotide content alone.

Despite these limitations, some basic agreement between the predicted and observed genome degradation rates was observed. Most importantly, the difference between genome degradation for all three viruses was predicted to be small, maximally 10% (Table 3.2). This is consistent with our findings, in which only small differences in the genome degradation rate constants were observed amongst the three viruses and UV<sub>254</sub>, <sup>1</sup>O<sub>2</sub>, and FC treatments (Table 3.4). In addition, this was consistent with the observed inactivation trends: for those disinfectants affecting the genome (UV<sub>254</sub>, singlet oxygen and FC), only small differences were found between the inactivation of the three phages (Figs. 3.2 and 3.3, Table 3.3). However, if investigated in detail, it is apparent that discrepancies do exist between the predicted and the experimentally determined order of genome degradation and inactivation. In the following paragraphs, the observed trends are discussed for each disinfectant individually.

### 3.4.2 UV<sub>254</sub>

Uracil dimers are the main product following RNA irradiation by UV<sub>254</sub>,<sup>142</sup> hence, adjacent uracils are the genome feature most prone to degradation by UV<sub>254</sub>. Among the three viruses, GA contains most adjacent uracils (Table 3.2), and hence, GA's genome is expected to degrade most rapidly. The experimental findings, however, show that inactivation by UV<sub>254</sub> caused no significant difference in the

extent of genome damage among the three viruses (Fig. 3.4; Table 3.4). This thus suggests that the composition of the genome is not the only factor determining its degradation rate. Instead, the secondary and tertiary structure of the genome may also influence its degradation.

Given that the genome is the main target of  $UV_{254}$ , inactivation of the three phages was expected to be directly related to their extent of genome damage. However, despite their similar extent of genome damage, GA was inactivated more rapidly than MS2 (Figs. 3.2 and 3.3, Table 3.3). In addition, its genome damage was insufficient to account for inactivation (Figs. 3.3 and 3.5). Overall, this implies that the mechanism of  $UV_{254}$  inactivation differs between the phages: while genome damage may be the main inactivation mechanism for MS2<sup>56</sup> and fr, protein damage must contribute to the inactivation of GA.

### 3.4.3 Singlet oxygen

For singlet oxygen, damage to the genome (oxidative genome lesions<sup>56,132</sup> as well as RNA-protein crosslinks)<sup>146</sup> has been identified as the main inactivating factor. Therefore inactivation was expected to follow the same trend as genome degradation. Based on genome composition, fr should inactivate faster than GA or MS2, since its genome contains the most guanines (Table 3.2). This was seen to some extent in our results; indeed, fr did exhibit faster genome decay than GA and MS2 (Figs. 3.3 and 3.4, Table 3.4), though comparison with MS2 did not yield a statistically significant difference. Correspondingly, inactivation was faster for fr than for MS2 and GA (Figs. 3.2 and 3.3, Table 3.3). Differences in genomic content among the three viruses may thus be responsible for the observed inactivation rate differences.

The extent of genome degradation in fr and MS2 roughly corresponded to its extent of inactivation by  $^1O_2$  ( $N/N_0 = C_v/C_{v,0}$ ; Fig 3.5). Notably, however, genome damage was not extensive enough to account for the inactivation of GA ( $N/N_0 < C_v/C_{v,0}$ ; Figs. 3.5). There must consequently be an additional protein component that controls the inactivation of GA. Similar to what was observed for  $UV_{254}$ , the mechanism of inactivation is thus different for GA than for the other two phages.

### 3.4.4 Free chlorine

Our previous results showed that FC caused extensive genome damage, but that inactivation was also accompanied by significant protein damage as well.<sup>56</sup> Other reports suggest that genome damage is entirely responsible for inactivation by FC.<sup>55,147</sup> The findings herein confirm that FC caused extensive genome damage in all three phages. However, fr's genome was found to degrade slower than GA's and



MS2's (Figs. 3.3 and 3.4, Table 3.4). This finding was surprising for two reasons: first, the high guanine content of fr should make it the most reactive; second, another oxidant,  $^1\text{O}_2$ , reacted fastest with the fr genome. These arguments support the conclusion that structural features of the RNA have varied impacts on different oxidants.

Regardless of their different genome degradation rates, the three bacteriophages inactivated at a similar rate (Figs. 3.2 and 3.3, Table 3.3). This is consistent with our previous findings for MS2<sup>56</sup> that despite the major role of genome degradation, inactivation is in part controlled by a protein component.

In this context it should be emphasized that our approach to measure genome damage by q-PCR may only be an approximation of the actual biologically relevant damage. The first step in the q-PCR method relies on a reverse transcriptase to create a DNA strand from viral RNA. In contrast, in the infectivity assay, genome replication involves RNA-dependent RNA polymerases. Different polymerases are known to differ in their read-through capacity of genome lesions;<sup>148–152</sup> therefore it is possible that these two enzymes exhibit a different level of tolerance when exposed to damaged genomes. Our method may overestimate genome damage by detecting both the lesions that cause inactivation, as well as lesions that are not lethal. Hence, even though extensive genome damage upon FC treatment was measured by q-PCR, it is possible that only a small fraction of it led to virus inactivation.

### 3.4.5 Chlorine dioxide

Inactivation by  $\text{ClO}_2$  did not lead to quantifiable genome degradation (Fig. 3.4), confirming our previous results and other reports that the mechanism of bacteriophage inactivation is entirely protein dependent.<sup>56,106,153</sup> The lack of genome damage is surprising given the rather large predicted genome degradation rate constants (Table 2). In addition, the rather small size of the chlorine dioxide molecule should allow it to penetrate the virus capsid by way of the 1-2 nm pores in the capsid, and to access the genome. The absence of genome damage may be explained by the fact that chlorine dioxide reacts more rapidly with some amino acids than with nucleotides (e.g., tryptophan reacts at least 75 times faster than the most susceptible nucleotide G, Table 3.1)<sup>128,154</sup>. Hence by the time detectable genome damage has accumulated, the virus may have already been inactivated as a result of protein damage.

### 3.4.6 Location in genome damage influences degradation

To better understand the discrepancies between the measured and predicted trends in genome degradation, we individually analyzed the degradation behavior of smaller genome segments (amplicons) distributed throughout the genome, and compared them against each other, as well as to their predicted degradation rate constants (Fig. 3.6 and Table 3.5). According to predictions, UV<sub>254</sub> should damage MS2's amplicon 1809-2125 most and 3258-3528 least, whereas for the three other oxidants, amplicon 344-678 should be the most susceptible and 1530-1818 the most resistant. As shown in Fig. 3.6, however, the damage was not distributed as predicted. Notably, amplicon 657-959 incurred the most damage for all treatments (except ClO<sub>2</sub>, for which no significant damage was measured), whereas 344-678 incurred the least damage by UV<sub>254</sub> and <sup>1</sup>O<sub>2</sub>. Similar arguments can be made for GA and fr (Table 3.5). It appears that there is little correlation between predicted and actual genome damage, even if small segments are considered individually. As discussed above, this suggests that oxidants were not able to access certain genome regions, resulting in a poor correlation between experimental and predicted genome degradation. In contrast to oxidants, UV<sub>254</sub> is not limited by solvent-accessibility, and may thus be able to access the entirety of the genome. Surprisingly, however, this was not confirmed by our results, indicating that RNA structural features also protect parts of the genome from UV<sub>254</sub>.

Finally, the experimental degradation rates for free chlorine and chlorine dioxide were found to be much smaller than the predicted ones, whereas those for UV<sub>254</sub> and <sup>1</sup>O<sub>2</sub> were of similar magnitude. We suggest that this is due to the fact that FC and ClO<sub>2</sub> are non-specific oxidants that can readily react with the proteins surrounding the genome. This lowers their effective concentration available to damage the genome. Close vicinity of genome and protein may thus protect the genome from degradation by FC and ClO<sub>2</sub> but not from UV<sub>254</sub> and <sup>1</sup>O<sub>2</sub>.

### 3.5 Conclusion

In conclusion, this study showed that despite the similarity of MS2, fr and GA, small differences in their composition alter their response to disinfection. Notably, the greatest difference in inactivation among viruses was observed for inactivation by  $\text{ClO}_2$ , which disinfects without inducing any measurable genome damage. Differences were subtler for treatments such as  $\text{UV}_{254}$ , which acts mainly on the genome. We contend that for disinfectants with a significant genome-damaging component, the extent of genome decay provided a reasonable estimate of inactivation. However, the relative order of inactivation among the viruses could not be explained by genome damage alone. This was attributed to the finding that - despite their similarity - the viruses could exhibit different inactivation mechanisms for the same disinfectant. Finally, we have shown that knowledge of the length and composition of the genome are not sufficient to predict genome degradation, and consequently inactivation. Instead, structural features of the genome play an important role in determining the extent of degradation. In order to predict inactivation of viruses based on related species or unrelated surrogate organisms, good knowledge of the dominant mechanisms of inactivation, as well as of the relevant structural features, is thus important. Unless these differences are understood, predicting the rates of disinfection of a virus based on those of a surrogate will remain a challenge.

For a more complete picture of the mechanisms that govern inactivation of the three phages studied herein, the implications of differences in their protein composition on inactivation will be discussed in chapter 4.



# Subtle differences in virus composition affect disinfection kinetics and mechanisms: effect of protein composition

## 4.1 Introduction

Virus inactivation kinetics by many disinfectants have been extensively studied in the past decades.<sup>48,52,132,133,155–157</sup> Nevertheless, their mechanisms of inactivation remain poorly understood. The factors governing a disinfectant's mode of action appear to be complex, as different mechanisms have been reported for the inactivation of different viruses inactivated by the same disinfectant.<sup>127,158</sup> Even among closely related viruses, small differences in virus composition have been shown to exhibit differences in susceptibility to disinfectants.<sup>52,133</sup> In order to understand these discrepancies, a molecular-level understanding of virus inactivation mechanisms is essential.

Both the viral genome and proteins can be affected during virus inactivation, but the relative contribution of genome and protein damage to inactivation differs, depending on the disinfectant used and the virus considered. In previous work, we examined the mechanisms of inactivation of MS2 coliphage by five disinfectants.<sup>56</sup> It was shown that UV<sub>254</sub> and singlet oxygen (<sup>1</sup>O<sub>2</sub>) mainly caused inactivation by damaging the genome to an extent that replication was inhibited. Genome damage also occurred during treatment by free chlorine (FC), but inactivation additionally involved a protein contribution. Finally, upon exposure to chlorine dioxide (ClO<sub>2</sub>) and heat, the genome stayed intact and the virus was inactivated solely via protein degradation.

With the mode of action of these disinfectants established, the goal of this work was to determine how differences in virus composition affect their inactivation kinetics and mechanisms. To do so, we

compared the genome and protein degradation of MS2 with that of two related phages, fr and GA during inactivation by UV<sub>254</sub>, <sup>1</sup>O<sub>2</sub>, FC and ClO<sub>2</sub>. In the first part of this study (chapter 3), we compared the inactivation kinetics of these three viruses, and analyzed the contribution of genome damage to overall inactivation. We determined that for disinfectants acting on the genome (UV<sub>254</sub>, <sup>1</sup>O<sub>2</sub>, FC), small but significant differences in kinetics occurred. These differences were much more pronounced for ClO<sub>2</sub>, which did not cause measurable genome damage. Furthermore, we established that even for the treatments acting strongly on the genome, genome damage alone could not always account for the observed inactivation of a single virus, or for the relative inactivation trends between the three viruses; this suggests that protein degradation must play a role in the inactivating mechanisms. The objective of this second part of the study was to evaluate the importance of protein damage to inactivation, and to assess if differences in the capsid protein degradation of MS2, fr and GA could explain those inactivation trends that are not attributable to genome damage alone.

The studied viruses all belonged to the *Leviviridae* family and consisted of a positive sense, single-stranded RNA genome (approximately 3500 nucleotides), which is surrounded by an icosahedral capsid containing 180 copies of a capsid protein (composed of 129 amino acids), as well as one copy of an assembly protein (A protein; composed of 393 amino acids for MS2 and fr; 390 for GA). Among the three phages, MS2 and fr are the most closely related. Their capsid proteins are 87% homologous, whereas those of MS2 and GA exhibit a homology of 62%, and fr and GA of 63% (Fig. 1.7).<sup>159</sup> Differences in the A-protein composition are more pronounced, with MS2 and fr exhibiting 78% homology, MS2 and GA 38%, and fr and GA 36%. These differences in protein composition may be particularly important for those disinfectants acting wholly or partially by viral protein degradation.

## 4.2 Materials and methods

### 4.2.1 Chemicals

The following reagents were used in addition to those described in chapter 3: trifluoroacetic acid (TFA), formic acid (FA), thiamine hydrochloride (98.5-101.5%),  $\text{Na}_2\text{HPO}_4 \cdot 12\text{H}_2\text{O}$  (99%) and HPLC grade acetonitrile were purchased from Acros Organics (Geel, Belgium).  $\text{KH}_2\text{PO}_4$  (99%), M9 minimum salts, L-cysteine (98.5%), iodoacetamide, sinapinic acid (98%), bromophenol blue and  $\alpha$ -cyano-4-hydroxycinnamic acid were obtained from Sigma-Aldrich (Germany). Glycerin (electrophoresis reagent purity) and  $\text{MgSO}_4 \cdot 7\text{H}_2\text{O}$  (cell culture grade) were purchased from AppliChem (Darmstadt, Germany).  $^{15}\text{NH}_4\text{Cl}$  (99%  $^{15}\text{N}$ ) was purchased from Cambridge Isotope Laboratories (Andover, MA). Trypsin and Chymotrypsin were purchased from Worthington Biochemical Corporation (Lakewood, NJ). Protein mid range standard, pre-casted 12% gels, electrophoresis reagent purity sodium dodecyl sulfate (SDS) and glycine were obtained from BioRad (Hercules, CA). Dithiothreitol was purchased from Fisher Scientific (Waltham, MA).  $\beta$ -mercaptoethanol was obtained from Promega (Madison, WI). SimplyBlue SafeStain was purchased from Invitrogen (Carlsbad, CA). All aqueous solutions were prepared in ultrapure water ( $>18 \text{ M}\Omega\text{cm}^{-1}$ ).

### 4.2.2 Microorganisms

A description of the phages used, their *E. coli* hosts, as well as the associated enumeration, propagation and purification methods are described in Chapter 3. In addition, *E. coli* C-3000 (ATTC 15597) was purchased from LGC Standards (Molsheim, France) for the propagation of isotopically [ $^{15}\text{N}$ ]-labeled bacteriophages.

### 4.2.3 Propagation of $^{15}\text{N}$ -labeled bacteriophages

To produce labeled *E. coli*, four sequential overnight cultures were prepared in M9 minimal media supplemented with  $1 \times 10^{-4} \text{ M}$   $\text{CaCl}_2$ ,  $3 \times 10^{-5} \text{ M}$  thiamine,  $2 \times 10^{-3} \text{ M}$   $\text{MgSO}_4$ , 0.2% D-glucose and  $1.84 \times 10^{-2} \text{ M}$   $\text{NH}_4\text{Cl}$  as the principal nitrogen source. A  $^{15}\text{NH}_4\text{Cl}$  nitrogen source was used for the last two overnight cultures. The resulting  $^{15}\text{N}$ -labeled *E. coli* was then grown to an optical density (600 nm) of 0.3, 0.04, and 0.2, and the cultures were spiked with MS2, fr, or GA at a multiplicity of infection of 1, 0.01, and 1, respectively. The virus propagation was stopped after 24 hours by the addition of chloroform to lyse the bacteria, and the resulting  $^{15}\text{N}$ -labeled virus were purified as previously described.<sup>108</sup>

#### 4.2.4 Disinfection assays for protein damage assessment

Virus inactivation experiments were conducted using three different viruses (MS2, fr and GA) and four disinfectants (UV<sub>254</sub>, <sup>1</sup>O<sub>2</sub>, FC and ClO<sub>2</sub>). Experimental details of the disinfection assays are described in Chapter 3. In brief, experiments were conducted in triplicate, in sacrificial, stirred reactors at room temperature. For UV<sub>254</sub> and <sup>1</sup>O<sub>2</sub>, experiments were carried out in 2 mL of dilution buffer (DB: 5 mM PO<sub>4</sub><sup>2-</sup>, 10 mM NaCl, pH 7.4) containing 5x10<sup>11</sup> pfu (plaque forming units) MS2/mL. For FC and ClO<sub>2</sub>, reactors contained 10 mL DB with 10<sup>11</sup> pfu MS2/mL. Initial concentrations of fr and GA were 10-fold lower. Experiments with FC, <sup>1</sup>O<sub>2</sub>, and UV<sub>254</sub> were conducted at constant disinfectant concentrations of 1.3-1.5 mg/L FC, 3.5·10<sup>-7</sup> mg/L <sup>1</sup>O<sub>2</sub>, or a UV<sub>254</sub> irradiance of 23.0 W/m<sup>2</sup> for MS2 and 2.4 W/m<sup>2</sup> for GA and fr. The disinfection experiments were stopped at several time points. For FC, this was achieved by quenching the residual FC with Tris buffer, and for UV<sub>254</sub> and <sup>1</sup>O<sub>2</sub> by removing the reactors from the light source. For ClO<sub>2</sub> experiments, quenchers were found to back-reduce oxidized protein residues; therefore disinfection was halted by dilution and evaporation of ClO<sub>2</sub>. The ClO<sub>2</sub> concentration was thus not constant, but decreased over the course of the experiments. To achieve different ClO<sub>2</sub> doses, experiments were conducted in reactors with a range of initial ClO<sub>2</sub> concentrations (0.4-1.6 mg/L).

Throughout the disinfection experiments, sample aliquots of 10-100 µL were periodically removed and were enumerated for infective viruses. The remaining volume was processed for protein quantification as described below.

#### 4.2.5 Analysis of peptide damage by Matrix Assisted Laser Desorption Ionization (MALDI)

All MALDI measurements were performed with an ABI 4800 MALDI tandem time of flight (TOF-TOF) mass spectrometer (Applied Biosystems, Rotkreuz, Switzerland), using the instrument settings and sample deposition methods described previously.<sup>61</sup>

After disinfection, each sample was spiked with its corresponding untreated [<sup>15</sup>N]-labeled virus, where it served as an internal standard for quantification of the MALDI measurements. If necessary, the spiked samples were first concentrated to 2 mL (for FC and ClO<sub>2</sub>) with 100-kDa Microcon centrifugal filters (Millipore, Billerica, MA). Then, the samples were split into two parts, one for trypsin and one for chymotrypsin digestion. Prior to digestion, samples were concentrated to a final volume of 20 µL. Of



these, 2  $\mu$ l were removed and subjected to MALDI linear mode analysis to detect cleavage products of the capsid protein.

The concentrated samples were denatured for 10 minutes at 95°C. Cysteines were immediately acetylated with fresh iodoacetamide (5  $\mu$ L, 25 mM, in Tris buffer (50 mM, pH 8)) at 37°C in the dark for 60 minutes, to prevent oxidation. Excess iodoacetamide was then quenched with cysteine (5  $\mu$ L, 50 mM, in Tris buffer (50 mM, pH 8)) and the samples were incubated for 15 minutes in the dark. Finally, 25  $\mu$ L Tris buffer (50 mM, pH 8) containing 2 mM  $\text{CaCl}_2$  was added to the samples and they were digested overnight with freshly prepared trypsin or chymotrypsin at a 50:1 capsid protein-to-enzyme ratio. Prior to analysis, pure acetonitrile was added to the digested samples to enhance crystallization on the MALDI plate. Samples were then subjected to MALDI analysis in reflectron mode. The *in silico* digestion products for each proteolytic enzyme (PeptideMass software, Swiss-Prot database) are shown in Table 4.1. Table D1 of appendix D shows the masses (M+1) of each analyzed peptide and the mass of its corresponding  $^{15}\text{N}$ -labeled peptide. For MS2, MALDI analysis covered 98% of the capsid protein, whereas fr and GA had a coverage of 100 and 93%, respectively.

Subtle differences in virus composition affect disinfection kinetics and mechanisms: effect of protein composition

**Table 4.1: Peptide sequences for each virus and each protease.** Underlined peptides indicate analyzed sequences (dotted line shows peptides including a missed cleavage site). Total coverage: MS2: 98.4%; fr: 100%; GA: 93.8% (PDB code: 2MS2, 1frs, 1GAv).

Bacteriophage	Protease	Sequence
MS2	Trypsin	ASNFTQFVLV <sup>10</sup> DNGGTGDVTV <sup>20</sup> APSNFANGVA <sup>30</sup> EWISSNSR
		<u>SQ<sup>40</sup>AYK</u> <u>VTCSVR</u> <u>Q<sup>50</sup>SSAQR</u> K YTI <sup>60</sup> K
		VEVPK <u>VATQ<sup>70</sup>TVGGVELPVA<sup>80</sup>AWR</u>
		<u>SYLNMEI<sup>90</sup>TIPIFATNSD<sup>100</sup>CELIVK</u> <u>AMQG<sup>110</sup>LLK</u>
		<u>DGNPIP<sup>119</sup>SAIAANSIY<sup>129</sup></u>
	Chymotrypsin	ASNFTQF VLV <sup>10</sup> DNGGTGDVTV <sup>20</sup> APSNF ANGVA <sup>30</sup> EW
		ISSNSRSQ <sup>40</sup> AY KVTCSVRQ <sup>50</sup> SSAQRKY
		TI <sup>60</sup> KVEVPKVATQ <sup>70</sup> TVGGVELPVA <sup>80</sup> AW RSY L NM
		EL <sup>90</sup> TIPIF ATNSD <sup>100</sup> CEL IVKAM QG <sup>110</sup> L L
		KDGNPIP <sup>119</sup> SAIAANSIY <sup>129</sup>
fr	Trypsin	ASNFEFVLV <sup>10</sup> DNGGTGDVK V <sup>20</sup> APSNFANGVA <sup>30</sup> EWISSNSR
		<u>SQ<sup>40</sup>AYK</u> <u>VTCSVR</u> <u>Q<sup>50</sup>SSANNR</u> KYTV <sup>60</sup> K VEVPK
		<u>VATQ<sup>70</sup>VQGGVELPVA<sup>80</sup>AWR</u>
		<u>SYNMEL<sup>90</sup>TIPVFATNDD<sup>100</sup>CALIVK</u> <u>ALQG<sup>110</sup>TFK</u>
		<u>TGNPIA<sup>119</sup>TAIAANSIY<sup>129</sup></u>
GA	Trypsin	ATLR SFVLVD <sup>10</sup> NGGTGNVTVV <sup>20</sup> PVSNANGVAE <sup>30</sup> WLSNNSR
		<u>SQA<sup>40</sup>YR</u> <u>VTASYR</u> AS <sup>50</sup> GADK R K YTIK <sup>60</sup>
		LEVPK <u>IVTQV<sup>70</sup>VNGVELPVSA<sup>80</sup>WK</u>
		<u>AYASIDLT<sup>90</sup>IPIFAATDDV<sup>100</sup>TVISK</u> <u>SLAGL<sup>110</sup>FK</u>
		<u>VGNPIAEA<sup>120</sup>ISSQSGFYA<sup>129</sup></u>
	Chymotrypsin	ATL RSF VL VD <sup>10</sup> NGGTGNVTVV <sup>20</sup> PVSNANGVAE <sup>30</sup> W
		L SNNSRSQA <sup>40</sup> Y RVTASY <u>RAS<sup>50</sup>GADKRKY</u> TIK <sup>60</sup> L
		<u>EVPKIVTQV<sup>70</sup>VNGVELPVSA<sup>80</sup>W</u> KAY ASIDL T <sup>90</sup> IPIF
		AATDDV <sup>100</sup> TVISKSL AGL <sup>110</sup> F KVGNPPIAEA <sup>120</sup> ISSQSGF
		Y A <sup>129</sup>

Calibration curves for each peptide were established using digested samples with known  $^{14}\text{N}/^{15}\text{N}$ -labeled virus ratios. The ratio of the  $^{14}\text{N}/^{15}\text{N}$  MALDI peak intensities was proportional to the ratio of native to heavy virus concentrations, as was discussed elsewhere<sup>56</sup> and can be observed in Fig. 4.1. The peptide degradation during disinfection was then quantified by monitoring the change in  $^{14}\text{N}/^{15}\text{N}$  peak intensity ratio with increasing disinfectant doses.

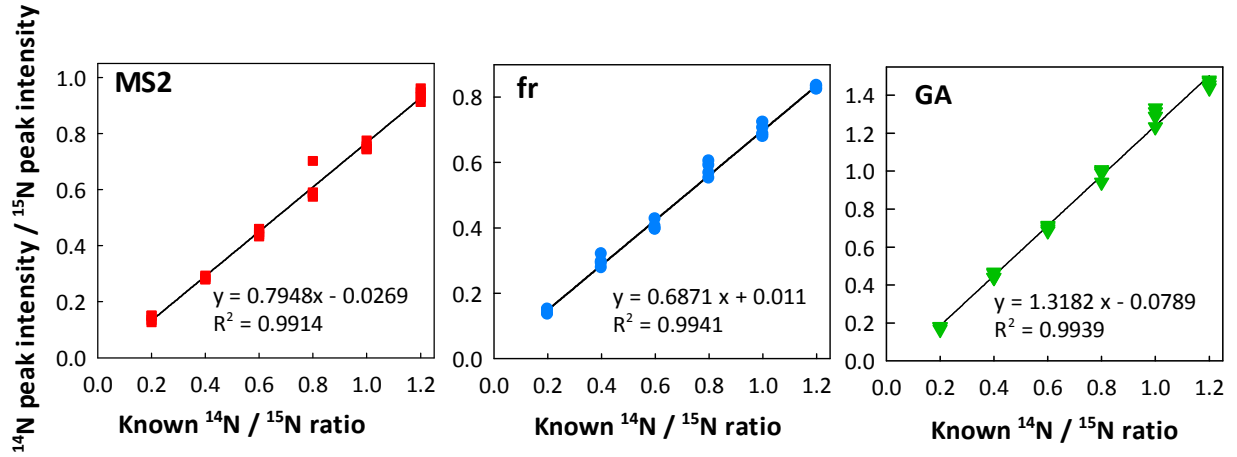


**Figure 4.1:** Example calibration curves for the quantification of peptides. Peptide sequences shown are for: MS2: 67-83; fr: 1-19; GA: 106-112.

Degradation rate constants for individual peptides ( $k_{\text{peptide}}$ ) were determined as a function of inactivation, according to Eq. 4.1:

$$\ln(p/p_0) = -k_{\text{peptide}} \log(C_v/C_{v,0}) \quad \text{Eq. 4.1}$$

where  $p$  indicates a specific capsid protein peptide concentration at time  $t$  and  $C_v$  and  $C_{v,0}$  are the concentration of infective viruses at time  $t$  and 0 respectively. Selected peptide products were subjected to tandem mass spectrometry (MS/MS) analysis in order to determine which amino acids within the peptide were modified during disinfection.

In addition to capsid proteins, the A protein of GA was also analyzed following disinfecting treatments with  $\text{UV}_{254}$  and  $^1\text{O}_2$ . After reactions were quenched, the A proteins were separated from the more abundant capsid proteins with SDS PAGE using 12% polyacrylamide gels and Coomassie blue staining.<sup>56,160</sup> The A protein lane (42 kDa) was cut and immediately subjected to cysteine acetylation

Subtle differences in virus composition affect disinfection kinetics and mechanisms: effect of protein composition

followed by in-gel digestion with trypsin.<sup>161</sup> The *in silico* digestion products of the GA A protein (PeptideMass software, Swiss-Prot database) are shown in Table 4.2. Due to the low abundance of the A protein in GA compared to the capsid protein (one copy of A protein versus 180 copies of the capsid protein), only 15% of the A protein's 390 amino acids could be detected. Furthermore, <sup>15</sup>N-labeled internal standards could not be used for A protein analysis, because labeled A protein concentrations were too low for MALDI detection. Instead, peptide peak intensities were normalized to that of an A protein peptide presumed stable (due to the absence of residues susceptible to UV<sub>254</sub> or <sup>1</sup>O<sub>2</sub>; peptide 154-160 in Table 4.2). As such, this analysis was only semi-quantitative.

**Table 4.2: A protein peptide sequence for GA digested by trypsin.** Underlined peptides indicate sequences detected by MALDI. Total coverage: 15%.

Bacteriophage	Sequence						
GA	MFPK	SNIDR	N <sup>10</sup> YK	VK	LISYDK <sup>20</sup>	K	GK
	LVSDDSF <sup>30</sup>	EQVENYLFQN <sup>40</sup>	R	<u>STTYKPGYI<sup>50</sup></u>	R	DFR	<u>RPTNF<sup>60</sup>WNGYR</u>
	<u>CFNQP<sup>70</sup>VGTFTR</u>	K	LSD <sup>80</sup> GGR	QVADYGI <sup>90</sup>	VNPNK		
	FTANS <sup>100</sup>	QHLGDNMVIY <sup>110</sup>	PGPFSINIDQ <sup>120</sup>	R	ASVEVLNK		
	L <sup>130</sup> SQSNLNIGVA <sup>140</sup>	IAEAK	MTASL <sup>150</sup>	LAK	<u>QSIALIR<sup>160</sup></u>	AYTAAK	R
	GNW <sup>170</sup>	R	<u>EVLSQLLIS<sup>180</sup></u>	EHR	FR	APAK	D <sup>190</sup> LGGR
	WLELQY <sup>200</sup>	GWLPLMSDLK <sup>210</sup>	AAYDLLTQTK <sup>220</sup>		LPAFMPLR	VT <sup>230</sup>	R
	<u>TVGGTHNYK<sup>240</sup></u>	VR	NVESAGDT <sup>250</sup>	WSYR	HR	LSVN <sup>260</sup>	YR
	IWYFISDP <sup>270</sup>	R	LAWASSLGL <sup>280</sup>	LNPLEYWEK <sup>290</sup>			
	TPWSFVVDWF <sup>300</sup>	LPVGNLIEAM <sup>310</sup>	SNPLGLDIIS <sup>320</sup>	GTK	TWQLESK <sup>330</sup>		
	LNATLPASGW <sup>340</sup>	SGTAK	LTAYA <sup>350</sup>	K	AYDR	STFYS <sup>360</sup>	FPTPLPYVK
	S <sup>370</sup> PLSGLHLANA <sup>380</sup>	LALINQR	LK	R <sup>390</sup>			

#### 4.2.6 Quantification of capsid protein degradation

The proportion of undamaged capsid protein ( $CP/CP_0$ ) was determined by the product of the intact fractions of the individual peptides ( $cp_i/cp_{i,0}$ ) (Eq. 4.2):

$$CP / CP_0 = (\prod cp_i / cp_{i,0}) \quad \text{Eq. 4.2}$$

The capsid protein degradation rate constant ( $k_{CP}$ ) was calculated for all treatments except  $ClO_2$  according to a first-order model versus disinfectant dose (Eq. 4.3):

$$\ln (CP/CP_0) = -k_{CP} C_d t \quad \text{Eq. 4.3}$$

where  $C_d t$  is the disinfectant dose. For  $ClO_2$ , protein degradation was described by a Hom-type model (Eq. 4.4):

$$\ln (CP/CP_0) = -k_{CP,H} C_d^n t^{m-1} \quad \text{Eq. 4.4}$$

Where  $k_{CP,H}$  is the Hom protein degradation rate constant [ $(\text{mgL}^{-1}\text{sec}^{m-1})^{-1}$ ],  $n$  is the dilution coefficient (set to 1 in accordance with inactivation experiments (see 3.2.4), and  $m$  is the constant for the inactivation rate law, which describes the deviation from the ideal first-order model (Eq. 4.3). The  $ClO_2$  concentration varied over time, due to autodecomposition and evaporation.  $ClO_2$  has been reported to degrade exponentially as follows (Eq. 4.5):<sup>107</sup>

$$C_d = C_{d,0} e^{-k_{ClO_2} t} \quad \text{Eq. 4.5}$$

where  $C_{d,0}$  and  $C_d$  are the chlorine dioxide concentration at times 0 and  $t$  [sec] respectively, and  $k_{ClO_2}$  is the first order  $ClO_2$  decay rate constant. Recall that the  $ClO_2$  experiments for protein damage assessment were conducted in sacrificial reactors at different initial  $ClO_2$  concentrations. The integration of Eq. 4.5 over time thus provided the respective  $ClO_2$  dose for each reactor. The average  $C_d$  in each reactor (input parameter for the Hom model) was then obtained by dividing the dose by the time of exposure,  $t$ . The parameters for the Hom model were fitted in Sigmaplot (version: 12.0, 2011).

Subtle differences in virus composition affect disinfection kinetics and mechanisms: effect of protein composition

For all treatments, the capsid degradation rate constant ( $k_{CP,inact}$ ) was also calculated according to a first-order model versus inactivation (Eq. 4.6):

$$\ln (CP/CP_0) = -k_{CP,inact} \log (C_v / C_{v,0}) \quad \text{Eq. 4.6}$$

where  $C_v$  and  $C_{v,0}$  are the concentration of infective viruses at time  $t$  and 0 respectively.

To determine if protein degradation differed among the three viruses and from zero, rate constants were compared by ANCOVA analysis, whereby a  $p$  value of  $<0.05$  was deemed significant.

#### **4.2.7 Prediction of capsid protein degradation rate constants**

Degradation of free amino acids by the disinfectants considered herein has been extensively studied, and the reported second order rate constants for the reactions with  $^1O_2$ , FC and  $ClO_2$ , as well as the quantum yields and molar absorptivities for photolysis by  $UV_{254}$  are summarized in Table 4.3. Based on these values, in conjunction with the abundance of each amino acid in the different capsid proteins, a capsid degradation rate constant for each virus and disinfectant was predicted.

Table 4.3: Summary of reaction rate constants, molar absorptivities ( $\epsilon$ ) and quantum yields ( $\phi$ ) for the reactions of free amino acids with the disinfectants considered herein.

Amino acid	$^1\text{O}_2$	FC	$\text{ClO}_2$	$\text{UV}_{254}$	
	$k [\text{M}^{-1}\text{s}^{-1}]^{162}$	$k [\text{M}^{-1}\text{s}^{-1}]^{163}$	$k [\text{M}^{-1}\text{s}^{-1}]^{140}$	$\epsilon [\text{M}^{-1}\text{cm}^{-1}]^{164}$	$\Phi [\%]^{63}$
Methionine	$1.6 \cdot 10^7$	$3.8 \cdot 10^7$			
Cysteine	$9 \cdot 10^6$	$3.0 \cdot 10^7$	$1.0 \cdot 10^7$		
Histidine	$3.2 \cdot 10^7$	$1.0 \cdot 10^5$			
Tryptophane	$3.0 \cdot 10^7$	$1.1 \cdot 10^4$	$3.4 \cdot 10^4$	2760	$9 \cdot 10^{-3}$
Tyrosine	$8.0 \cdot 10^6$	$4.4 \cdot 10^1$	$1.8 \cdot 10^5$	341	$2.2 \cdot 10^{-2}$
Phenilalanine				139.6	$1.9 \cdot 10^{-2}$
Lysine		$5.0 \cdot 10^3$			
Arginine		$2.6 \cdot 10^1$			
Backbone N		$1.0 \cdot 10^1$			
Asparagine		$3.0 \cdot 10^{-2}$			
Glutamine		$3.0 \cdot 10^{-2}$			
Terminal amine		$1.0 \cdot 10^5$			

#### 4.2.8 Computational modeling of methionine oxidation in fr and MS2

The free energy difference of oxidation reaction of Met88 by  $^1\text{O}_2$  in fr and MS2 was evaluated by combined molecular dynamics and thermodynamic integration simulations using the NAMD package.<sup>165</sup> The Amber force field (parm10) (AMBER 11; D. A. Case et al., University of California, San Francisco)<sup>166</sup> was used to describe the protein environment, while additional parameters required for the methionine sulfoxide residue were generated using the Gaussian 03 (M. Frisch et al., Gaussian Inc., Walling-ford, CT)<sup>167</sup> quantum mechanical software package and the restrained electrostatic potential (RESP) procedure for the point electrostatic charges and the General Amber Force Field<sup>168</sup> for the remaining parameters. Pressure was set to 100 kPa and the temperature was set to 300 K. Additional details are given in

appendix D (paragraph D1 and Fig. D1).

Poisson Boltzmann calculations were performed to investigate the stability of the capsid at different ionic strengths. Ion charges of 1 and -1 with radii of 2 Å were used and the biomolecule and solvent dielectric constants were set to 2 and 78 respectively. Additional details are given in Appendix D (paragraph D2 and Fig D2).

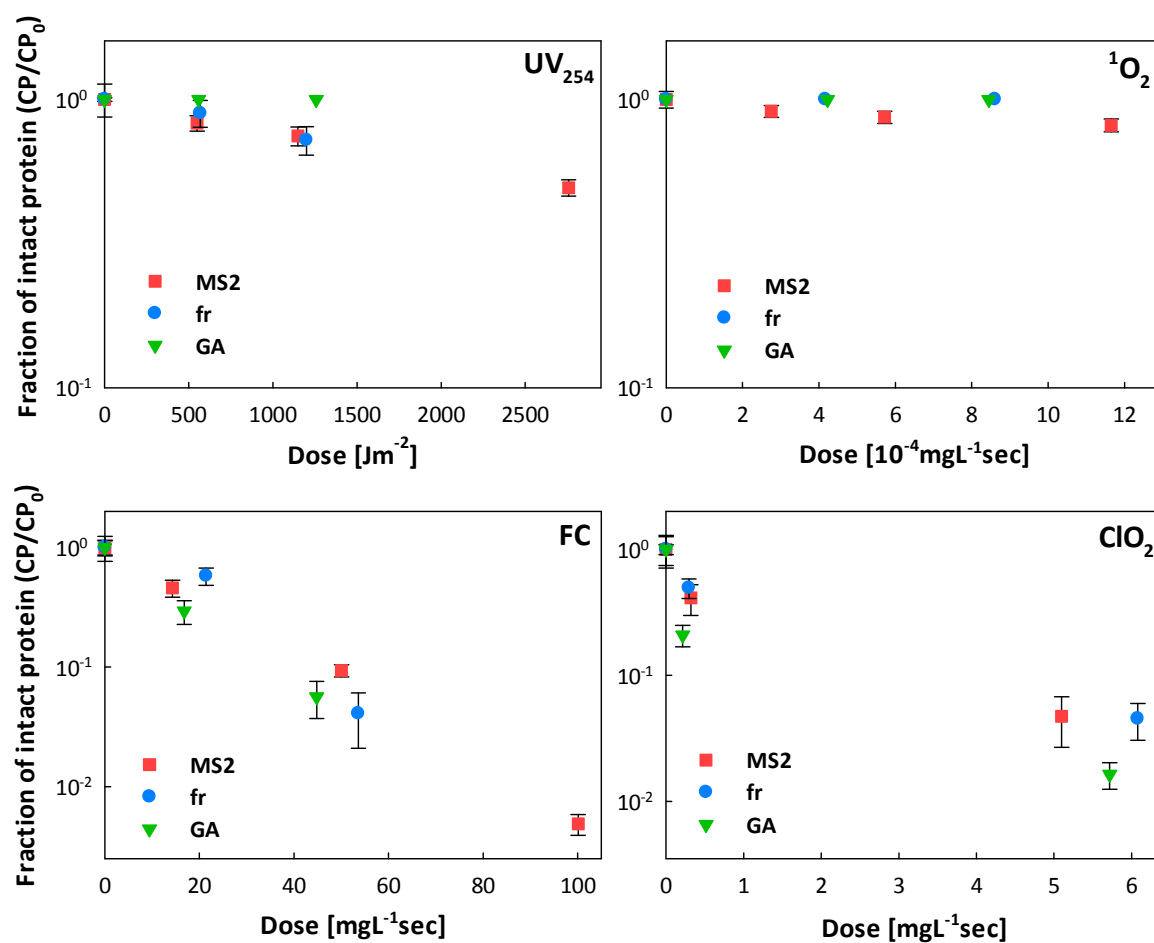
The solvent-accessible surface area (SASA) for the MS2 and fr sulfur atoms was calculated using VMD.<sup>169</sup> Each reported SASA is an average of ten SASAs obtained using the structures extracted for the Adaptive Poisson-Boltzmann Solver (APBS) calculations. The probe radius was set to 1.4 Å.

## 4.3 Results

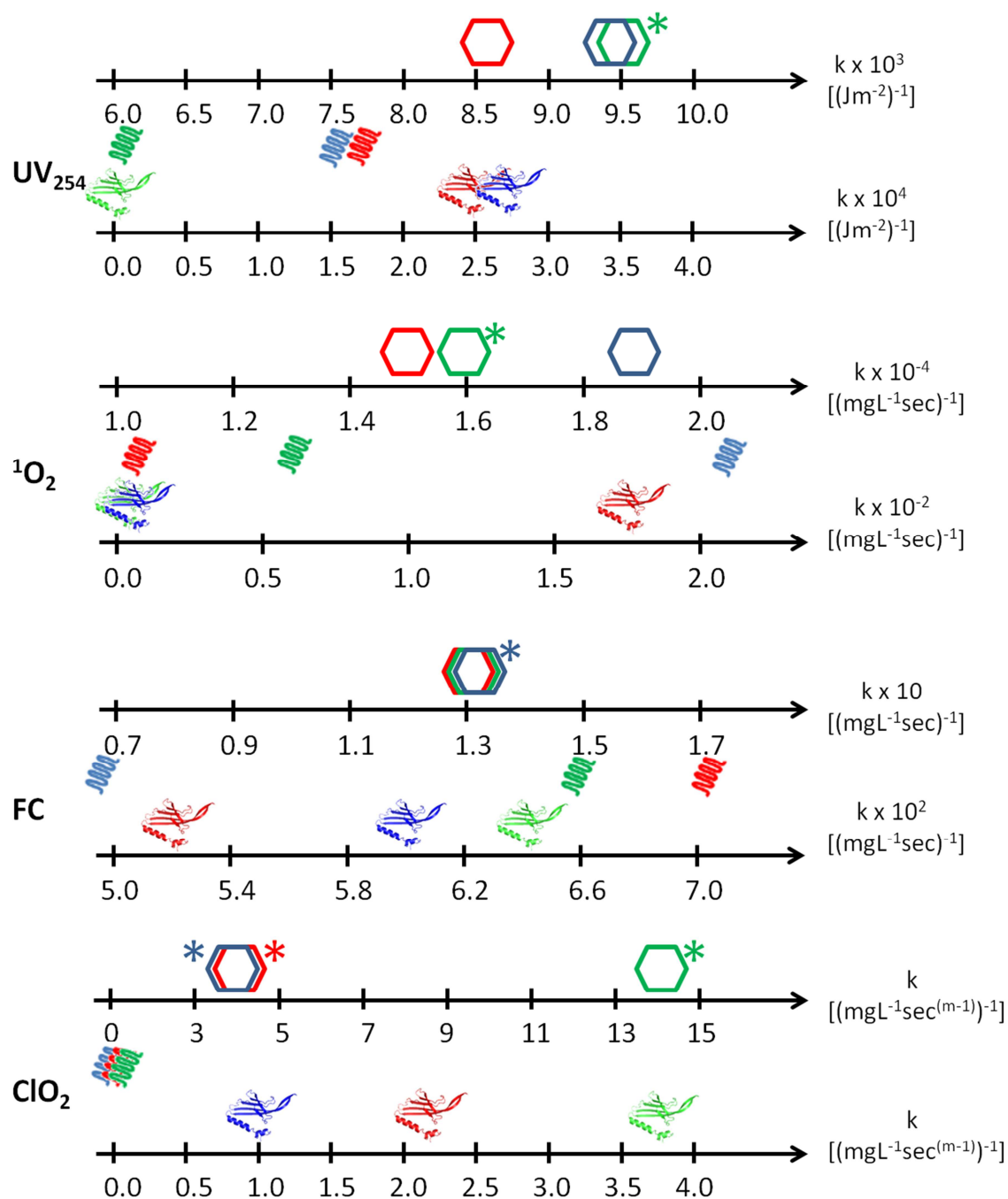
### 4.3.1 Comparison of capsid protein degradation

Fig. 4.2 shows capsid protein degradation as a function of disinfectant dose for all viruses and disinfectants. The corresponding rate constants and their associated errors are listed in Table 4.4. These results are also represented in Fig 4.3 along with the inactivation rate constants and genome degradation rate constants (obtained from chapter 3). In addition, the virus-treatment combinations for which genome degradation could account for inactivation are also depicted. For the viruses that exhibited significant protein degradation by UV<sub>254</sub>, <sup>1</sup>O<sub>2</sub> or FC, protein degradation followed first-order kinetics with respect to disinfectant dose. ClO<sub>2</sub>, in contrast, caused tailing with increasing dose, similar to the corresponding inactivation curves (Fig. 3.2). However, if analyzed as a function of inactivation (Fig. 4.4), capsid protein degradation by ClO<sub>2</sub> also followed a first-order model.





**Figure 4.2: Comparison of capsid protein damage versus disinfectant dose between the three viruses upon inactivation by the four disinfectants.** Error bars represent the standard error. Statistically significant differences in protein degradation were found for the following combinations: FC: MS2-GA ( $p = 0.007$ ); ClO<sub>2</sub>: fr-GA ( $p < 0.01$ ).



**Figure 4.3: Overview of inactivation, genome degradation and protein degradation rate constants.** Hexagons: inactivation rate constants ( $k_{CW}$  or  $k_H$ , chapter 3); Protein monomers: capsid protein degradation rate constants ( $k_{CP}$ , or  $k_{CP,H}$ ); spirals: genome degradation rate constants ( $k_G$ ) for all four disinfecting treatments. MS2 is shown in red, fr in blue and GA in green. The asterisk indicates virus/treatment pairs where genome degradation could not account for inactivation (see chapter 3). Exact protein degradation rate constants and associated values are listed in Table 4.4.

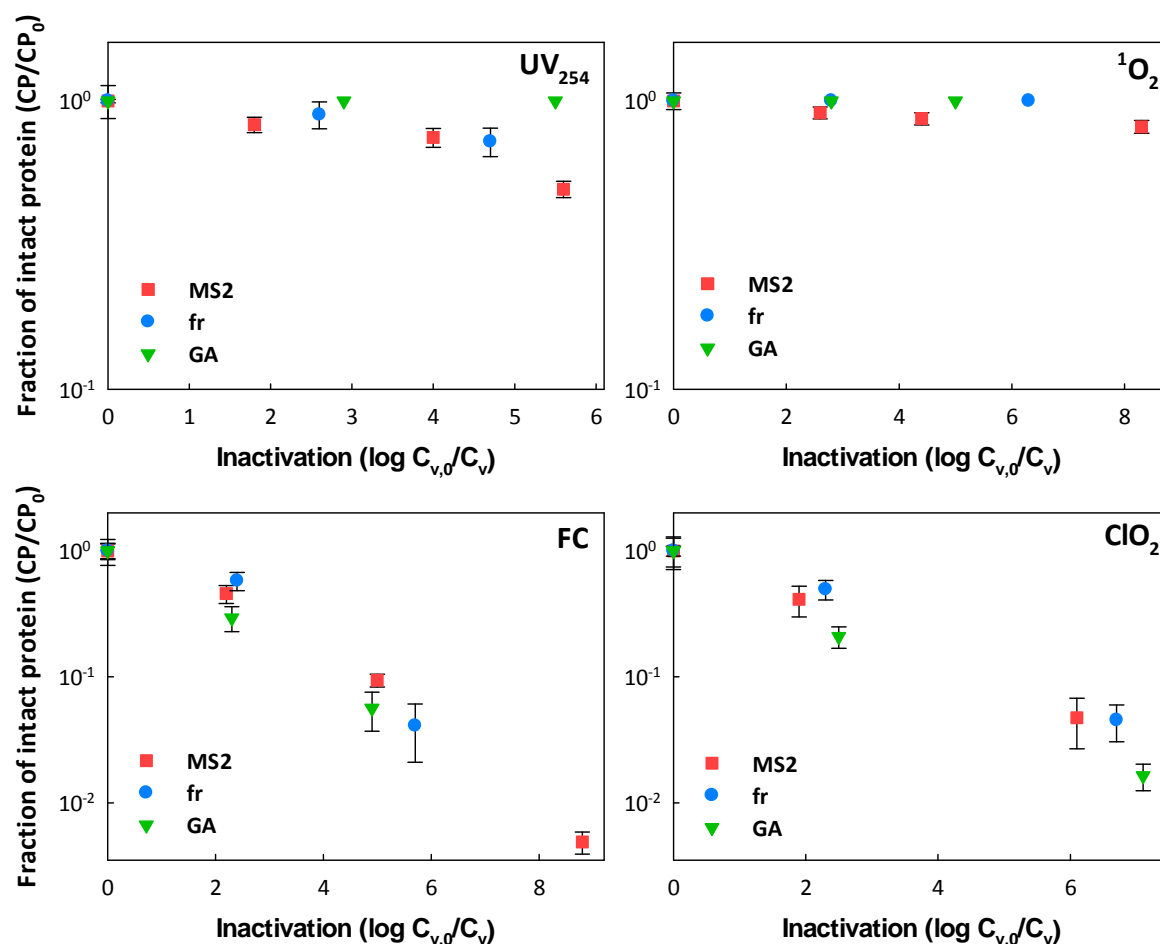


**Figure 4.4: Protein degradation per log inactivation between the three viruses upon inactivation by the four disinfectants.** Error bars represent standard errors. Statistically significant differences in protein degradation were found for the following combinations: UV<sub>254</sub>: MS2-fr ( $p = 0.038$ ); ClO<sub>2</sub>: fr-GA ( $p = 0.027$ ).

The effects of UV<sub>254</sub> and singlet oxygen on the capsid proteins were generally subtle. Upon treatment by UV<sub>254</sub>, only MS2 and fr sustained a statistically significant amount of capsid protein damage, while GA's capsid protein remained unaffected. Singlet oxygen caused slight, but significant damage to MS2 only. Free chlorine as well as ClO<sub>2</sub>, in contrast, rapidly degraded the capsid proteins of all viruses. Upon exposure to the same dose, free chlorine acted more efficiently on the GA capsid than on MS2 ( $p = 0.007$ ), though the degradation rate constants differed by a factor of only 1.2. If analyzed as a function of inactivation, however, the three virus capsids degraded at indistinguishable rates (Fig. 4.4). Finally, chlorine dioxide treatment exhibited significantly different degradation rate constants for fr and GA ( $p < 0.01$ ).

**Table 4.4: Experimental and predicted single protein degradation rate constants.** The uncertainty is represented by the standard error. NS indicates non-significant decay.

Phage	UV <sub>254</sub>			<sup>1</sup> O <sub>2</sub>		
	Predicted	Experimental	Experimental	Predicted	Experimental	Experimental
	k <sub>CP</sub> [(Jm <sup>-2</sup> ) <sup>-1</sup> ]	k <sub>CP</sub> [(Jm <sup>-2</sup> ) <sup>-1</sup> ]	k <sub>CP,inact</sub> [(log C <sub>v</sub> /C <sub>v,0</sub> ) <sup>-1</sup> ]	k <sub>CP</sub> [(mgL <sup>-1</sup> sec) <sup>-1</sup> ]	k <sub>CP</sub> [(mgL <sup>-1</sup> sec) <sup>-1</sup> ]	k <sub>CP,inact</sub> [(log C <sub>v</sub> /C <sub>v,0</sub> ) <sup>-1</sup> ]
<b>MS2</b>	2.00·10 <sup>-5</sup>	2.5·10 <sup>-4</sup> ± 0.2·10 <sup>-4</sup>	1.2·10 <sup>-1</sup> ± 0.2·10 <sup>-1</sup>	4.43·10 <sup>3</sup>	1.7·10 <sup>2</sup> ± 0.3·10 <sup>2</sup>	2.4·10 <sup>-2</sup> ± 0.3·10 <sup>-2</sup>
<b>fr</b>	2.06·10 <sup>-5</sup>	2.7·10 <sup>-4</sup> ± 0.5·10 <sup>-4</sup>	6.8·10 <sup>-2</sup> ± 1.3·10 <sup>-2</sup>	4.43·10 <sup>3</sup>	NS	NS
<b>GA</b>	2.16·10 <sup>-5</sup>	NS	NS	3.13·10 <sup>3</sup>	NS	NS
Phage	FC			ClO <sub>2</sub>		
	Predicted	Experimental	Experimental	Predicted	Experimental	Experimental
	k <sub>CP</sub> [(mgL <sup>-1</sup> sec) <sup>-1</sup> ]	k <sub>CP</sub> [(mgL <sup>-1</sup> sec) <sup>-1</sup> ]	k <sub>CP,inact</sub> [(log C <sub>v</sub> /C <sub>v,0</sub> ) <sup>-1</sup> ]	k <sub>CP</sub> [(mgL <sup>-1</sup> sec) <sup>-1</sup> ]	k <sub>CP,H</sub> [(mgL <sup>-1</sup> sec <sup>(m-1)</sup> ) <sup>-1</sup> ]	k <sub>CP,inact</sub> [(log C <sub>v</sub> /C <sub>v,0</sub> ) <sup>-1</sup> ]
<b>MS2</b>	2.60·10 <sup>3</sup>	5.2·10 <sup>-2</sup> ± 0.2·10 <sup>-2</sup>	6.0·10 <sup>-1</sup> ± 0.3·10 <sup>-1</sup>	3.08·10 <sup>2</sup>	2.1 ± 0.7 m = 1.7 ± 0.1	5.1·10 <sup>-1</sup> ± 0.3·10 <sup>-1</sup>
<b>fr</b>	2.60·10 <sup>3</sup>	6.1·10 <sup>-2</sup> ± 0.8·10 <sup>-2</sup>	5.7·10 <sup>-1</sup> ± 0.9·10 <sup>-1</sup>	3.08·10 <sup>2</sup>	1.0 ± 0.5 m = 1.8 ± 0.1	4.8·10 <sup>-1</sup> ± 0.9·10 <sup>-1</sup>
<b>GA</b>	3.03	6.4·10 <sup>-2</sup> ± 0.4·10 <sup>-2</sup>	5.9·10 <sup>-1</sup> ± 0.4·10 <sup>-1</sup>	1.44·10 <sup>1</sup>	3.7 ± 0.4 m = 1.5 ± 0.1	5.7·10 <sup>-1</sup> ± 0.4·10 <sup>-1</sup>

#### 4.3.2 Identification of susceptible capsid protein domains

To identify and compare the susceptible capsid domains for each combination of virus and disinfectant, we monitored the degradation of individual protein regions (peptides) of the capsid protein during disinfection. A summary of the resulting peptide degradation rate constants, determined as a function of inactivation, are shown in Figure 4.5. The effect of UV<sub>254</sub> and <sup>1</sup>O<sub>2</sub> on the different peptides was small, whereas FC and ClO<sub>2</sub> caused extensive degradation. While ClO<sub>2</sub> caused damage to selected peptides only, FC was less specific and reacted with all parts of the capsid.

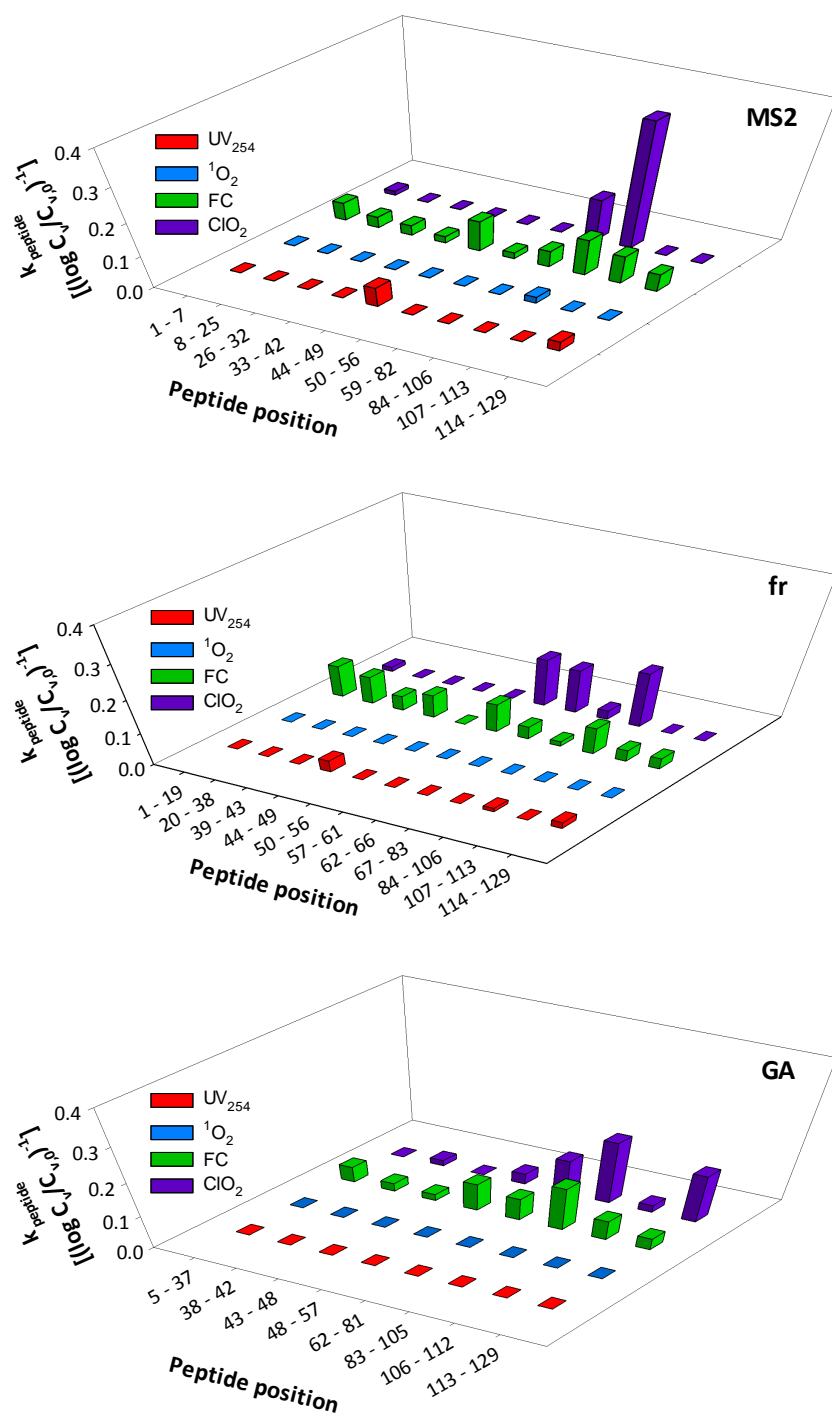


**Figure 4.5:** Degradation rate constants  $k_{\text{peptide}}$  for the individual peptides within the capsid proteins of the three viruses. Rate constants were calculated according to Eq. 4.1. The numbers on the x-axis correspond to the positions of the peptides.

Among the three viruses, subtle differences in the damage pattern could be observed. For MS2, at least one peptide was degraded by each disinfectant: UV<sub>254</sub> mainly affected peptides 44-49 and 114-129, singlet oxygen selectively degraded peptide 84-106, ClO<sub>2</sub> degraded peptide 84-106 and the adjacent peptide 59-82, and free chlorine affected all peptides. The fr damage pattern was very similar to that observed for MS2, although peptide 84-106 was not degraded by singlet oxygen. Finally, GA did not sustain any measurable peptide degradation by UV<sub>254</sub> or singlet oxygen.

MALDI analysis of the undigested capsid protein revealed instances of protein backbone cleavage after treatment by UV<sub>254</sub> and free chlorine (Fig. 4.6). For these two disinfectants, protein degradation could thus be attributed to both protein backbone cleavage and modifications of the amino acid side chains. UV<sub>254</sub> only induced backbone cleavage in MS2 and fr. In both cases, a single cleavage occurred around residues Cys46 and Ser47, consistent with the observed loss of peptide 44-49 (Fig. 4.5). Treatment by free chlorine led to capsid protein fragmentation in all three viruses at various locations. Among the observed fragmentation products, a dominant fragment resulted from cleavage between residues 50 and 51 in all three viruses (Fig. 4.6). Specifically, the main cleavage products detected after FC treatment had masses of 5280, 5335 and 5258 Da for MS2, fr and GA respectively; the predicted mass of peptide 1-50 corresponds to 5278 Da for MS2, 5335 Da for fr and 5254 Da for GA. Singlet oxygen and ClO<sub>2</sub> did not result in measurable backbone cleavage. Protein degradation by these two disinfectants was thus mainly attributed to modifications of the side chains.

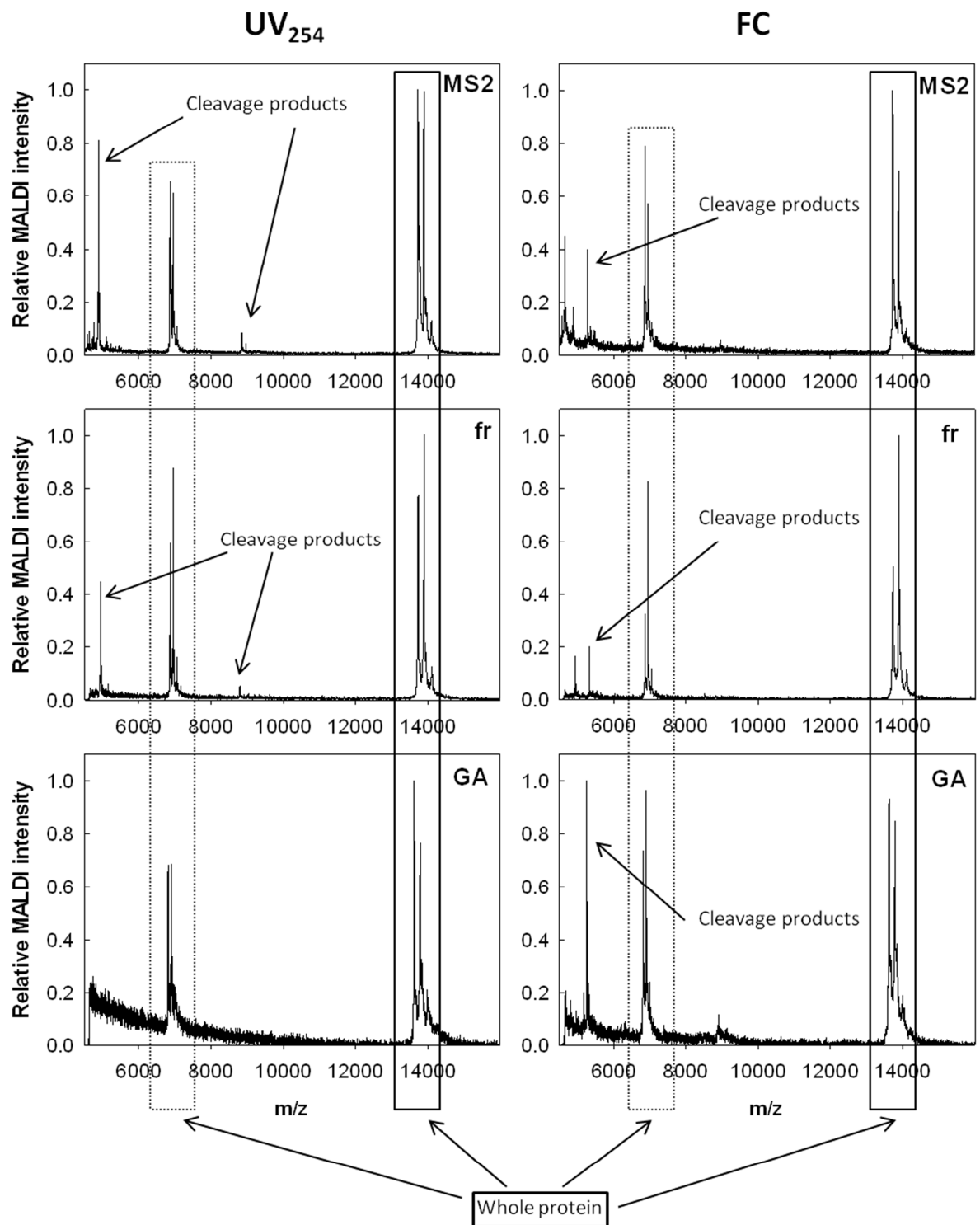


**Figure 4.6:** Linear mode MALDI spectra after disinfection by UV<sub>254</sub> and free chlorine. The whole protein indicates the M<sup>+1</sup> (indicated by solid box) and M<sup>+2</sup> (dotted box) of the entire peaks. Double peaks are visible due to the presence of <sup>15</sup>N-labeled capsid proteins, which have a mass offset compared to native capsid proteins.

### 4.3.3 Identification of susceptible A protein domains

UV<sub>254</sub> and <sup>1</sup>O<sub>2</sub> did not cause any detectable capsid protein degradation in GA; yet the observed inactivation by these two treatments could not be accounted for by genome damage alone (Chapter 3, Fig. 3.5). We therefore additionally analyzed the effect of these two disinfectants on the last remaining virus component, the A protein. Despite the low coverage, it was evident that both UV<sub>254</sub> and <sup>1</sup>O<sub>2</sub> caused the A protein to degrade (Fig. 4.7): peptides 42-51 and 172-183 were damaged by UV<sub>254</sub> irradiation, and peptide 56-65 degraded during treatment by <sup>1</sup>O<sub>2</sub>.

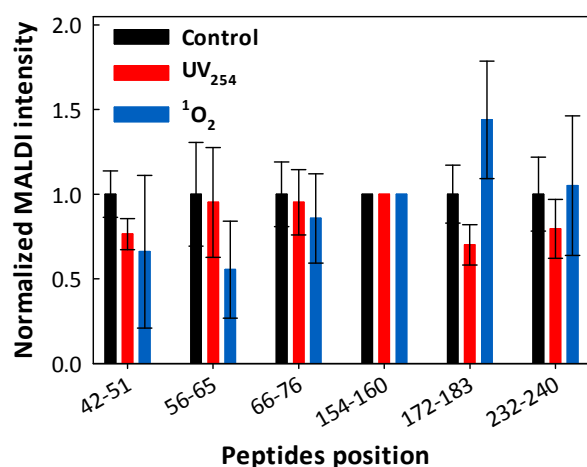


**Figure 4.7: GA A protein peptide degradation after UV<sub>254</sub> and <sup>1</sup>O<sub>2</sub>.** Peptide 154-160 was used as internal standard. Error bars represent the standard deviation. UV<sub>254</sub> peptides 42-51, 172-183 and <sup>1</sup>O<sub>2</sub> peptide 56-65 are significantly different from the control ( $p < 0.02$ ).

### 4.3.4 MS/MS identification of amino acids modified by singlet oxygen

The capsid protein peptide analysis (Fig. 4.5) showed that in MS2 only one peptide was degraded by singlet oxygen, and a single product with a mass shift of +16, corresponding to an oxidation event, was generated (data not shown). MS/MS analysis was performed on this product, and revealed that residue Met88 was oxidized (Fig. 4.8). Because GA does not contain any methionine residues, no corresponding product formed. Interestingly, however, this product also did not form in fr despite the fact that it does contain Met88.



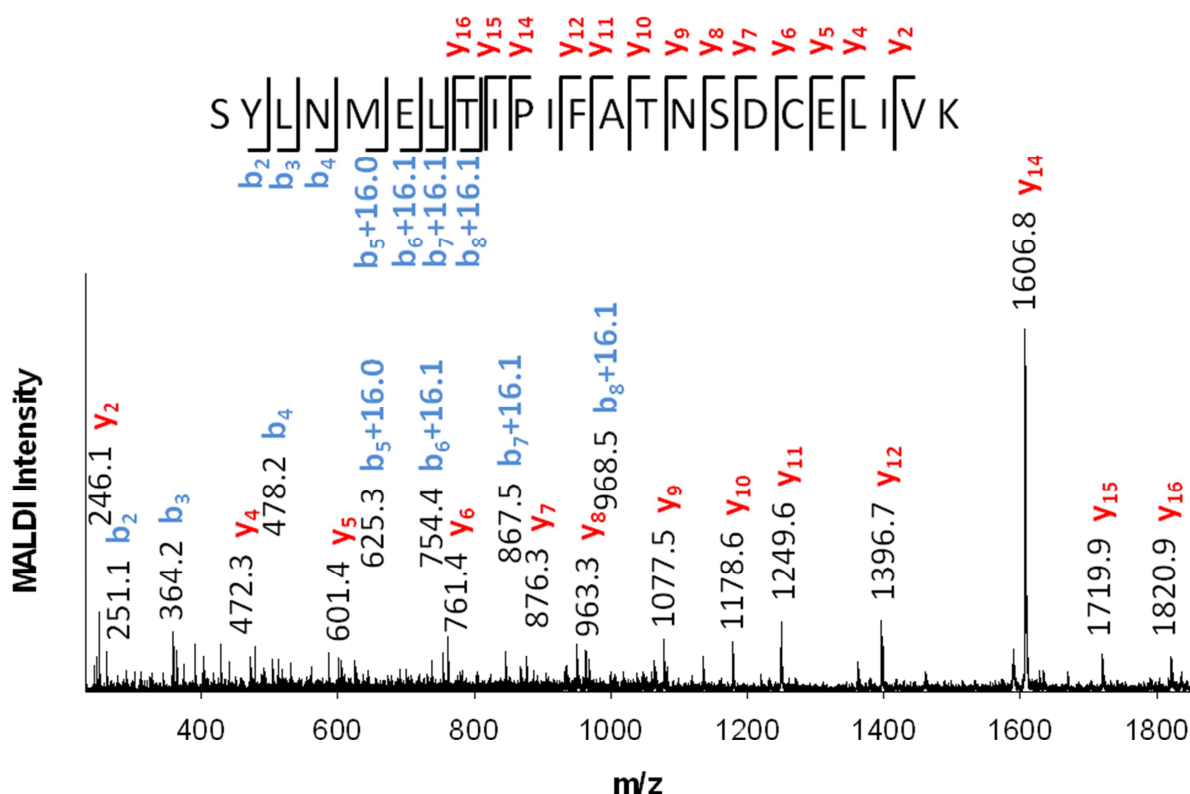


**Figure 4.8: MALDI-TOF-TOF fragmentation spectra of oxidation product m/z 2687.89.** This corresponds to oxidized trypsin peptide S84-K106 after  $^1\text{O}_2$  oxidation of MS2's capsid protein, showing the oxidation of Met88 (mass shift of +16).

#### 4.3.5 Computational rationalization of singlet oxygen findings

To explain the absence of Met88 oxidation by singlet oxygen in fr, this residue was compared to the corresponding residue in MS2 using a range of computational tools. Three factors were considered: the energy cost associated with the oxidation process, the strength of intracapsid binding (i.e. binding between capsid protein triplets) and the solvent-accessible surface area (SASA) surrounding the Met88 residue. Thermodynamic integration revealed that the two viruses had similar free energy of oxidation costs of approximately 4 kcal/mol (see appendix D, Table D2). APBS calculations (see appendix D, Table D3) showed that both shared similar electrostatic components to intracapsid binding. Calculating the SASA using the sulfur atoms of Met88 (highlighted in Fig. 4.9 A and B), however, showed a marked difference between MS2 and fr. The SASA for MS2 was measured to be  $1.6 \pm 0.2 \text{ \AA}^2$  while the SASA for fr was only at  $0.4 \pm 0.2 \text{ \AA}^2$ . This difference is illustrated in Fig. 4.9 C and D, where representative structures used to calculate the SASAs are shown.

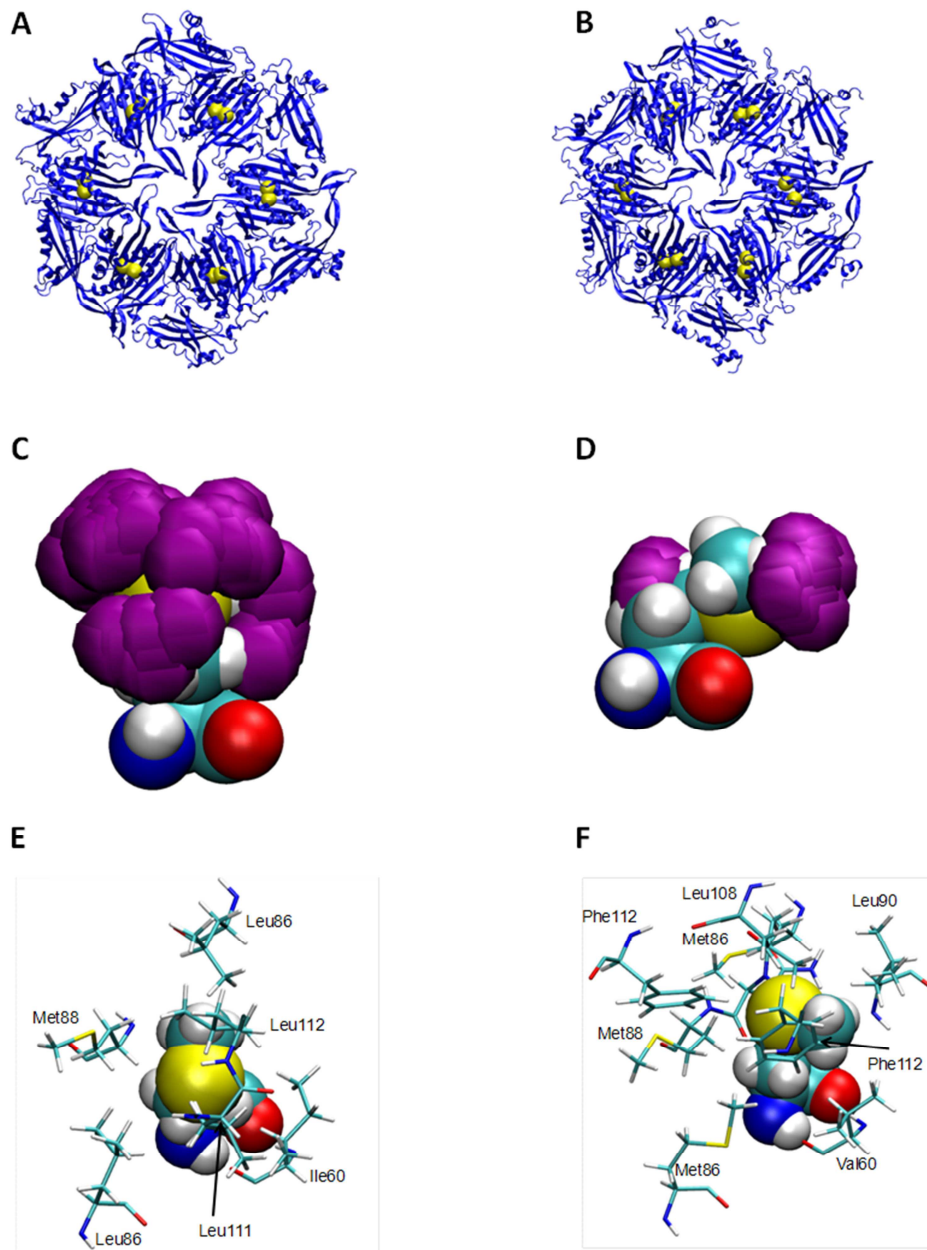


**Figure 4.9: Capsid protein views of MS2 and fr.** A and B: Plan views of fragments of the MS2 (A) and fr (B) capsid where each fragment contains six copies of the triplet. The sulfur atoms of the Met88 are shown as yellow spheres. C and D: Purple spheres represent the SASA of one of the 12 Met88 residues used to calculate the SASA for MS2 (C) and fr (D). The images show the accumulation of 10 equidistant snapshots taken from simulations of 2ns duration. The surrounding protein is not shown so as to aid clarity. The oxygen atoms are colored red, nitrogens are blue, carbons are cyan, sulfurs are yellow and hydrogens are white. E and F: Residues within 5 Å of the sulfur atom of Met88 chain A for MS2 (E) and fr (F), where Met88 is shown in the space-filling VDW representation and the surrounding residues are shown in licorice representation.

## 4.4 Discussion

According to previous work,<sup>56</sup> MS2 is inactivated by chlorine dioxide and to a smaller extent by free chlorine via protein damage, whereas UV<sub>254</sub> and <sup>1</sup>O<sub>2</sub> act mainly on the genome. Similar results were found for the three viruses investigated herein, as summarized in Fig. 4.3: we previously found that the contribution of genome damage by UV<sub>254</sub> and <sup>1</sup>O<sub>2</sub> was large for all viruses, though not sufficient to fully account for inactivation of GA. In contrast, ClO<sub>2</sub> caused no genome damage in the time frame of inactivation, confirming that the protein contribution is essential. Finally, all viruses were inactivated by FC at the same rate, whereas their genome damage varied substantially; it was therefore concluded that inactivation by FC must in part be controlled by protein damage.

Based on these findings, we thus expected protein damage to be important for inactivation by ClO<sub>2</sub> and free chlorine, and of little importance for inactivation by UV<sub>254</sub> and <sup>1</sup>O<sub>2</sub>. As can be seen in Figs. 4.2 and 4.4, this expectation was confirmed: capsid protein degradation was subtle for UV<sub>254</sub> irradiation and singlet oxygen treatment and extensive for free chlorine and chlorine dioxide.

### 4.4.1 Influence of protein composition on degradation and inactivation

As for the genome, protein composition, length and structure are likely to influence degradation. Based on amino acid reactivity (Table 4.3), significantly slower protein degradation was expected for GA compared to the two other viruses. This is due to the fact that MS2 and fr capsid proteins contain two cysteines and two methionines, the two amino acids most reactive toward oxidants (Table 4.3), whereas the GA capsid protein has neither. As such, the absence of cysteine and methionine implies that the capsid protein of GA may degrade more slowly than those of MS2 and fr upon disinfection by oxidants. Experimentally, however, the extents of capsid protein damage were similar for all three viruses (Figs. 4.2 and 4.4). This suggests that the composition of the viral protein is not the most important factor governing its degradation, but that protein structure may also play an important role. For example, studies have shown that despite their high reactivity, cysteines in bacteriophage f2, a virus similar to the ones investigated here, were not degraded by ClO<sub>2</sub> due to their poor accessibility.<sup>153</sup>

In the following paragraphs, we present a detailed discussion of the observed effects of each disinfectant on the capsids of the three viruses, and interpret these findings in the context of protein composition and structure, as well as the concurrent inactivation and genome damage.

#### 4.4.2 UV<sub>254</sub>

Several aromatic amino acids can be affected by UV<sub>254</sub> irradiation (Table 4.3), yet only little degradation of peptides containing these residues was observed (Fig. 4.5). This can be explained by the nucleotides' greater sensitivity to degradation by UV<sub>254</sub> compared to that of amino acids (Table 4.3), which implies that the three viruses were inactivated by genome degradation before substantial damage to aromatic amino acids in the capsid protein could accumulate. For MS2 and fr, however, slight capsid degradation was observed in peptide 44-49, which contains no UV<sub>254</sub>-susceptible amino acids (Fig. 4.5). In previous work,<sup>170</sup> it was shown that the degradation of peptide 44-49 in MS2 was caused by backbone cleavage around amino acids Cys46 and Ser47. This cleavage event was facilitated by the presence of both RNA and cysteine at the cleavage site. fr also contains the relevant cysteine in its capsid protein, whereas in GA this cysteine is absent. Consequently, cleavage at the same site was found for fr but not for GA (Fig. 4.6). The cleavage event is thought to contribute to MS2 inactivation by preventing it from injecting its genome into the host.<sup>56</sup> Besides genome degradation, capsid cleavage thus contributes to a small extent to the inactivation of MS2, and presumably fr, while this mechanism is not present in GA.

Since neither genome degradation nor capsid protein cleavage could account for the inactivation of GA by UV<sub>254</sub> (Fig. 4.3), GA's inactivation must involve a relevant contribution of the A protein. Consistent with this hypothesis, significant degradation of the A protein was observed (Fig. 4.7). Furthermore, it cannot be excluded that the viruses underwent protein modifications, which are not measurable with the methods used here, such as structural changes that inhibit the virus from binding to its host.

#### 4.4.3 Singlet oxygen

Previous work has shown that inactivation of MS2 by <sup>1</sup>O<sub>2</sub> was mostly caused by genome damage.<sup>56</sup> In addition, a small portion of inactivation was caused by a loss in MS2's ability to attach to its host, which was attributed to degradation of the A protein. Similar to MS2, the extent of genome degradation in fr roughly corresponded to its extent of inactivation by <sup>1</sup>O<sub>2</sub>. However, this was not the case for GA, for which genome degradation was too small to account for inactivation (Fig. 4.3). This discrepancy could not be explained by contribution of the capsid protein to inactivation, since GA's capsid remained unaffected by this disinfection method. Similar to what was observed with UV<sub>254</sub>, GA's inactivation by <sup>1</sup>O<sub>2</sub> must therefore involve a significant contribution of the A protein. The A protein analysis revealed degradation of peptide 56-65, which contain <sup>1</sup>O<sub>2</sub>-susceptible residues tryptophan and tyrosine (Fig. 4.7, Table 4.2). Only a small part of the A protein was analyzed; it is, however, likely that unanalyzed parts of

the protein also degrade, as was previously observed for MS2.<sup>56</sup> Furthermore, singlet oxygen is known to cause protein cross-linkages,<sup>131</sup> which may not be detected with the methods used here but may further contribute to inactivation.

In MS2,  $^1\text{O}_2$  caused oxidation of the capsid protein Met88 residue (Figs. 4.5 and 4.8). Interestingly, fr's capsid protein Met88 was not affected by  $^1\text{O}_2$ . From a thermodynamic standpoint (see appendix D, Table D2), if MS2's Met88 is oxidized, then fr's Met88 should also be oxidized. Furthermore, the magnitude of binding energy between capsid triplets was found to be similar, and the electrostatic component of the MS2 intracapsid binding energy was even slightly stronger than that of fr (see appendix D, Table D3); therefore, the observed Met88 oxidation difference was not due to differences in capsid stability. An explanation could be found, however, by considering the solvent-accessible surface area (SASA) of the Met88 sulfur atoms, which did show a marked difference between MS2 and fr. The SASA for fr was measured to be four times smaller than that of MS2 (Fig. 4.9 C-D). The difference in SASA is attributed primarily to the position of the Leu90 residue (see appendix D, Fig. D3), which allows the region surrounding the sulfur of Met88 to more easily accommodate a  $^1\text{O}_2$  atom in MS2 than the same region in fr. The residues within 5 Å of the sulfur atom of Met88 for both capsid proteins are shown in Fig. 4.9 E-F. In both cases the protein surrounding the sulfur atoms is hydrophobic, a more amenable environment to  $^1\text{O}_2$  than water. In addition water exhibits a slightly higher penetration of the capsid structure of fr than that of MS2 (see appendix D, Fig. D4).

Our calculations thus indicate that in the vicinity of Met88,  $^1\text{O}_2$  can have faster diffusion kinetics in MS2 than in fr due to both a larger accessible space and smaller hindrance originating from buried waters that must be displaced to access the Met88 site. We note here that the local environment and accessibility to a specific site have been reported as being crucial elements in accounting for protein reactivity toward  $^1\text{O}_2$ .<sup>171</sup>

#### 4.4.4 Free chlorine

Free chlorine is known to inactivate viruses by both a genome and a protein component.<sup>56,64,147,172</sup> This is consistent with our previous findings for MS2<sup>56</sup> that despite the major role of genome degradation, inactivation is in part controlled by a protein component. Indeed, free chlorine-induced capsid protein damage was extensive for all three viruses (Figs. 4.2 and 4.4). The strong and slightly variable effects of FC on the capsid proteins is in agreement with our finding that all three viruses were inactivated by FC at

the same rate (Fig. 4.3). In other words, even though the viruses incurred different inactivating events, the overall damage to genomes and proteins resulted in a similar inactivation rate.

The peptide degradation pattern (Fig. 4.5) shows that compared to the other treatments, degradation of proteins by free chlorine treatment was less specific. The relatively homogeneous distribution of damage in the various regions of the capsid protein is due to FC's ability to not only react with amino acid side chains, but also to cleave protein backbones (Fig. 4.6, Table 4.3). Nevertheless, the peptides most readily degraded tended to contain FC-susceptible residues (methionine, cysteine and tryptophane) (e.g., peptides 84-106, 107-113 and 44-49 in MS2), whereas the peptides lacking susceptible residues were more resistant to FC (e.g., peptides 50-56, 39-43 and 107-113 in fr).

#### **4.4.5 Chlorine dioxide**

Chlorine dioxide has been reported to have no effect on the viral genome, and inactivates viruses solely via protein degradation.<sup>56,128</sup> So as expected, we found a complete absence of genome damage for all three viruses after disinfection with ClO<sub>2</sub> (Fig. 4.3), whereas extensive capsid protein degradation was found (Figs. 4.2 and 4.4). Protein degradation was fastest for GA, which corresponds to the order of observed inactivation rates (Fig. 4.3). This suggests that virus inactivation is governed by capsid protein degradation, a point that is further supported by the fact that capsid protein degradation was directly proportional to inactivation (Fig. 4.4).

The peptide results (Fig. 4.5) showed a pattern of localized degradation with the majority of capsid protein degradation occurring between amino acids 61 and 106. Interestingly, not all of the peptides in this region contained amino acids susceptible to ClO<sub>2</sub> (cysteine, tryptophane and tyrosine, Table 4.3). Their degradation can be rationalized by the fact that ClO<sub>2</sub> is a one-electron acceptor that can create radicals upon reaction.<sup>154</sup> This can trigger radical chain reactions that damage adjacent parts of the protein, as has been observed previously with hydroxyl radicals.<sup>173</sup> Spatially, the affected regions are located around the pores and then propagate to the inside space between the pores (Fig. 4.10). This confirms that only readily accessible residues, but not those buried within the protein, were affected by ClO<sub>2</sub>.

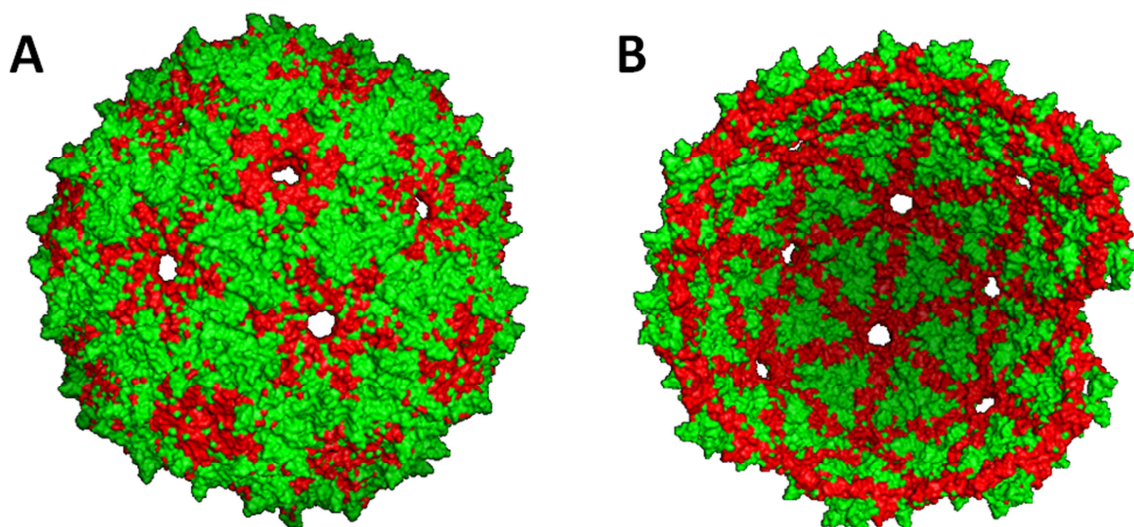


**Figure 4.10:** Location of degraded peptides after  $\text{ClO}_2$  treatment on the outside (A) and inside (B) of the MS2 capsid. Intact regions are shown in green; degraded regions are shown in red.

Our findings regarding the extent of genome and protein degradation provide some preliminary conclusions regarding the prevailing disinfection mechanisms. First, the main target of  $\text{UV}_{254}$  and  $^1\text{O}_2$  is the genome, which may result in the inability of a virus to replicate. In these cases, the contribution of capsid degradation was minor, and could not explain the relative trends in inactivation among the three viruses. Instead, the A protein was identified as a more important target for inactivation. Free chlorine can target both genome and proteins, leading to a loss in replication, as well as protein-mediated functions involved in infection (i.e., host attachment, genome injection into the host). Consistently, both genome and protein damage was shown to contribute to disinfection by FC, though their contribution varied between the three viruses. For  $\text{ClO}_2$ , on the other hand, capsid protein degradation showed similar trends as inactivation, suggesting that viruses disinfected by  $\text{ClO}_2$  may retain the ability to replicate, but cannot penetrate the host cell. Finally, the relative trends of capsid protein damage could in part be rationalized by considering structural (solvent-accessible surface area) as well as compositional features (involvement of cysteines in  $\text{UV}_{254}$  disinfection, or methionines as targets in  $^1\text{O}_2$  disinfection).

Overall, these findings are consistent with previous work,<sup>56</sup> in which the loss of the individual functions of MS2 upon disinfection were investigated. Interestingly, however, the subtle differences in genome and protein composition of fr and GA compared to MS2 were nevertheless sufficient to cause some alterations in the prevailing inactivation mechanisms.

## 4.5 Conclusion

In conclusion, this study (along with chapter 3) illustrates the complexity involved in predicting virus inactivation. Depending on the disinfectant, the three related viruses exhibited equal, similar, or very different inactivation rates. Furthermore, the relative susceptibilities of the three viruses varied with the different disinfectants. This could be explained by differences in both, the mode of action of the four inactivating treatments, and the inactivation mechanisms among the viruses.

For treatments with a strong genome-damaging component ( $UV_{254}$ ,  $^1O_2$  and FC), inactivation kinetics were generally similar among the three phages. In contrast, the protein-damaging  $ClO_2$  led to much greater differences in inactivation. This finding leads to the hypothesis that it may be possible to predict the inactivation kinetics of experimentally not tractable viruses based on related species, as long as the disinfectant is primarily targeting the genome. On the other hand, if a protein component is involved such predictions are not likely to be accurate. We caution, however, that this hypothesis remains to be tested with greater sets of related viruses. In particular, it may only be valid for viruses with similar genome length, such as the three species studied herein.

To allow for accurate predictions of virus inactivation, we need to improve our understanding of the factors that govern genome and protein susceptibility to disinfectants beyond composition alone. This may include better knowledge of the disinfectants' mode of action, and a comprehensive understanding of the effect of structure on genome and protein reactivity. Finally, it would be desirable to know the relevant virus domains involved in the infectious cycle, in particular host attachment sites. This would enable more conclusive statements of the impact of protein degradation on inactivation, and would allow a more targeted analysis.



# MS2 and Qbeta inactivation at the copper-water interface

## 5.1 Introduction

For purposes of drinking water disinfection, much work has been done with respect to dissolved disinfectants as for example chlorine, ozone or chlorine dioxide. The kinetics for these treatments have been studied in depth for many different microorganisms<sup>105,174,175</sup> and the molecular-level mechanisms of inactivation are increasingly being investigated.<sup>56,112</sup> However, less is known about heterogeneous disinfection, i.e, inactivation processes involving surfaces or particles.

The association of viruses with surfaces and particles is often reported to protect viruses from inactivation by homogeneous disinfectants, by mechanisms such as light shielding or consumption of the disinfectant.<sup>66,67,176</sup> However, surfaces may in some cases also cause inactivation. In a noteworthy study, Murray and Laband<sup>92</sup> showed that copper and aluminum oxides inactivate Poliovirus effectively, whereas iron oxide (hematite  $\text{Fe}_2\text{O}_3$ ) did not. In a more recent study,<sup>177</sup> different iron oxides and hydroxides were assessed for their inactivating properties and it was found that only one iron oxide (magnetite,  $\text{Fe}_3\text{O}_4$ ) had the capacity to inactivate bacteriophages. Finally, it has also been reported that  $\text{Fe}^{\text{II}}$  as well as zero-valent iron inactivate MS2 bacteriophage efficiently.<sup>178</sup>

An inactivating surface that has received special scrutiny is metallic copper. Copper jars are common storage containers in many Indian homes. They have been shown to possess a very good disinfection capacity against important pathogens.<sup>73</sup> The inactivation of bacteria in copper jars has been extensively studied by Sharan et al., who observed that inactivation was more efficient at higher temperatures.<sup>179</sup> They also studied the influence of presence of organic and inorganic matter inside the copper jars, and determined that the presence of natural organic matter (NOM) or degraded proteins reduced the inactivation capacity of the copper jar. The presence of NOM furthermore resulted in increased

concentrations of dissolved copper, though its complexation with NOM resulted in low bioavailability.<sup>180</sup> The drawback concerning the storage of water in copper jars is that the dissolved copper concentration in the presence of organic matter may exceed the maximum concentration recommended for drinking water (2 mg/L according to WHO guidelines),<sup>181</sup> which could lead to gastrointestinal disease or even chronic liver cirrhosis.<sup>180</sup> The other inconvenience of copper jars is that they are becoming expensive and not all the households in India can afford them. In order to provide a cheaper disinfection method, Sudha et al. developed an inexpensive copper coil that could be added to all containers to efficiently inactivate the microorganisms in solution.<sup>182</sup> In addition to the fact that it is cheap, the copper coil is reusable, does not need fuel or sunshine and its maintenance is easy.

Copper has also shown effective disinfection of fungi and algae,<sup>75</sup> as well as various viruses including bacteriophages,<sup>183</sup> Rotavirus<sup>73</sup> and Influenza virus.<sup>184</sup> Inactivation rates differ greatly between viruses, which could not be attributed to the type of genome (RNA or DNA), suggesting that some other key element may be responsible for inactivation. For example, inactivation of HIV-1 by copper induced the degradation of a protease essential to viral replication.<sup>185</sup> Finally, a comparison of polyethylene and copper pipes showed that the latter greatly reduced the biomass formation rate.<sup>76</sup>

The biocidal properties of copper surfaces are thus evident, yet the mechanisms involved are not understood. To further exploit copper surfaces for disinfection purposes, or to optimize current applications, it is imperative to study the interactions between copper and microorganisms, to better understand the processes governing adsorption and inactivation. The main goal of this study was to assess the mechanisms by which interactions of viruses with copper lead to inactivation. Specifically, we aimed to identify the type of interactions involved in inactivation, and to characterize the damage inflicted on the viruses.

Several different interactions may lead to the association of viruses with surfaces. These interactions exhibit different strengths and include (in order of increasing strength per interaction):<sup>186</sup> van der Waals interactions (4-5 kJ/mol), hydrophobic interactions (~10 kJ/mol), hydrogen bonds (16-20 kJ/mol), electrostatic interactions (~30 kJ/mol) and covalent bonds (between 150 and 900 kJ/mol depending on the atoms involved). In order to determine which interactions can cause virus adsorption or inactivation, they must be separated and tested individually. For this purpose, an ideal approach is the use of Self-Assembled Monolayers (SAMs). SAMs consist of alkyl chains of chosen length terminated on one end by a thiol group bound to a gold substrate, and on the other one by a functional group. The thiol end of the carbon chain binds to gold efficiently and in an ordered fashion,<sup>187</sup> while the functional group forms the interface to the solution phase and promotes a specific interaction type.<sup>188</sup> SAMs thus provide a system

to study virus adsorption in detail by isolating each type of interaction (electrostatic, hydrophobic, etc.) on a flexible but defined surface.<sup>189,190</sup> The simplicity and reliability of SAM preparation, the reproducibility of the generated surface, the flexibility of generating a wide range of surfaces and the multiple techniques to characterize SAMs have made them of great interest to many technological domains, including material sciences (e.g. microelectrodes, microscopy probes)<sup>191</sup> or biotechnology (e.g., mimicking of natural cell surfaces, biosensors).<sup>192,193</sup> In the domain of environmental science, they have been used to represent the properties of natural organic matter.<sup>194</sup>

In the framework of this study, we used SAMs terminated in functional groups that induce either electrostatic (amine ( $-\text{NH}_3^+$ ) and carboxyl ( $-\text{COO}^-$ ) terminated SAMs) or hydrophobic interactions (methyl ( $-\text{CH}_3$ ) terminated SAMs), or that could be involved in hydrogen bonding (hydroxyl ( $-\text{OH}$ ) terminated SAMs). Finally, interactions of the virus with the naked gold surface are mainly governed by van der Waals interaction. Any of these interactions may contribute to virus adherence to copper surfaces.

Bacteriophages were used as test organisms in this study. They are commonly used surrogates for human viruses,<sup>25</sup> but are easier to culture and safer to work with. Specifically, we used MS2 and Qbeta, two bacteriophages from the *Leviviridae* family (Fig. 5.1).

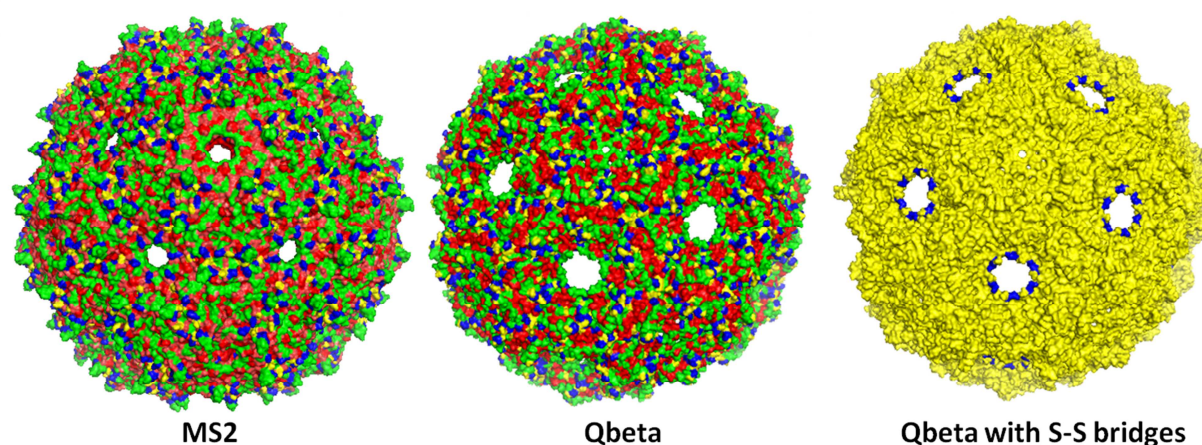


**Figure 5.1: MS2 and Qbeta bacteriophage, surface characteristics.** Left: MS2; middle: Qbeta; Distribution of negatively charged (blue), positively charged (yellow), hydrophobic (red), inducing H-bonding (green) amino acids on the surface using software *pymol*. Right: Qbeta with highlighted disulfide bridges (blue). (PDB codes: 2MS2, 1qbe).

These organisms are very similar in size and shape and are composed of a positive single-stranded RNA (3569 and 4160 nucleotides for MS2 and Qbeta, respectively) surrounded by a capsid protein composed of 180 copies of one single protein (129 amino acids for MS2 and 132 for Qbeta). Additionally, both

phages contain one copy of a maturation protein, also called A protein. One of the major differences between MS2 and Qbeta is that Qbeta possesses disulfide bridges that connect the individual capsid proteins (right panel in Fig. 5.1).<sup>31</sup> These bonds lead to an enhanced stability of the capsid. However, they could also be a weak point with respect to disinfection as they can easily be reduced, causing deformation or disintegration of the capsid. The second important difference between MS2 and Qbeta resides in the fact that they exhibit different isoelectric points (IEP), around 3.5 for MS2 and around 5.3 for Qbeta.<sup>195</sup> This implies that, depending on the pH of the solution, the two viruses exhibit opposite charges which will lead to opposite electrostatic interactions with charged surfaces.

## 5.2 Materials and methods

Two experimental setups were used in this study. The first involved batch systems, which were used to assess inactivation kinetics as well as damage on virus genome and capsid proteins. This system allowed us to take liquid samples at various time points and to increase the concentration of viruses in solution. The second setup consisted of a flow-through system. Specifically, measurements of adsorption onto SAMs and resulting inactivation were performed in a flow cell coupled to a Quartz Crystal Microbalance with Dissipation monitoring (QCM-D). The adsorption experiments were performed by our collaborators (Antonius Armanious and Michael Sander at ETHZ), and the corresponding inactivation experiments were performed in our laboratories using the same setup. All the experiments were performed at room temperature.

### 5.2.1 Chemicals

NaCl (99.5%), NaH<sub>2</sub>PO<sub>4</sub>·H<sub>2</sub>O (99%), CaCl<sub>2</sub>·2H<sub>2</sub>O (99%), D-glucose (for analysis), HPLC grade acetonitrile and aminoethanethiol (95%) were purchased from Acros Organics (Geel, Belgium). Bis-Tris (≥98%), polyethylene glycol 6000 (PEG 6000), streptomycin sulfate, copper foil (99.98%, thickness 0.5 mm), 1-dodecanethiol (≥98%), sinapinic acid (98%), L-cysteine (98.5%), iodoacetamide, 11-mercapto-1-undecanol (99%), 11-mercaptoundecanoic acid (98%) and α-cyano-4-hydroxycinnamic acid were obtained from Sigma-Aldrich (Germany). HCl (25%), CH<sub>3</sub>COOH (100%), meat extract (for microbiology) and H<sub>2</sub>SO<sub>4</sub> (95-97%) were obtained from Merck (Darmstadt, Germany). H<sub>2</sub>O<sub>2</sub> (30%) and glycine (99%) were obtained from Fluka (Steinheim, Germany). Yeast extract (for microbiology) was obtained from Chemie Brunschwig (Basel, Switzerland). Bactotryptone was obtained from AxonLab (Baden, Switzerland). Sodium dodecyl sulfate (SDS, research grade) was obtained from SERVA (Heidelberg,

Germany). Absolute ethanol (analytical reagent grade) was obtained from Fisher Scientific (Waltham, MA). Trypsin and Chymotrypsin were purchased from Promega (Madison, WI). Ultrapure water ( $>18 \text{ M}\Omega\text{cm}^{-1}$ ) was used for all aqueous solutions.

### 5.2.2 Microorganisms

Bacteriophage MS2 (DSMZ 13767) and Qbeta (DSMZ 13768) as well as their *Escherichia coli* host (DSMZ 5695) were purchased from the German Collection of Microorganisms and Cell Cultures (DSMZ, Braunschweig, Germany). The viruses were propagated in *E. coli* and subsequently concentrated. The virus was initially inoculated into 1 liter of LB medium (10 g of Bactotryptone, 1 g of yeast extract, 8 g of NaCl supplemented with 1 g of D-glucose, 0.3 g of  $\text{CaCl}_2$  and 2 mg of streptomycin sulfate containing log-phase *E. coli* at roughly  $10^7$  CFU/ml) at a multiplicity of infection (MOI) of 0.1 (for both MS2 and Qbeta) as described previously.<sup>108</sup> Five hours post-inoculation, the liter of bacterial-viral suspension was mixed with 5 ml of chloroform to induce the lysis of all bacteria. The suspension was centrifuged for 15 min at 4'000 g to separate the bacterial debris from the virus. The supernatant was then filtered and concentrated with 100 kDa Microcon centrifugal filters (Millipore, Billerica, MA) to a volume of about 1 mL, and finally was washed twenty times with dilution buffer (DB: 5 mM  $\text{PO}_4^{2-}$ , 10 mM NaCl, pH 7.4). Infectivity was assessed by enumeration of plaque forming units (pfu) using the double agar layer method.<sup>109</sup> All virus manipulations (dilutions for plating, washing) were conducted in dilution buffer (DB).

### 5.2.3 Batch experiments with copper

Two types of batch experiments were performed; one in presence of copper foil ("*Cu foil*") and one after removal of the foil only in presence of dissolved copper ("*dissolved Cu*"). This setup served to distinguish between the effect of the foil and the effect of dissolved copper.

To assess the effect of the copper surface on virus infectivity (*Cu foil* experiment), 15 mL of acetate buffer (3 mM acetic acid, ionic strength (IS) 10 mM adjusted by NaCl, pH 5 adjusted with NaOH (0.1 M)) were placed in a glass beaker and were spiked to a final virus concentration (MS2 or Qbeta) of  $5 \times 10^7$  pfu/mL. A copper foil with a  $2 \text{ cm}^2$  surface area was added to the solution and mixed on a stir plate at 200 rpm. 100  $\mu\text{L}$  samples were taken at regular intervals and were analyzed by plaque assay to monitor inactivation, and by quantitative Polymerase Chain Reaction (q-PCR; detailed below) to evaluate the decrease in the number of genome copies (a proxy for virus adsorption). At the end of each experiment, the viruses were desorbed by addition of 15 mL of a beef extract solution (BE, containing 6% meat extract and 0.1 M glycine at pH 9.3) as described previously.<sup>196</sup> Before each experiment, the copper foil

was subjected to cleaning with piranha solution ( $\text{H}_2\text{SO}_4:\text{H}_2\text{O}_2$  3:1) and was thoroughly rinsed in working buffer. These experiments were conducted in duplicates with good reproducibility.

In the *Cu dissolved* experiment, the copper foil was first immersed in the acetate buffer for 20 minutes and then removed before addition of the virus.

The copper dissolution rate in the *Cu foil* experiments was measured by Inductive Coupled Plasma Atomic Emission Spectroscopy (ICP-AES, ICPE 9000, Shimadzu, Kyoto, Japan).

#### 5.2.4 RNA extraction and quantitative Polymerase Chain Reaction (q-PCR)

200  $\mu\text{L}$  samples were extracted with a PureLink<sup>TM</sup> Viral RNA/DNA Kit (Invitrogen). Extracts were reverse transcribed and amplified with a Rotorgene 3000 quantitative PCR platform (Corbett Life Science, Sydney, Australia) using the thermocycling conditions described previously.<sup>108</sup> The primer sets M2 and Q2 (Table C1) were used to monitor the concentration of MS2 and Qbeta genome copies in the supernatant of *Cu foil* batch experiments. The thermocycle conditions used were: 10 min at 42 °C, 20 s at 95 °C, 45 cycles of 95 °C for 15 s, 60 °C for 20 s, and 72 °C for 20 s, followed by a melting ramp from 72 to 95 °C, holding for 45 s on the first step (72 °C) followed by 5-s holds on all subsequent temperatures.

#### 5.2.5 Analysis of copper disinfection kinetics

Two analyses were performed to model inactivation kinetics. First, inactivation was analyzed as a function of time, using a first-order model (Eq. 5.1):

$$\ln(C_v/C_{v,0}) = -kt \quad \text{Eq. 5.1}$$

Here,  $t$  corresponds to the duration of the experiment (in minutes),  $C_v$  and  $C_{v,0}$  correspond to the infectious virus concentrations (in pfu/mL) at time  $t$  and 0, respectively, and  $k$  is the first-order inactivation rate constant (in  $\text{min}^{-1}$ ). In addition, inactivation was assessed as a function of the dissolved Cu dose, using a Chick-Watson model (Eq. 5.2):

$$\ln(C_v/C_{v,0}) = -k_{\text{CW}} C_{\text{Cu}} t \quad \text{Eq. 5.2}$$

where  $C_{\text{Cu}} t$  is the dissolved copper dose, expressed as the product of the time of exposure (in minutes) and the dissolved copper concentration  $C_{\text{Cu}}$  (in mg/L),  $C_v$  and  $C_{v,0}$  are the infective virus concentrations (in

pfu/mL) at a copper dose of  $C_{Cu,t}$  or 0 respectively, and  $k_{CW}$  is the Chick-Watson inactivation rate constant (in  $[mg/L \cdot min]^{-1}$ ).

To determine if significant differences existed between inactivation in the presence and absence of the foil, rate constants were compared by ANCOVA analysis, whereby a p value of  $<0.05$  was deemed significant.

### 5.2.6 Self-assembled monolayers (SAMs): description and preparation

SAMs are alkane chains of various lengths (n) terminated on one side by a thiolate group bound to a gold substrate and on the other end by a specific selected chemical function (R). They can be prepared by immersion of the substrate in either the alkylthiol solution ( $HS-(CH_2)_n-R$ ) or in a dialkyl disulfide solution ( $R-(CH_2)_n-S-S-(CH_2)_n-R$ ); both will spontaneously react to form a covalent thiolate bond with the gold as shown in Fig. 5.2.

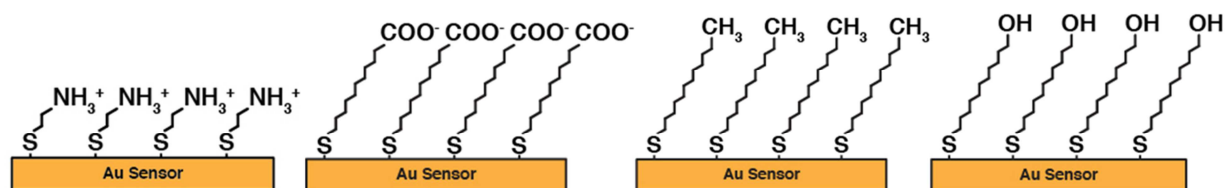
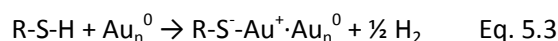


**Figure 5.2: Representation of the self-assembled monolayers on gold sensors used in this study.** The alkyl chain can be of various lengths and can be terminated by different chemical functions. Representations provided by Antonius Armanious (ETHZ).

Even though the alkylthiol is more efficient at forming the thiolate-gold bond than the dialkyl sulfide,<sup>197</sup> the resulting surfaces are undistinguishable. The suggested mechanism for the alkylthiol reaction is an initial oxidative addition of the S-H bond, followed by a reductive elimination of the hydrogen, resulting in the formation of a thiolate bond as described in Eq 5.3:<sup>198</sup>



The dialkyl disulfide was suggested to react via oxidative addition according to Eq. 5.4:<sup>198</sup>



This first step (thiolate-gold bond formation) to the assembly of the monolayer is a fast process whereas the rearrangement of the alkyl chain via inter-chain van der Waals interactions is much slower.<sup>188</sup> As the alkyl chains repel each other, they align to minimize the interactions between them, yielding a very ordered system and allowing the tails to form a uniform surface.<sup>187,198</sup> The alkyl chains were found to be tilted from the perpendicular to the surface by an angle of 26-28°, and the thickness of such monolayers is usually between 1 and 3 nm.<sup>199</sup>

Herein, four differently terminated SAMs were studied (Table 5.1). They were prepared from alkylthiols on QCM-D gold sensors (LOT-QuantumDesign, Darmstadt Germany) according to a published protocol<sup>200</sup> with slight modifications. In brief, the gold sensor was sonicated in 2% SDS for 15 minutes. After sonication, rinsing and drying with N<sub>2</sub>, the surface was subjected to piranha cleaning for 2 minutes. It was then intensively rinsed with ethanol (96%) and water and finally dried with N<sub>2</sub> before being immersed into the corresponding alkylthiol solution (0.5-1 mM in pure ethanol). The sensor was left in solution for 18-24 hours under gentle shaking. Before use, it was sonicated in ethanol for 2 minutes in order to remove any unbound alkylthiol and dried with N<sub>2</sub>.

**Table 5.1: Description of SAMs.** Grey colored materials: hydrophobic surfaces; no color: hydrophilic surfaces.

Name of alkylthiol	Chemical formula	Abbreviation	Interaction type
None	Au	Au	Van der Waals
aminoethanethiol	HS(CH <sub>2</sub> ) <sub>2</sub> NH <sub>2</sub>	-NH <sub>3</sub> <sup>+</sup>	Electrostatic
11-mercaptoundecanoic acid	HS(CH <sub>2</sub> ) <sub>10</sub> COOH	-COO <sup>-</sup>	Electrostatic H-bonding*
11-mercapto-1-undecanol	HS(CH <sub>2</sub> ) <sub>11</sub> OH	-OH	H-bonding
1-dodecanethiol	HS(CH <sub>2</sub> ) <sub>11</sub> CH <sub>3</sub>	-CH <sub>3</sub>	Hydrophobic

\* Because the pKa of the functional group is 4.95, this surface also contains the protonated -COOH groups, which may undergo H-bonding



### 5.2.7 Adsorption and inactivation experiments in a teflon QCM-D flow-through cell

Virus adsorption onto gold and SAMs was assessed by our collaborators at ETHZ using a Quartz Crystal Microbalance with Dissipation monitoring (QCM-D).<sup>201</sup> This method allows real-time quantification of adsorption of biomacromolecules onto a sensor with an extremely high sensitivity ( $< 1 \text{ ng/cm}^2$ ). The QCM-D method detects changes in oscillation frequency of the sensor due to virus adsorption over time, which is then converted to adsorbed mass. An output obtained by QCM-D measurement is shown in Fig. 5.3. From the change in resonance frequency (yellow and red lines in Fig. 5.3), the adsorbed mass can be calculated, and the change in dissipation factor (blue lines in Fig. 5.3) gives information about the viscoelasticity of the layer. For homogeneous, non-dissipative films, the Sauerbrey equation can be used to describe the mass adsorbed according to the change in resonance frequency per surface unit (Eq. 5.5):<sup>202,203</sup>

$$M = C/n \cdot \Delta f \quad \text{Eq. 5.5}$$

Where  $M$  is the adsorbed mass [ $\text{ng/cm}^2$ ],  $C$  is the mass sensitivity constant (equal to  $-17.7 \text{ [ng}\cdot\text{cm}^{-2}\cdot\text{Hz}^{-1}]$ ),  $n$  is the overtone number (equal to 1, 3, etc.) and  $\Delta f$  is the change in resonance frequency. It is important to note that the mass  $M$  measured includes water, which represents about 80% of the total mass of the virus.<sup>204</sup> A full monolayer of viruses corresponds to an adsorbed mass  $M$  of  $2\,500 \text{ ng/cm}^2$ , which corresponds to about  $5 \times 10^{10}$  viral particles/ $\text{cm}^2$ .

The adsorption rate is determined from the initial, linear phase of the adsorption curve. Comparing the adsorption rates of different surfaces can give information about the virus' relative affinity to these surfaces. Herein, the adsorption data are represented as relative attachment efficiencies. These were calculated as adsorption rate/maximum adsorption rate, whereby the rate of adsorption to the positively charged SAM ( $-\text{NH}_3^+$ ) served as the proxy for the maximum adsorption rate.

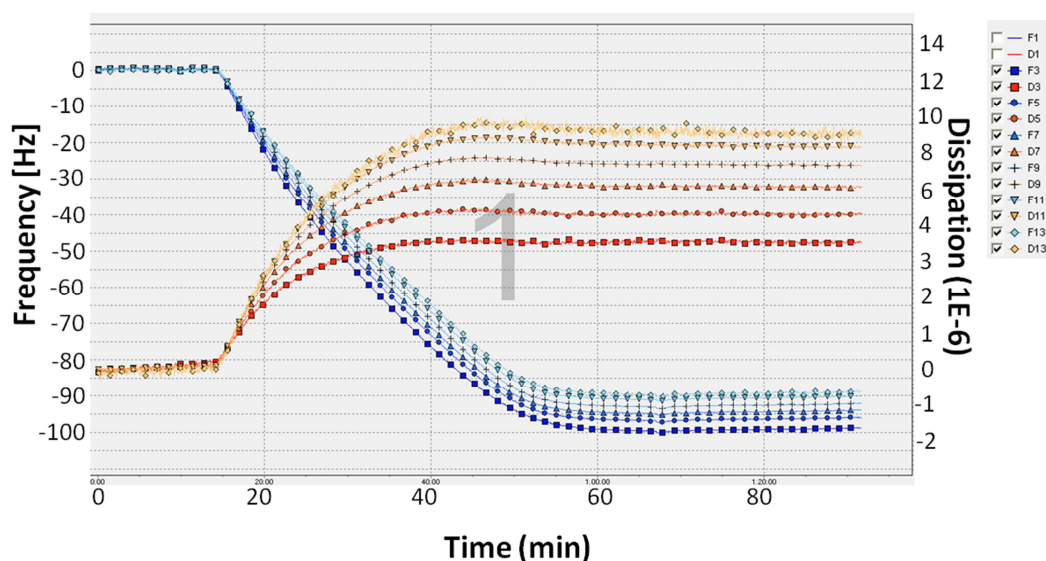


**Figure 5.3: QCM-D output for adsorption monitoring.** Typical output obtained for adsorption of viruses on SAMs (here MS2 on  $\text{NH}_3^+$ ). The yellow and red lines represent the change in resonance frequency [Hz] for the different overtones and the blue lines represent the change in dissipation.

The protocol used to monitor inactivation caused by adsorption is outlined in Fig. 5.4. Specifically, the sensor was placed in a QCM-D teflon cell and buffer was passed through the system at a 50  $\mu\text{L}/\text{min}$  rate by means of a peristaltic pump (KdScientific, Holliston, MA). The buffer used was generally Bis-Tris (3 mM) at pH 6 and the ionic strength was adjusted to 10 mM with NaCl, except for the carboxyl terminated SAM (3 mM acetate buffer, pH 5 and IS adjusted to 10 mM with NaCl) and for the naked gold surface (3 mM Bis-Tris, pH 6 and IS adjusted to 250 mM with NaCl). After 30 minutes of buffer exposure, the running solution was changed to the buffer containing virus ( $5 \times 10^{10}$  pfu/mL), of which 3.8 mL were passed over the sensor (about 60 minutes). This exposure of virus solution to the surface has shown to induce a complete monolayer of viruses.<sup>201</sup> Then the surface was rinsed with buffer for 60 minutes to remove any unbound viruses. The pump was then turned off and the sensor was left in contact with the viruses. After three hours, the cell was opened and the sensor was removed and immediately immersed in 3 mL beef extract solution for 30 minutes while gently shaking. A sample of the starting virus solution (before adsorption) and of the final beef extract solution (viruses desorbed after adsorption onto the sensor) were taken and analyzed for infective viruses by culturing and genome copies by q-PCR. Control samples showed that no inactivation occurred after 4 hours of contact between the virus and the different buffers used in these studies. These experiments were performed in triplicates for Qbeta with good reproducibility and in duplicate for MS2.

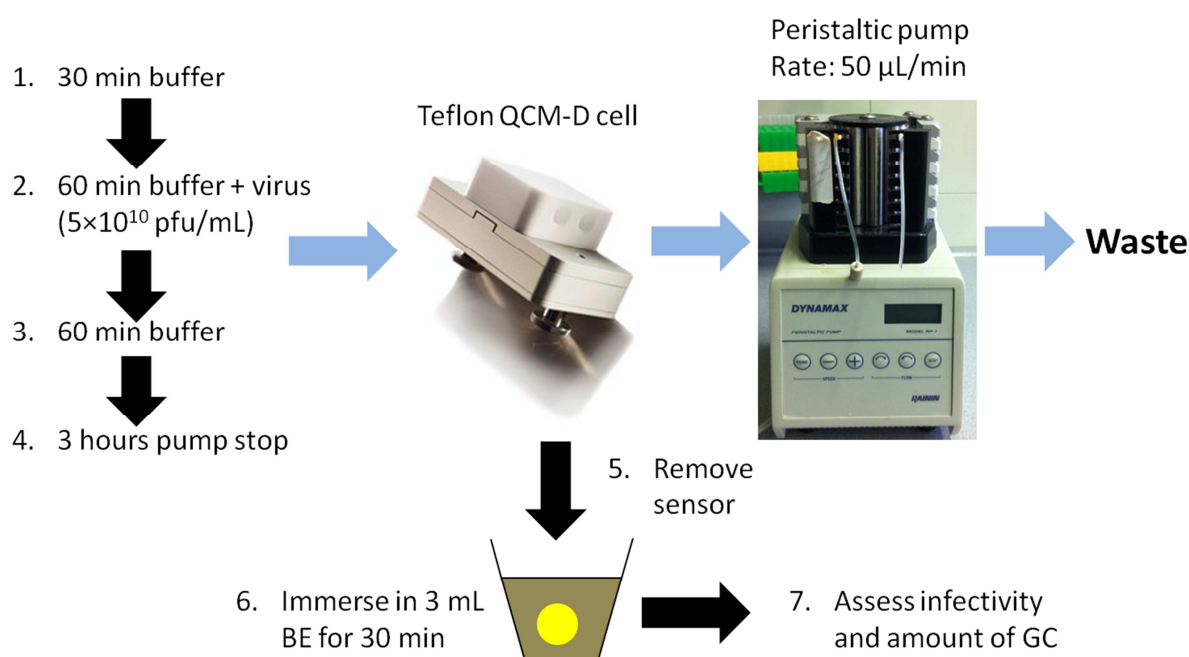


**Figure 5.4: Schematic representation of inactivation experiments on SAMs.** Blue arrows represent the liquid flow, black arrows shows experimental steps. BE = Beef extract, GC = genome copies.

### 5.2.8 Analysis of Qbeta genome damage by q-PCR

To assess genome damage by copper treatment, two genome segments (Q1 and Q2) were amplified by q-PCR as described previously.<sup>135</sup> Details pertaining to the location and length of each analyzed amplicon are given in Table C1. Combined, the two segments achieved 14% genome coverage. Damage to the entire genome was estimated by extrapolation as described elsewhere.<sup>135</sup> RNA standards were prepared for both viruses as described previously.<sup>108</sup>

### 5.2.9 Analysis of Qbeta capsid protein damage by Matrix Assisted Laser Desorption Ionization (MALDI)

To assess the effect of copper on the Qbeta capsid proteins, 15 mL batch experiments were conducted as described above, except that the virus concentration was raised to  $5 \times 10^9$  pfu/mL to meet the detection limit of the mass spectrometer. After the experiment, the viruses were digested by a proteolytic enzyme (trypsin), and the resulting peptides were analyzed by MALDI. To obtain a quantitative measure of peptide degradation, the peptides of the Cu-inactivated viruses were compared to those of an untreated, internal control added prior to the enzymatic digestion. Ideally, the internal control is a  $^{15}\text{N}$ -labeled version of the virus.<sup>56</sup> For Qbeta, however, insufficient labeled virus could be produced for use as

an internal standard. Therefore MS2 was added as the internal standard, and all the peptide peaks were compared to peptide 84-106 from MS2. Hereby it should be noted that the comparison to another peptide peak than the corresponding  $^{15}\text{N}$ -labeled one only yields semi-quantitative results, as different peptides may exhibit different ionization efficiencies during the analysis. All MALDI measurements were performed with an ABI 4800 MALDI-TOF-TOF (Applied Biosystems, Rotkreuz, Switzerland), using the instrument settings and sample deposition methods described previously.<sup>61</sup> This method enabled coverage of the capsid protein of 69.7 % Qbeta. The capsid protein sequence and peptides resulting from enzymatic cleavage is shown in Table 5.2. The results are shown as the intact fractions of the individual peptides ( $\text{cp}_i/\text{cp}_{i,0}$ ).  $\text{cp}_i$  and  $\text{cp}_{i,0}$  represent the intensity of the measured peptide peak divided by the intensity of the standard peak (peptide 84-106 of MS2) after and before treatment respectively.

**Table 5.2: Peptide sequences for Qbeta after trypsin digestion.** Underlined peptides indicate analyzed sequences.

Bacteriophage	Protease	Sequence
<b>Qbeta</b>	Trypsin	AK <u>LETVTLGN<sup>10</sup>IGK</u> DGK <u>QTLV<sup>20</sup>LNPR</u>
		<u>GVNPTN<sup>30</sup>GVASLSQAGA<sup>40</sup>VPALK</u> R <u>VTV<sup>50</sup>SVSQPSR</u>
		NR    K <sup>60</sup> NYK    VQVK
		<u>IQN<sup>70</sup>PTACTANGSC<sup>80</sup>DPSVTR</u> <u>QAYA<sup>90</sup>DVTFSTQYS<sup>100</sup>TDEER</u>
		AFVR    T <sup>110</sup> ELAALLASPL <sup>120</sup> LIDAIQQLNP <sup>130</sup> AY

## 5.3 Results and discussion

### 5.3.1 Inactivation kinetics by copper

In a copper jar, inactivation of viruses may occur via two pathways: either viruses interact with the surface and inactivate, or the viruses do not interact directly with the surface and the dissolved copper that has leached from the surface is responsible for inactivation. Fig. 5.5 shows the inactivation of MS2 and Qbeta in both *Cu foil* and *dissolved Cu* experiments. The first thing to notice is that, as expected, the presence of the copper foil leads to a decrease in the concentration of both studied viruses. The decay in infective virus concentration was mainly due to inactivation, not adsorption onto the foil. This was evident from the concurrent q-PCR measurements (Fig. 5.5). q-PCR measures the total concentration of virus genomes, arising from both infective and inactivated viruses present in solution. A decrease in genome concentration over time is thus indicative of removal from the solution phase by adsorption onto the foil. The q-PCR results show that the concentration of virus genomes in solution stayed constant (MS2) or decreased only minimally (Qbeta;  $k_{\text{obs}} = 7 \times 10^{-2} \pm 2 \times 10^{-2} \text{ [min}^{-1}\text{]}$ ,  $p < 0.01$ ), indicating that the suspended virus concentration was only minimally influenced by the copper foil.

Furthermore, it can be seen that both viruses were inactivated in the absence of copper foil. Inactivation of MS2 in fact occurred more rapidly if the foil was not present, whereas similar disinfection rates were observed for Qbeta independent of the presence of the foil (Fig. 5.5A). The inactivation in the absence of the foil indicates that dissolved copper alone can lead to inactivation. This is in agreement with previous studies on Herpes Simplex virus, Poliovirus and MS2, which showed that copper ions (generated electrolytically or by addition of  $\text{CuCl}_2$ ) showed an efficient inactivation capacity.<sup>205,206</sup> To determine if dissolved copper alone caused inactivation in the *Cu foil* system, or if the foil contributed, the kinetic data was additionally analyzed as a function of the dissolved copper dose (Fig. 5.5B), using the Chick-Watson model (Eq. 5.2). To do so, the copper concentrations in both experimental systems at any given time had to be determined.

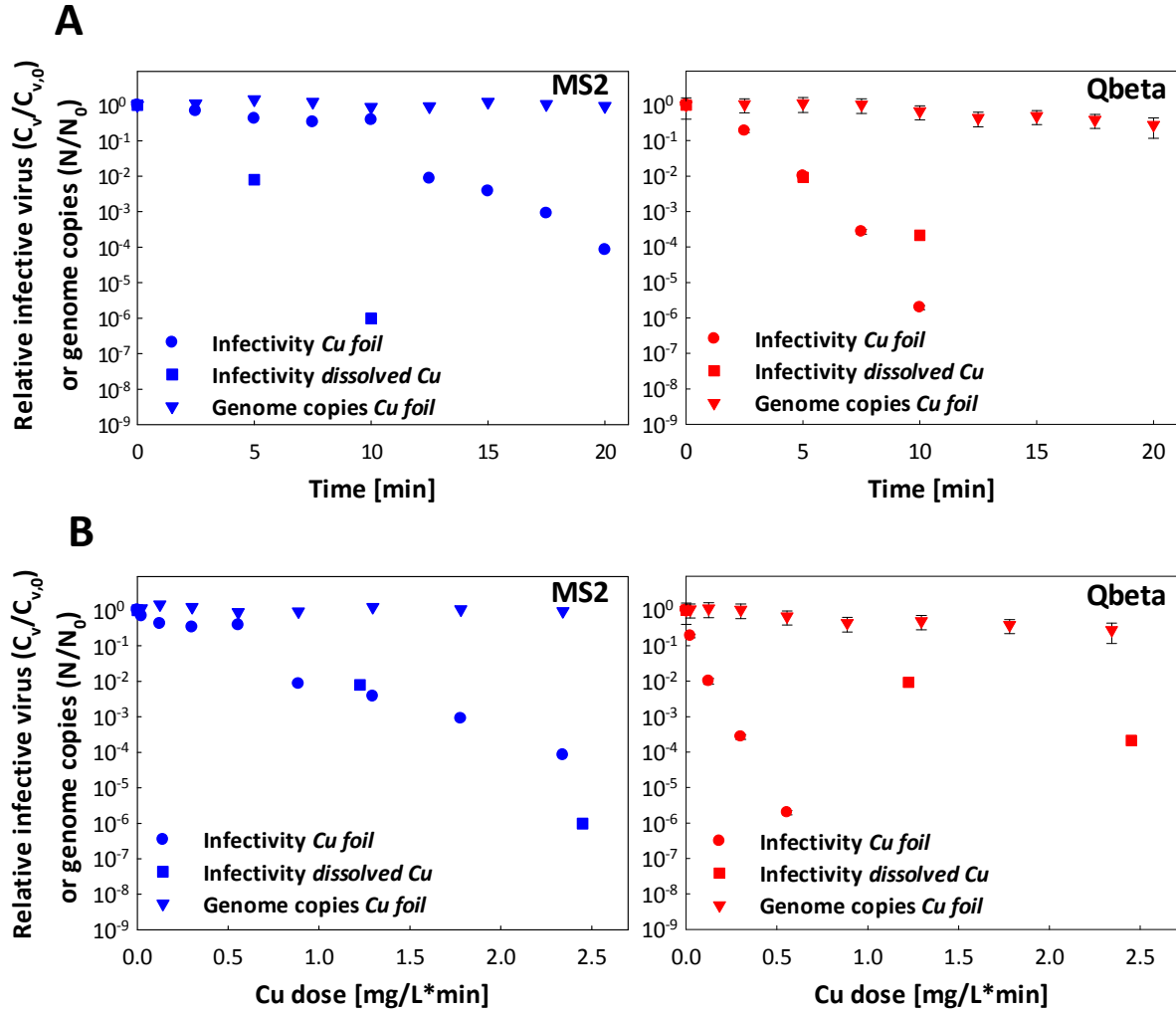


**Figure 5.5: Inactivation kinetics of MS2 and Qbeta with copper.** A: Inactivation ( $C_v/C_{v,0}$ ) and genome loss ( $N/N_0$ ) measured versus time; B: Inactivation ( $C_v/C_{v,0}$ ) and genome loss ( $N/N_0$ ) measured versus dissolved copper dose; Left: MS2 (blue); Right: Qbeta (red); Squares: Infectivity *Cu foil*; Circles: Infectivity *dissolved Cu*; Triangles: Genome copies *Cu foil*.

Metallic copper dissolves in the experimental solutions under the influence of oxygen, carbonate and acetate.<sup>207</sup> Upon addition of the copper foil to the experimental buffer in the *Cu foil* experiments, dissolution followed a zero-order model (Fig. 5.6), which could be expressed by the following equation (Eq. 5.6):

$$C_{Cu} = k_{Cu}t + C_{Cu,0} \quad \text{Eq. 5.6}$$

where  $C_{Cu}$  and  $C_{Cu,0}$  are the dissolved copper (present either as free ions or in complexes) concentrations (in mg/L) at time  $t$  and  $t_0$  respectively,  $t$  is the time of reaction (in minutes) and  $k_{Cu}$  is the dissolution rate

constant (in  $\text{mg/L} \cdot \text{min}^{-1}$ ). The slope of Fig. 5.6 thus corresponds to  $k_{\text{Cu}}$ , which was equal to  $0.012 \pm 0.002$   $[\text{mg/L} \cdot \text{min}^{-1}]$ . The concentration after 20 minutes (duration of the *Cu foil* experiments) was 0.245  $\text{mg/L}$  (3.9  $\mu\text{M}$ ). This concentration corresponded to that in the *dissolved Cu* experiments, where the foil was removed prior to virus addition, such that the copper concentration remained constant.

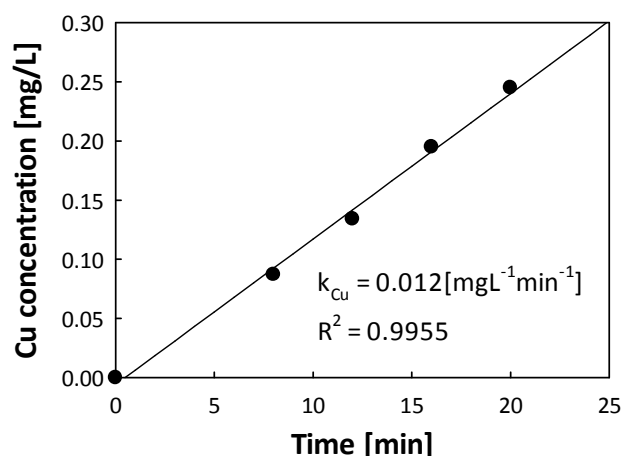


**Figure 5.6: Kinetics of copper dissolution.** Dissolution of copper in acetate buffer as a function of time.

For the *Cu foil* system, the copper dose ( $C_{\text{Cu}}t$ ) was then calculated by integrating Eq. 5.6 over time. For the *dissolved Cu* experiments, the copper dose was calculated from the multiplication of the (constant) copper concentration (0.245  $\text{mg/L}$ ) with time.

The Chick-Watson analysis (Fig. 5.5B) revealed that the two viruses were impacted by the foil in drastically different ways. For MS2, the  $k_{\text{CW}}$  obtained in both systems (*Cu foil* and *dissolved Cu*) only differed by a factor of 1.4, with the *dissolved Cu* system exhibiting a slightly larger  $k_{\text{CW}}$  ( $p = 0.033$ ). This suggests that the inactivation process between the two tested conditions was similar; i.e., the dissolved Cu was responsible for inactivation in both systems. However a different scenario was observed for Qbeta, where the  $k_{\text{CW}}$  in the *Cu foil* experiment was 6-7 times greater than in *dissolved Cu* ( $p < 0.01$ ), indicating that the copper surface had an important effect on this virus. Finally, in the *Cu foil* experiment, Qbeta inactivated significantly more readily than MS2 ( $p = 0.027$ ), while this was not the case in the *dissolved Cu* system, indicating that different inactivation processes acted on the two viruses in the *Cu foil* system.

Two hypotheses can be formulated to understand the observed differences between the two viruses in the *Cu foil* experiment: *i*) MS2 did not interact with the copper foil, whereas Qbeta did, and hence only

Qbeta was subject to surface-mediated inactivation; or *ii*) both bacteriophages interacted with the foil, but only Qbeta was inactivated. In the following paragraphs, we aim to shed light on these hypotheses by comparing different surface interactions of the two viruses, as well as the resulting inactivation trends.

### 5.3.2 Surface interactions of MS2 and Qbeta

To determine if the two viruses differ in their surface interactions, the susceptibility of both viruses to undergo adsorption by specific interactions was explored. Because the exact type of interactions exhibited by the Cu foil are not known, we tested a series of four SAM surfaces, along with a clean gold surface, that promoted interactions that may also be involved in virus-copper adsorption: electrostatic attraction and repulsion, hydrogen bonding, hydrophobic interactions and van der Waals interactions (Table 5.1).

Previous studies have shown that interaction between proteins and surfaces in aqueous solutions is stronger for hydrophobic surfaces than for hydrophilic ones, implying that the proteins are less tightly bound to hydrophilic surfaces.<sup>208</sup> It has been suggested that this is due to the fact that hydrophobic interactions are multistep interactions initiated firstly by hydrophobic residues, and followed by multipoint interaction due to various degree of protein denaturation.<sup>209</sup> This would indicate that more parts of the protein are bound to a hydrophobic surface than to a hydrophilic one, leading to stronger interaction. The hydrophobic parts of a virus capsid are usually oriented to the interior of the protein, to avoid contact with water. However several hydrophobic residues do point to the outside (Fig. 5.1), and they are expected to act as sites for association with other hydrophobic moieties.<sup>210</sup> According to this observation, adsorption of viruses on  $-CH_3$  should lead to the most stable virus layer.

Virus adsorption experiments were assessed by QCM-D. Fig. 5.7 shows the results of attachment studies for MS2 and Qbeta. It can be seen that, except in the case of electrostatic repulsion of MS2, all interactions tested caused adsorption for both viruses. For MS2, the attachment efficiency followed the order:  $-NH_3^+ > -CH_3 > -OH > Au > -COO^-$ . Qbeta's adsorption efficiency sequence was slightly different:  $-NH_3^+ > -COO^- \approx Au \approx -CH_3 > -OH$ . These sequences reflect the tendency of the surfaces to adsorb the viruses as a function of time; they do not, however, give any indication concerning the strength and the reversibility of the interaction. The electrostatic attraction exerted by the positively charged surface is thus a more rapid process than the hydrophobic interaction that may rely on inducing conformational changes. Notably, it was observed that all surfaces (except for  $-COO^-$  with MS2) were covered by a



monolayer of viruses (corresponding to about  $5 \times 10^{10}$  viral particles) at the end of the experiments, indicating that all the surfaces adsorbed the viruses extensively, only at different rates.

Generally, the differences in the attachment efficiency to the different surfaces were much greater for MS2 than for Qbeta. This shows that Qbeta was generally less influenced by the type of surface under these experimental conditions. This is probably a result of the different IEPs of the two viruses: while MS2 carries an overall negative charge at the working pH, the higher IEP of Qbeta renders its overall charge close to neutral. MS2 is therefore strongly attracted by the positive surface and strongly repelled by the negative one, and thus spans a large range of adsorption efficiencies. Qbeta, in contrast, can interact similarly well with all surfaces.

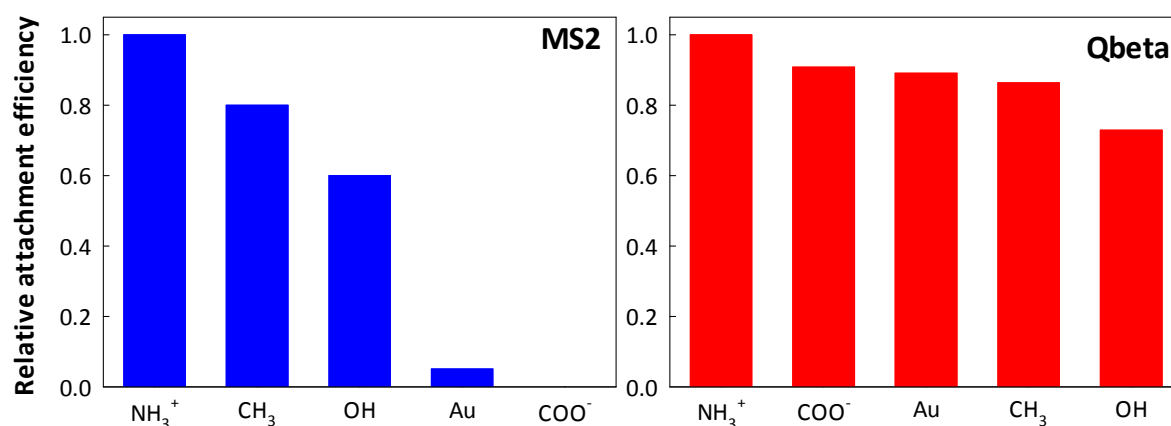


**Figure 5.7: Adsorption efficiency onto SAMs.** Relative attachment efficiency of MS2 (left-blue) and Qbeta (right-red) to different SAMs at pH 5 and IS 10 mM (NaCl). This data was obtained by Antonius Armanious (ETHZ).<sup>201</sup>

Two major differences in the adsorption behavior can be seen between the two bacteriophages: first, MS2 did not adsorb onto the negatively charged surface, whereas Qbeta did. As discussed above, this can be rationalized by the fact that MS2 is negatively charged at the experimental pH, leading to repulsive interactions with the negative carboxylate groups, whereas the low overall charge of Qbeta allowed it to interact. Second, adsorption to gold was more important for Qbeta than for MS2. This may be explained by the presence of disulfide bridges in the capsid of Qbeta (but not MS2; Fig. 5.1), which are known to react to form thiolates attached to the gold surface. Similar processes can also occur with metallic copper.<sup>211</sup> In contrast, the thiol groups of cysteine, which are present on both viruses, require a higher activation energy to form thiolate-gold bonds.<sup>212</sup> In addition, the cysteines are buried inside the viral capsids, rendering them poorly accessible for interaction with the surface.

As can be seen from Fig. 5.7, MS2 did not adsorb very efficiently on gold in these conditions. To allow a better adsorption rate, the ionic strength was increased to 250 mM (NaCl) in the following experiments. An increase in ionic strength has been found to enhance adsorption, though the reasons for this enhancement are not clear.

### 5.3.3 Probing the effect of different interactions on virus infectivity

Starting from the adsorption results, we then assessed if virus-SAM interactions caused inactivation of the viruses. To assess if any inactivation occurred, the genome copies ( $N_0$ ) and infectivity ( $C_{v,0}$ ) were measured in solution before the surface interaction, and were re-measured after desorption from the surface ( $N$ ,  $C_v$ ). In Fig. 5.8 the different possible outcomes of this experiment are depicted. Hereby, the relative concentration of genome copies in solution after desorption ( $N/N_0$ ) determines the adsorption reversibility, and the relative infectivity measured after desorption ( $C_v/C_{v,0}$ ) determines a surface's inactivation potency. As can be seen from Fig. 5.8, this analysis enables us to differentiate between five situations: A) Adsorption is reversible and no inactivation occurs; B) Adsorption is reversible and inactivation occurs; C) Adsorption is not fully reversible and no inactivation occurs; D) Adsorption is not fully reversible and inactivation occurs; E) Adsorption of non-infective viruses present in the starting solution is favored.

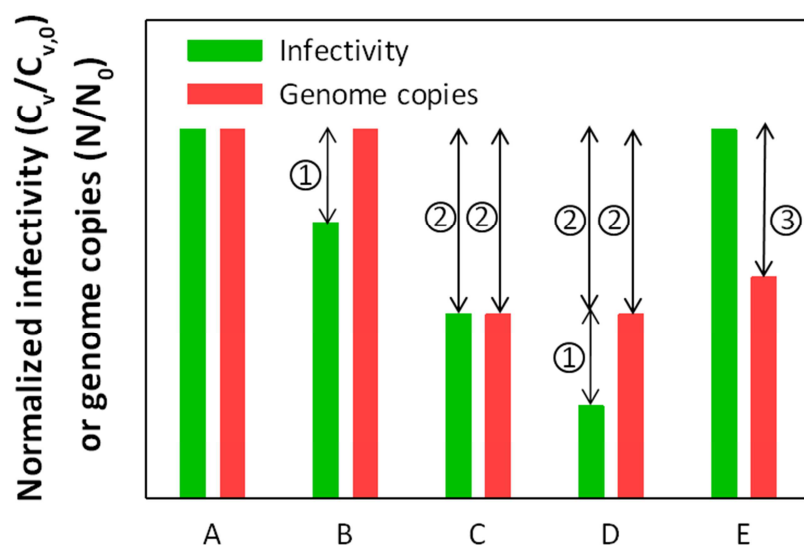


**Figure 5.8: Infectivity and genome concentration after adsorption-desorption to a surface.** The y-axis reflects the concentration of genome copies ( $N/N_0$ ) or infective viruses ( $C_v/C_{v,0}$ ) after an adsorption-desorption process compared to that of a starting solution. A) Adsorption is reversible and no inactivation occurs; B) Adsorption is reversible and inactivation occurs; C) Adsorption is not fully reversible and no inactivation occurs; D) Adsorption is not fully reversible and inactivation occurs; E) Adsorption of non-infective viruses present in the starting solution is favored. Process 1 is due to virus inactivation; process 2 is due to irreversible adsorption; process 3 is due to irreversible adsorption of non-infective viruses.

The last scenario (E in Fig. 5.8) indicates if a loss of genome copies occurs without a concurrent loss in inactivation. While this outcome may appear counterintuitive, it in fact implies that non-infective viral particles preferentially adsorb to the surface. As measured in our virus stock solutions, for each infective MS2 bacteriophage, there are about 10 genome copies present in solution that are associated with non-infective viruses (note that this is the case for many viruses; for example for Hepatitis A virus, the ratio is 1 infective virus to 80 genome copies).<sup>213</sup> Preferential adsorption of these non-infectious particles thus leads to a decrease in the q-PCR signal, but not in infectivity.

The results of inactivation on the SAMs of MS2 and Qbeta are shown in Fig. 5.9. To enable comparison with the scenarios depicted in Fig. 5.8, the results are presented as (Eq. 5.7 and 5.8):

$$\text{Normalized infective viruses} = C_v / C_{v,\max} \quad \text{Eq. 5.7}$$

$$\text{Normalized amount of genome copies} = N / N_{\max} \quad \text{Eq. 5.8}$$

Where  $C_v$  is the concentration of viruses after desorption by beef extract,  $C_{v,max}$  is the maximum infective virus concentration (in pfu/mL),  $N$  is the concentration of desorbed genome copies, and  $N_{max}$  is the maximum GC concentration (in GC/mL). The maximum infective virus or genome copies concentration is based on the assumption that a full monolayer of viral particles adsorbed on the sensor and that adsorption was fully reversible. As mentioned above, a full monolayer represents  $5 \times 10^{10}$  viral particles/cm<sup>2</sup>, and the surface of the sensor is 1 cm<sup>2</sup>.<sup>201</sup> The maximum concentration in the 3 mL beef extract used to desorb the viruses is then  $1.7 \times 10^{10}$  GC/mL, and given that there are 10 times fewer infective than total viruses, the maximum infective viruses concentration is  $1.7 \times 10^9$  pfu/mL.

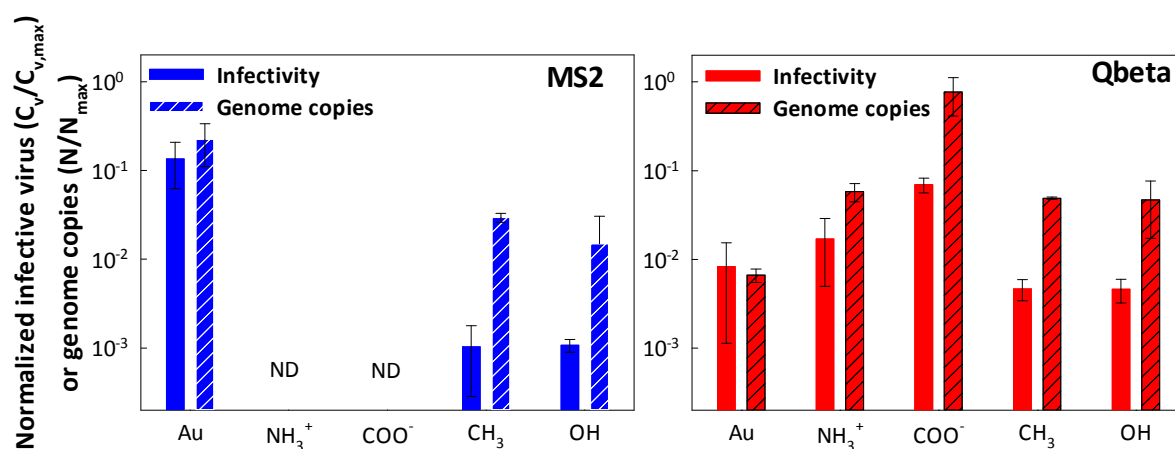


**Figure 5.9: Inactivation after adsorption-desorption on SAMs.** Left: MS2 (blue); right: Qbeta (red). The full bar shows the loss in infectivity ( $C_v/C_{v,max}$ ) and the hashed bar represents the loss in genome copies ( $N/N_{max}$ ). Error bars represent the standard deviation. ND = not determined.

Inactivation of Qbeta was assessed for all SAMs as well as the gold surface. Qbeta's interaction with Au followed case C, indicative of partial desorption but no inactivation. Adsorption to -NH<sub>3</sub><sup>+</sup>, -CH<sub>3</sub> and -OH terminated SAMs followed case D, indicating that partial desorption occurred, and some of the desorbed viruses were inactivated. Finally, adsorption to the -COO<sup>-</sup> SAM followed case B, where the viruses fully desorbed, accompanied by partial inactivation.

As MS2 did not adsorb onto the carboxylic acid SAM (Fig. 5.7), and as only little inactivation was observed for Qbeta on NH<sub>3</sub><sup>+</sup> (Fig. 5.9), inactivation was only assessed for the -CH<sub>3</sub> and -OH terminated SAMs as well as for the gold surface. As for Qbeta, adsorption-inactivation of MS2 on Au followed case C (Fig. 5.8), and adsorption to the -CH<sub>3</sub> and -OH terminated SAMs followed case D. Both viruses thus exhibited similar inactivation behavior as a function of surface interaction.

The finding that neither virus was inactivated by adsorption onto gold suggests that Van der Waals interactions do not cause inactivation. Similarly, positive electrostatic interactions only caused little inactivation. This latter finding was surprising, as electrostatic attraction onto positively charged surfaces led to the most efficient adsorption of MS2 and Qbeta. This suggests that the attachment efficiency is not a good indicator of inactivation. This finding furthermore contradicts the work by Ryan et al.,<sup>93</sup> who suggested that electrostatic interactions lead to capsid disintegration. On the other hand, the -OH, -CH<sub>3</sub> as well as (for Qbeta only) the -COO<sup>-</sup> terminated SAM induced a significant loss in infectivity of 1-1.5 logs for both viruses. This may be due to the fact that hydrophobic interactions and H-bonding cause conformational changes in the capsid, which result in loss of infectivity (note that the -COO<sup>-</sup> terminated SAM may have undergone H-bonding with Qbeta; Table 5.1). This hypothesis is supported by literature reports, which suggest denaturation of viral protein as a consequence of adsorption to hydrophobic surfaces. Specifically, disinfection on hydrophobic polycations has been observed before for Poliovirus and Rotavirus<sup>214</sup> and the mechanism of inactivation has been studied on Influenza virus, showing that proteins were bound irreversibly to the surface and that the genome was allowed to escape from the capsid.<sup>215</sup>

From our findings using SAMs and gold, conclusions can be drawn regarding MS2 and Qbeta inactivation by copper foil. First, we have found that both viruses exhibited similar inactivation trends if a given virus-surface interaction is established on a SAM. However, the two viruses differed in their tendencies to undergo adsorption. The different inactivation behavior in the presence of the copper foil discussed above (Fig. 5.5) must thus stem from differences in the surface interactions, rather than differences in the surface's ability to inactivate each virus. Our findings are thus supportive of hypothesis *i*) established in section 5.3.1.

Second, conclusions regarding the nature of virus-copper interactions can be drawn for each virus. Because MS2 exhibited neither detectable adsorption nor inactivation in the Cu foil experiment, we can conclude that MS2 was neither subjected to hydrophobic interactions nor H-bonding, as these interactions would result in its inactivation. Electrostatic attraction between MS2 and the Cu foil are also unlikely, as this interaction exhibited a rapid adsorption rate, which would have led to detectable MS2 adsorption. Interaction via van der Waals interactions, however, cannot be excluded. Because the corresponding rate of adsorption is slow, and because van der Waals interactions did not lead to inactivation, this interaction may have occurred but gone undetected. For Qbeta, the picture is more complex. Qbeta exhibited slight adsorption as well as inactivation. Its interaction with the surface may

thus include hydrophobic interactions or H-bonding. Electrostatic attractions and van der Waals interactions are less likely to be the dominant interactions, as their inactivation potencies were small or nil. Finally, the more extensive adsorption and inactivation of Qbeta compared to MS2 may also result from an important difference in the two viruses, namely the presence of disulfide bridges on Qbeta's capsid (Fig. 5.1), which could lead to the formation of thiolate-copper bonds.<sup>216</sup> In fact, the observed interactions with the gold surface support the notion that disulfide bridges enhanced Qbeta's adsorption, as adsorption was less reversible for Qbeta compared to MS2 ( $N/N_{\max}$  (MS2) >  $N/N_{\max}$  (Qbeta) in Fig. 5.9). Besides forming thiolate bonds, the redox-active copper foil may furthermore cause reduction of the disulfide bridges, leading to a destabilization of the capsid and hence to inactivation. This process could not be tested on a SAM, as there was no redox-active surface that could interact as destructively with the disulfide bridge.

#### 5.3.4 Assessment of the mechanism of inactivation by copper

Qbeta exhibited different inactivation processes in the *Cu foil* and the *dissolved Cu* experiments. In the final portion of this work, we aimed to understand how these processes differed with respect to their impact on the viral constituents. Specifically, the damage induced on the genome as well as on the capsid were assessed.

First, we assessed if dissolved and metallic copper cause changes to the genome that render it non-readable by the replication enzymes. Fig. 5.10 shows the extent of damage to the genome induced by the two copper systems, along with the corresponding infectivity loss measured in the same samples.

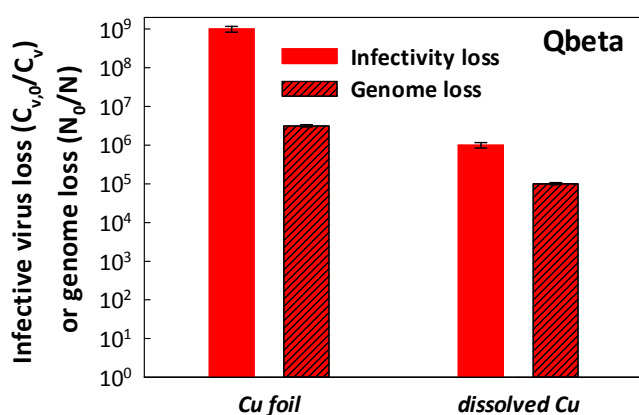


**Figure 5.10: Qbeta genome damage after exposure to copper.** The inactivation was about 6 logs in *dissolved Cu* and about 9 logs in *Cu foil*. Error bars represent the analytical error (95% confidence interval) associated with the q-PCR measurement and plaque assay.

It can be observed that under the *dissolved Cu* experimental conditions, the extent of genome damage was approximately 10-fold smaller than the corresponding extent of inactivation. This indicates that, while genome damage may be partly responsible for inactivation, a contribution of protein damage to inactivation must also occur. This is in accordance with previous results by Warnes et al., who observed Norovirus genome damage after inactivation by copper alloys, and who attributed inactivation to dissolved copper.<sup>217</sup>

In the *Cu foil* experiment the genome loss only accounted for a minimal extent of inactivation (ca. 1/1000), suggesting that protein damage dominates inactivation. This confirms that, in the presence of the foil, inactivation is governed by a different process from that of dissolved copper.

To confirm the occurrence of protein damage in general and the involvement of disulfide bridges in particular, the capsid protein damage of Qbeta was assessed. Fig 5.11 summarizes the degradation of the capsid protein as a function of dissolved copper dose. Specifically, it shows the degradation of the individual peptides resulting from proteolytic digestion of the capsid protein after inactivation by copper.

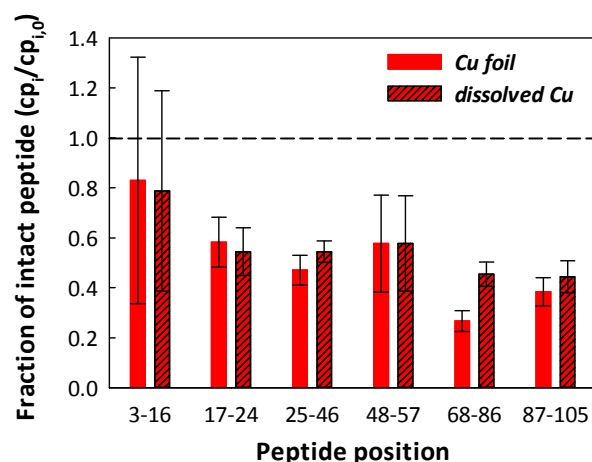


**Figure 5.11: Qbeta peptide damage after treatment with copper.** Bars indicate the residual fraction of intact peptide ( $cp_i/cp_{i,0}$ ) after treatment. The dashed line represents ratio of intact peptide ( $cp_i/cp_{i,0}$ ) in the untreated control sample. The errors represent the standard deviation of four MALDI measurements of the same sample.

Firstly it can be observed that extensive peptide degradation occurs in both systems, indicating that the proteins are an important target of copper. This is in good agreement with previous studies on interaction of copper (II) with proteins or peptides, which have shown that Cu can bind to the N-terminal and become coordinated to the carboxyl group.<sup>218</sup> In addition, if the pH is raised, this reaction can

continue until Cu is coordinated to four amines, leading to drastic changes in the conformation of the protein. It has also been previously observed that after inactivation of influenza by copper, analysis by electron microscopy revealed morphological abnormalities of the Cu(II)-treated virus.<sup>219</sup>

Furthermore, copper degraded the protein non-specifically, as most peptides were degraded to a similar extent for a specific experimental condition. One exception, however, was peptide 68-86, which is the only Qbeta peptide that incurred significantly more damage in the *Cu foil* experiment than in *dissolved Cu*. This peptide contains the cysteines involved in disulfide bonding, which are located at positions 74 and 80 (see Figs 1.7 and 5.1)). The degradation of this particular peptide lends support to the hypothesis that degradation of the disulfide bridges is involved in Qbeta adsorption and inactivation. This observation thus supports the notion that the presence of disulfide bridges in the capsid protein of a virus renders it more susceptible to copper treatment.

The observed influence of disulfide bonds on virus inactivation is interesting with respect to assessing the inactivation of additional microorganisms. Several other viruses, such as Papillomavirus, Polyomavirus, Herpes Simplex virus, and foot-and-mouth disease virus contain disulfide bonds in their capsids,<sup>220,221</sup> and these could be a target for an antiviral drugs or specific disinfectants against these species.

### 5.3.5 Limitations of the current study

The methodologies used in this study have some limitations. Firstly, adsorption to copper was only studied in batch experiments with low sensitivity. For more accurate results, it would be of interest to study the adsorption of the viruses on copper by QCM-D. Unfortunately, as copper is not stable in water (production of copper oxide on the surface, followed by dissolution of copper ions), the adsorption cannot be quantified accurately. Secondly, SAM inactivation experiments exhibited significant variability in the results. Better reproducibility of the SAM experiments could be achieved if a different experimental setup allowing direct periodic sampling in the cell could be designed. This would enable simultaneous assessment of adsorption and inactivation kinetics at the surface. Thirdly, the inactivation on SAMs was determined based on the infectivity of desorbed viruses. However, except for interaction of Qbeta with  $\text{-COO}^-$ , the desorption efficiency corresponded only to 1-10% of the adsorbed virus. This implies that the effect of the interaction could only be assessed for a small portion of the viruses. The infectivity of the irreversibly adsorbed viruses could unfortunately not be assessed. In addition as only 10% of the total viral particles are infective, it is difficult to ensure that the adsorption behaviors



observed are representative of the infective viruses. Finally, to assess the extent of damage to the viral proteins higher virus concentrations are required than those adsorbed to the sensors.

## 5.4 Conclusion

This work confirms that copper has antiviral properties, and is thus a suitable storage material to obtain and maintain safe water. We furthermore showed that - depending on the virus and its properties - only the dissolved copper leached from the surface, or the dissolved copper in conjunction with the copper surface cause inactivation. Disinfection by copper could be particularly interesting for local populations where disinfection of water is not yet optimal, after natural catastrophes or also for travelers. For this purpose, previously suggested<sup>182</sup>, small reusable devices that contain copper and can be immersed in water may be a more practical design than copper pots.

In the distribution system, water pipes made of copper may be beneficial compared to other materials (e.g. cast iron), as they could allow a continuous inactivation of microorganisms during water transport. Further research is needed to determine if such pipe-mediated disinfection is sufficiently effective to replace the commonly applied chlorine residual, which is known to produce toxic byproducts.

Downsides of applying copper for water treatment are its costs, and the necessity to ensure that dissolved copper concentrations stay below the regulatory limit. Therefore, it may be preferable to design novel materials that contain the beneficial properties of copper, but avoid the associated complications. For example, such new materials should take into account that most viruses and other microorganisms are negatively charged at neutral pH, and are thus repelled by negatively charged materials. In order to benefit from enhanced inactivation via surface interactions, new materials should therefore exhibit neutral or positively charged surfaces. Furthermore, as observed in this work, incorporation of hydrophobic functions may lead to particularly efficient inactivation.



# Conclusions and perspectives

Every year more than a million people die due to diarrheal diseases arising from waterborne illnesses, often caused by viruses. Vaccination campaigns of children have efficiently decreased the transmission of several viruses; however, vaccines are not available for all waterborne viruses. In addition, viruses have high mutation rates, which make the development of vaccines particularly challenging. Vaccination often also requires to be renewed to generate an efficient protection against mutated viruses. In developing countries, especially in rural areas, this is difficult to realize, as they may lack the infrastructure necessary for the implementation of followed vaccination control. It is therefore of great interest to prevent virus transmission by other means. An important example is the development of good sanitation and hygiene habits as well as the application of sustainable disinfection methods.

Compared to the removal and disinfection of other pathogenic microorganisms, viruses present three major challenges: they are extremely small, allowing them to pass through filters and sedimentation tanks; some viruses have shown greater resistance to common disinfectants such as chlorine or UV compared to many other microorganisms; and they are shed at very high loads, while causing infection at minimal doses. Viruses may thus remain present and infective after water treatment when other microorganisms are inactivated or removed to innocuous levels. For these reasons, it is of importance to recognize the fundamental mechanisms underlying virus inactivation, to ensure protection from waterborne viral diseases.

Despite the importance of virus disinfection, much remains to be discovered regarding the processes and mechanisms that govern inactivation. Researchers have assessed the disinfection kinetics of various waterborne viruses with a wide range of disinfectants. Several of these studies have reported deviations from the classic first-order Chick-Watson disinfection kinetics. However, little effort has been dedicated

to unraveling the causes of these deviations. Similarly, it is well-known that viruses have vastly different susceptibilities to disinfection, yet the source of these discrepancies has not been unraveled. In particular, we are still lacking knowledge regarding the molecular-level mechanisms that promote virus inactivation by different disinfectants. This lack of knowledge may be due to the fact that the necessary tools to study virus disinfection at a molecular level have only relatively recently become available. The advent of PCR has led to an increasing number of studies that investigate genome damage during disinfection. In contrast, detailed analyses of the impact of disinfection on viral proteins are encountered less frequently.

Finally, the majority of disinfection studies to date have been performed in homogeneous solutions; yet during water treatment, the probability of a virus encountering a solid phase (particles or surfaces) is high. The interactions between viruses and solids have been studied fairly extensively, but their impact on inactivation remains ambiguous. Whereas some virus-solid interactions are reported to have a protective effect against disinfectants, others have shown to enhance inactivation. The factors promoting inactivation via solid interactions, however, are not understood.

Overall, it can thus be said that our understanding of the mechanisms underlying virus inactivation in both homogeneous and heterogeneous disinfection systems still has important gaps. This thesis contributes to filling some of these gaps by adding mechanistic knowledge on various important aspects of virus disinfection. Specifically, the mechanistic knowledge gained was used to explain deviations from ideal disinfection kinetics, and to provide molecular-level insights into inactivation as a function of virus and solution composition. A particularly novel aspect of this work is that it has investigated inactivation not only from a genomic, but also a proteomic perspective. By working with phage models, the challenge of meeting analytical detection limits of protein analysis was overcome, and new insights into the role of protein modifications during disinfection were gained.

The following paragraphs describe the principal findings of this thesis and deliberates the future perspectives. The findings are discussed in the framework of how mechanistic knowledge of virus inactivation helps understand some of the conundrums of virus disinfection. Furthermore, conclusions are drawn with respect to how the knowledge gained can optimize the practice of disinfection, and how it may be used to assess one of the holy grails of virus disinfection, namely the disinfection of nonculturable viruses.

## 6.1 Inactivation mechanism determines disinfection model

Deviations from the ideal first-order Chick-Watson model have been frequently observed but little to no explanations have been offered with respect to the mechanisms underlying these behaviors. During chlorine dioxide treatment in particular, a tailing phenomenon has been observed for both bacteria and viruses. Tailing was usually attributed to either reduction in the disinfectant dose, to alteration of the inactivating capacity of the disinfectant or to the presence of heterogeneous populations of microorganisms. In this study we were able to show that neither of these common explanations was in fact responsible for the observed tailing of bacteriophage inactivation by  $\text{ClO}_2$ . Instead, the results indicated that an adduct was deposited onto the capsid protein of the viruses during the disinfection process, protecting it from further inactivation.

It can be argued that  $\text{ClO}_2$  exhibits this self-limiting effect on disinfection because it was found to mainly act on the viral proteins. As such, deposition of adducts on the proteins directly block the disinfectant from its target. In contrast, genome-active disinfectants are expected to be less inhibited by this barrier. Indeed, no such effect was observed with any of the other homogeneous disinfectants used in this thesis, all of which were mainly found to act on the viral genomes. A disinfectant's mechanism of action can thus be invoked to rationalize the observed deviation from first-order disinfection kinetics. Similarly, deviations from first-order kinetics may be indicative of the disinfection mechanisms at hand.

Viruses have already been shown to possess the ability to protect themselves from disinfection. For example, it is known that DNA viruses may benefit from the DNA repair mechanism of the host cells to recover their infectivity. But to our knowledge, this is the first report that the inactivation process itself could protect viruses from further disinfection. This is an important outcome, because viruses that are increasingly protected during disinfection are a threat to treatment performance. The standard minimum decrease in viruses that has been formulated by the US EPA for water treatment is a 4-log reduction in infectivity, corresponding to an inactivation of 99.99% of viruses. In case of a tailing inactivation curve, a 4-log removal may never be reached. Furthermore, even if a 4-log removal is possible for a given virus, its close relatives may be removed less efficiently. Such a scenario was observed in this work: even though MS2, GA and fr are very similar in size, shape, types of genome and capsid protein composition, their inactivation by chlorine dioxide showed remarkably different

inactivation kinetics. They all exhibited significant tailing, but the tailing's onset occurred already after 2 logs inactivation for fr, whereas it occurred after 4 and 6 logs of inactivation for MS2 and GA, respectively. This finding highlights that extrapolating the disinfection behavior of a model virus to that of a related (nonculturable) target virus may not be reliable.

Overall, the study on tailing mechanisms shows that before implementing a disinfection treatment, it is important to assess all the possible outcomes of inactivation kinetics. If a deviation (especially tailing) from the ideal Chick-Watson model is observed, it is essential to ensure that the inactivation level of the target microorganisms is reached. Inevitably, a tailing effect will also importantly increase the costs of the treatment.

## **6.2 Mechanistic information explains differences in viruses' susceptibility to disinfection**

Virus inactivation kinetics can exhibit different rates for a specific treatment, even among related viruses. However, the reasons behind these discrepancies are not well understood, as the underlying inactivation mechanisms haven't been elucidated. This work shed light on this problematic by investigating mechanistic details of virus inactivation. The strategy adopted was to expose three related bacteriophages to common disinfectants, assess their differences in inactivation rates, and relate the observed differences to differences in genome and protein degradation. It was found that for genome-active disinfectants, the inactivation rates as well as the measured genome degradation were similar for the related viruses studied. In contrast for protein-active disinfectants, inactivation kinetics varied greatly among related viruses. By determining the extent of protein degradation, which varied depending on the virus and which was proportional to the extent of inactivation, the kinetic behavior could be rationalized.

In addition to rationalizing observed differences in virus susceptibilities to disinfection, mechanistic information may ultimately also allow us to determine the disinfection of nonculturable viruses. The mere detection of viruses is nowadays possible for almost all viruses by means of q-PCR. However, q-PCR does not allow assessing if viruses still are infective. Therefore, disinfection kinetics of nonculturable viruses still rely on the inactivation observed for model viruses used as surrogates. These surrogates are chosen by their similarities in shape, size, types of genome and capsid protein to the target organism. While this practice is common for lack of better options, it is well known that the approach can be

unreliable. Methods to directly determine the infectivity of nonculturable viruses are therefore considered the silver bullet of disinfection research.

This work has shown that the use of surrogates is potentially valid for treatments that mainly target the genome: for viruses with similar genome type and size, inactivation rates corresponded well, independent of the exact genome composition. Furthermore, direct measurement of the degradation of the entire genome provided a reasonable estimate of the extent of inactivation. For genome-active disinfectants, whole-genome degradation assays can thus be proposed as tools to directly measure inactivation, even for nonculturable viruses. For protein-active disinfectants, the surrogate approach is less advisable, as inactivation rates among viruses varied greatly. However, the determination of protein integrity could be proposed as a superior alternative to assess the inactivation of nonculturable viruses. There are important limitations to overcome to make this proposition feasible: most importantly, in order to assess protein damage accurately, high protein concentrations are needed, which are difficult to obtain for human viruses. Furthermore, protein mass spectrometric methods are expensive and they involve long and delicate protocols. It is likely, however, that newer generations of mass spectrometers will achieve a better sensitivity at lower cost, thus ultimately allowing for the development of mass spectrometric methods to monitor virus infectivity.

### **6.3 Interactions leading to heterogeneous inactivation**

A wide range of interactions can occur between viruses and surfaces in heterogeneous systems. These interactions are important to take into consideration when assessing the fate of viruses in water, as they are often adsorbed onto particles in environmental samples. Similarly, viruses in the distribution system may adhere to the walls of the pipes. The effect of such virus-solid interactions may be beneficial to virus inactivation, if the interactions are such that they interfere with virus infectivity. Here, we showed that hydrophobic interactions, as well as hydrogen bonding, efficiently inactivate two viruses, whereas electrostatic attractive forces did not.

The use of self-assembled monolayers (SAMs) allowed studying one by one the interactions between viruses and surfaces. They thus allowed isolating the different components of the complex mixture of interactions occurring at a virus-surface interface. This methodology is novel and relevant, as it provides knowledge on the potency of different interactions to cause adsorption of viruses and furthermore their inactivation. By studying the adsorption and inactivation of viruses on well-defined surfaces inducing

specific interactions, it was possible to draw conclusions regarding the mechanism of inactivation induced by a more complex surface.

This mechanistic insight into surface-induced virus inactivation could ultimately allow the development of new materials with enhanced adsorption or inactivation potency of microorganisms. These materials could, for example, be used in water pipes to replace or minimize the problematic practice of disinfectant residuals. Additional uses could also involve membrane development, which could have sufficiently small pores to retain bacteria and a special coating on which viruses would efficiently adsorb and inactivate. In addition, it might be of interest to develop reactors or storage containers with engineered walls or moving-bed type particles in order to increase the water-solid interface and enhance virus inactivation.

### **6.4 Future work**

These studies were performed with bacteriophages as models for human viruses in very simple and controlled solution conditions. To reach conclusions that are directly relevant to real-world systems, additional work should be conducted which focus on the following points:

Firstly, laboratory solution conditions in which these experiments were performed were very clean, whereas future research should be conducted in real water systems containing dissolved organic matter and particulate material. A more complex matrix may influence the disinfection outcomes. Specifically, a tailing behavior may change if adducts formed during disinfection adsorb onto particulate matter instead of adsorbing to and protecting the viruses. This would then lead to a decrease in the tailing phenomenon as part of the virus protection would be lost. Or inversely, if environmental solution constituents adsorb to the surface of the viruses, they could contribute to the protection of the virus from disinfectants, thus causing a more pronounced onset of tailing, and an even further reduced inactivation. In addition, if adsorbed solution constituents protect viral proteins from degradation, this may shift the inactivation mechanism toward a more important contribution of genome degradation. The dominant inactivation mechanisms determined in clean laboratory solutions should thus be confirmed in environmental samples.

Secondly, this work was performed on bacteriophages. Aspects of this work should, however, be confirmed with actual human viruses. For example, the results from this thesis suggest that



appropriately chosen surrogate/disinfectant combinations allow estimating the infectivity of experimentally non-tractable viruses. Before generalizing this statement, it needs confirmation with viruses more relevant to public health. To do so, viruses from the same genus could be used (e.g., different members of the Echovirus or Coxsackievirus genus). The results of this sort of experiment could potentially validate the use of closely related surrogates to assess inactivation of nonculturable viruses, and could additionally validate the use of bacteriophages to study inactivation mechanisms.

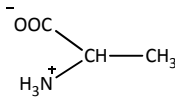
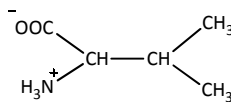
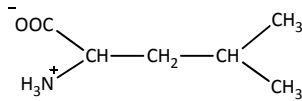
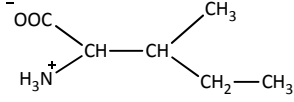
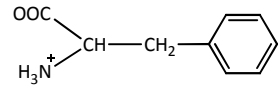
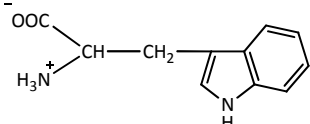
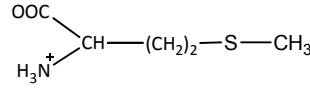
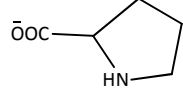
Thirdly, SAMs could be created that are more reflective of solid phases encountered in real systems. For example, SAMs could be used to study two or more interactions at the same time. This would allow assessing if the combination of interactions could have synergistic effects to adsorb and inactivate viruses more efficiently. Furthermore they could also be used to immobilize a monolayer of viruses and allow the assessment of adsorption of for example natural organic matter on them. This could give valuable information on the behavior of viruses in natural water systems.

Finally, this work showed that knowledge of virus inactivation mechanism advances our understanding of disinfection. However, *ab initio* predictions of virus disinfection remain challenging, even if the mechanisms are understood. Specifically, the knowledge of the composition of viral genome and proteins alone is not sufficient to obtain a correct estimation of their degradation during disinfection. Instead, virus structure also determines which genome and protein regions get degraded or adsorbed, and at which rates. It would thus be of interest to combine the information regarding virus composition and structure with knowledge of the location of regions vital to virus infectivity (as for example the virus' host binding site). Understanding how a disinfectant's potency is influenced by these viral features may allow us to move closer to *ab initio* methods to predict virus disinfection.

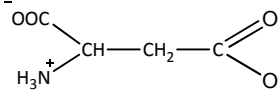
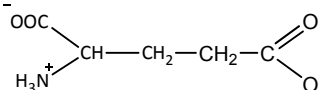


## Appendix A – Chapter 1

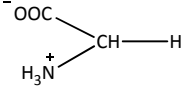
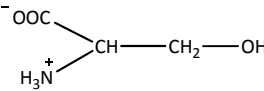
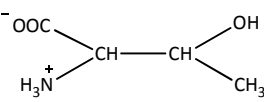
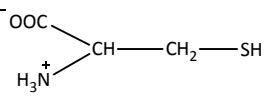
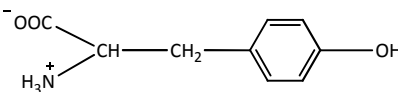
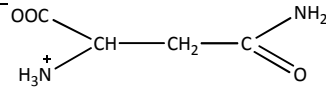
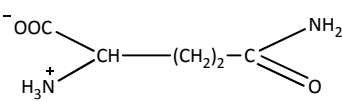
### Nonpolar, hydrophobic

Alanine Ala A MW = 89	
Valine Val V MW = 117	
Leucine Leu L MW = 131	
Isoleucine Ile I MW = 131	
Phenylalanine Phe F MW = 131	
Tryptophan Trp W MW = 204	
Methionine Met M MW = 149	
Proline Pro P MW = 115	

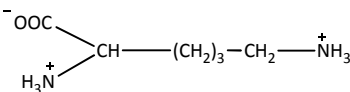
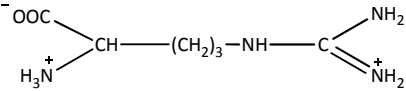
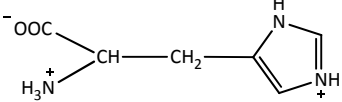
### Polar acidic

Aspartic acid Asp D MW = 133	
Glutamic acid Glu E MW = 147	

### Polar, uncharged

Glycine Gly G MW = 75	
Serine Ser S MW = 105	
Threonine Thr T MW = 119	
Cysteine Cys C MW = 121	
Tyrosine Tyr Y MW = 181	
Asparagine Asn N MW = 132	
Glutamine Gln Q MW = 146	

### Polar basic

Lysine Lys K MW = 146	
Arginine Arg R MW = 174	
Histidine His H MW = 155	

**Figure A.1: Table of amino acids.** Names, abbreviations, extended formulas, molar masses and their physico-chemical properties are depicted.



Appendix B – Chapter 2

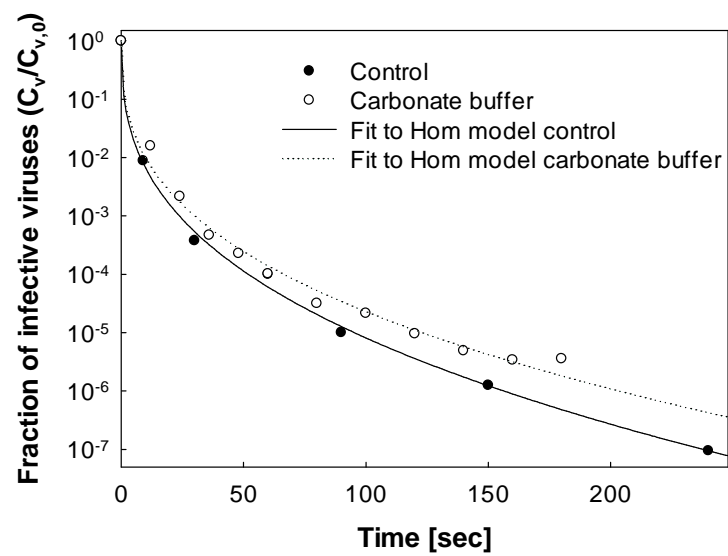


Figure B.1: Inactivation curve with fit to the Hom model for a control and for the experiment with added carbonate buffer instead of DB.

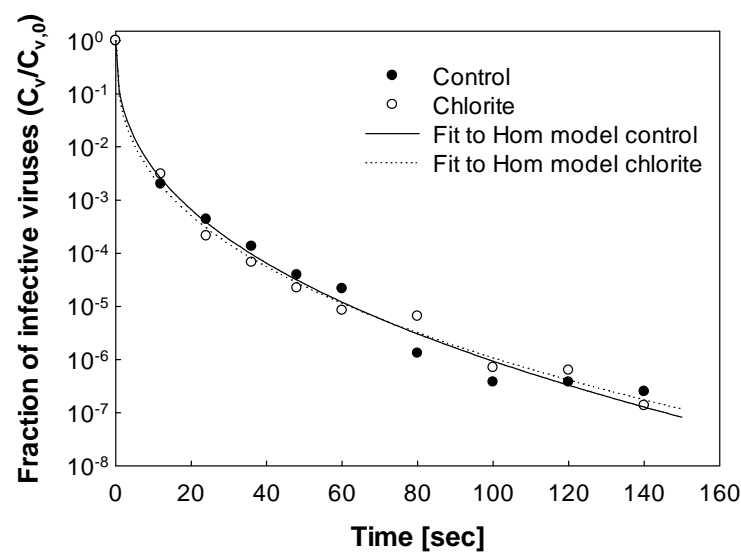


Figure B.2: Inactivation curve with fit to the Hom model for a control and for the experiment with added chlorite in the beginning.

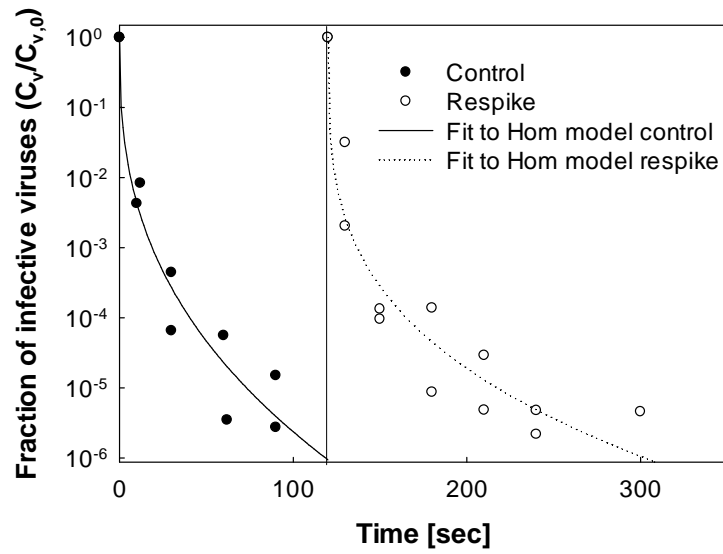


Figure B.3: Inactivation curve with fit to the Hom model for a control and for the second spike of MS2 in the spent solution.

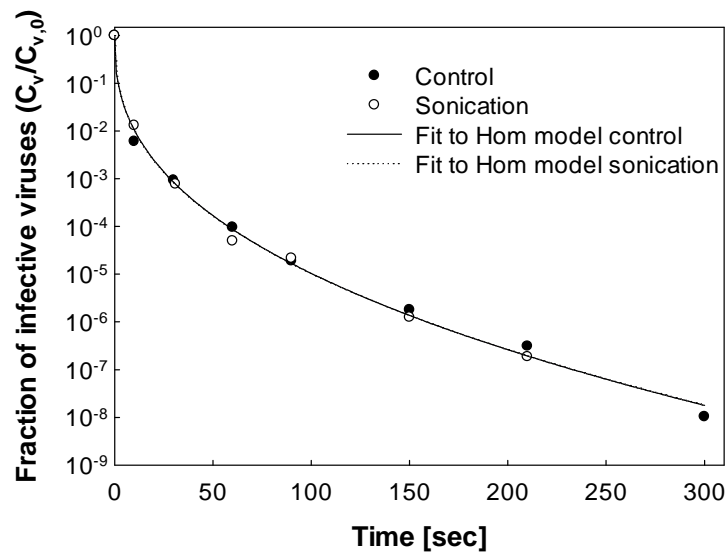


Figure B.4: Inactivation curve with fit to the Hom model for a control and for the experiment with sonication pre-treated virus stock.

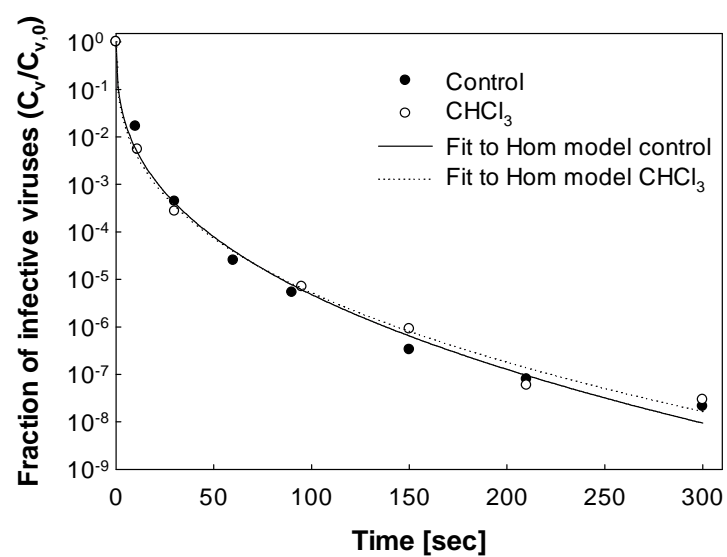


Figure B.5: Inactivation curve with fit to the Hom model for a control and for the experiment with chloroform pre-treated virus stock.

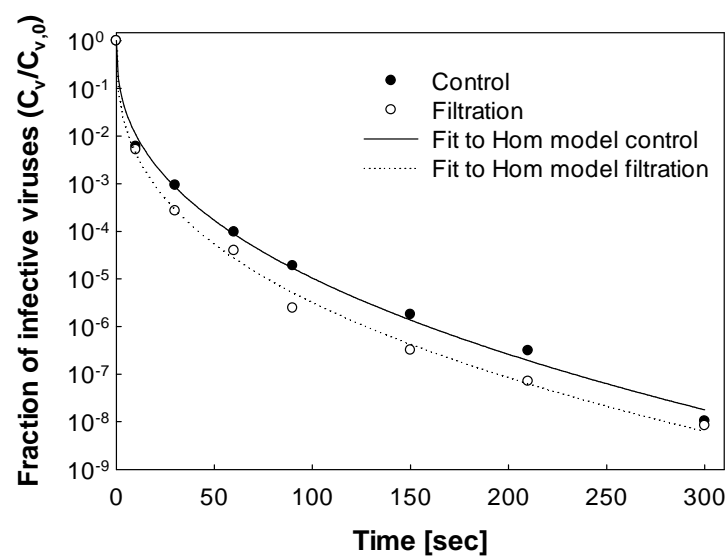


Figure B.6: Inactivation curve with fit to the Hom model for a control and for the experiment with 0.1  $\mu\text{m}$  filtered virus stock.

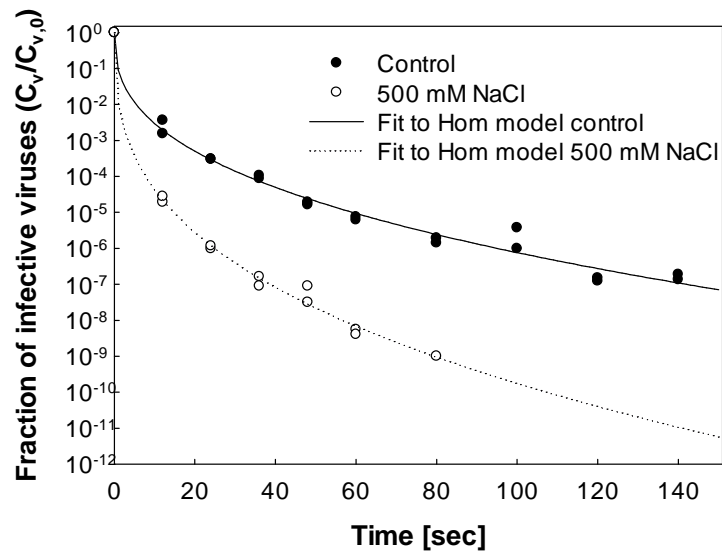


Figure B.7: Inactivation curve with fit to the Hom model for a control and for the experiment in high ionic strength (500 mM NaCl).

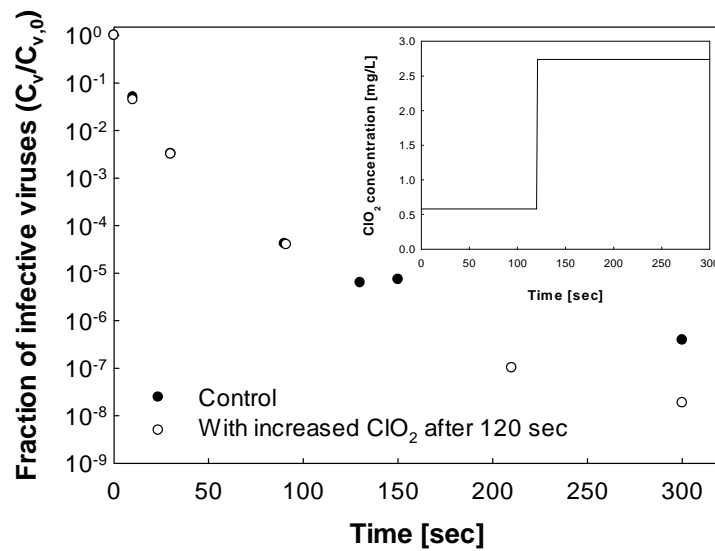


Figure B.8: Inactivation curve of a control experiment and a sample with increased  $\text{ClO}_2$  concentration after 120 seconds. In the top right corner, the  $\text{ClO}_2$  concentration is depicted.



## Appendix C – Chapter 3

**Table C.1: Description of primers for PCR.** NCBI accession numbers: MS2: NC\_001417; fr: NC\_001333; GA: NC\_001426; Qbeta: AY099114.

Virus	Name of primer set	Location of amplicon	Length	Direction	Sequence
MS2	M1	344-678	335	FORWARD	AAGGTGCCTACAAGCGAAGT
				REVERSE	TTCGTTTAGGGCAAGGTAGC
	M2	657-959	303	FORWARD	CCGCTACCTTGCCCTAAAC
				REVERSE	GACGACAACCATGCCAAAC
	M3	1530-1818	289	FORWARD	CCTAAAGTGGCAACCCAGAC
				REVERSE	AAAGATCGCGAGGAAGATCA
	M4	1809-2125	317	FORWARD	CGCGATCTTTCTCTCGAAAT
				REVERSE	GACGATCGGTAGCCAGAGAG
	M5	2724-3033	310	FORWARD	ATAGTCAAAGCGACCCAAATC
				REVERSE	GGCGTGGATCTGACATACCT
fr	F1	90-765	676	FORWARD	GCTGTAGGTAGCCGCAATTC
				REVERSE	CACCTTGATATCGCTGAGA
	F2	1935-2566	632	FORWARD	CCTAGGGGATGGTAACGACG
				REVERSE	CGTCGTTACCATCCCCTAGG
	F3	3018-3503	486	FORWARD	AATAGCAGACCCACGCCTCT
				REVERSE	CTAGAGGGCGAACCCTCACC
GA	G1	967-1559	593	FORWARD	CTCGGGCTTCTTAACCCTTT
				REVERSE	CAGGCAGCTCAACACCATT
	G2	1587-1945	359	FORWARD	TCGACCTGACCATCCCTATC
				REVERSE	GCGTCCGAATTACTGTCTCC
	G3	2143-2523	381	FORWARD	GAGCCTCACAAGGGTTCAAG
				REVERSE	TAGTAGCGAGCGAACCATCA
	G4	2533-2926	394	FORWARD	GTAGCGCTAGCGATTCCATC
				REVERSE	GGTTTCATGTCGGCATCTTT
	G5	2958-3343	386	FORWARD	CCCATGTCATGTTGCTATG
				REVERSE	GAGAGAACGCAGGCCTCTAA
QBeta	Q1	314-560	247	FORWARD	TGTTGACTGGGATTTGCGTA
				REVERSE	TAAATCGCCACGCTTAACAG
	Q2	1164-1401	238	FORWARD	TACAGCCGACTCCATACGAG
				REVERSE	ACGCCGTTAGTGGGATTAC

**Table C.2: q-PCR thermocycling conditions.** 1: Reverse transcriptase; 2: Denaturation and activation of enzymes; 3: genome amplification.

Primer set	1	2	3 - 45 cycles
<b>M1, M2 ,M3, M4, M5, M6</b>			95°C 15 sec
<b>G2, G3, G5</b>	42°C 20 min	95°C 10 sec	60°C 20 sec
<b>Q1, Q2</b>			72°C 20 sec
			95°C 15 sec
<b>F1, F2</b>	42°C 20 min	95°C 30 sec	60°C 20 sec
			72°C 60 sec
			95°C 15 sec
<b>F3</b>	42°C 20 min	95°C 30 sec	60°C 20 sec
			72°C 40 sec
			95°C 15 sec
<b>G1</b>	42°C 20 min	95°C 30 sec	60°C 20 sec
			72°C 50 sec
			95°C 15 sec
<b>G4</b>	42°C 20 min	95°C 30 sec	60°C 20 sec
			72°C 30 sec

## Appendix D – Chapter 4

**Table D.1: Location and mass of each peptide with its corresponding [ $^{14}\text{N}$ ] and [ $^{15}\text{N}$ ] peak mass.** (cysteines are protected with iodoacetamide). \* indicates a missed cleavage site.

Bacteriophage	Position in sequence	[ $^{14}\text{N}$ ] Peptide mass [Da]	[ $^{15}\text{N}$ ] peptide mass [Da]	Protease
MS2	1-7*	814.4	823.4	Chymotrypsin
	8-25*	1761.9	1781.9	Chymotrypsin
	26-32	746.3	755.3	Chymotrypsin
	33-42	1112.5	1127.5	Chymotrypsin
	44-49	721.4	730.4	Trypsin
	50-56	790.4	803.4	Trypsin
	59-82	2492.4	2520.4	Chymotrypsin
	84-106	2671.3	2697.3	Trypsin
	107-113	760.4	769.4	Trypsin
	114-129	1559.8	1577.8	Trypsin
fr	1-19	1997.9	2019.9	Trypsin
	20-38	2005.9	2029.9	Trypsin
	39-43	596.3	603.3	Trypsin
	44-49	721.3	730.3	Trypsin
	50-56	776.3	787.3	Trypsin
	57-61*	638.4	645.4	Trypsin
	62-66	571.3	576.3	Trypsin
	67-83	1780.9	1801.9	Trypsin
	84-106	2645.3	2671.3	Trypsin
	107-113	764.4	773.4	Trypsin
	114-129	1533.8	1551.8	Trypsin
GA	5-37	3373.7	3417.7	Trypsin
	38-42	624.4	633.4	Trypsin
	43-48	696.4	705.4	Trypsin
	48-57	1151.6	1169.6	Chymotrypsin
	62-81	2164.2	2190.2	Chymotrypsin
	83-105	2424.3	2448.3	Trypsin
	106-112	735.4	743.4	Trypsin
	113-129	1710.8	1729.8	Trypsin

### D.1 Thermodynamic integration simulation

The local environment of Met88 in the MS2 and fr capsids was modeled in each case by considering a cluster of 4 capsid proteins. The coordinates for the three capsid proteins comprising the respective capsid triplet subunits were taken from the Protein Data Bank (PDB code: 2MS2<sup>222</sup> and 1FRS<sup>29</sup>) with the position of the fourth capsid protein determined using VIPERdb.<sup>223</sup> The proteins were described using the Amber force field (parm10).<sup>166</sup> Additional parameters required for the methionine sulfoxide residue were generated using the Gaussian 03<sup>167</sup> quantum mechanical software package and the General Amber Force Field.<sup>168</sup> The proteins were neutralized with 4 Cl<sup>-</sup> ions in each instance, solvated using 30,638 TIP3P<sup>224</sup> water molecules and equilibrated at 300 K and 1 bar for 2 ns using the Gromacs<sup>225</sup> molecular dynamics package version 4.5.4. The conversion from Amber to Gromacs format was performed using Amb2gmx.<sup>226</sup> The single methionine/methionine sulfoxide in water systems were treated in a similar manner.

The difference in the relative free energy between the chain A Met88 and its sulfoxide,  $\Delta\Delta G = \Delta G_{\text{WAT}} - \Delta G_{\text{PRO}} = \Delta G_{\text{S-H}} - \Delta G_{\text{S=O}}$ , was calculated for both MS2 and fr using the free energy cycle shown in Fig. D1 and thermodynamic integration given by (Eq. D1):

$$\Delta G = \int_0^1 \left\{ \frac{\delta V(\lambda)}{\delta \lambda} \right\}_\lambda d\lambda \quad \text{Eq. D1}$$

Where  $\Delta G$  is the difference in Gibbs energy for one arm of the Gibbs energy cycle,  $\lambda$  is a coupling constant which enables the gradual alchemical mutation from Met-S  $\rightarrow$  Met-S=O and likewise for the reverse reaction of Met-S=O  $\rightarrow$  Met-SH.

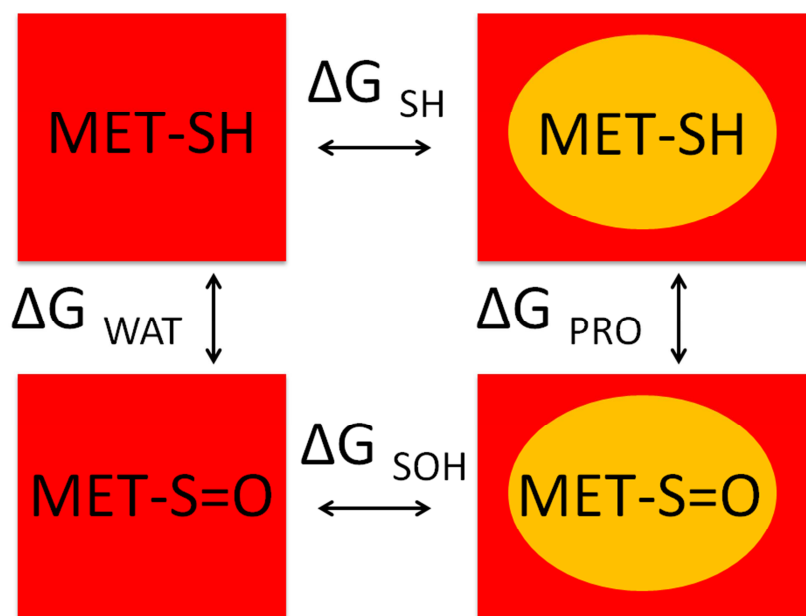


**Figure D.1:** Schematic representation of the thermodynamic cycle used for the calculation of energy difference in the oxidation of methionine in an aqueous environment relative to a protein environment. The red rectangles on the left represent the single Met-SH and Met-S=O residues in a box of water while the red rectangles with yellow ellipses on the right represent the capsid proteins in a water box.

The transformation was performed in three stages: 1) the charges were turned off; 2) the methionine was mutated into methionine sulfoxide; 3) the charges were then turned back on. At each stage 11 equidistance  $\lambda$  values, in the range 0 to 1, were used with the final conformation of a preceding simulation at a given  $\lambda$  value being used as the initial conformation in the succeeding  $\lambda$  value simulation. Each  $\lambda$  value simulation was equilibrated for 0.1 ns followed by 0.2 ns of productions (with the output saved every 2 ps), summing to approximately 10 ns per reaction. A time step of 2 fs was used throughout. Electrostatic interactions were treated using the Particle-mesh Ewald method. The Parrinello-Rahman barostat and the leap-frog stochastic dynamics integrator were used with the pressure set to 1 bar and the temperature to 300 K. Images were generated using the VMD program.<sup>169</sup>

## D.2 Poisson Boltzmann calculations

To obtain starting structures for Poisson Boltzmann calculations, capsid fragments containing six triplet for both the MS2 and fr virus capsids were generated, solvated and equilibrated for 2 ns followed by a further 2 ns of simulation, using the Amber force and the NAMD<sup>165</sup> molecular dynamics software package. In each case two neighboring triplets were extracted from the simulation at ten equi-distance

time intervals. These structures were used as inputs structures for the Poisson Boltzmann equation solver, APBS,<sup>227</sup> by which the electrostatic component of the inter-triplet capsid binding energy was calculated. This binding energy,  $\Delta G_{\text{binding}} = \Delta G_{\text{desol\_triplet\_1}} + \Delta G_{\text{desol\_triplet\_2}} + \Delta G_{\text{electrostatic}}$ , was calculated according to the thermodynamic cycle shown in Fig. D2.<sup>228</sup> The APBS grid parameters were set using the APBS tool psize.py. Ions charges of 1 and -1 were used with a radius of 2 Å and the biomolecule and solvent dielectric constants were set to 2 and 78 respectively.

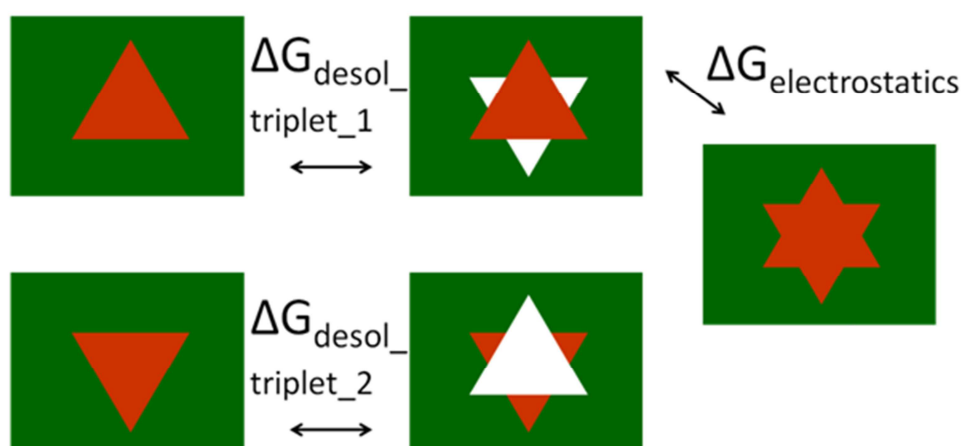


**Figure D.2:** Schematic representation of the thermodynamics cycle used for the calculation of the electrostatic component of the inter-triplet capsid binding energy. The orange triangles represent individual charged triplets, while the white triangles represent triplets in which the charges have been turned off. The green rectangles represent water.

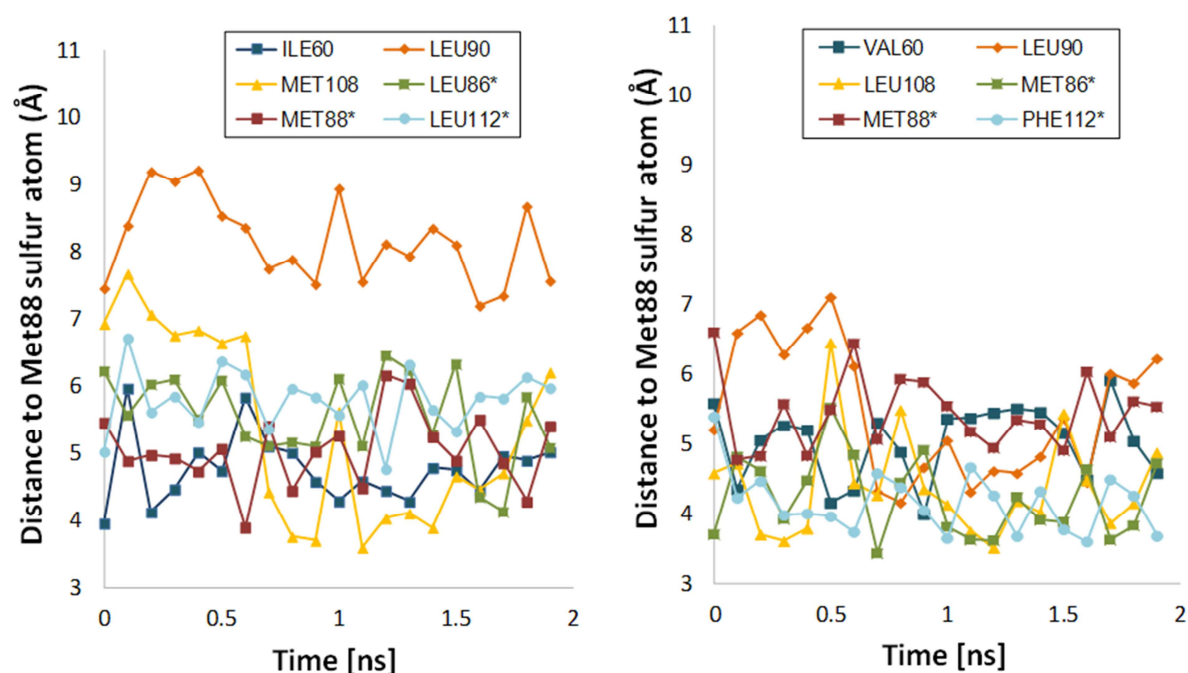


**Figure D.3: Distance to the sulfur atom of Met88 for a single atom in the surrounding residues.** Left: MS2; Right: fr. \* Indicates that the residue is from a neighboring triplet. The single atoms selected were those considered to be closest to the sulfur atom of the Met88 residue overall. The residues in fr are on average closer ( $4.8 \pm 0.8$  Å) to the Met88 sulfur atom than the equivalent residues in MS2 ( $5.8 \pm 1.3$  Å). The largest contributor to this increase is Leu90 which in fr has an average distance of  $5.5 \pm 1$  Å while in MS2 this increases to  $8.2 \pm 0.6$  Å. Also of note are Phe112 in fr with an average distance of  $4.2 \pm 0.4$  Å, for the equivalent residue in MS2, Leu112, this increases to  $5.8 \pm 0.5$  Å; likewise Leu108 in fr has an average distance of  $4.4 \pm 0.7$  Å while the equivalent residue in MS2, Met108, has an average distance of  $5.4 \pm 1.4$  Å. The resultant difference in the sasa is illustrated in Figs. 8C and D which show the contributions to the sasa for one of the Met88 residues, overall twelve such residues were used to calculate the sasa with sampling performed once every 0.2 ps for 2ns.

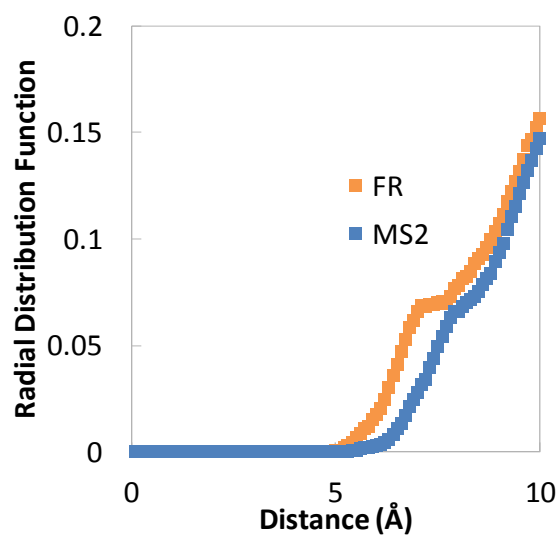


Figure D.4: Radial distribution function of the Met 88 sulfur atom in chain A and the oxygen atoms of water for the MS2 and fr virus capsid.

Table D.2: The change in Gibbs energy for the oxidation of methionine in a capsid protein environment relative to an aqueous environment.

Phage	Reaction	Charges Off	Mutation	Charges On	Overall
		[kcal/mol]	[kcal/mol]	[kcal/mol]	[kcal/mol]
<b>MS2</b>	Met88-SH -> Met88-S=O	-44 ± 6	0 ± 3	+48 ± 4	+4 ± 7
<b>MS2</b>	Met88-S=O -> Met88-SH	+44 ± 6	+1 ± 2	-49 ± 4	-4 ± 7
<b>fr</b>	Met88-SH -> Met88-S=O	-44 ± 6	0 ± 1	+49 ± 5	+4 ± 7
<b>fr</b>	Met88-S=O -> Met88-SH	+43 ± 6	0 ± 3	-48 ± 4	-5 ± 8



**Table D.3: The APBS calculated electrostatic component of the MS2 and fr intra-capsid binding energies and its ionic strength dependency.**

Phage	Ion concentration	Binding energy
	[mM]	[kcal/mol]
<b>MS2</b>	15	-15 ± 2
<b>MS2</b>	100	-16 ± 2
<b>MS2</b>	500	-15 ± 1
<b>fr</b>	15	-13 ± 2
<b>fr</b>	100	-15 ± 2
<b>fr</b>	500	-14 ± 2



# References

1. Carpenter, E. J., Lin, S. & Capone, D. G. Bacterial activity in South Pole snow. *Appl. Environ. Microbiol.* **66**, 4514–4517 (2000).
2. Horneck, G. Survival of microorganisms in space: A review. *Adv. Sp. Res.* **1**, 39–48 (1981).
3. Olsson, K., Keis, S., Morgan, H. W., Dimroth, P. & Cook, G. M. Bioenergetic properties of the thermoalkaliphilic *Bacillus* sp. strain TA2.A1. *J. Bacteriol.* **185**, 461–465 (2003).
4. Fields, B. N., Knipe, D. M. & Howley, P. M. *Fields virology*. (Wolters Kluwer Health/Lippincott Williams & Wilkins, 2007).
5. Dolja, V., Koonin, E. & Forterre, P. The origin of viruses and their possible roles in major evolutionary transitions. *Virus Res.* **117**, 5–16 (2006).
6. Lawrence, C. M. *et al.* Structural and functional studies of archaeal viruses. *J. Biol. Chem.* **284**, 12599–603 (2009).
7. Bergh, O., Børshheim, K. Y., Bratbak, G. & Heldal, M. High abundance of viruses found in aquatic environments. *Nature* **340**, 467–8 (1989).
8. Suttle, C. A. Marine viruses--major players in the global ecosystem. *Nat. Rev. Microbiol.* **5**, 801–12 (2007).
9. Koplow, D. A. *Smallpox: The fight to eradicate a global scourge*. (2004).
10. Dixon, C. W. *Smallpox*. (Churchill, London, 1962).
11. Taubenberger, J. & Morens, D. 1918 Influenza: the mother of all pandemics. *Emerg. Infect. Dis. J. - CDC* **12**, (2006).
12. Flint, S. J., Enquist, L. W., Racaniello, V. R. & Skalka, A. M. *Principles of virology*. (ASM Press, 2003).
13. Atmar, R. L. *et al.* Norwalk virus shedding after experimental human infection. *Emerg. Infect. Dis.* **14**, 1553–7 (2008).
14. Stott, E. J. & Heath, G. F. Factors affecting the growth of Rhinovirus 2 in suspension cultures of L 132 cells. *J. Gen. Virol.* **6**, 15–24 (1970).
15. Paranchych, W., Krahn, P. M. & Bradley, R. D. Stages in phage R17 infection. *Virology* **41**, 465–473 (1970).

## References

16. Bosch, A. Human enteric viruses in the water environment: a minireview. *Int Microbiol* **1**, 191–196 (1998).
17. WHO | Water, sanitation and hygiene links to health. (2004). at <[http://www.who.int/water\\_sanitation\\_health/publications/facts2004/en/](http://www.who.int/water_sanitation_health/publications/facts2004/en/)>
18. Howard, G. & Bartram, J. WHO | Domestic water quantity, service level and health. (2003). at <[http://www.who.int/water\\_sanitation\\_health/diseases/wsh0302/en/](http://www.who.int/water_sanitation_health/diseases/wsh0302/en/)>
19. Emmanuelle Guillot, J.-F. L. *Waterborne pathogens: Review for the drinking water industry*. (IWA Publishing, 2010).
20. Girones, R. *et al.* Molecular detection of pathogens in water - The pros and cons of molecular techniques. *Water Res.* **44**, 4325–4339 (2010).
21. Cabelli, V. J. in *Bact. Indic. Hazards Assoc. with Water* (Hoadley, A. W. & Dutka, B. J.) 222–238 (American Society for Testing and Materials, 1977).
22. Bonde, G. J. Bacteriological methods for estimation of water pollution. *Health Lab. Sci.* **3**, 124–8 (1966).
23. Sobsey, M. Inactivation of health-related microorganisms in water by disinfection processes. *Water Sci. Technol.* **21**, 179 – 195 (1989).
24. Havelaar, A. H., van Olphen, M. & Drost, Y. C. F-specific RNA bacteriophages are adequate model organisms for enteric viruses in fresh water. *Appl. Envir. Microbiol.* **59**, 2956–2962 (1993).
25. Grabow, W. O. K. Bacteriophages: update on application as models for viruses in water. *Water Sa* **27**, 251–268 (2001).
26. Havelaar, A. H. *et al.* Bacteriophages as model viruses in water-quality control. *Water Res.* **25**, 529–545 (1991).
27. ViralZone of the Swiss Institute of Bioinformatics. at <<http://viralzone.expasy.org/>>
28. Roberts, J. W. & Steitz, J. E. A. Reconstitution of infective bacteriophage R17. *Proc. Natl. Acad. Sci. U. S. A.* **58**, 1416–& (1967).
29. Liljas, L., Fridborg, K., Valegard, K., Bundule, M. & Pumpens, P. Crystal-structure of bacteriophage-fr capsids at 3.5-angstrom resolution. *J. Mol. Biol.* **244**, 279–290 (1994).
30. Berlett, B. S. & Stadtman, E. R. Protein oxidation in aging, disease, and oxidative stress. *J. Biol. Chem.* **272**, 20313–20316 (1997).
31. Golmohammadi, R., Fridborg, K., Bundule, M., Valegård, K. & Liljas, L. The crystal structure of bacteriophage Q $\beta$  at 3.5 Å resolution. *Structure* **4**, 543–554 (1996).

32. Gerba JB, C. R. Viruses in source and drinking water. *Drink. Water Microbiol. Recent Dev.* 380–396 (1990).
33. Christman, K. A. *Chlorine*.
34. Xie, Y. F. *Disinfection byproducts in drinking water; Formation, analysis and control*. 161 (Lewis Publisher, 2004).
35. Villanueva, C. M. *et al.* Disinfection byproducts and bladder cancer: a pooled analysis. *Epidemiology* **15**, 357–67 (2004).
36. Rahman, M. B., Driscoll, T., Cowie, C. & Armstrong, B. K. Disinfection by-products in drinking water and colorectal cancer: a meta-analysis. *Int. J. Epidemiol.* **39**, 733–45 (2010).
37. White, P. A. *et al.* Occurrence, genotoxicity, and carcinogenicity of regulated and emerging disinfection by-products in drinking water: A review and roadmap for research. *Mutat. Res. Mutat. Res.* **636**, 178–242 (2007).
38. U. S. Environmental Protection Agency, *National primary drinking water regulations: Stage 2 disinfectants and disinfection byproducts rule*. *Fed. Regist.* Vol. 71, (2), pp 387–493 (2006).
39. Jeong, C. H. *et al.* Occurrence and toxicity of disinfection byproducts in European drinking waters in relation with the HIWATE epidemiology study. *Environ. Sci. Technol.* **46**, 12120–8 (2012).
40. Lazarova, V. *et al.* Advanced wastewater disinfection technologies: Short and long term efficiency. *Water Sci. Technol.* **38**, 109–117 (1998).
41. Sharma, V. K. Potassium ferrate(VI): an environmentally friendly oxidant. *Adv. Environ. Res.* **6**, 143–156 (2002).
42. Aieta, E. M. & Berg, J. D. A review of chlorine dioxide in drinking-water treatment. *J. Am. Water Work. Assoc.* **78**, 62–72 (1986).
43. Kohn, T. & Nelson, K. L. Sunlight-mediated inactivation of MS2 coliphage via exogenous singlet oxygen produced by sensitizers in natural waters. *Environ. Sci. Technol.* **41**, 192–197 (2007).
44. Kohn, T., Grandbois, M., McNeill, K. & Nelson, K. L. Association with natural organic matter enhances the sunlight-mediated inactivation of MS2 coliphage by singlet oxygen. *Environ. Sci. Technol.* **41**, 4626–4632 (2007).
45. Chick, H. An investigation of the laws of disinfection. *J. Hyg. (Lond)*. **8**, 92–158 (1908).
46. Watson, H. E. A note on the variation of the rate of disinfection with change in the concentration of the disinfectant. *J. Hyg. (Lond)*. **8**, 536–542 (1908).
47. Hiatt, C. W. Kinetics of inactivation of viruses. *Bacteriol. Rev.* **28**, 150–& (1964).

## References

48. Clevenger, T., Wu, Y., DeGruson, E., Brazos, B. & Banerji, S. Comparison of the inactivation of *Bacillus subtilis* spores and MS2 bacteriophage by MIOX, ClorTec and hypochlorite. *J. Appl. Microbiol.* **103**, 2285–2290 (2007).
49. Koivunen, J. & Heinonen-Tanski, H. Inactivation of enteric microorganisms with chemical disinfectants, UV irradiation and combined chemical/UV treatments. *Water Res.* **39**, 1519–1526 (2005).
50. Gerba, C. P., Gramos, D. M. & Nwachuku, N. Comparative inactivation of Enteroviruses and Adenovirus 2 by UV light. *Appl. Environ. Microbiol.* **68**, 5167–5169 (2002).
51. Shin, G. A., Linden, K. G. & Sobsey, M. D. Low pressure ultraviolet inactivation of pathogenic enteric viruses and bacteriophages. *J. Environ. Eng. Sci.* **4**, S7–S11 (2005).
52. Engelbrecht, R. S., Weber, M. J., Salter, B. L. & Schmidt, C. A. Comparative inactivation of viruses by chlorine. *Appl. Environ. Microbiol.* **40**, 249–256 (1980).
53. Shang, C., Cheung, L. M. & Liu, W. MS2 coliphage inactivation with UV irradiation and free chlorine/monochloramine. *Environ. Eng. Sci.* **24**, 1321–1332 (2007).
54. Shin, G. A. & Sobsey, M. D. Inactivation of Norovirus by chlorine disinfection of water. *Water Res.* **42**, 4562–4568 (2008).
55. Li, J. W., Xin, Z. T., Wang, X. W., Zheng, J. L. & Chao, F. H. Mechanisms of inactivation of Hepatitis A virus by chlorine. *Appl. Environ. Microbiol.* **68**, 4951–4955 (2002).
56. Wigginton, K. R., Pecson, B. M., Sigstam, T., Bosshard, F. & Kohn, T. Virus inactivation mechanisms: impact of disinfectants on virus function and structural integrity. *Env. Sci Technol* **46**, 12069–78 (2012).
57. Bosshard, F., Armand, F., Hamelin, R. & Kohn, T. Mechanisms of human Adenovirus inactivation by sunlight and UVC light as examined by quantitative PCR and quantitative proteomics. *Appl. Environ. Microbiol.* **79**, 1325–32 (2013).
58. Hawkins, C. L., Pattison, D. I. & Davies, M. J. Hypochlorite-induced oxidation of amino acids, peptides and proteins. *Amino Acids* **25**, 259–274 (2003).
59. Sano, D., Pinto, R. M., Omura, T. & Bosch, A. Detection of oxidative damages on viral capsid protein for evaluating structural integrity and infectivity of human Norovirus. *Environ. Sci. Technol.* **44**, 808–812 (2010).
60. Simonet, J. & Gantzer, C. Inactivation of Poliovirus 1 and F-specific RNA phages and degradation of their genomes by UV irradiation at 254 nanometers. *Appl. Environ. Microbiol.* **72**, 7671–7677 (2006).
61. Wigginton, K. R., Menin, L., Montoya, J. P. & Kohn, T. Oxidation of virus proteins during UV254 and singlet oxygen mediated inactivation. *Environ. Sci. Technol.* **44**, 5437–5443 (2010).

62. Eischeid, A. C. & Linden, K. G. Molecular indications of protein damage in Adenoviruses after UV disinfection. *Appl. Environ. Microbiol.* **77**, 1145–1147 (2011).
63. Khoroshilova, E. V, Repeyev, Y. A. & Nikogosyan, D. N. UV photolysis of aromatic-amino-acids and related dipeptides and tripeptides . *J. Photochem. Photobiol. B-Biology* **7**, 159–172 (1990).
64. Page, M. A., Shisler, J. L. & Marinas, B. J. Mechanistic aspects of Adenovirus serotype 2 inactivation with free chlorine. *Appl. Environ. Microbiol.* **76**, 2946–2954 (2010).
65. Carlson, G. F., Woodard, F. E., Wentworth & Sproul, O. J. Virus inactivation on clay particles in natural waters. *J. Water Pollut. Control Fed.* **40**, R89–& (1968).
66. Stagg, C. H., Wallis, C. & Ward, C. H. Inactivation of clay-associated bacteriophage-MS2 by chlorine. *Appl. Environ. Microbiol.* **33**, 385–391 (1977).
67. Templeton, M. R., Andrews, R. C. & Hofmann, R. Inactivation of particle-associated viral surrogates by ultraviolet light. *Water Res.* **39**, 3487–3500 (2005).
68. Gerba, C. P., Stagg, C. H. & Abadie, M. G. Characterization of sewage solid-associated viruses and behavior in natural-waters. *Water Res.* **12**, 805–812 (1978).
69. Chrysikopoulos, C. V & Syngouna, V. I. Attachment of bacteriophages MS2 and ΦX174 onto kaolinite and montmorillonite: extended-DLVO interactions. *Colloids Surf. B. Biointerfaces* **92**, 74–83 (2012).
70. Babich, H. & Stotzky, G. Reductions in inactivation rates of bacteriophages by clay minerals in lake water. *Water Res.* **14**, 185–187 (1980).
71. Loveland, J. ., Ryan, J. ., Amy, G. . & Harvey, R. . The reversibility of virus attachment to mineral surfaces. *Colloids Surfaces A Physicochem. Eng. Asp.* **107**, 205–221 (1996).
72. Gassilloud, B. & Gantzer, C. Adhesion-aggregation and inactivation of Poliovirus 1 in groundwater stored in a hydrophobic container. *Appl. Environ. Microbiol.* **71**, 912–20 (2005).
73. Preethi Sudha, V. B., Ojit Singh, K., Ramani, S., Paul, A. & Venkatasubramanian, P. Inactivation of Rotavirus in water by copper pot. *J. Water, Sanit. Hyg. Dev.* **1**, 165 (2011).
74. Borkow, G. & Gabbay, J. Putting copper into action: copper-impregnated products with potent biocidal activities. *FASEB J.* **18**, 1728–30 (2004).
75. Borkow, G. & Gabbay, J. Copper as a biocidal tool. *Curr. Med. Chem.* **12**, 2163–2175 (2005).
76. Lehtola, M. J. *et al.* Microbiology, chemistry and biofilm development in a pilot drinking water distribution system with copper and plastic pipes. *Water Res.* **38**, 3769–3779 (2004).
77. Gerba, C. P. Applied and theoretical aspects of virus adsorption to surfaces. *Adv. Appl. Microbiol.* **30**, 133–168 (1984).

## References

78. Van Oss, C. J. Acid—base interfacial interactions in aqueous media. *Colloids Surfaces A Physicochem. Eng. Asp.* **78**, 1–49 (1993).
79. Boström, M., Williams, D. & Ninham, B. Specific ion effects: Why DLVO theory fails for biology and colloid systems. *Phys. Rev. Lett.* **87**, 168103 (2001).
80. Yoon, R.-H., Flinn, D. H. & Rabinovich, Y. I. Hydrophobic interactions between dissimilar surfaces. *J. Colloid Interface Sci.* **185**, 363–370 (1997).
81. Langlet, J., Gaboriaud, F., Gantzer, C. & Duval, J. F. L. Impact of chemical and structural anisotropy on the electrophoretic mobility of spherical soft multilayer particles: The case of bacteriophage MS2. *Biophys. J.* **94**, 3293–3312 (2008).
82. Dika, C., Ly-Chatain, M. H., Francius, G., Duval, J. F. L. & Gantzer, C. Non-DLVO adhesion of F-specific RNA bacteriophages to abiotic surfaces: Importance of surface roughness, hydrophobic and electrostatic interactions. *Colloids Surfaces A Physicochem. Eng. Asp.* **435**, 178–187 (2013).
83. Kessick, M. A. & Wagner, R. A. Electrophoretic mobilities of virus adsorbing filter materials. *Water Res.* **12**, 263–268 (1978).
84. Farrah, S. R. Chemical factors influencing adsorption of bacteriophage-MS2 to membrane filters. *Appl. Environ. Microbiol.* **43**, 659–663 (1982).
85. Michen, B. & Graule, T. Isoelectric points of viruses. *J. Appl. Microbiol.* **109**, 388–97 (2010).
86. Lewis, J. A. Colloidal processing of ceramics. *J. Am. Ceram. Soc.* **83**, 2341–2359 (2004).
87. Sposito, G. *The environmental chemistry of aluminum*. (CRC Press, 1995).
88. Cornell, R. M. & Schwertmann, U. *The iron oxides: Structure, properties, reactions, occurrences and uses*. (Wiley-VCH, 2003).
89. Preocanin, T. & Kallay, N. Point of zero charge and surface charge density of TiO<sub>2</sub> in aqueous electrolyte solution as obtained by potentiometric mass titration. *Croat. Chem. ACTA* **79**, 95–106 (2006).
90. De Wit, J. C. M., Van Riemsdijk, W. H., Nederlof, M. M., Kinniburgh, D. G. & Koopal, L. K. Analysis of ion binding on humic substances and the determination of intrinsic affinity distributions. *Anal. Chim. Acta* **232**, 189–207 (1990).
91. Gianfreda, L., Rao, M. A. & Violante, A. Adsorption, activity and kinetic-properties of urease on montmorillonite, aluminum hydroxide and Al(OH)X-montmorillonite complexes. *Soil Biol. Biochem.* **24**, 51–58 (1992).
92. Murray, J. P. & Laband, S. J. Degradation of Poliovirus by adsorption on inorganic surfaces. *Appl. Environ. Microbiol.* **37**, 480–486 (1979).



93. Ryan, J. N. *et al.* Field and laboratory investigations of inactivation of viruses (PRD1 and MS2) attached to iron oxide-coated quartz sand. *Environ. Sci. Technol.* **36**, 2403–2413 (2002).
94. Koizumi, Y. & Taya, M. Kinetic evaluation of biocidal activity of titanium dioxide against phage MS2 considering interaction between the phage and photocatalyst particles. *Biochem. Eng. J.* **12**, 107–116 (2002).
95. Gerrity, D., Ryu, H., Crittenden, J. & Abbaszadegan, M. Photocatalytic inactivation of viruses using titanium dioxide nanoparticles and low-pressure UV light. *J. Environ. Sci. Heal. Part A-Toxic/Hazardous Subst. Environ. Eng.* **43**, 1261–1270 (2008).
96. Jin, M. *et al.* Chlorine dioxide inactivation of Enterovirus 71 in water and its impact on genomic targets. *Environ. Sci. Technol.* **47**, 4590–4597 (2013).
97. Zoni, R., Zanelli, R., Riboldi, E., Bigliardi, L. & Sansebastiano, G. Investigation on virucidal activity of chlorine dioxide. Experimental data on feline Calicivirus, HAV and Coxsackie B5. *J. Prev. Med. Hyg.* **48**, 91–95 (2007).
98. Chauret, C. P., Radziminski, C. Z., Lepuil, M., Creason, R. & Andrews, R. C. Chlorine dioxide inactivation of *Cryptosporidium parvum* oocysts and bacterial spore indicators. *Appl. Environ. Microbiol.* **67**, 2993–3001 (2001).
99. Huang, J. L. *et al.* Disinfection effect of chlorine dioxide on viruses, algae and animal planktons in water. *Water Res.* **31**, 455–460 (1997).
100. Li, J. W., Yu, Z. B., Cai, X. P., Gao, M. & Chao, F. H. Trihalomethanes formation in water treated with chlorine dioxide. *Water Res.* **30**, 2371–2376 (1996).
101. Harakeh, M. & Butler, M. Inactivation of human Rotavirus, SA11 and other enteric viruses in effluent by disinfectants. *J. Hyg. (Lond)*. **93**, 157–163 (1984).
102. Cerf, O. Tailing of survival curves of bacterial-spores. *J. Appl. Bacteriol.* **42**, 1–19 (1977).
103. Thurston-Enriquez, J. A., Haas, C. N., Jacangelo, J. & Gerba, C. P. Inactivation of enteric Adenovirus and feline Calicivirus by chlorine dioxide. *Appl. Environ. Microbiol.* **71**, 3100–3105 (2005).
104. Berman, D. & Hoff, J. C. Inactivation of simian Rotavirus SA11 by chlorine, chlorine dioxide, and monochloramine. *Appl. Environ. Microbiol.* **48**, 317–323 (1984).
105. Chen, Y. S. & Vaughn, J. M. Inactivation of human and simian Rotaviruses by chlorine dioxide. *Appl. Environ. Microbiol.* **56**, 1363–1366 (1990).
106. Lim, M. Y., Kim, J. M. & Ko, G. Disinfection kinetics of murine Norovirus using chlorine and chlorine dioxide. *Water Res.* **44**, 3243–3251 (2010).
107. Hornstra, L. M., Smeets, P. & Medema, G. J. Inactivation of bacteriophage MS2 upon exposure to very Low concentrations of chlorine dioxide. *Water Res.* **45**, 1847–1855 (2010).

## References

108. Pecson, B. M., Martin, L. V & Kohn, T. Quantitative PCR for determining the infectivity of bacteriophage MS2 upon inactivation by heat, UV-B radiation, and singlet oxygen: advantages and limitations of an enzymatic treatment to reduce false-positive results. *Appl. Environ. Microbiol.* **75**, 5544–5554 (2009).
109. Walter, W. G. Standard methods for the examination of water and wastewater (11th ed.). *Am. J. Public Heal. Nations Heal.* **51**, 940 (1961).
110. Gates, D. *The chlorine dioxide handbook*. 177 (American Water Works Association, 1998).
111. Hoigne, J. & Bader, H. Kinetics of reactions of chlorine dioxide (OCIO) in water. 1. Rate constants for inorganic and organic-compounds. *Water Res.* **28**, 45–55 (1994).
112. Sigstam, T. *et al.* Subtle differences in virus composition affect disinfection kinetics and mechanisms. *Appl. Environ. Microbiol.* **79**, 3455–3467 (2013).
113. Haas, C. N. & Joffe, J. Disinfection under dynamic conditions - modification of Hom model for decay. *Environ. Sci. Technol.* **28**, 1367–1369 (1994).
114. Xue, B. *et al.* Effects of chlorine and chlorine dioxide on human Rotavirus infectivity and genome stability. *Water Res.* **47**, 3329–3338 (2013).
115. Mattle, M. J. *et al.* Impact of virus aggregation on inactivation by peracetic acid and implications for other disinfectants. *Environ. Sci. Technol.* **45**, 7710–7717 (2011).
116. Mattle, M. J. & Kohn, T. Inactivation and tailing during UV254 disinfection of viruses: Contributions of viral aggregation, light shielding within viral aggregates, and recombination. *Environ. Sci. Technol.* **46**, 10022–10030 (2012).
117. Napolitano, M. J., Green, B. J., Nicoson, J. S. & Margerum, D. W. Chlorine dioxide oxidations of tyrosine, N-acetyltyrosine, and dopa. *Chem. Res. Toxicol.* **18**, 501–508 (2005).
118. Sharp, D. G., Floyd, R. & Johnson, J. D. Nature of surviving plaque-forming unit of Reovirus in water containing bromine. *Appl. Microbiol.* **29**, 94–101 (1975).
119. Thurston-Enriquez, J. A., Haas, C. N., Jacangelo, J. & Gerba, C. P. Chlorine inactivation of Adenovirus type 40 and feline Calicivirus. *Appl. Environ. Microbiol.* **69**, 3979–3985 (2003).
120. Hejkal, T. W., Wellings, F. M., Lewis, A. L. & Larock, P. A. Distribution of viruses associated with particles in waste-water. *Appl. Environ. Microbiol.* **41**, 628–634 (1981).
121. Floyd, R. & Sharp, D. G. Aggregation of Poliovirus and Reovirus by dilution in water. *Appl. Environ. Microbiol.* **33**, 159–167 (1977).
122. Delgado, A. V, Gonzalez-Caballero, E., Hunter, R. J., Koopal, L. K. & Lyklema, J. Measurement and interpretation of electrokinetic phenomena - (IUPAC technical report). *Pure Appl. Chem.* **77**, 1753–1805 (2005).

123. Floyd, R. & Sharp, D. G. Viral aggregation - Effects of salts on aggregation of Poliovirus and Reovirus at low-pH. *Appl. Environ. Microbiol.* **35**, 1084–1094 (1978).
124. Rodriguez-Lazaro, D. *et al.* Virus hazards from food, water and other contaminated environments. *Fems Microbiol. Rev.* **36**, 786–814 (2012).
125. Kahler, A. M., Cromeans, T. L., Roberts, J. M. & Hill, V. R. Source water quality effects on monochloramine inactivation of Adenovirus, Coxsackievirus, Echovirus, and murine Norovirus. *Water Res.* **45**, 1745–1751 (2011).
126. Park, G. W., Linden, K. G. & Sobsey, M. D. Inactivation of murine Norovirus, feline Calicivirus and Echovirus 12 as surrogates for human Norovirus (NoV) and coliphage (F+) MS2 by ultraviolet light (254 nm) and the effect of cell association on UV inactivation. *Lett. Appl. Microbiol.* **52**, 162–167 (2011).
127. Alvarez, M. E. & O'Brien, R. T. Mechanisms of inactivation of Poliovirus by chlorine dioxide and iodine. *Appl. Environ. Microbiol.* **44**, 1064–1071 (1982).
128. Napolitano, M. J., Stewart, D. J. & Margerum, D. W. Chlorine dioxide oxidation of guanosine 5' -monophosphate. *Chem. Res. Toxicol.* **19**, 1451–1458 (2006).
129. Kurosaki, Y. *et al.* Pyrimidine dimer formation and oxidative damage in M13 bacteriophage inactivation by ultraviolet C irradiation. *Photochem. Photobiol.* **78**, 349–354 (2003).
130. Eischeid, A. C., Meyer, J. N. & Linden, K. G. UV disinfection of Adenoviruses: molecular indications of DNA damage efficiency. *Appl. Environ. Microbiol.* **75**, 23–28 (2009).
131. Hotze, E. M., Badireddy, A. R., Chellam, S. & Wiesner, M. R. Mechanisms of bacteriophage inactivation via singlet oxygen generation in UV illuminated fullerol suspensions. *Environ. Sci. Technol.* **43**, 6639–6645 (2009).
132. Schneider, J. E. *et al.* Methylene-blue and Rose-Bengal photoinactivation of RNA bacteriophages - Comparative-studies of 8-oxoguanine formation in isolated RNA. *Arch. Biochem. Biophys.* **301**, 91–97 (1993).
133. Baxter, C. S., Hofmann, R., Templeton, M. R., Brown, M. & Andrews, R. C. Inactivation of Adenovirus types 2, 5, and 41 in drinking water by UV light, free chlorine, and monochloramine. *J. Environ. Eng.-Asce* **133**, 95–103 (2007).
134. Rahn, R. O. Potassium iodide as a chemical actinometer for 254 nm radiation: Use of iodate as an electron scavenger. *Photochem. Photobiol.* **66**, 450–455 (1997).
135. Pecson, B. M., Ackermann, M. & Kohn, T. Framework for using quantitative PCR as a nonculture based method to estimate virus infectivity. *Environ. Sci. Technol.* **45**, 2257–2263 (2011).
136. Du, H., Fuh, R. C. A., Li, J. Z., Corkan, L. A. & Lindsey, J. S. PhotochemCAD: A computer-aided design and research tool in photochemistry. *Photochem. Photobiol.* **68**, 141–142 (1998).

## References

137. Wilkinson, F., Helman, W. P. & Ross, A. B. Rate constant for the decay and reactions of the lowest electronically excited singlet-state of molecular-oxygen in solution - an expanded and revised compilation. *J. Phys. Chem. Ref. Data* **24**, 663–1021 (1995).
138. Prutz, W. A. Hypochlorous acid interactions with thiols, nucleotides, DNA, and other biological substrates. *Arch. Biochem. Biophys.* **332**, 110–120 (1996).
139. Prutz, W. A. Interactions of hypochlorous acid with pyrimidine nucleotides, and secondary reactions of chlorinated pyrimidines with GSH, NADH, and other substrates. *Arch. Biochem. Biophys.* **349**, 183–191 (1998).
140. Ison, A., Odeh, I. N. & Margerum, D. W. Kinetics and mechanisms of chlorine dioxide and chlorite oxidations of cysteine and glutathione. *Inorg. Chem.* **45**, 8768–8775 (2006).
141. Gorner, H. Photochemistry of DNA and related biomolecules - Quantum yields and consequences of photoionization. *J. Photochem. Photobiol. B-Biology* **26**, 117–139 (1994).
142. Miller, R. L. & Plageman, P. G. Effect of ultraviolet-light on Mengovirus - Formation of uracil dimers, instability and degradation of capsid, and covalent linkage of protein to viral-RNA. *J. Virol.* **13**, 729–739 (1974).
143. Vøllestad, K., Murray, J. B., Stockley, P. G., Stonehouse, N. J. & Liljas, L. Crystal-structure of an RNA-bacteriophage coat protein-operator complex. *Nature* **371**, 623–626 (1994).
144. Koning, R. *et al.* Visualization by cryo-electron microscopy of genomic RNA that binds to the protein capsid inside bacteriophage MS2. *J. Mol. Biol.* **332**, 415–422 (2003).
145. Weissman, C., Billeter, M. A., Goodman, H. M., Hindley, J. & Weber, H. Structure and function of phage RNA. *Annu. Rev. Biochem.* **42**, 303–328 (1973).
146. Schneider, J. E. *et al.* Potential mechanisms of photodynamic inactivation of virus by methylene blue - I. RNA-protein crosslinks and other oxidative lesions in Q beta bacteriophage. *Photochem. Photobiol.* **67**, 350–357 (1998).
147. Dennis, W. H., Olivieri, V. P. & Kruse, C. W. Mechanism of disinfection - Incorporation of Cl<sub>2</sub> into f2 virus. *Water Res.* **13**, 363–369 (1979).
148. Ericson, G. & Wollenzien, P. Use of reverse transcription to determine the exact locations of psoralen photochemical crosslinks in RNA. *Anal. Biochem.* **174**, 215–223 (1988).
149. Shibutani, S., Takeshita, M. & Grollman, A. P. Insertion of specific bases during DNA-synthesis past the oxidation-damaged base 8-oxodG. *Nature* **349**, 431–434 (1991).
150. Kim, S. K., Yokoyama, S., Takaku, H. & Moon, B. J. Oligoribonucleotides containing 8-oxo-7,8-dihydroguanosine and 8-oxo-7,8-dihydro-2'-O-methylguanosine: Synthesis and base pairing properties. *Bioorg. Med. Chem. Lett.* **8**, 939–944 (1998).

151. Wurtmann, E. J. & Wolin, S. L. RNA under attack: Cellular handling of RNA damage. *Crit. Rev. Biochem. Mol. Biol.* **44**, 34–49 (2009).
152. Smith, C. A., Baeten, J. & Taylor, J. S. The ability of a variety of polymerases to synthesize past site-specific cis-syn, trans-syn-II, (6-4), and Dewar photoproducts of thymidyl-(3' → 5')-thymidine. *J. Biol. Chem.* **273**, 21933–21940 (1998).
153. Noss, C. I., Hauchman, F. S. & Olivieri, V. P. Chlorine dioxide reactivity with proteins. *Water Res.* **20**, 351–356 (1986).
154. Stewart, D. J., Napolitano, M. J., Bakhmutova-Albert, E. V & Margerum, D. W. Kinetics and mechanisms of chlorine dioxide oxidation of tryptophan. *Inorg. Chem.* **47**, 1639–1647 (2008).
155. Li, J. W., Xin, Z. T., Wang, X. W., Zheng, J. L. & Chao, F. H. Mechanisms of inactivation of Hepatitis A virus in water by chlorine dioxide. *Water Res.* **38**, 1514–1519 (2004).
156. Sirikanchana, K., Shisler, J. L. & Marinas, B. J. Inactivation kinetics of Adenovirus serotype 2 with monochloramine. *Water Res.* **42**, 1467–1474 (2008).
157. Hu, L. *et al.* Inactivation of bacteriophage MS2 with potassium ferrate(VI). *Environ. Sci. Technol.* **46**, 12079–87 (2012).
158. Hauchman, F. S., Noss, C. I. & Olivieri, V. P. Chlorine dioxide reactivity with nucleic-acids. *Water Res.* **20**, 357–361 (1986).
159. Tars, K., Bundule, M., Fridborg, K. & Liljas, L. The crystal structure of bacteriophage GA and a comparison of bacteriophages belonging to the major groups of Escherichia coli leviviruses. *J. Mol. Biol.* **271**, 759–773 (1997).
160. Laemmli, U. K. Cleavage of structural proteins during assembly of head of bacteriophage-T4. *Nature* **227**, 680–& (1970).
161. Shevchenko, A., Wilm, M., Vorm, O. & Mann, M. Mass spectrometric sequencing of proteins from silver stained polyacrylamide gels. *Anal. Chem.* **68**, 850–858 (1996).
162. Davies, M. J. Reactive species formed on proteins exposed to singlet oxygen. *Photochem. Photobiol. Sci.* **3**, 17–25 (2004).
163. Pattison, D. I. & Davies, M. J. Absolute rate constants for the reaction of hypochlorous acid with protein side chains and peptide bonds. *Chem. Res. Toxicol.* **14**, 1453–1464 (2001).
164. Mihalyi, E. Numerical values of absorbances of aromatic amino acids in acid, neutral and alkaline solutions. *J. Chem. Eng. Data* **13**, 179–& (1968).
165. Phillips, J. C. *et al.* Scalable molecular dynamics with NAMD. *J. Comput. Chem.* **26**, 1781–1802 (2005).

## References

166. D.A. Case, T.E. Cheatham, III, C.L. Simmerling, J. Wang, R.E. Duke, R. Luo, R.C. Walker, W. Zhang, K.M. Merz, B. Roberts, B. Wang, S. Hayik, A. Roitberg, G. Seabra, I. Kolossváry, K.F. Wong, F. Paesani, J. Vanicek, J. Liu, X. Wu, S.R. Brozell, T. Steinbre, T. A. D. AMBER 11. (2010).
167. M. Frisch, H. Schlegel, G. Scuseria, M. Robb, J. Cheeseman, J. Montgomery, T. Vreven, K. Kudin, J. Burant, J. Millam, S. Iyengar, J. Tomasi, V. Barone, B. Mennucci, M. Cossi, G. Scalmani, N. Rega, G. Petersson, H. Nakatsuji, M. Hada, M. Ehara, K. Toyota, G. T. Gaussian 03. (2003).
168. Wang, J. M., Wolf, R. M., Caldwell, J. W., Kollman, P. A. & Case, D. A. Development and testing of a general amber force field. *J. Comput. Chem.* **25**, 1157–1174 (2004).
169. Humphrey, W., Dalke, A. & Schulten, K. VMD: Visual molecular dynamics. *J. Mol. Graph. Model.* **14**, 33–38 (1996).
170. Wigginton, K. R. *et al.* UV radiation induces genome-mediated, site-specific cleavage in viral proteins. *Chembiochem A Eur. J. Chem. Biol.* **13**, 837–845 (2012).
171. Jensen, R. L., Arnbjerg, J. & Ogilby, P. R. Reaction of singlet oxygen with tryptophan in proteins: A pronounced effect of the local environment on the reaction rate. *J. Am. Chem. Soc.* **134**, 9820–9826 (2012).
172. O'Brien, R. T. & Newman, J. Structural and compositional changes associated with chlorine inactivation of Polioviruses. *Appl. Environ. Microbiol.* **38**, 1034–1039 (1979).
173. Davies, M. J. The oxidative environment and protein damage. *Biochim. Biophys. Acta-Proteins Proteomics* **1703**, 93–109 (2005).
174. Jensen, H., Thomas, K. & Sharp, D. G. Inactivation of Coxsackie-viruses B3 and B5 in water by chlorine. *Appl. Environ. Microbiol.* **40**, 633–640 (1980).
175. Shin, G.-A. & Sobsey, M. D. Reduction of Norwalk virus, Poliovirus 1, and bacteriophage MS2 by ozone disinfection of water. *Appl. Environ. Microbiol.* **69**, 3975–3978 (2003).
176. Hejkal, T. W., Wellings, F. M., LaRock, P. A. & Lewis, A. L. Survival of Poliovirus within organic solids during chlorination. *Appl. Environ. Microbiol.* **38**, 114–8 (1979).
177. Nieto-Juarez, J. I. & Kohn, T. Virus removal and inactivation by iron (hydr)oxide-mediated Fenton-like processes under sunlight and in the dark. *Photochem. Photobiol. Sci.* (2013). doi:10.1039/c3pp25314g
178. Kim, J. Y. *et al.* Inactivation of MS2 coliphage by ferrous ion and zero-valent iron nanoparticles. *Environ. Sci. Technol.* **45**, 6978–84 (2011).
179. Sharan, R., Chhibber, S., Attri, S. & Reed, R. H. Inactivation and injury of Escherichia coli in a copper water storage vessel: effects of temperature and pH. *Antonie Van Leeuwenhoek* **97**, 91–7 (2010).

180. Sharan, R., Chhibber, S., Attri, S. & Reed, R. H. Inactivation and sub-lethal injury of *Escherichia coli* in a copper water storage vessel: effect of inorganic and organic constituents. *Antonie Van Leeuwenhoek* **98**, 103–15 (2010).
181. WHO | Copper in drinking-water. (2004). at <[http://www.who.int/water\\_sanitation\\_health/publications/copper/en/index.html](http://www.who.int/water_sanitation_health/publications/copper/en/index.html)>
182. Sudha, V. B. P., Singh, K. O., Prasad, S. R. & Venkatasubramanian, P. Killing of enteric bacteria in drinking water by a copper device for use in the home: laboratory evidence. *Trans. R. Soc. Trop. Med. Hyg.* **103**, 819–22 (2009).
183. Li, J. & Dennehy, J. J. Differential bacteriophage mortality on exposure to copper. *Appl. Environ. Microbiol.* **77**, 6878–83 (2011).
184. Noyce, J. O., Michels, H. & Keevil, C. W. Inactivation of Influenza A virus on copper versus stainless steel surfaces. *Appl. Environ. Microbiol.* **73**, 2748–50 (2007).
185. Borkow, G. *et al.* Neutralizing viruses in suspensions by copper oxide-based filters. *Antimicrob. Agents Chemother.* **51**, 2605–7 (2007).
186. Pollard, T. D., Earnshaw, W. C. & Lippincott-Schwartz, J. *Cell Biology*. (2007).
187. Poirier, G. E. & Pylant, E. D. The self-assembly mechanism of alkanethiols on Au(111). *Science (80-. J.)* **272**, 1145–1148 (1996).
188. Bain, C. D. *et al.* Formation of monolayer films by the spontaneous assembly of organic thiols from solution onto gold. *J. Am. Chem. Soc.* **111**, 321–335 (1989).
189. Prime, K. & Whitesides, G. Self-assembled organic monolayers: model systems for studying adsorption of proteins at surfaces. *Science (80-. J.)* **252**, 1164–1167 (1991).
190. Prime, K. L. & Whitesides, G. M. Adsorption of proteins onto surfaces containing end-attached oligo(ethylene oxide): a model system using self-assembled monolayers. *J. Am. Chem. Soc.* **115**, 10714–10721 (1993).
191. Kumar, A., Biebuyck, H. A. & Whitesides, G. M. Patterning self-assembled monolayers: Applications in materials science. *Langmuir* **10**, 1498–1511 (1994).
192. Revell, D. J., Knight, J. R., Blyth, D. J., Haines, A. H. & Russell, D. A. Self-assembled carbohydrate monolayers: Formation and surface selective molecular recognition. *Langmuir* **14**, 4517–4524 (1998).
193. Ferretti, S., Paynter, S., Russell, D. A., Sapsford, K. E. & Richardson, D. J. Self-assembled monolayers: A versatile tool for the formulation of bio-surfaces. *TrAC Trends Anal. Chem.* **19**, 530–540 (2000).

## References

194. Azmi, A. A., Ebralidze, I. I., Dickson, S. E. & Horton, J. H. Characterization of hydroxyphenol-terminated alkanethiol self-assembled monolayers: Interactions with phosphates by chemical force spectrometry. *J. Colloid Interface Sci.* **393**, 352–360 (2013).
195. Dowd, S. E., Pillai, S. D., Wang, S. & Corapcioglu, M. Y. Delineating the specific influence of virus isoelectric point and size on virus adsorption and transport through sandy soils. *Appl. Environ. Microbiol.* **64**, 405–10 (1998).
196. Pecson, B. M., Decrey, L. & Kohn, T. Photoinactivation of virus on iron-oxide coated sand: enhancing inactivation in sunlit waters. *Water Res.* **46**, 1763–70 (2012).
197. Bain, C. D., Biebuyck, H. A. & Whitesides, G. M. Comparison of self-assembled monolayers on gold: coadsorption of thiols and disulfides. *Langmuir* **5**, 723–727 (1989).
198. Ulman, A. Formation and structure of self-assembled monolayers. *Chem. Rev.* **96**, 1533–1554 (1996).
199. Nuzzo, R. G. & Allara, D. L. Adsorption of bifunctional organic disulfides on gold surfaces. *J. Am. Chem. Soc.* **105**, 4481–4483 (1983).
200. Love, J. C., Estroff, L. A., Kriebel, J. K., Nuzzo, R. G. & Whitesides, G. M. Self-assembled monolayers of thiolates on metals as a form of nanotechnology. *Chem. Rev.* **105**, 1103–69 (2005).
201. Armanious, A. & Sander, M. (In prep).
202. Reviakine, I., Johannsmann, D. & Richter, R. P. Hearing what you cannot see and visualizing what you hear: interpreting quartz crystal microbalance data from solvated interfaces. *Anal. Chem.* **83**, 8838–48 (2011).
203. Vörös, J. The density and refractive index of adsorbing protein layers. *Biophys. J.* **87**, 553–61 (2004).
204. Kuzmanovic, D. A., Elashvili, I., Wick, C., O’Connell, C. & Krueger, S. Bacteriophage MS2: Molecular weight and spatial distribution of the protein and RNA components by small-angle neutron scattering and virus counting. *Structure* **11**, 1339–1348 (2003).
205. Sagripanti, J. L., Routson, L. B. & Lytle, C. D. Virus inactivation by copper or iron ions alone and in the presence of peroxide. *Appl. Environ. Microbiol.* **59**, 4374–4376 (1993).
206. Yahya, M. T., Straub, T. M. & Gerba, C. P. Inactivation of coliphage-MS2 and Poliovirus by copper, silver, and chlorine. *Can. J. Microbiol.* **38**, 430–435 (1992).
207. Dortwegt, R. & Maughan, E. The chemistry of copper in water and related studies planned at the advanced photon source. *Conf.Proc.* **C0106181**, 1456–1458 (2001).
208. Norde, W. Adsorption of proteins from solution at the solid-liquid interface. *Adv. Colloid Interface Sci.* **25**, 267–340 (1986).



209. Silin, V., Weetall, H. & Vanderah, D. J. SPR studies of the nonspecific adsorption kinetics of human IgG and BSA on gold surfaces modified by self-assembled monolayers (SAMs). *J. Colloid Interface Sci.* **185**, 94–103 (1997).
210. Tanford, C. Interfacial free-energy and the hydrophobic effect. *Proc. Natl. Acad. Sci. U. S. A.* **76**, 4175–4176 (1979).
211. Seymour, D. L. *et al.* A mercaptide intermediate on Cu(111). *Surf. Sci.* **189-190**, 529–534 (1987).
212. Grönbeck, H., Curioni, A. & Andreoni, W. Thiols and disulfides on the Au(111) surface: the headgroup–gold interaction. *J. Am. Chem. Soc.* **122**, 3839–3842 (2000).
213. Deng, M. Y., Day, S. P. & Cliver, D. O. Detection of Hepatitis A virus in environmental samples by antigen-capture PCR. *Appl. Environ. Microbiol.* **60**, 1927–33 (1994).
214. Larson, A. M. *et al.* Hydrophobic polycationic coatings disinfect Poliovirus and Rotavirus solutions. *Biotechnol. Bioeng.* **108**, 720–3 (2011).
215. Hsu, B. B., Yinn Wong, S., Hammond, P. T., Chen, J. & Klibanov, A. M. Mechanism of inactivation of Influenza viruses by immobilized hydrophobic polycations. *Proc. Natl. Acad. Sci. U. S. A.* **108**, 61–6 (2011).
216. Itoh, S., Nagagawa, M. & Fukuzumi, S. Fine tuning of the interaction between the copper(I) and disulfide bond. Formation of a bis(  $\mu$  -thiolato)dicopper(II) complex by reductive cleavage of the disulfide bond with copper(I). *J. Am. Chem. Soc.* **123**, 4087–4088 (2001).
217. Warnes, S. L. & Keevil, C. W. Inactivation of Norovirus on dry copper alloy surfaces. *PLoS One* **8**, (2013).
218. Kozłowski, H., Bal, W., Dyba, M. & Kowalik-Jankowska, T. Specific structure–stability relations in metallopeptides. *Coord. Chem. Rev.* **184**, 319–346 (1999).
219. Horie, M. *et al.* Inactivation and morphological changes of avian Influenza virus by copper ions. *Arch. Virol.* **153**, 1467–72 (2008).
220. Logan, D. *et al.* Structure of a major immunogenic site on foot-and-mouth disease virus. *Nature* **362**, 566–8 (1993).
221. Szczepaniak, R. *et al.* Disulfide bond formation contributes to Herpes Simplex virus capsid stability and retention of pentons. *J. Virol.* **85**, 8625–34 (2011).
222. Golmohammadi, R., Valegard, K., Fridborg, K. & Liljas, L. The refined structure of bacteriophage-MS2 at 2-center-dot-8-angstrom resolution. *J. Mol. Biol.* **234**, 620–639 (1993).
223. Carrillo-Tripp, M. *et al.* VIPERdb(2): an enhanced and web API enabled relational database for structural virology. *Nucleic Acids Res.* **37**, D436–D442 (2009).

## References

- 224. Jorgensen, W. L., Chandrasekhar, J., Madura, J. D., Impey, R. W. & Klein, M. L. Comparison of simple potential functions for simulating liquid water. *J. Chem. Phys.* **79**, 926–935 (1983).
- 225. Hess, B., Kutzner, C., van der Spoel, D. & Lindahl, E. GROMACS 4: Algorithms for highly efficient, load-balanced, and scalable molecular simulation. *J. Chem. Theory Comput.* **4**, 435–447 (2008).
- 226. Mobley, D. L., Chodera, J. D. & Dill, K. A. On the use of orientational restraints and symmetry corrections in alchemical free energy calculations. *J. Chem. Phys.* **125**, (2006).
- 227. Baker, N. A., Sept, D., Joseph, S., Holst, M. J. & McCammon, J. A. Electrostatics of nanosystems: Application to microtubules and the ribosome. *Proc. Natl. Acad. Sci. U. S. A.* **98**, 10037–10041 (2001).
- 228. Wang, T., Tomic, S., Gabdoulline, R. R. & Wade, R. C. How optimal are the binding energetics of barnase and barstar? *Biophys. J.* **87**, 1618–1630 (2004).

# Thérèse Sigstam

Rue de la Tour 6, 1004 Lausanne  
therese.sigstam@gmail.com  
20.09.1982, Swedish and Swiss citizen

---

## EDUCATION

- 2010-2014: **PhD in Environmental Chemistry**, at Ecole Polytechnique Fédérale de Lausanne, Switzerland supervised by Prof. Tamar Kohn  
*"Mechanistic insight into virus disinfection: Influence of virus characteristics, solution composition and surface interactions"*
- 2005-2007: **Master studies in biological and molecular chemistry** at Ecole Polytechnique Fédérale de Lausanne, Switzerland  
Master project at University of Seville (Spain) (with Prof. I. Robina-Ramirez (Seville) and Prof. P. Vogel (Lausanne))  
*"7-Azabicyclo[2.2.1]hept-2-enes as synthetic intermediates for the preparation of 2,5-disubstituted pyrrolidines-synthesis of both enantiomers of cis-5-methylproline"*
- 2002-2005: **Bachelor studies** in chemistry at Ecole Polytechnique Fédérale de Lausanne, Switzerland

## WORKING EXPERIENCE

- 2007-2009: **Project manager formulation**, at Medipol SA, Lausanne Switzerland
- 2007: **Internship** at the Pathology Institute at CHUV, Lausanne, Switzerland

## LANGUAGES

- Swedish: Mother tongue  
French: Mother tongue  
English: Very good spoken and written knowledge  
Spanish: Good spoken and written knowledge  
German: Good understanding and speaking

## PERSONAL INTERESTS

Sports: capoeira, ski (downhill and back-country) and badminton  
Traveling

## PUBLICATIONS

1. **Sigstam T.**, Rohatschek A., Zhong Q., Brennecke M., and Kohn T. On the cause of the tailing phenomenon during virus disinfection by chlorine dioxide. *Water Res.*, vol. 48, pp. 82–89, **2014**.
2. **Sigstam T.**, Gannon G., Cascella M., Pecson B. M., Wigginton K. R., and Kohn T. Subtle differences in virus composition affect disinfection kinetics and mechanisms. *Appl Env. Microbiol*, vol. 79, no. 11, pp. 3455–3467, **2013**.
3. Wigginton K. R., Menin L., **Sigstam T.**, Gannon G., Cascella M., Ben Hamidane H., Tsybin Y. O., Waridel P., and Kohn T. UV Radiation Induces Genome-Mediated, Site-Specific Cleavage in Viral Proteins. *Chembiochem A Eur. J. Chem. Biol.*, vol. 13, no. 6, pp. 837–845, **2012**.
4. Wigginton K. R., Pecson B. M., **Sigstam T.**, Bosshard F., and Kohn T. Virus inactivation mechanisms: impact of disinfectants on virus function and structural integrity. *Env. Sci Technol*, vol. 46, no. 21, pp. 12069–78, **2012**.
5. Hu L., Page M. A., **Sigstam T.**, Kohn T., Mariñas B. J., and Strathmann T. J. Inactivation of Bacteriophage MS2 with Potassium Ferrate(VI). *Env. Sci Technol*, no. VI, **2012**.
6. Moreno-Clavijo E., Moreno-Vargas A. J., Kieffer R., **Sigstam T.**, Carmona A. T., and Robina I. Exploiting the ring strain in bicyclo[2.2.1]heptane systems for the stereoselective preparation of highly functionalized cyclopentene, dihydrofuran, pyrroline, and pyrrolidine scaffolds. *Org. Lett.*, vol. 13, no. 23, pp. 6244–7, **2011**.

## CONFERENCE PRESENTATIONS

**17<sup>th</sup> International symposium on  
health-related water  
microbiology**

Florianopolis, Brazil

15<sup>th</sup> – 20<sup>th</sup> September 2013

Adsorption and inactivation of viral pathogens upon surface interaction. **Sigstam, T.**, Armanious, A., Sander, M. and Kohn T. Oral presentation

**Goldschmidt conference**

Florence, Italy

25<sup>th</sup> – 30<sup>th</sup> August 2013

Adsorption of MS2 virus to natural organic matter and model surfaces. Armanious, A., **Sigstam, T.**, Kohn, T., and Sander, M. Oral presentation

**IIE Green days**

Arolla, Switzerland

29<sup>th</sup> – 30<sup>th</sup> August 2013

On the causes of the tailing phenomenon during virus disinfection by chlorine dioxide. **Sigstam, T.**, Rohatschek, A., Zhong, Q., Brennecke M. and Kohn T. Oral presentation

**ENAC research day**

EPFL, Lausanne

23<sup>rd</sup> April 2013

Influence of virus composition on inactivation and associated protein and genome damage by different disinfectants. **Sigstam, T.** and Kohn, T. Poster presentation

**3<sup>rd</sup> Food and environmental  
virology conference**

Lisboa, Portugal

7<sup>th</sup> – 10<sup>th</sup> October 2012

Influence of subtle changes in virus composition on inactivation by UV<sub>254</sub> and ClO<sub>2</sub>. **Sigstam, T.** and Kohn, T. Poster presentation

**3<sup>rd</sup> Food and environmental  
virology conference**

Lisboa, Portugal

7<sup>th</sup> – 10<sup>th</sup> October 2012

A mechanistic investigation of virus inactivation by oxidants, UV and heat. Wigginton, K.R., **Sigstam, T.**, Pecson, B.M., Bosshard, F., and Kohn, T. Oral presentation

**Gordon research conference on  
environmental sciences: Water**

Plymouth, NH, USA

24<sup>th</sup> – 29<sup>th</sup> June 2012

Influence of subtle changes in virus composition on inactivation by UV<sub>254</sub> and ClO<sub>2</sub>. **Sigstam, T.** and Kohn, T. Poster presentation

<b>ENAC research day</b> EPFL, Lausanne 15 <sup>th</sup> June 2012	Influence of subtle changes in virus composition on inactivation by UV <sub>254</sub> and ClO <sub>2</sub> . <b><u>Sigstam, T.</u></b> and Kohn, T. Poster presentation
<b>242<sup>nd</sup> American Chemical Society National Meeting</b> Denver, USA 28 <sup>th</sup> August – 1 <sup>st</sup> Sept. 2011	Comparison of protein and genome damage and virus function loss with disinfection of two different bacteriophages. <b><u>Sigstam, T.</u></b> , Wigginton, K. R. And Kohn, T. Poster presentation
<b>242<sup>nd</sup> American Chemical Society National Meeting</b> Denver, USA 28 <sup>th</sup> August – 1 <sup>st</sup> Sept. 2011	Virus inactivation mechanisms upon exposure to heat, oxidants, and UV irradiation. <u>Wigginton, K.R.</u> , Pecson, B.M., <b><u>Sigstam, T.</u></b> , Bosshard, F. and Kohn, T. Oral presentation
<b>Meeting of the Association of Environmental Engineering and Science Professors (AEESP)</b> Tampa, USA 10 <sup>th</sup> – 12 <sup>th</sup> July 2011	Quantitative assessment of virus protein and genome damage upon inactivation by common disinfectants. <u>Wigginton, K.R.</u> , Pecson, B.M., <b><u>Sigstam, T.</u></b> , Bosshard, F. and Kohn, T. Oral presentation
<b>111<sup>th</sup> General Meeting of the American Society of Microbiology</b> New Orleans 21 <sup>st</sup> – 24 <sup>th</sup> May 2011	The mechanisms responsible for virus Inactivation upon exposure to oxidants, germicidal UV, and heat. <u>Wigginton, K.R.</u> , Pecson, B.M., Bosshard F, <b><u>Sigstam, T.</u></b> and Kohn, T. Poster presentation
<b>2011 FEMS conference</b> Geneva, Switzerland 26 <sup>th</sup> – 30 <sup>th</sup> June 2011	Virus inactivation mechanisms upon exposure to heat, oxidants and UV-light. <u>Bosshard. F.</u> , Wigginton, K.R., Pecson, B.M., <b><u>Sigstam, T.</u></b> and Kohn, T. Poster presentation.
<b>2<sup>nd</sup> COST 929 symposium “Future Challenges in Food and Environmental Virology”</b> Istanbul, Turkey 7 <sup>th</sup> – 9 <sup>th</sup> October 2010	Quantitative assessment of genome and protein damage upon virus inactivation by chlorine, heat, UVC and sunlight. <u>Wigginton, K.R.</u> , Pecson, B.M., <b><u>Sigstam, T.</u></b> and <u>Kohn T.</u> Oral presentation

